

NUREG/CR-2189, Vol. 5
UCID-18967, Vol. 5
RM

Probability of Pipe Fracture in the Primary Coolant Loop of a PWR Plant

Volume 5: Probabilistic Fracture Mechanics Analysis Load Combination Program Project I Final Report

Manuscript Completed June 1981
Date Published August 1981

Prepared by
D. O. Harris, B. Y. Lim, D. D. Dedhia
Science Applications, Inc
Lawrence Livermore Laboratory
7000 East Avenue
Livermore, CA 94550

Prepared for
Division of Engineering Technology
Office of Nuclear Regulatory Research
U.S. Nuclear Regulatory Commission
Washington, D.C. 20535
NRC FIN No. A-0133

ABSTRACT

The purpose of the portion of the Load Combination Program covered in this volume was to estimate the probability of a seismic induced loss-of-coolant accident (LOCA) in the primary piping of a commercial pressurized water reactor (PWR). Such results are useful in rationally assessing the need to design reactor primary piping systems for the simultaneous occurrence of these two potentially high stress events. The primary piping system at Zion I was selected for analysis. Attention was focussed on the girth butt welds in the hot leg, cold leg and cross-over leg, which are centrifugally cast austenitic stainless steel lines with nominal outside diameters of 32 - 37 inches.

A fracture mechanics model of structural reliability was employed to estimate the piping failure probability. This model assumes piping failure to occur as the result of the subcritical and catastrophic growth of cracks introduced into weldments during fabrication. Part-circumferential interior surface cracks are considered to be present with a probability that depends on their size, and a bivariate crack size distribution is employed which is estimated from the literature. The size distribution is altered by pre- and in-service inspections by a crack detection probability that depends on crack size. The cracks that are present after the pre-service inspection and proof test form the initial conditions for fracture mechanics calculation of how these cracks would grow due to cyclic stresses imposed in service. Seismic events of a specified magnitude at a specified time were included in the stress history thereby providing information on the influence of such events on the piping reliability.

The results generated by a specially written computer code indicated that the stress history was dominated by the heatup-cooldown cycle, and that seismic events generally did not have a strong influence. Pre-service inspection and the initial proof test provided a significant reduction in the failure probabilities. The leak and LOCA probabilities were calculated to be on the order of 10^{-6} and 10^{-12} per plant lifetime (respectively) for the complete primary system. Large variations in the input parameters (such as initial crack size distribution) were required before these values were significantly altered. Hence, it appears that the probability of a sudden and complete pipe severance in the large primary piping at Zion I is very low. The probability of a seismic induced LOCA is even lower.

TABLE OF CONTENTS

<u>Section</u>	<u>Page</u>
LIST OF FIGURES.....	viii
LIST OF TABLES.....	xiv
ACKNOWLEDGEMENTS.....	xvi
EXECUTIVE SUMMARY.....	xvii
1.0 INTRODUCTION.....	1
1.1 Basic Methodology.....	2
1.2 Plant Description.....	2
1.3 Review of Relevant Stresses.....	7
1.3.1 Non-Seismic Stresses.....	7
1.3.2 Seismic Stresses.....	8
1.3.3 Radial Gradient Thermal Stresses.....	8
2.0 FRACTURE MECHANICS MODEL.....	12
2.1 Overview and Review of Past Work.....	12
2.2 Summary and Discussion of Major Assumptions.....	16
2.3 Initial Crack Distribution.....	20
2.3.1 Depth Distribution.....	24
2.3.2 Aspect Ratio Distribution.....	28
2.3.3 Resulting Area and Length Distributions....	33
2.3.4 Crack Existence Probabilities.....	43
2.4 Inspection Detection Probabilities.....	49
2.4.1 Review of Past Results.....	49
2.4.2 Model for Influence of Surface Length.....	54
2.4.3 Specialization to Austenitic Weldments.....	56
2.5 Material Fracture Characteristics.....	59
2.5.1 Fatigue Crack Growth.....	62
2.5.2 Final Fracture.....	72
2.6 Fatigue Crack Growth Calculation Procedures.....	77
2.6.1 Relevant Stress Intensity Factors for Part-Through Cracks.....	77
2.6.2 Cycle Counting and Load Interactions.....	80
2.7 Stress Intensity Factors.....	86
2.8 Leak Models.....	93
2.8.1 Prediction of Flashing Water Flow-Through PWR Pipe-Wall Cracks.....	93
2.8.2 Crack Opening Displacements.....	101

Table of Contents (cont'd)

<u>Section</u>	<u>Page</u>
2.8.3 Leak Detection Probabilities.....	104
2.9 Failure Criteria.....	105
3.0 NUMERICAL SIMULATION PROCEDURES.....	110
3.1 Monte Carlo Simulation.....	115
3.2 Sample Space Definition.....	117
3.3 Stratified Sampling.....	120
3.4 Initial Crack Size Distribution.....	123
3.4.1 Transformation of Variables.....	123
3.4.2 Pre-Service Inspection and Hydrostatic Proof Test.....	128
3.5 Arrival Time for Events.....	132
3.6 Crack Growth Calculation.....	134
3.7 Influence of Earthquakes on Crack Growth.....	138
3.8 Statistical Variance.....	143
4.0 APPLICATIONS TO REACTOR PIPING.....	148
4.1 Transient Frequencies.....	150
4.2 Joint and System Reliability.....	153
4.3 Results and Discussion.....	154
4.3.1 Results for all Transients.....	155
4.3.2 Results for Base Case Conditions.....	157
4.3.3 Influence of Input Parameters on Results.....	190
4.3.4 Additional Discussion of Results.....	198
5.0 SUMMARY AND CONCLUSIONS.....	206
SUMMARY OF MAJOR NOTATION.....	209
REFERENCES..	214

Appendices

<u>Section</u>	<u>Page</u>
A. INTRODUCTION AND REVIEW OF STRESS INTENSITY FACTOR ANALYSIS.....	233
A.1 Desired Solutions.....	234
A.2 Review of Previously Existing Stress Intensity Solutions.....	235
A.3 Review of Boundary Integral Equation Techniques.....	249
B. STRESS INTENSITY FACTOR RESULTS FROM BOUNDARY INTEGRAL EQUATION CALCULATIONS.....	251
B.1 Complete Circumferential Crack.....	254
B.2 Longitudinal Semi-Elliptical Cracks.....	257
B.3 Circumferential Semi-Elliptical Cracks.....	269
C. INFLUENCE FUNCTIONS.....	277
C.1 Introductory Remarks.....	278
C.2 Underlying Theory.....	283
C.3 Curve Fit to g_1	289
C.4 Curve Fit to g_2	293
D. APPLICATIONS TO COMPLEX STRESSES.....	299
D.1 Integration Procedures.....	300
D.2 Verification of the Integration Procedures.....	304
D.2.1 Uniform Stresses.....	304
D.2.2 Non-Uniform Stresses.....	305
D.3 Comparison With Existing Solutions.....	309
D.3.1 Uniform Stress.....	309
D.3.2 Non-Uniform Stresses.....	309
D.4 Applications to Radial Gradient Thermal Stresses.....	315
GLOSSARY.....	349

LIST OF FIGURES

<u>Figure</u>		<u>Page</u>
1-1	Schematic Representation of Various Portions of Project to Determine Necessity of Coupling LOCA's and Seismic Events.....	3
1-2	Diagram of Primary Piping Analyzed Showing Locations of Welds Considered.....	5
2-1	Schematic Diagram of Steps in Analysis of Reliability of a Given Weld Location.....	13
2-2	Geometry of Part-Circumferential Internal Surface Crack Considered in this Investigation.....	22
2-3	Various Complementary Cumulative Marginal Crack Depth Distributions	26
2-4	Various Complementary Cumulative Marginal Distributions of Crack Aspect Ratio.....	32
2-5	Complementary Cumulative Distribution of Crack Area. Exponential Depth Distribution and Shifted Lognormal Aspect Ratio Distribution of Various Values of ρ	38
2-6	Comparison of Feldman Data on Crack Area Distributions with Results Using Marshall Exponential on Depth and "Shifted" Lognormal on Aspect Ratio, with $\rho = 10^{-4}$	39
2-7	Complementary Cumulative Distribution of Half Surface Crack Length for Marginal Exponential Depth Distribution and Marginal Lognormal Aspect Ratio Distribution.....	42
2-8	Probability of Non-Detection of a Crack as a Function of its Depth for an Ultrasonic Inspection — Data From Literature....	50
2-9	Crack Geometry Versus Beam Diameter for the Two Dimensional Model of Probability of Non-Detection Based on Crack Area.....	55
2-10	Two Dimensional Lognormal Model of Probability of Non-Detection of a Crack Based on Crack Area Plotted on Lognormal Probability Paper.....	57
2-11	Two Dimensional Lognormal Model of Probability of Non-Detection of a Crack Based on Crack Area Plotted on Linear Scales..	58
2-12	P_{ND} Data for Wrought Materials (Same as Figure 2-8) and the Model for Cast Austenitic Material.....	60

List of Figures (cont'd)

<u>Figure</u>		<u>Page</u>
2-13	Two Dimensional Lognormal Model for Probability of Non-Detection of a Crack in Cast Austenitic Material.....	61
2-14	Fatigue Crack Growth Rate Data as a Function of Effective Stress Intensity Shown Along with Least Square Curve-Fit.....	65
2-15	Frequency Histogram of $\ln(C)$ for $m = 4.0$	69
2-16	Cumulative Distribution of C Plotted on a Lognormal Probability Paper.....	70
2-17	Schematic Representation of J-Integral R Curve.....	74
2-18	Schematic Representation of a Stress-Time History Showing Means of Counting Stress Cycles and Corresponding $\Delta\sigma_i$	82
2-19	Schematic Representation of a Time History for Stress Intensity Factor for a Transient That Produces Radial Gradient Thermal Stresses During Steady State Plant Operation.....	83
2-20	K_t/σ_a^2 for a Part-Circumferential Crack in a Pipe With Uniform Stress in the Pipe Wall.....	88
2-21	K_t/σ_a^2 for a Part-Circumferential Crack in a Pipe With Uniform Stress in the Pipe Wall.....	89
2-22	Two-Phase Flow Through a Long, Narrow Crack (From Wallis 80)..	94
2-23	Solution Method. HEM Model/Isenthalpic Flow $P_{in} = 2250$ psia, $T_{in} = 550^\circ\text{F}$, $R_2 - R_1 = 1.8$	100
2-24	Crack Flows. $P_{in} = 2250$ psia, $h = 1.8$ in., $T_{sat} = 652^\circ\text{F}$	103
2-25	Geometry of Part-Circumferential Interior Surface Crack Used for Calculation of Critical Crack Area.....	108
3-1	Simplified PRAISE Flowchart.....	116
3-2	Sample Space for PRAISE Code.....	118
3-3	Schematic Representation of Typical Stratification Employed in PRAISE Calculations.....	122
3-4	Algorithm for Crack Growth Calculations.....	135
3-5	Algorithm for "Evaluation" Earthquakes.....	140

List of Figures (cont'd)

<u>Figure</u>	<u>Page</u>
A-2	Weight Function for an Internal Circumferential Surface Crack in a Section of Straight Pipe (from Labbens 76)..... 239
A-3	A Comparison of K for Internal Surface Circumferential Cracks in Pipes Subjected to Uniform Axial Stress. Results are from Labbens 76 and are for straight pipe runs unless otherwise noted..... 240
A-4	Stress Intensity Factor for Edge Crack in a Flat Plate and for Long Longitudinal and Complete Circumferential Crack in a Pipe with $R_1/h = 10$. Pipe Results are from Labbens 76..... 241
A-5	Function $i_j(\phi)$ for $\frac{a}{h} = 0.25$ (from Heliot 79)..... 243
A-6	Functions $i_j(\phi)$ for $\frac{a}{h} = 0.50$ (from Heliot 79)..... 244
A-7	Functions $i_j(\phi)$ for $\frac{a}{h} = 0.80$ (from Heliot 79)..... 245
A-8	$K_{max}/\sigma a^2$ as a Function of γ for $\beta = 1$ and 5 and $\alpha = 0.6$. Results are from Kobayashi 77 and are for uniform or pressure stress..... 247
A-9	Normalized Angular Variation of K Along Crack Front for Selected Cases of Uniform or Pressure Stress..... 248
B-1	Boundary Integral Equation Nodalization for Complete Circumferential Crack..... 255
B-2	Various Comparisons of K From BIE Calculations With Corresponding Results Obtainable From Labbens 76..... 256
B-3	Stress Intensity Factor as a Function of Position on Crack Front for Pressure Loading on a Small Area of Crack Surface... 258
B-4	Nodalization for BIE Analysis of a Longitudinal Semi-Elliptical Crack in a Pipe..... 259
B-5	Comparison of Normalized Variation of K Along Crack Front of Semi-Elliptical Interior Surface Longitudinal Crack in a Pipe..... 262
B-6	Comparison of Normalized Variation of K Along Crack Front of Semi-Elliptical Interior Surface Longitudinal Crack in a Pipe..... 263

List of Figures (cont'd)

<u>Figure</u>	<u>Page</u>
B-7	Comparison of Normalized Variation of K Along Crack Front of Semi-Elliptical Interior Surface Longitudinal Crack in a Pipe..... 264
B-8	Various Comparisons of Normalized Variation of K Along Crack Front for Semi-Elliptical Longitudinal Surface Cracks in Pipe, Plates and Half Spaces..... 266
B-9	Various Comparisons of $K(\phi=0)$ for Longitudinal Semi-Elliptical Cracks in Pipes..... 268
B-10	Geometry of Part-Circumferential Cracked Pipe of Interest Showing Nodalization Scheme Employed in BIE Calculations.... 270
B-11	Normalized Variation of K Along the Crack Front for Various Longitudinal and Circumferential Semi-Elliptical Cracks in Pipes as Obtained by BIE Calculations..... 274
B-12	Normalized Variation of K Along the Crack Front for Various Longitudinal and Circumferential Semi-Elliptical Cracks in Pipes as Obtained by BIE Calculations..... 275
C-1	Schematic Representation of a Crack Growing Only in the "a" Degree-of-Freedom..... 281
C-2	Comparison of Curve-Fit and BIE Data Points for the Function G_1 295
D-1	Coordinate System for Integration Scheme for Integrating Over a Semi-Elliptical Area..... 303
D-2	\bar{K}_a for Uniform Stress Obtained by IF Method Compared With Direct Results From BIE (Section 2.7)..... 310
D-3	\bar{K}_b for Uniform Stress Obtained by IF Method Compared With Direct Results From BIE 311
D-4	Comparison of IF Solutions for Non-Uniform Stresses With Existing Solutions..... 313
D-5	Comparison of IF Solutions for Non-Uniform Stresses With Existing Solutions..... 314
D-6	Plant Loading and Unloading at a Rate of 5% per Minute..... 318
D-7	Ten Percent Step Load Decrease From 100 Percent Power..... 319

List of Figures (cont'd)

<u>Figure</u>	<u>Page</u>
D-8 Ten Percent Step Load Increase From 90 Percent Power.....	320
D-9 Large Step Decrease in Load With Steam Dump.....	321
D-10 Loss of Load From Full Power.....	322
D-11 Loss of Power.....	323
D-12 Loss of Flow in One Loop.....	324
D-13 Loss of Flow in Other Loops.....	325
D-14 Steam Line Break From no Load.....	326
D-15 Reactor Trip From Full Power.....	327
D-16 Radial Gradient Thermal Stresses at Various Times From the Start of the Transient for a 2.5 in. Thick Weld in the Hot Leg.....	329
D-17 $\delta\bar{K}_I$ as a Function of Time for Three Crack Geometries for a 2.5 Inch Thick Weld in the Hot Leg.....	330
D-18 Maximum $\delta\bar{K}_I$ During Reactor Trip as a Function of Crack Geometry for a 2.5 Inch Thick Weld in the Hot Leg.....	332
D-19 Maximum $\delta\bar{K}_I$ During Reactor Trip as a Function of Crack Geometry for 2.5 Inch Thick Weld in the Hot Leg.....	333
D-20 Maximum and Minimum $\delta\bar{K}_I$ During the Transient Loss of Load From Full Power for a 2.5 Inch Thick Weld in the Hot Leg.....	335
D-21 Maximum and Minimum $\delta\bar{K}_I$ During the Transient Loss of Load From Full Power for a 2.5 Inch Thick Weld in the Hot Leg.....	336

LIST OF TABLES

<u>Table</u>		<u>Page</u>
1-1	Materials of Piping and Related Components Along With Selected Mechanical Properties.....	6
1-2	Summary of Various Non-Seismic Stresses for Each of the Weld Locations. Dimensional Information is Also Included.....	9
1-3	Summary of Maximum Load Controlled Stress and Value of S-Factor for Each Weld Location and Seismic Event Magnitude Considered.....	10
2-1	Values of Complementary Cumulative Distribution of Crack Area, $P(> A)$, for Marshall Exponential Depth Distribution and Various Marginal Aspect Ratio Distributions.....	37
2-2	Summary of Value of Crack Frequencies From Cramond 74.....	45
2-3	The Probability of Non-Detection of a Defect of Depth 'a' as a Function of 'a' For Ultrasonic Inspection.....	52
2-4	The Probability of Non-Detection of a Defect of Depth 'a' as a Function of 'a' For Ultrasonic Inspection.....	53
2-5	Summary of Flow Rate Experiment Data (From Collier 80)	97
2-6	Comparison of Experimental Critical Values with Predicted Limits (From Agostinelli 58).....	99
2-7	Crack Flows Q' (gal/min-ft).....	102
3-1	Illustration of Procedure Used in Monte Carlo Simulation to Account for Influence of Pre-Service Inspection.....	131
4-1	List of Transients and Postulated Number of Occurrences in 40 Years.....	152
4-2	Tabulation of Values of $P[t_{LOCA} < t Eq(g,t)]$ for Weld Joints Considered-Results Conditional on a Crack Being Initially Present.....	158
4-3	Tabulation of Values of $P[t_{leak} < t Eq(g,t)]$ for Weld Joints Considered-Results Conditional on a Crack Being Initially Present.....	172
4-4	Estimates of Influence of In-Service Inspection for Various Times of First Inspection.....	201

List of Tables (cont'd)

<u>Table</u>	<u>Page</u>
B-1	Comparisons of $K(\phi=0)/\sigma a^{1/2}$ for Uniform Stress on a Longitudinal Interior Surface Semi-Elliptical Crack in a Pipe with $R_1/h=10$, $b/a=3$, Various $\alpha=a/h$261
B-2	Comparison of $K(\phi=0)/\sigma a^{1/2}$ for Uniform Stress on a Longitudinal Semi-Elliptical Crack in a Pipe for Various γ , α and β . All Results Generated by BIE, and are not Corrected to Account for Consistently Low BIE Results.....267
B-3	Comparison of $K(\phi=0)/\sigma a^{1/2}$ for Uniform Stress on Semi-Elliptical Cracks in Pipes with Various γ Showing Direct Comparison of Longitudinal and Circumferential Cracks.....272
C-1	Strain Energies for Surface and Buried Cracks.....291
C-2	g_1 for Various Sizes of Surface Cracks.....292
C-3	g_1 for Various Crack Geometries-Results From Curve-Fit.....294
D-1	\bar{K}_a for Buried Elliptical Defect in an Infinite Body Under Uniform Stress-Comparison of Results Obtained by the Integration Scheme with the Existing Solutions.....306
D-2	\bar{K}_b for Buried Elliptical Defect in an Infinite Body Under Uniform Stress-Comparison of Results Obtained by the Integration Scheme with the Existing Solutions.....307
D-3	\bar{K}_a and \bar{K}_b for Buried Circular Defect Under Non-Uniform Stress, in an Infinite Body--Comparison of Analytical Results with that Obtained by the Integration Scheme.....308
D-4	Description of the Transients, Including Maximum ΔT in Hot Leg.....317
D-5	Normalized RMS Stress Intensity Factors $(\frac{\delta K_1}{\alpha \sqrt{E \Delta T} \sqrt{a}})$ for Transients in the Hot Leg of ZION 1.....338

ACKNOWLEDGEMENTS

We would like to take this opportunity to acknowledge the many persons who contributed to the efforts resulting in this report. The initial efforts of Dr. Pedro Albrecht, now at the University of Maryland, in initiating this project are greatly appreciated, and the continuing support of John O'Brien and Milt Vagins was essential to this work. The contributions of C.K. Chou and his colleagues at Lawrence Livermore National Laboratory are also gratefully acknowledged. The cooperation of T. Cruse of Pratt and Whitney Aircraft, East Hartford, Connecticut, and P. Besuner of Failure Analysis Associates, Palo Alto, California in providing the boundary integral equation code was invaluable in generation of the numerical stress intensity factor results. Additionally, the assistance provided by P. Besuner in the early stages of running the code, and in formulation of the influence functions provided essential inputs to these key phases of the project. Numerous co-workers at Science Applications, Inc., provided essential assistance in this work. The analysis provided by Dr. Verne Denny, as reported in Section 2.8.1, was especially helpful. The key discussions with Stanley Basin at various stages of this work are also gratefully acknowledged. The assistance provided in running and developing the PRAISE code provided by Douglas Smith of SAI and the University of California at Berkeley, and the BIE nodalization and calculations performed by Richard Northrup of SAI and the University of Cincinnati are especially noteworthy. It is also a pleasure to acknowledge the helpful discussions held with various consultants, including D. Iglehart of Stanford University, P. C. Paris of Washington University, and A.S. Kobayashi of the University of Washington. Finally (in a departure from SAI tradition) we would like to acknowledge the skillful typing provided by John Ann Carlisle-Webb, formerly of SAI.

EXECUTIVE SUMMARY

The Code of Federal Regulations requires that structures, systems, and components that affect the safe operation of nuclear power plants be designed to withstand combinations of loads that can be expected to result from natural phenomena, normal operating conditions, and postulated accidents. One load combinations requirement — the combination of the most severe LOCA (loss-of-coolant accident) load and SSE (safe shutdown earthquake) loads — has been controversial because both events occur with very low probabilities. This issue became more controversial in recent years because postulated large LOCA and SSE loads were each increased by a factor of 2 or more to account for such phenomena as asymmetric blowdown and because better techniques for defining loading have been developed.

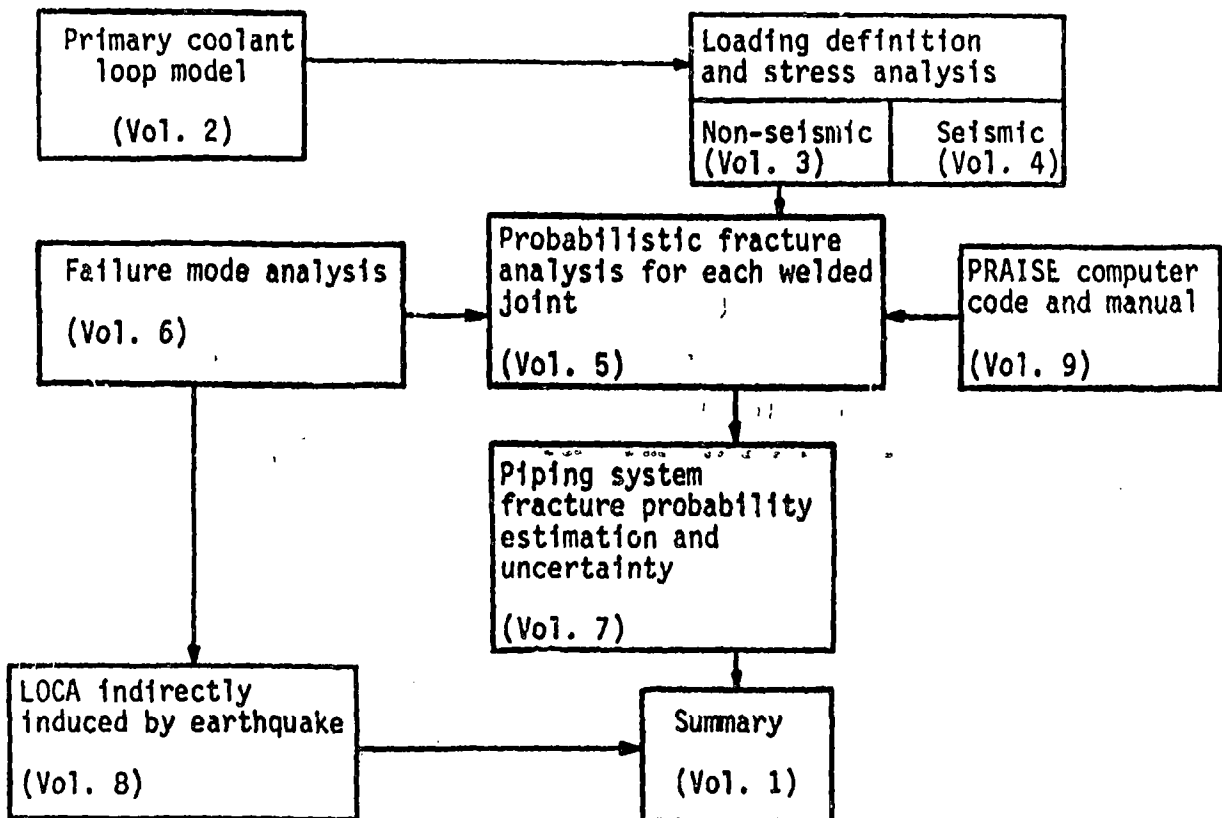
The original objective of Load Combinations Project I was to estimate the joint probability of simultaneous occurrence of both events and to develop a technical basis for the NRC (Nuclear Regulatory Commission) to use in determining whether it could relax its requirement on the combination of SSE and large LOCA for nuclear power plants. However, in the process of probability estimation we have not only estimated the probability of simultaneous occurrence of a large LOCA and an earthquake, but also estimated the probability of a large LOCA caused by normal and abnormal loading conditions without an earthquake. The estimates provide very useful information on the likelihood of asymmetric blowdown, which is a subset of large LOCA. Also, the probabilistic fracture mechanics model that we developed can be used to estimate the probability of pipe rupture with or without prior leak. That is, we can estimate the proportion of pipes that will leak detectably before rupture under normal operation, accident, or upset conditions. We can also evaluate the piping reliability in general. After a sufficient parametric study is done, we will be able to recommend a more rational basis for postulating pipe rupture locations.

If earthquakes and large LOCAs are independent events, the probability of their simultaneous occurrence is small. However, this probability is expected to be greater if an earthquake can induce pipe failure that leads to a LOCA. This LOCA could result directly (i.e., ground motion causes a pipe break in the primary cooling system) or indirectly (i.e., an earthquake causes a structural, mechanical, or electrical failure that in turn causes a pipe

break in the primary cooling system).

In the first-phase study reported in these nine volumes, we concentrated on determining the probability of a large LOCA in a PWR plant directly induced by an earthquake. The expert consensus is that such a directly induced LOCA is most likely to result from the growth of cracks formed in the pipes during fabrication. We selected a demonstration plant for study (Unit 1 of the Zion Nuclear Power Plant), modeled its primary cooling loop (Vol. 2), analyzed the best estimated responses of that piping system to non-seismic and seismic stresses (Vols. 3 and 4), developed a probabilistic fracture mechanics model of that piping system (Vols. 5, 6, and 7), analyzed failure mode (Vol. 6), and developed a computer code, PRAISE, to simulate the life history of a primary coolant system (Vol. 9). Finally, we examine the probability with which an earthquake can indirectly induce a LOCA (Vol. 8).

In Volume 5, we present a probabilistic fracture analysis for each welded joint. The relation between this volume and the rest of the report is shown in the following drawing:



1.0 INTRODUCTION

This is the final report of work through September 1980 performed by Science Applications, Inc. (SAI) under subcontract to Lawrence Livermore National Laboratory (LLNL) on the Load Combinations Program Project I: Event Decoupling. Current regulations covering the design of primary piping in commercial power reactors require consideration of various combinations of loads hypothesized to occur during the plant lifetime. The types of loads to be considered, and the means of combining them, are often ill-defined and not based on current best understandings of the phenomena involved. The LLNL Load Combinations Program was initiated to update techniques for a rational combination of loads in the design of reactor components. Seismic events that may occur during the life of the plant are of special concern, because the frequency and magnitude of such events are ill-defined. Specifically, combining seismic loads with those resulting from a loss-of-coolant accident (LOCA) can result in large loads on piping, pressure vessel, component supports and reactor vessel internals that are difficult to adequately design for. Additionally, designs resulting from requirements to combine the large loads from these rare events may be far from optimum for plant safety during normal operation. Significant seismic events and LOCAs are both rare events, and if it was known that the probability of both occurring simultaneously was very small, then requirements for combining the loads resulting from them could be relaxed.

If seismic events and LOCAs occurred independently of one another, then it is a simple matter to show that their simultaneous occurrence is a very low probability event. However, it is possible that the stresses resulting from a seismic event could induce a LOCA. Hence, these events do not necessarily occur independently, and means of estimating the probability of a seismic event leading directly and rapidly to a LOCA are of interest. If the probability of a seismic induced LOCA was very low, then perhaps requirements for combining the loads could be eliminated — with resulting simplification of plant design, reduction of costs, and (perhaps) a favorable influence on plant integrity during normal operation.

1.1 Basic Methodology

The primary purpose of the Load Combination Program covered in this report is to estimate the probability of a seismic induced LOCA in the primary piping of a commercial pressurized water reactor (PWR). Best estimates, rather than upper bound results are desired. This was accomplished by use of a fracture mechanics model that employs a random distribution of initial cracks in the piping welds. Estimates of the probability of cracks of various sizes initially existing in the welds are combined with fracture mechanics calculations of how these cracks would grow during service. This then leads to direct estimates of the probability of failure as a function of time and location within the piping system. The influence of varying the stress history to which the piping is subjected is easily determined. Seismic events enter into the analysis through the stresses they impose on the pipes. Hence, the influence of various seismic events on the piping failure probability can be determined, thereby providing the desired information.

The purpose of work presented here is to construct and exercise the fracture mechanics piping reliability model. The stress analysis of the piping was supplied to SAI (Chan 81, Lu 81), and the results obtained here were combined with the probability of seismic events of various magnitudes (George 81) to provide inputs to a possible load decoupling criterion. Figure 1-1 shows the various components of an overall program to assess the need to couple LOCA and seismic events, with identification of the portion of the work to be covered in this report. Details of the methodologies employed and results obtained are included in later sections of the report.

1.2 Plant Description

A specific plant was selected for analysis so that the results obtained would be applicable to a real situation. Zion I was chosen for analysis. This is a 1100 MWe plant of Westinghouse design. It is located on the shore of Lake Michigan some 40 miles north of Chicago. The plant is owned and operated by Commonwealth Edison.

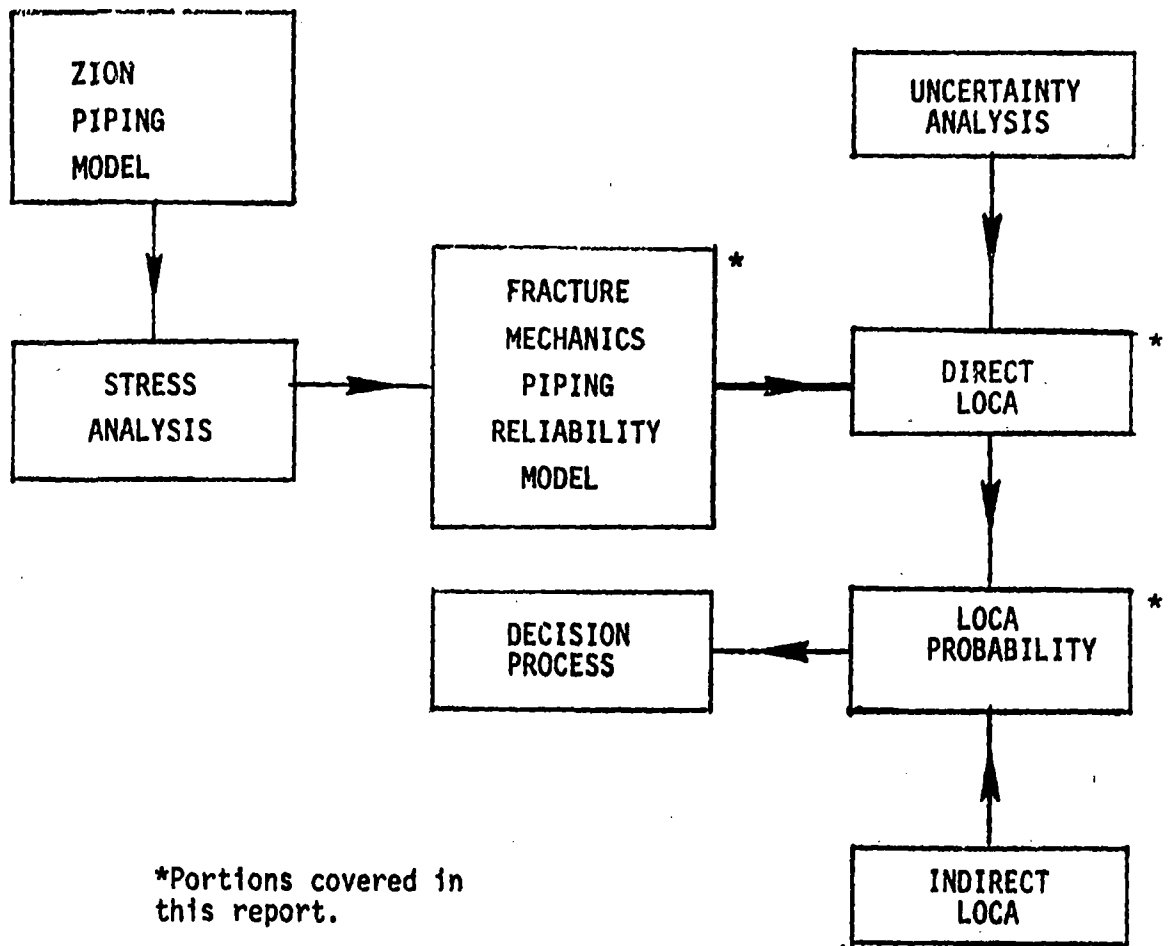


Figure 1-1. Schematic Representation of Various Portions of Project to Determine Necessity of Coupling LOCA s and Seismic Events.

The large primary piping was selected for consideration because a LOCA in these pipes is of particular concern. Figure 1-2 presents a schematic of the pipes considered, which consisted of the hot leg, cross-over leg, and cold leg. The nominal sizes of these pipes are as follows (FSAR):

<u>Name</u>	<u>Inside Diameter, in.</u>	<u>Wall Thickness, in.</u>
hot leg	29.0	2.50
cross-over leg	31.0	2.66
cold leg	27.5	2.38

Sudden and complete pipe severances are of particular concern in this work. Such piping failures will be called LOCAs*. Leaks and LOCAs are most likely to occur at welds, and attention here will be restricted to welds. Additionally, LOCAs are much more likely to occur at a circumferential than at a longitudinal weld. The reasons for this are two-fold: geometrically, a longitudinal weld would result only in a slot fracture rather than directly in a complete severance, and axial piping stresses tend to be higher than hoop stresses. Attention will therefore be focused on circumferential girth butt welds--the locations of which are shown in Figure 1-2. As far as the primary piping is concerned, all four loops have the same weld configuration. Stress analyses performed as another part of the Load Combinations Program (Chan 81, Lu 81) revealed that all four loops have virtually identical stresses. Attention was therefore concentrated on a single loop, with the results being representative of all four loops. The weld numbering system used in this report is included in Figure 1-2, which shows the locations of the 14 circumferential girth butt pipe welds considered in this analysis.

The materials used in fabrication of the pipes and related components (FSAR) are shown in Table 1-1, along with their selected properties (ASTM 80). These materials are basically austenitic stainless steel, predominantly of the centrifugally cast variety. The piping itself is seamless. Hence, the only longitudinal welds are in the elbows.

* In this report, a LOCA is taken to be a sudden and complete pipe severance, rather than the more conventional definition of any event that can produce a loss-of-coolant. A double ended pipe break (DEPB) would perhaps be a better term.

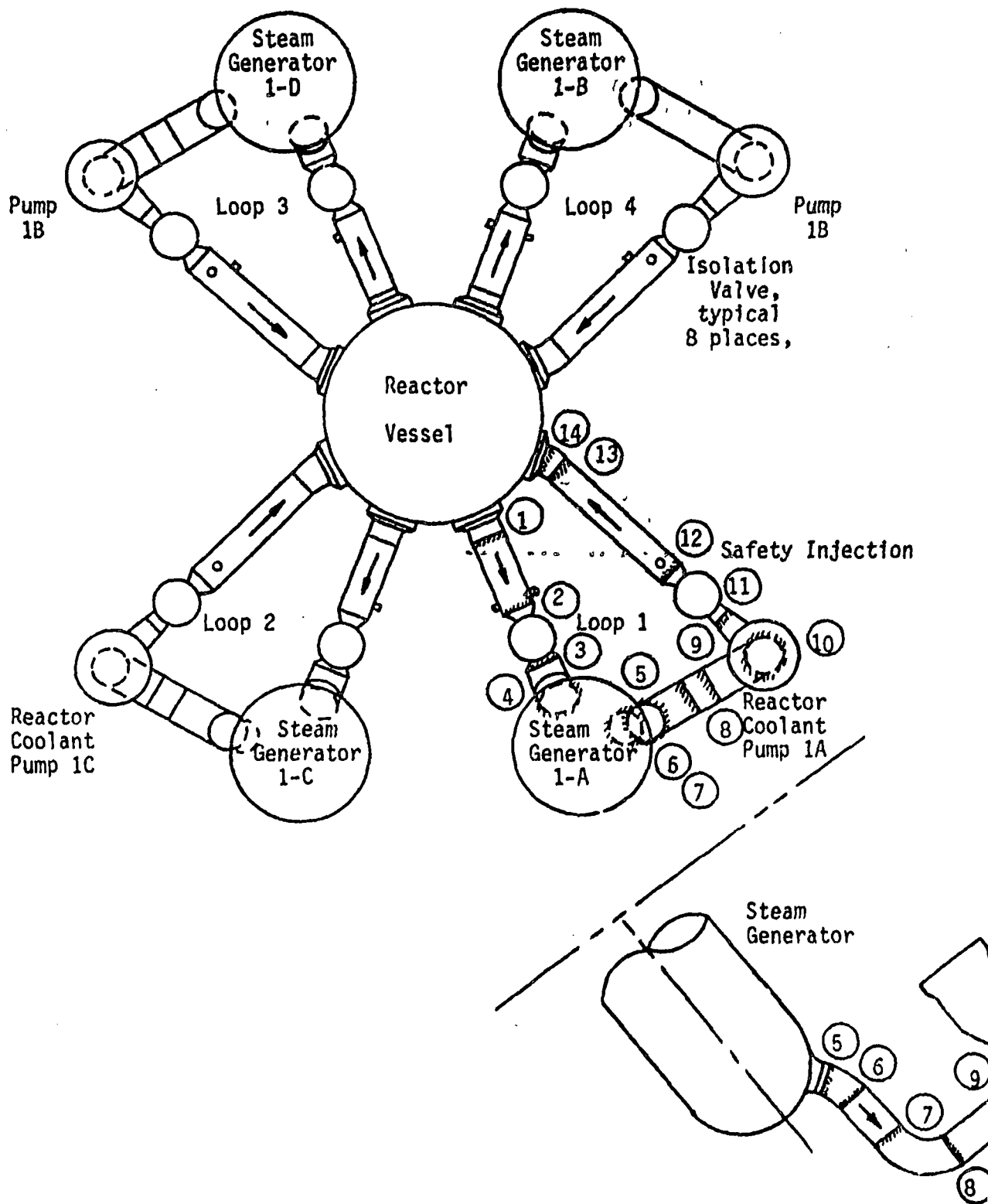


Figure 1-2. Diagram of Primary Piping Analyzed Showing Locations of Welds Considered.

Table 1-1

Materials of Piping and Related Components Along With Selected Mechanical Properties

Component	Material	Min. Tensile strength, ksi	Min. Yield strength, ksi	Min. Percent Elongation
pipes	A-376 type 316	75	30	35
pipe fittings	A-351 Gr CF8M	70	30	30
pipe nozzles	A-182 Gr F316	75	30	30
pump casing	A-351 Gr CF8	70	30	35
valves (pressure retaining parts)	A-351 Gr CF8M	70	30	30

1.3 Review of Relevant Stresses

Details of the stress analysis and procedures are presented elsewhere (Chan 81, Lu 81), as was discussed in Section 1.1. The purpose of this section is to briefly present the major results of the stress analysis that are applicable to the fracture mechanics analysis. Only axial piping stresses are considered, since they are generally the largest and are oriented in the manner to most influence crack growth in the circumferential girth butt welds considered in this analysis. In most cases, torsional components of stress are negligible. In cases where they are not, they are combined with the axial stress to provide the maximum principal stress, which is then used in the crack growth calculations as if it was oriented along the axis of the pipe.

Stresses resulting from bending loads will vary around the pipe circumference and through the wall thickness. Such variations will be ignored, and the maximum bending stress at the inner pipe wall will be taken to be uniformly distributed throughout the pipe cross section. Stresses resulting from axial and transverse forces will be neglected, because they are small compared to the stresses resulting from bending moments. Non-seismic, seismic and radial gradient thermal stresses will be covered individually in the following sections.

1.3.1 Non-Seismic Stresses

Non-seismic stresses are induced by pressure, dead weight and restraint of thermal expansion. The axial component of the pressure stress is taken as $pR_i/2h$, with p equal to the design pressure of 2235 psig. At no pressure and room temperature, the piping stress is taken to be equal to dead weight stress — which is directly obtainable from the calculated piping moments. Welding residual stresses could also be present at no load, but are not considered in the current analysis. If known, they could be easily included, but this is left for future efforts. The steady state stress at the normal operating temperature of 550°F (σ_{NO}) was obtained by vector addition of dead weight (DW) and restraint of thermal expansion (TE) moments calculating the resulting maximum inside wall stress, and then adding the

component of the pressure stress. At joints where thickness transitions occurred (such as straight pipe run to elbow welds), the stresses in the thinner section were employed. Results for the various stress components for each of the 14 welds considered are summarized in Table 1-2, which also includes information on wall thickness and pipe diameters.

1.3.2 Seismic Stresses

Stresses at various locations were calculated for various magnitude seismic events (Lu 81). Calculations revealed that the stresses were virtually the same in each of the four loops, and were very close to the same for an event of a given magnitude--the magnitude being expressed as the peak acceleration. Time dependent calculations of seismically induced bending moments were performed. These moments were vectorially added to the deadweight and restraint of thermal expansion moments in order to calculate the maximum cyclic stresses in the joint as a function of time. The axial component of the pressure stress was then added on to the results of such calculations. These cyclic stresses were combined in an appropriate manner to provide a measure of the influence of seismic events on crack growth. This measure is denoted as S , and will be discussed in Section 2.6.2. Values of S were evaluated at 48 locations around the pipe circumference and the maximum value used in subsequent calculations. The seismic bending moments were also vectorially added to the dead weight bending moments. The maximum bending stress was then calculated, to which was added the axial component of the pressure stress. This was considered to be the load controlled stress during a seismic event. The maximum value for each weld location and for each seismic event was evaluated, with results being summarized in Table 1-3. A safe shutdown earthquake (SSE) at Zion I is equal to 0.17g. These values are useful in the analysis of the influence of seismic events on subcritical and fast crack growth in reactor piping.

1.3.3 Radial Gradient Thermal Stresses

Temperature fluctuations of the reactor coolant give rise to stresses in addition to those resulting from restraint of thermal expansion. Such stresses are called radial gradient thermal stresses. They are self-equilibrating through the wall thickness, and can be determined from the temperature

Table 1-2

Summary of Various Non-Seismic Stresses for Each of the Weld Locations. Dimensional Information is Also Included.

Joint No.	h, in.	R ₁ in.	σ_{DW} ksi	σ_p ksi	σ_{NO} ksi	Node No. of Finite Element Model
1	2.50	14.5	2.08	6.49	15.07	1
2	2.50	14.5	.04	6.49	7.47	5
3	3.28	15.0	.51	5.11	7.28	7
4	3.28	15.0	.59	5.11	8.56	9
5	3.312	15.5	.34	5.23	7.27	26
6	2.66	15.5	.41	6.52	7.43	27
7	2.66	15.5	.30	6.52	8.63	28
8	2.66	15.5	.18	6.52	7.07	31
9	2.66	15.5	.10	6.52	7.74	35
10	3.312	15.5	.29	5.23	8.02	37
11	4.00	14.5	.21	4.06	4.28	48
12	2.38	13.74	.15	6.46	6.90	51
13	2.38	13.74	.62	6.46	7.19	58
14	3.03	13.75	.44	5.07	5.66	59

Thickness and ID at thinner part of thickness transition joint.

Table 1-3

Summary of Maximum Load Controlled Stress and Value of S-Factor for Each Weld Location and Seismic Event Magnitude Considered.

Joint No.	OBE		SSE		SSSE		BSSE	
	Max. σ_{LC} , ksi	S, (ksi) ⁴	Max. σ_{LC} , ksi	S, (ksi) ⁴	Max. σ_{LC} , ksi	S, (ksi) ⁴	Max. σ_{LC} , ksi	S, (ksi) ⁴
1	8.76	521.6	9.06	2958.3	10.56	63430.	10.62	162000.
2	6.75	31.18	6.85	105.8	7.17	627.8	7.09	1195.4
3	5.75	318.0	6.09	1418.5	7.12	10570.	6.81	19986.
4	6.14	619.5	6.52	2805.8	7.67	17100.	7.70	27400.
5	5.70	189.2	5.92	1270.3	7.82	19100.	7.29	33500.
6	7.04	53.54	7.25	338.4	8.58	4960.	8.25	8260.
7	6.91	25.31	7.05	153.0	7.30	2570.	7.62	5230.
8	6.81	9.40	6.90	48.80	7.30	825.	7.41	1405.
9	6.83	276.6	7.01	1399.2	8.86	13500.	8.71	26100.
10	5.04	259.9	6.11	1308.1	7.42	14500.	7.49	32900.
11	5.05	200.7	5.46	1487.2	8.04	22100.	7.39	42800.
12	7.11	917.7	8.08	6863.5	11.93	105900.	11.08	200100.
13	7.36	235.2	7.97	1828.3	11.56	27690.	10.08	56680.
14	5.81	114.1	6.16	644.0	7.97	11450.	7.12	26100.

history of the coolant and the thermal and elastic properties of the piping material). The radial gradient thermal stresses were evaluated considering the temperatures to be uniform along a long straight run of piping. These stresses are both time and space dependent, and are different for each of the plant operating transients. They are discussed in detail by Chan 81, and in Appendix D.

This concludes the introductory remarks, and attention will now be turned to presentation of the fracture mechanics model of piping reliability. Section 2 will provide details of the model, and Section 3 will discuss the numerical procedures devised to obtain results. Then in Section 4 attention will again be turned to actual application of the procedures to evaluation of the reliability of the primary piping at Zion.

history of the coolant and the thermal and elastic properties of the piping material. The radial gradient thermal stresses were evaluated considering the temperatures to be uniform along a long straight run of piping. These stresses are both time and space dependent, and are different for each of the plant operating transients. They are discussed in detail by Chan 81, and in Appendix D.

This concludes the introductory remarks, and attention will now be turned to presentation of the fracture mechanics model of piping reliability. Section 2 will provide details of the model, and Section 3 will discuss the numerical procedures devised to obtain results. Then in Section 4 attention will again be turned to actual application of the procedures to evaluation of the reliability of the primary piping at Zion.

Only failure due to the growth of cracks introduced during fabrication are

fracture mechanics procedures, which requires knowledge of the stress history at the location of interest. The critical sizes of cracks for leaks and complete pipe severance (LOCA) can be obtained from appropriate failure criteria. The probability of a leak or LOCA within a given time is equal to the probability of a crack growing to the corresponding critical size within that time. Other factors, such as the influence of leak detection systems and proof tests, can be included in the analysis.

Figure 2-1 provides a schematic representation of the various components and their interrelationships in the model of piping reliability. Piping failures are assumed to result from the growth of crack-like defects introduced during fabrication. The development of a leak or a complete pipe severance is considered to be a failure. Cracks are generally concentrated in welds, and attention will therefore be focussed on these locations. Each weld location can be considered discretely, and the procedures shown schematically in Figure 2-1 can be applied individually to each weld location considered. Initial populations of crack-like defects at a given weld will be considered to be randomly distributed in size. These initial cracks will be found with a certain probability during pre-service and in-service inspection. The probability of detection depends on the crack size. Those cracks that escape detection and repair can then grow due to subcritical crack growth. Fatigue crack growth will be considered in this investigation, but other growth mechanisms whose "growth law" is known could be treated. The fatigue crack growth is analyzed by fracture mechanics procedures, which requires knowledge of the stress history at the location of interest. The critical sizes of cracks for leaks and complete pipe severance (LOCA) can be obtained from appropriate failure criteria. The probability of a leak or LOCA within a given time is equal to the probability of a crack growing to the corresponding critical size within that time. Other factors, such as the influence of leak detection systems and proof tests, can be included in the analysis.

2.1 Overview and Review of Past Work

Details of the fracture mechanics model of piping reliability will be presented in this section. An overview of the model will first be included, followed by a review of past related work and detailed discussions of the various components of the model.

2.0 FRACTURE MECHANICS MODEL

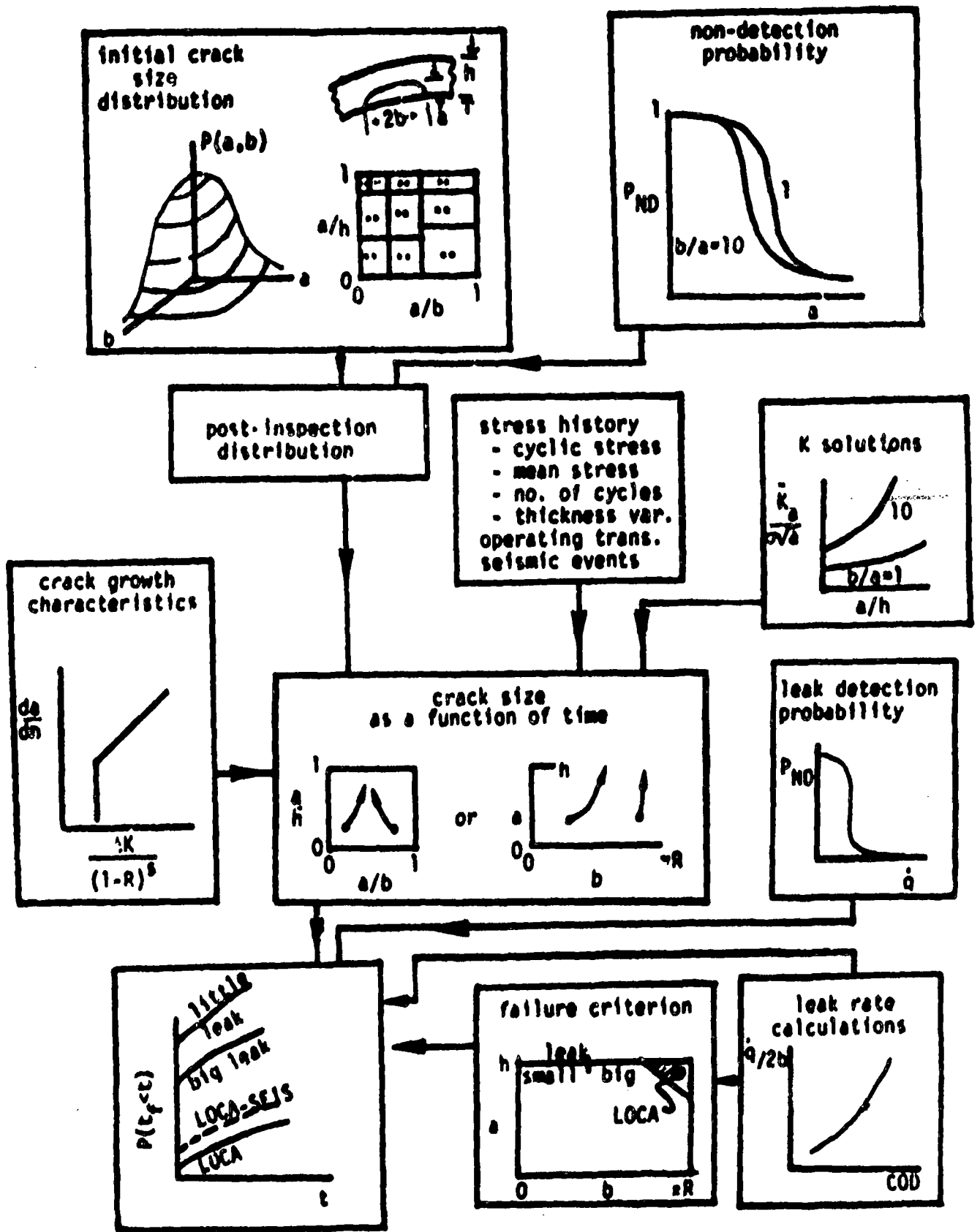


Figure 2-1. Schematic Diagram of Steps in Analysis of Reliability of a Given Weld Location.

considered. Design and assembly errors are therefore omitted from consideration, except as they would influence the existence of crack-like defects. The influence of errors during operation of the plant that could contribute to piping failures are also not considered. Further assumptions employed in this analysis will be presented and discussed in Section 2.2.

Attention will now be turned to a brief discussion of past work in applying fracture mechanics to the calculation of structural reliability. No attempt is made to provide an all-inclusive review.. The earliest work in this area appears to have been related to aircraft applications (Shin-ozuka 69, Heer 71, Yang 74) although general early discussions were provided by Graham 74 and Cramond 74. Becher and Pederson (Becher 74) provide one of the earliest examples of the use of such techniques in the nuclear power industry, by applying the methodology to estimation of the reliability of the reactor pressure vessel. Generally speaking, most recent applications also consider nuclear reactor pressure vessels (Arnett 76, Marshall 76, Nilsson 77, Schmidt 77, Collier 77, Dufresne 78, Lidgard 78, Vesely 78, Lucia 79), with analyses of piping reliability receiving somewhat less attention (Wilson 74, Harris 76, 77a, 77b, 78a, 79, 81, Burns 78, Derby 77, Schmidt 79). General discussions of the methodologies employed, without emphasis on reactor applications are also available (Besuner 77a, Harris 77c, 78b, Johnston 78a, 78b, Gallagher 79) and are of interest when applying such techniques to other structural components.

The vast majority of past applications of probabilistic fracture mechanics employ two features that greatly simplify the analysis:

- (i) Stress variations through the thickness of the part are either ignored or taken to be linear. This is consistent with the spirit of the ASME Boiler and Pressure Vessel Code, Section XI (ASME 1980). The only known exceptions to this are Harris 79, 81 in which cases nonlinear stress gradients through the pipe wall are accounted for.
- (ii) Crack shapes are taken to be simplified by considering either line cracks, complete circumferential cracks, or cracks with a constant length-to-depth ratio. The

latter case is again consistent with the ASME Code (ASME 1980), and, when used in conjunction with the uniform or linear stress variations, leads to particularly straightforward crack growth analyses.

However, actual cracks can have a wide variety of surface length-to-depth ratios, and these ratios can change during crack growth. The manner in which they change depends on the nature of the stresses--especially on thickness gradients. Therefore, it is desirable to account for changes in the length-to-depth ratio during crack growth. This is especially true if it is desired to differentiate between pipe leaks and LOCAs, which is the case in the current investigation. In order to be able to separately distinguish these two failure modes, a two-dimensional distribution of crack sizes is required, and a bivariate distribution will be used in this investigation. This more closely models reality, but requires stress intensity factor solutions beyond those available--especially when thickness variations of the stress are considered. Therefore, an appreciable portion of this work was devoted to the development of suitable stress intensity factor formulations. These will be presented in detail in subsequent sections of this report, with the Appendices containing the bulk of the information in this area.

Considerable work has been published on fracture mechanics analysis of crack behavior in pressure vessels and piping, without regard to any statistical considerations. The results of such work have provided assurances that large initial cracks are generally required before leaks or catastrophic failure would occur. An extensive review of such deterministic analyses will not be included here. The work of Mayfield, et al. (Mayfield 80) provides such a comprehensive review. Of special interest, Witt 78 and Griesbach 80 provide deterministic analyses of the influence of seismic events on crack growth in reactor piping.

Each of the components of the piping reliability model depicted in Figure 2-1 will be discussed in detail in the following sections of this report. Prior to this, the major assumptions employed herein will be summarized in the following section.

2.2 Summary and Discussion of Major Assumptions

The major assumptions employed in the current investigation will be summarized and discussed in this section. Some of the assumptions are specific to the current work, and are not inherent in a probabilistic fracture mechanics formulation of piping reliability. Some of the major assumptions have already been presented in introductory sections, but they will be included here for the sake of completeness.

The following are the major assumptions:

- Piping failures occur due to the growth of crack-like defects introduced during fabrication. Therefore, design, fabrication and assembly errors are omitted from consideration except as they may (implicitly) affect the sizes of initial defects.
- The as-fabricated crack-like defects are confined to weld joints. Hence, failures due to defects in base material are not considered. This assumption is further refined to consider only defects in circumferential girth butt welds, because such welds are more likely to result in failures (especially LOCAs) due to geometric considerations. A further assumption is made that all defects are located on the interior surface of the pipe and are oriented perpendicular to the axis of the pipe. (Part-circumferential interior surface cracks.) The axial component of the stress is taken to be applied normal to the crack in cases where torsional stresses are small. When torsional stresses are not small, the maximum principal stress is determined, and the stress is then taken to be applied normal to the crack. This is a conservative way to treat torsional stresses within the framework of current fracture mechanics techniques.

- The as-fabricated initial defects in the weld joints are independently and identically distributed in size. In other words, the initial crack size distribution is taken to be the same in each weld joint, with minor modifications to account for varying pipe size and wall thickness.
- Cracks that are initially shorter than twice their depth are omitted from consideration.
- The subcritical growth of a crack-like defect is as a fatigue crack, and the growth rate can be predicted from laboratory linear-elastic fracture mechanics tests [$da/dn = F(\Delta K, R, \text{environment, etc.})$].
- The cyclic stress history controls fatigue crack growth, and is estimated from plant operating history regarding frequency and types of transients. Transient stresses of an unanticipated nature are therefore omitted from consideration.
- The influence of seismic events enters through their contribution to the cyclic stress history, and influence on maximum stresses.
- If more than one crack exists within a given weld, then the cracks don't interact with one another, and the critical conditions for unstable crack propagation are dependent only on the size of the largest crack present.
- The unstable final growth of a crack is determined either by a net section instability (exceedance of a critical net section stress) or tearing instability ($T_{\text{appl}} > T_{\text{mat}}$)-- whichever results in the smallest critical crack size at a given stress.

- The applied stress used in the failure criterion is stress that can not be relaxed by crack extension-- otherwise known as the "load controlled" stress. Such stresses consist of pressure, and deadweight. Additionally, seismic stresses will be taken to be load controlled.
- Axial pipe stresses induced by bending moments are taken to be uniformly distributed over the pipe cross-section at a value equal to the maximum bending stress at the inside pipe wall.
- The maximum principal stress, including the contributions of torsion and transverse shear, is assumed to act normal to the plane of the crack. Since torsional contributions are small, especially in the highly stressed joints, the values of the maximum principal stress and axial stress are usually quite close.
- Cracks are initially elliptical in shape, and remain elliptical as they grow, unless they develop into through-wall cracks.
- The growth of an elliptical (or semi-elliptical) surface) crack in the directions of its axes is controlled by an averaged (RMS) stress intensity factor associated with each axis.
- The growth rates for each axis of a crack at a given cyclic stress intensity factor can be determined from corresponding results on a planar specimen.
- Once a crack grows through the pipe wall, its outside surface length is equal to its inside surface length.
- Temporal variation of coolant temperature and pressure during a plant transient is given by values used in the original plant design. (The magnitude of the variations is taken from plant data where possible.)

- Leaks greater than 1 gallon per minute are always immediately found and repaired, except those that develop during seismic events which are not detected until after the seismic event.
- Cracks are found by nondestructive evaluation (NDE) with a probability which depends only on the current crack size (not a function of having been missed in earlier inspections).
- Cracks found by NDE are repaired, and removed from the crack population. Otherwise the crack population is not affected by repairs.
- Defects are not introduced during the repair process.

Numerous secondary assumptions are made in later portions of this report, which will be discussed at the point where they arise. Each of the components of the fracture mechanics model of piping reliability will now be presented in detail.

2.3 Initial Crack Distribution

The size distribution of initial cracks present in a piping weld forms a key input to the fracture mechanics model of piping reliability. The initial crack distribution will be composed of two components:

- (i) The size distribution given that a crack is present. This component is called the conditional crack size distribution.
- (ii) The probability that a crack is present to begin with. This component is called the crack existence probability, and will vary with the size of the weld.

As-fabricated cracks in piping welds can be either sub-surface or surface. For a given crack size and stress level, a surface crack will be more severe, because it will have a larger stress intensity factor. Interior surface cracks are generally of more concern than exterior surface cracks, because thermal stresses tend to be higher at the inner pipe wall, and interior surface cracks are subjected to the coolant which is often an adverse environment for cracks. Hence, attention is focussed on interior surface cracks, and cracks located totally within the pipe wall are omitted from consideration in the present analysis.

There is no inherent reason that embedded cracks could not be included in this model, but this refinement is left for future efforts. The consideration of only interior surface cracks will not significantly alter the calculated failure probabilities, especially if the probability of a crack existing within a weld is applied to interior surface defects. Nilsson 77 provides a discussion of straightforward techniques for treating embedded cracks.

Attention will be concentrated on circumferential welds, because such welds are generally subjected to higher stress, and their failure can lead to more severe consequences. This was discussed in earlier sections. The

axial stresses are the largest components, and cracks oriented normal to the pipe axis therefore have the most severe orientation. Consequently, attention will be focussed on part-circumferential cracks. In accordance with the previous paragraph, this is further restricted to interior surface cracks. Therefore, the crack geometry considered in this investigation is a part-circumferential interior surface crack--the geometry of which is shown in Figure 2-2. This geometry is much more realistic, and more general, than those used in earlier similar investigations, such as line cracks, complete circumferential cracks, circular cracks, or semi-elliptical cracks of a specified length-to-depth ratio.

The use of semi-elliptical cracks of arbitrary length-to-depth ratio allows a more general treatment of initial crack sizes and shapes, and also allows pipe failure modes, such as leaks versus complete pipe severances, to be distinguished. However, the use of this more general crack geometry significantly complicates the fracture mechanics analysis, as well as the statistical description of initial crack sizes. The crack geometry considered requires two length parameters for its specification--the crack depth, a , and surface length, $2b$. Hence, a bivariate crack size distribution is required. Mathematically, this can be represented by a probability density function, $p(a,b)$, where $p(a,b) da db$ is the probability of a crack falling within the size range $(a, a+da)$, $(b, b+db)$ -- given that a crack is present. The semi-elliptical surface cracks considered here will have depths between 0 and the wall thickness, h , and half-surface lengths (b) between 0 and half the pipe circumference. This upper limit on b will be neglected, which will not be seriously in error if the probability of a complete circumferential crack is very small compared to the probability of a part-circumferential crack. Taking a in the range 0 to h , and b from 0 to ∞ , the following expression will apply to the conditional bivariate crack size distribution

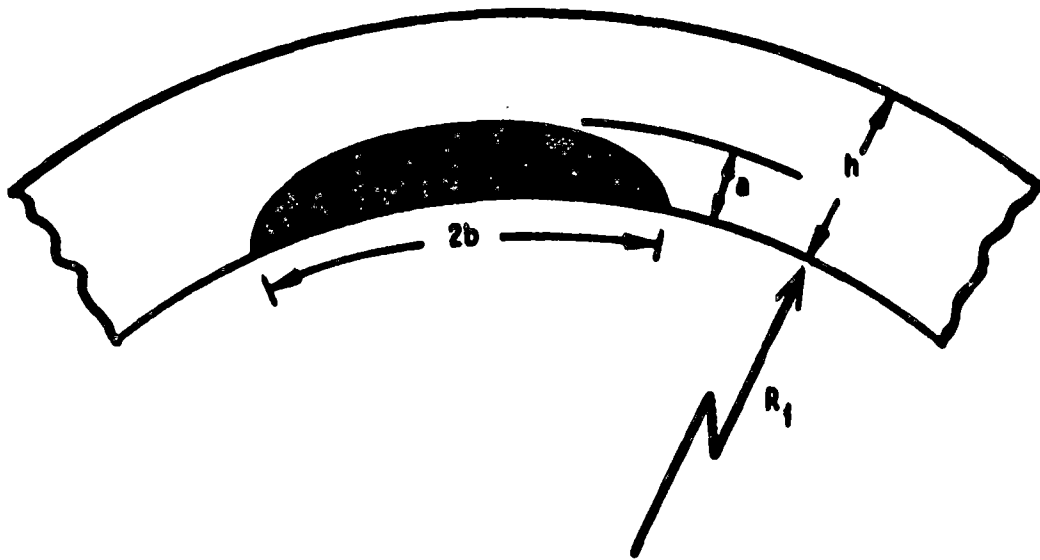


Figure 2-2. Geometry of Part-Circumferential Internal Surface Crack Considered in this Investigation.

$$\int_0^h \int_0^{\infty} p(a,b) db da = 1 \quad (2-1)$$

Information on bivariate crack size distributions is very sparse, with Wilson 74 providing the most information to adequately define the function $p(a,b)$. A fair amount of information is available on estimates of the depth distribution of cracks (which will be reviewed in Section 2.3.1), and it is desirable to use such information in estimating the size distribution of cracks considered in this analysis.

The density function of crack depths, $p(a)$, can be obtained from the bivariate distribution as follows:

$$p(a) = \int_0^{\infty} p(a,b) db \quad (2-2)$$

This univariate density function is called the marginal distribution of the crack depths and is directly comparable to information on depth distributions to be reviewed shortly. An expression analogous to Equation 2-3 can be written for the marginal distribution of b . Knowledge of the marginal distributions of the two length parameters is not sufficient to define the bivariate density function, because this latter function depends on the degree of correlation of the two variables (Hahn 67). Additionally, very little information is available on the length distribution of surface cracks, with Dvorak 72 providing a rare example of such information. Dvorak 72 suggests that the surface lengths should be lognormally distributed, but does not discuss any correlation with crack depth.

Some simplifying assumptions regarding the initial bivariate crack size distribution must be made in order to define this important variable. Assuming that the depth and surface length are independent does not seem reasonable, because a crack that is deep is more likely to be long than one that is shallow. An alternative assumption, that has some intuitive appeal, is that the crack depth and surface length-to-depth ratio are independent. Taking $s = b/a$, and calling this the "aspect ratio", this

assumption can be restated that the depth and aspect ratio are independent. This can be interpreted in words as follows: take a large population of cracks, and sort them out into separate "stacks" according to depth. Then measure the distribution of aspect ratio for each "stack". If a and b were independent, then the distribution of b would be the same for all "stacks"; i.e., b is independent of a . This assumption greatly simplifies the statistical description of initial crack sizes, and will be used throughout this investigation. This is a major assumption, and is in addition to those enumerated in Section 2.2. The information required to describe the initial conditional distribution of crack sizes is now reduced to specifying the distribution of crack depth, a , and aspect ratio, $b = b/a$. The statistical distribution of crack length, b , or crack area, A , can be calculated from this information. This will be described in succeeding sections.

2.3.1 Depth Distribution

The available information on crack size distributions is quite limited. Many investigators cited in Section 2.1 assume the crack depth (or length) to have a particular distribution, use assumed parameters, and then proceed with the analysis. An exponential distribution of crack depth is commonly assumed, which is a particularly simple distribution. (See Hahn 67 for a discussion of various standard distributions, such as exponential, normal, lognormal, Weibull, gamma, etc.). It is preferable to base the size distribution used on actual observations of cracks-preferably in steel weldments.

Information available on crack size distributions concentrates on the crack depth, because the depth dimension (a) has more influence on the stress intensity factor than the length dimension (b). Wilson 74 provides information on both depth and length, as was mentioned above. However, his estimates are based on judgement, rather than data. The Wilson distribution has been employed in previous analyses of reactor piping reliability (Harris 76, 77b, 78a, Burns 78), but adjustments were made so that only cracks exceeding a given surface length were included. Wilson's marginal distributions on a and b appear to be exponential. Marginal crack depth distributions employed using Wilson's data, with adjustments to include only cracks larger

than a certain value, were taken to be lognormal. The most complete set of crack depth information is that supplied by Becher and Hansen (Becher, no date), in which data on the depths of 228 surface cracks found during successive removal of layers of steel weldment is provided. They conclude that the depth distribution appeared lognormal, and the resulting distribution has been used in succeeding analyses (Nilsson 77, Harris 79). Nilsson took the cracks to be distributed according to a gamma distribution, which appears to fit the data equally well. In fact, the gamma distribution employed by Nilsson is nearly equal to an exponential distribution, and an exponential distribution also fits the Becher and Hansen data quite well. Other depth distributions, which were applied to reactor pressure-vessels, are suggested by Marshall 76, Vesely 78, and Lynn 77. These distributions are all approximately exponential, and fairly similar to one another. The Marshall data (Marshall 76, p. 126) is based on cracks found in US and UK nuclear vessels, along with other information on non-nuclear vessels. The data is used to estimate the crack depth distribution, which was found to be exponentially distributed with the following probability density function.

$$p_a(a) = \frac{1}{\mu} e^{-a/\mu} \quad (2-3)$$

$$\mu = 0.246 \text{ in.}$$

This value of μ is also the mean crack depth.

The complementary cumulative distribution corresponding to this density function is given by the following expression

$$P_a(>a) = \int_a^{\infty} p_a(x) dx = e^{-a/\mu} \quad (2-4)$$

The Marshall distribution, expressed as the complementary cumulative distribution, is shown in Figure 2-3. This figure also shows a lognormal fit to the Becher and Hansen data, the distribution from Wilson (initial surface lengths, b_0 , greater than 2 in.), and various estimates from Lynn 77. This figure shows that the Marshall distribution falls within the various estimates from Lynn 77, and is generally less than an order of magnitude different from the lognormal fit to Becher and Hansen. The Wilson $b_0 > 2$ distribution falls well below all the others, which is at least partially due to

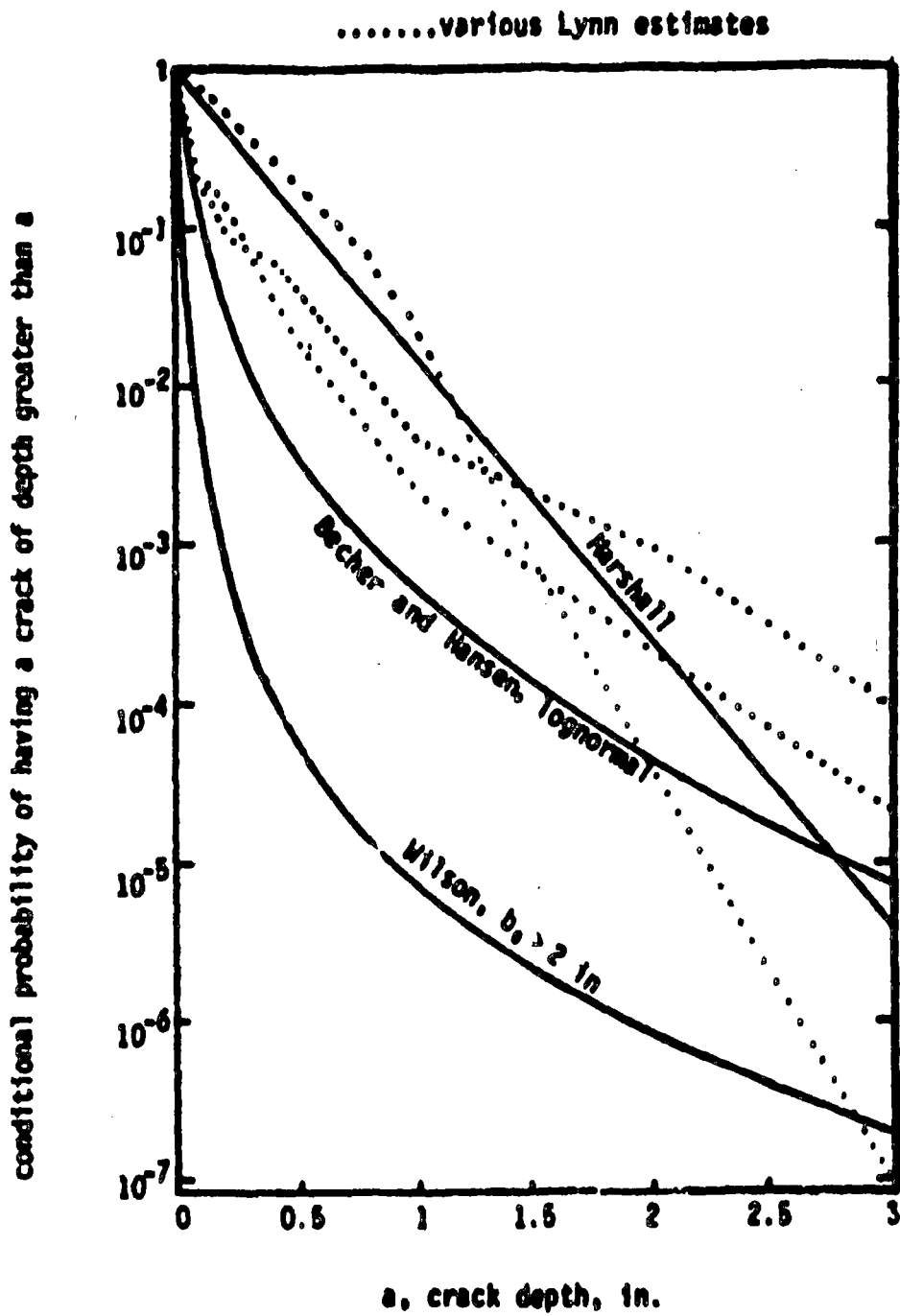


Figure 2-3. Various Complementary Cumulative Marginal Crack Depth Distributions.

its exclusion of cracks with initial surface lengths less than 4 in. ($2b_0 = 4$ in.). This modified Wilson distribution does not appear applicable to the current situation. The Marshall distribution will be used in succeeding portions of this investigation, because it appears to provide a realistic estimate of crack depths. It falls midway in the range of distributions shown in Figure 2-3, and does not differ drastically from the Becher and Hansen data.

Another aspect of the Becher and Hansen data is perhaps worth noting. As was mentioned above, the Becher and Hansen distribution can be adequately fit by an exponential distribution. The largest crack in the population found by Becher and Hansen was 0.45 in. (11.5 mm), and the data is actually better fit with an exponential distribution, with parameter, μ , of 0.067 in. A plot of this result would drop off the scale of Figure 2-3 at 1.08 in., which would put this distribution way below any of those shown in Figure 2-3 for crack depths exceeding about 0.5 in. In this context, a case could be made for the Marshall distribution being very conservative. Nevertheless, the Marshall distribution will be used in this investigation. The mean crack depth is 0.24 in., which is considerably greater than the corresponding values of 0.067 in. from Becher and Hansen (Becher, no date), or the value of 0.084 in. quoted on page 108 of Cramond 74.

Some modifications are required to the exponential distribution of equations 2-4 and 2-5 to eliminate the physical impossibility of having a crack depth exceeding the pipe wall thickness. This can be accomplished by renormalizing the density function. This leads to the following marginal density of crack depths

$$p_a(a) = \frac{e^{-a/\mu}}{\mu(1 - e^{-h/\mu})} \quad 0 \leq a \leq h \quad (2-5)$$

with $\mu = 0.246$ in.

As a sidelight, the complementary cumulative distribution of crack depth, mean value of a (\bar{a}) and median value of a (a_{50}) are easily obtained from the density function of equation 2-5 (Hahn 67). The results are easily

shown to be

$$P_a(>a) = \frac{e^{-a/\mu} - e^{-h/\mu}}{1 - e^{-h/\mu}} \quad (2-6)$$

$$\bar{a} = \mu \frac{1 - e^{-h/\mu} \left(1 + \frac{h}{\mu}\right)}{1 - e^{-h/\mu}} \sim \mu$$

$$a_{50} = \mu \left[\ln 2 - \ln(1 + e^{-h/\mu}) \right] \sim \mu \ln 2$$

For $h \gg \mu$, these all reduce to the standard definition for exponential distributions.

The marginal distribution of crack depth is now completely defined. The next step in the determination of the initial crack size distribution is to define the distribution of aspect ratios.

2.3.2 Aspect Ratio Distribution

The marginal distribution of the aspect ratio forms the remaining portion of the initial conditional crack size distribution to be defined. The aspect ratio is denoted as β , and is equal to b/a (see Figure 2-2). As mentioned earlier, cracks that initially have a surface length less than twice the depth will be omitted from consideration. Thus, the lower limit of aspect ratio corresponds to semi-circular cracks. Cracks with aspect ratio less than that corresponding to semi-circular are seldom observed, and would tend to grow toward a semi-circular shape. The omission of cracks with $\beta < 1$ is felt to have a negligible influence on the results.

Information on the distribution of aspect ratio is virtually non-existent. This distribution will therefore be assumed to be one of the standard forms, with slight modification to compensate for cracks with $\beta < 1$ being omitted. From earlier discussions, the upper limit on β will be taken to be infinity--even though this can result in cracks longer than the

pipe circumference being included. As will be seen, however, such cracks will be present with a very low probability. Truncation of the β distribution to eliminate cracks longer than the pipe circumference would greatly complicate the mathematical description of initial crack sizes without changing the end result.

Exponential and lognormal distributions of β will be considered. A "shifted" exponential density function of β that omits cracks with $\beta < 1$ is given by the following

$$p_{\beta}(\beta) = \begin{cases} 0 & \beta < 1 \\ C_{\beta} e^{-\beta/\lambda} & \beta > 1 \end{cases} \quad (2-7)$$

The values of C_{β} and λ can be determined if the percentage of cracks with $\beta > 5$ is specified. Denoting this percentage as ρ , the constants C_{β} and λ can be evaluated from the following general requirements

$$\int_1^{\infty} p_{\beta}(x) dx = 1$$

$$\int_5^{\infty} p_{\beta}(x) dx = \rho \quad (2-8)$$

The resulting values of λ and C_{β} are the following

$$\lambda = 4 / \{ \ln(1/\rho) \}$$

$$C_{\beta} = \frac{1}{\lambda} e^{1/\lambda} \quad (2-9)$$

The complementary cumulative distribution, mean, median and standard deviation of β corresponding to this shifted exponential distribution are easily shown to be

$$P_{\beta}(>\beta) = \begin{cases} 0 & \beta < 1 \\ e^{-(\beta - 1)/\lambda} & \beta > 1 \end{cases} \quad (2-10)$$

$$\beta_{50} = 1 + \lambda \ln 2$$

$$\bar{\beta} = 1 + \lambda$$

$$\beta_{sd} = \lambda$$

A suitable modified lognormal probability density function can be expressed by the following

$$p_{\beta}(R) = \begin{cases} 0 & \beta < 1 \\ \frac{C_{\beta}}{\lambda \beta (2\pi)^{1/2}} \exp\left[-\left(\ln \frac{R}{R_m}\right)^2 / (2\lambda^2)\right] & \beta > 1 \end{cases} \quad (2-11)$$

This density function will also be required to meet the conditions of Equations 2-8. This will provide two equations for the three unknowns C_{β} , λ and R_m . The necessary third equation can be obtained by requiring the mode of the lognormal distribution to be at $\beta = 1$. The mode of a lognormal density function is located at $R_m e^{-\lambda^2}$ (Hahn 67), which provides the third equation. The following three equations are the end result of the procedure

$$\begin{aligned} R_m e^{-\lambda^2} &= 1 \\ 2 &= C_{\beta} \operatorname{erfc}\left[\left(\ln \frac{1}{R_m}\right) / (\lambda 2^{1/2})\right] \\ 2\rho &= C_{\beta} \operatorname{erfc}\left[\left(\ln \frac{\rho}{R_m}\right) / (\lambda 2^{1/2})\right] \end{aligned} \quad (2-12)$$

The function $\operatorname{erfc}(x)$ is the complementary error function, which is discussed and tabulated by Abramowitz 64. These equations can be solved by trial and error once ρ is specified. The complementary cumulative distribution, median, mean and standard deviation of β are easily shown to be given by the following

$$\begin{aligned} P_{\beta}(\beta) &= \operatorname{erfc}\left(\frac{\ln \beta}{\lambda 2^{1/2}} - \frac{\lambda}{2^{1/2}}\right) / \left(2 - \operatorname{erfc} \frac{\lambda}{2^{1/2}}\right) \\ R_{50} &= R_m \exp\left[\lambda 2^{1/2} \operatorname{erfc}^{-1}\left(1 - \frac{1}{2} \operatorname{erfc} \frac{\lambda}{2^{1/2}}\right)\right] \\ \beta &= \frac{1}{2} R_m C_{\beta} e^{\lambda^2} \operatorname{erfc}\left[\frac{\ln(1/R_m)}{\lambda 2^{1/2}} - \frac{\lambda}{2^{1/2}}\right] \\ \sigma_{\beta}^2 + \beta^2 &= \frac{1}{2} R_m^2 C_{\beta}^2 e^{2\lambda^2} \operatorname{erfc}\left[\frac{\ln(1/R_m)}{\lambda 2^{1/2}} - 2^{1/2} \lambda\right] \end{aligned} \quad (2-13)$$

$\text{erfc}^{-1}(x)$ is taken to be the "inverse" complementary error function [i.e., $y = \text{erfc}^{-1}(x)$ means y is the value where $\text{erfc } y$ equals x]. Calculations of λ , \bar{a}_m , C_B , \bar{a}_{50} and \bar{B} are quite straightforward, and produce the following results for two values of ρ of particular interest

$\rho =$	10^{-2}	10^{-4}
λ	0.5382	0.3830
\bar{a}_m	1.336	1.158
C_B	1.419	1.5405
\bar{a}_{50}	1.638	1.379
\bar{B}	1.883	1.494
\bar{a}_{5d}	0.8570	0.4371
c.o.v.	0.46	0.29

Figure 2-4 is a plot of the complementary cumulative distribution of B for exponential and lognormal distributions for 1% and 0.01% of the cracks having a surface length greater than 10 times the depth ($\rho = 10^{-2}$ and 10^{-4}). This figure shows that the lognormal and exponential distributions are very similar for $B < 5$, but the lognormal distribution results in higher probabilities of long cracks as B exceeds 5. This is as expected, due to the large "tail" associated with lognormal distributions.

Very little information is available in the literature from which to estimate the appropriate distribution of aspect ratio. Cramond 74, page 108, estimates a mean value of B of 1.7, but this estimate can not be considered firm. A comparison of this with the above tabulated lognormal results suggests a value of $\rho [= P(B > 5)]$ of about 10^{-2} . Corresponding results for a "shifted" exponential distribution would predict $\rho = 3.3 \times 10^{-1}$ for $\bar{B} = 1.7$; a value some half order of magnitude below 10^{-2} .

Frost and Denton (Frost 67) provide results for 9 cracks that were initial defects in welded steel plates. Their resulting values of various parameters for B are as follows

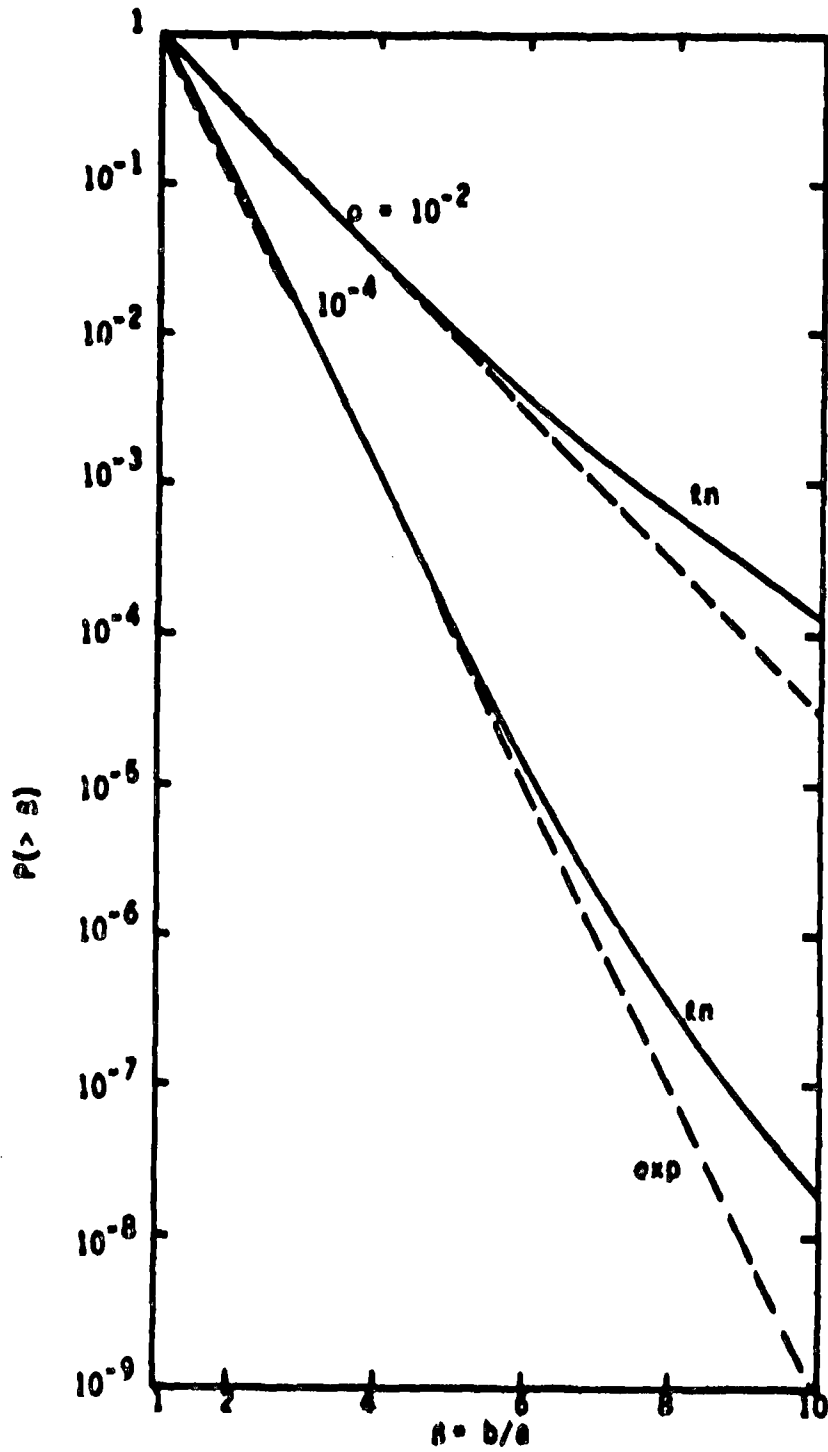


Figure 2-4. Various Complementary Cumulative Marginal Distributions of Crack Aspect Ratio.

$$\begin{aligned} \bar{B} &= 3.40 \\ \sigma_{B0} &= 2.67 \\ \sigma_{Bd} &= 2.44 \\ \text{c.o.v.} &= \sigma_{Bd} / \bar{B} = 0.72 \end{aligned}$$

The use of these values in a lognormal distribution would result in $\rho \gg 10^{-2}$. Using \bar{B} in the exponential distribution would predict $\rho = 0.19$, and a coefficient of variation of 0.71. The use of Frost and Denton's data would predict something like 20% of the initial cracks having $b/a > 5$. This seems like an excessive number of cracks with high aspect ratio. Additionally, these results are in marked contrast to Cramond 74 discussed above--in which a mean value of β of 1.7 was given.

Due to the lack of definitive information on the distribution of aspect ratio, the "shifted" lognormal distribution will be assumed to be applicable. This will result in a higher probability of having cracks with large β than if the "shifted" exponential distribution was employed. A value of ρ of 10^{-2} will be assumed to be applicable. This provides results in reasonable agreement with Cramond 74, but not with Frost and Denton (Frost 67). Additional discussions of the appropriateness of the lognormal distribution with $\rho = 10^{-2}$ will be provided in the following section, which provides information on the crack area and crack surface length distributions resulting from the above distribution of aspect ratio and crack depth.

2.3.3 Resulting Area and Length Distributions

The distribution of crack area and crack surface length can be calculated once the marginal distributions of a and β are defined, and the assumption that a and β are independent is made. This section will present the resulting distributions of crack area (A) and surface length ($2b$). Such results will provide additional information and insights into the appropriateness of the marginal a and β distributions, and will allow comparison with published results on crack area distributions (Feldman 68).

Considering the crack area first, take the cracks to be semi-elliptical in shape, and located in a flat plate. The distortion of the crack shape due to curvature of the pipe is therefore neglected. The crack area will then be equal to $A = \frac{\pi}{2} ab = \frac{\pi}{2} a^2 b$. As intermediate steps, let $c = a^2$ and $b' = \frac{\pi}{2} b$. Then $A = cb'$. The distribution of c is obtainable from the distribution of a , and is the following

$$p_c(x) = \begin{cases} \frac{p_a(x^h)}{2x^h} & 0 < c < h^2 \\ 0 & c > h^2 \end{cases} \quad (2-14)$$

The density functions are subscripted to denote what function it is. For instance, $p_a(x^h)$ for exponentially distributed a is equal to $\exp(-x^h/u) / [u(1-\exp(-h/u))]$ from equation 2-5. Similarly, an expression for the density function of b' is obtained

$$p_{b'}(y) = \frac{2}{h} p_b\left(\frac{2y}{h}\right) \quad \frac{h}{2} > y > 0 \quad (2-15)$$

The probability the crack area is greater than A can be stated in words as follows

(probability that crack area $> A$) = \sum (probability c lies between c and $c + dc$)

$$\times \left[\text{probability } b' > \begin{cases} A/c \\ h/2 \end{cases} - \text{biggest of these two} \right]$$

[The choice of A/c or $h/2$ must be made so as to exclude cracks with $b = b/a < 1$; one of the major assumptions enumerated in Section 2.2]. This can be restated mathematically as follows

$$\begin{aligned} (\text{probability that crack area } > A) &= P_A(>A) \\ &= \int_0^{2A/h} p_c(x) p_{b'}(>A/x) dx + \int_{2A/h}^{h^2} p_c(x) dx \end{aligned} \quad (2-16)$$

C_B , β_m and λ in this expression are defined implicitly in terms of ρ by Equations 2-12. Once again, the first expression is taken to be zero if it is negative, and the integral must be evaluated numerically. Results for exponential and lognormal marginal β distributions are presented in Table 2-1, which shows that the area distribution obtained using the two marginal distributions are very similar, with the lognormal results being only slightly higher. Results for the lognormal β are shown in Figure 2-5, from which it is seen that the value of ρ has an increasingly large influence as the crack area increases.

These results can be compared with data from Feldman 68 on crack area distributions. Results from Feldman are presented in Figure 2-6, along with corresponding results from the above analysis for $P(>A)$. Results for a "shifted" lognormal distribution of aspect ratio with 0.01% of the cracks having $b/a > 5$ ($\rho=10^{-4}$) are included. This figure shows that Feldman's data predicts a much lower probability of having cracks with large areas. This suggests that the value of ρ of 10^{-4} is too large (or that the marginal depth distribution is too high). However, even a value of $\rho = 10^{-4}$ seems low--especially in light of the fairly large mean aspect ratios reported by Frost 67, which was discussed at the end of Section 2.3.2.

In summary, it appears that the "shifted" lognormal distribution of β with $\rho = 10^{-4}$ provides reasonable estimates; providing high results in some cases (as compared to Feldman 68) and low results in others (as compared to Frost 67).

Additional insights can be gained by considering the statistical distribution of the surface length of cracks. This can be derived from the marginal distributions of a and β , along with the assumption of independence of these two parameters. The probability that b exceeds a value B is given by the following expression.

$$(\text{probability that } b > B) = \sum_{\beta} (\text{probability } \beta \text{ lies between } \beta \text{ and } \beta+d\beta) \\ \times (\text{probability } a > B/\beta)$$

Table 2-1

Values of Complementary Cumulative Distribution of Crack Area, $P(> A)$, for Marshall Exponential Depth Distribution and Various Marginal Aspect Ratio Distributions

A, in^2	exponential β		lognormal β	
	$\rho = 10^{-2}$	10^{-4}	10^{-2}	$\rho = 10^{-4}$
0.01	7.78×10^{-1}	7.57×10^{-1}	7.79×10^{-1}	7.62×10^{-1}
0.03	6.48×10^{-1}	6.19×10^{-1}	6.50×10^{-1}	6.25×10^{-1}
0.10	4.56×10^{-1}	4.17×10^{-1}	4.58×10^{-1}	4.25×10^{-1}
0.30	2.56×10^{-1}	2.22×10^{-1}	2.62×10^{-1}	2.29×10^{-1}
1	8.98×10^{-2}	6.59×10^{-2}	9.07×10^{-2}	6.96×10^{-2}
3	1.77×10^{-2}	9.79×10^{-3}	1.79×10^{-2}	1.07×10^{-2}
10	9.94×10^{-4}	2.69×10^{-4}	9.93×10^{-4}	3.08×10^{-4}
30	1.96×10^{-5}	2.06×10^{-6}	2.02×10^{-5}	2.27×10^{-6}
100	3.05×10^{-8}	5.74×10^{-10}	4.39×10^{-8}	5.88×10^{-10}

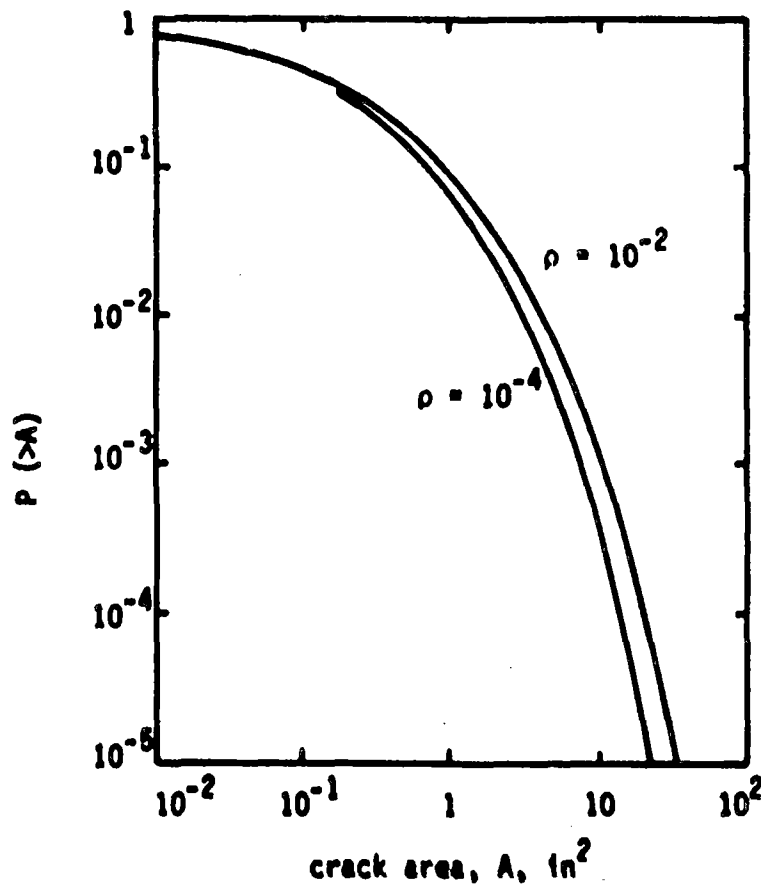


Figure 2-5. Complementary Cumulative Distribution of Crack Area. Exponential Depth Distribution and Shifted Lognormal Aspect Ratio Distribution for Various Values of ρ .

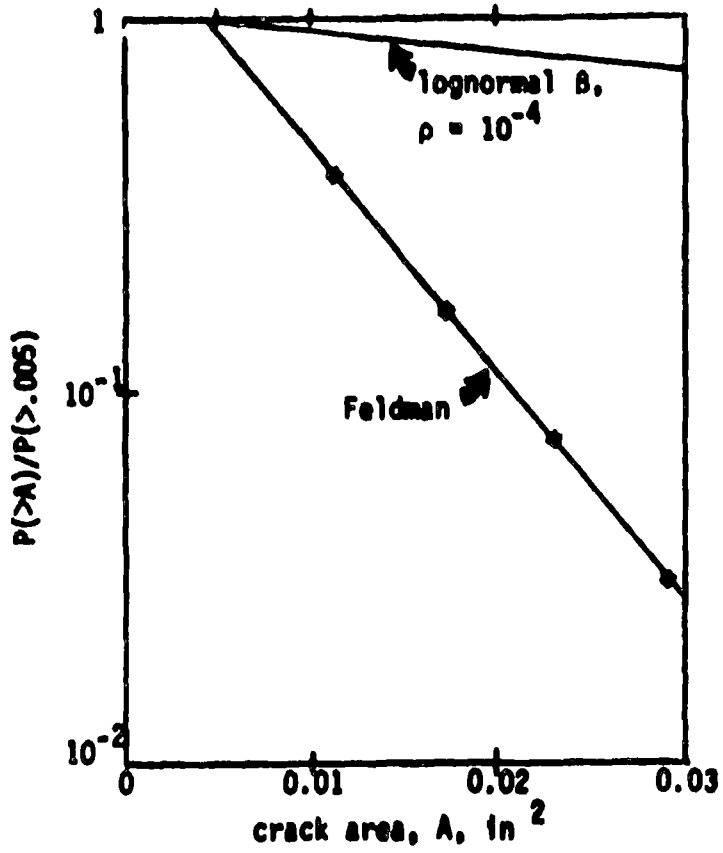


Figure 2-6. Comparison of Feldman Data on Crack Area Distributions with Results Using Marshall Exponential on Depth and "Shifted" log-normal on Aspect Ratio, with $\rho = 10^{-4}$.

This can be stated mathematically as follows:

$$P_b(b > B) = \int_{1 \text{ or } \frac{B}{h}}^{\infty} P_a(a > \frac{B}{\beta}) p_\beta(\beta) d\beta \quad (2-19)$$

Care must be taken in the limit of integration, because $\beta < 1$ and $a > h$ are excluded from consideration. For this reason, the lower limit is taken to be the bigger of the two numbers 1 or B/h . Only the case of an exponential distribution of crack depths and "shifted" lognormal distribution of aspect ratio will be considered. Using the appropriate density and complementary cumulative distributions from Sections 2.3.1 and 2.3.2 provides the following result.

$$P_b(b > B) = \int_{1 \text{ or } B/h}^{\infty} \frac{C_\beta}{\lambda x (2\pi)^{1/2}} e^{-(\ln x/\beta_m)^2 / (2\lambda^2)} \times \frac{e^{-B/x\mu} - e^{-h/\mu}}{1 - e^{-h/\mu}} dx \quad (2-20)$$

For convenience, define β_2 as the largest of 1 or B/h . Then making use of the definition of the complementary error function $\text{erfc } x$ (Abramowitz 64), and making appropriate changes of variable eventually leads to the following result

$$P_b(b > B) = \frac{C_\beta}{1 - e^{-h/\mu}} \left\{ \frac{1}{\lambda^{1/2}} \int_{(\ln \beta_2 / \beta_m) / 2^{1/2} \lambda}^{\infty} \exp \left[- \left(x^2 + \frac{h}{\mu \beta_m} e^{-\lambda x 2^{1/2}} \right) \right] dx \right. \\ \left. - \frac{1}{2} e^{-h/\mu} \text{erfc} \frac{1}{\lambda^{1/2}} \ln \frac{\beta_2}{\beta_m} \right\} \quad (2-21)$$

Once again, the integral must be evaluated numerically. In this case some care must be exercised, because the upper limit of integration is infinite. Problems in this regard can be eliminated by noting that the term

$$x^2 + \frac{B}{\mu B} e^{-\lambda x^2} \sim x^2$$

for x large. Numerical integration can be used to evaluate the integral from the lower limit out to where the above approximation is sufficiently accurate, and a closed form expression obtained for the value of the integral from there to infinity. Complementary error functions will result from such an operation.

Results of such calculations for $\rho = 10^{-2}$ are presented in Figure 2-7, with values of b being included out to a length corresponding to complete circumferential cracks in the hot leg ($h = 2.5$ in, $R_1 = 14.5$ in). Some rather startling results are shown in Figure 2-7, in that some very small probabilities are present. The marginal distributions of a and B (Figures 2-3 and 2-4) had numbers like 10^{-4} and above for representative complementary cumulative distributions ($\rho = 10^{-2}$), whereas numbers like 10^{-10} appear on Figure 2-7. This is undoubtedly because the very long cracks required for nearly complete circumferential cracks are way out in the tail of the aspect ratio distribution.

The Marshall exponential on a and "shifted" lognormal distributions of B with $\rho = 10^{-2}$ will be used as the base case for further work in this project. A case could be made that this is a conservative initial crack size distribution, because the resulting crack area distribution is far above the corresponding experimental results of Feldman 68, and the Marshall marginal distribution of crack depth is well above the Becher and Hansen (Becher, no date) experimental results. This crack size distribution appears to be a reasonable estimate based on current information, but could be significantly altered as more information becomes available in this area.

To summarize, the base case crack size distribution is given by the following marginal density functions of a and B , combined with the assumption that a and B are statistically independent

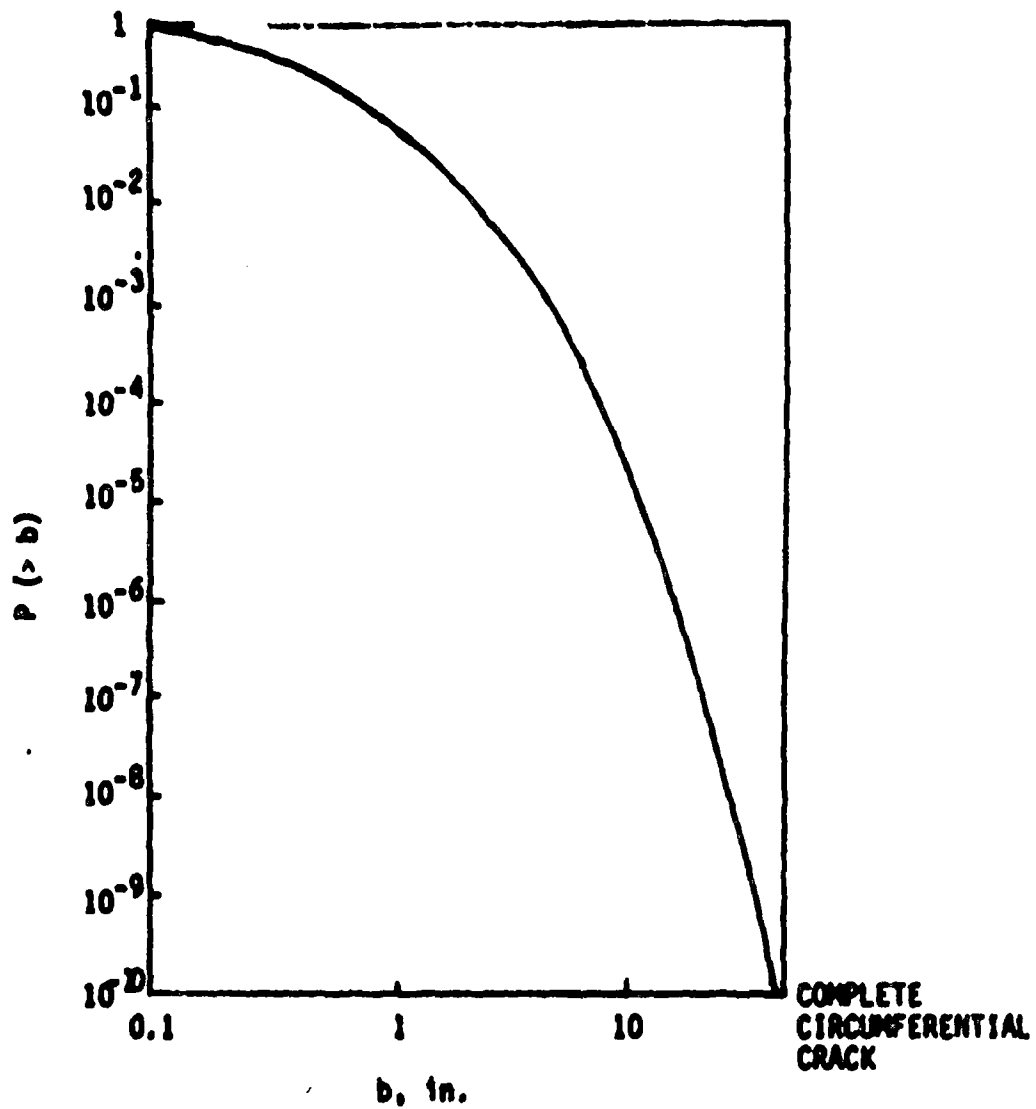


Figure 2-7. Complementary Cumulative Distribution of Half Surface Crack Length for Marginal Exponential Depth Distribution and Marginal Lognormal Aspect Ratio Distribution.

$$p_a(a) = \frac{e^{-a/\mu}}{\mu(1 - e^{-h/\mu})} \quad 0 \leq a \leq h$$

$$\mu = 0.246 \text{ in.} \quad (2-22)$$

$$p_B(B) = \frac{C_B}{\lambda B(2\pi)^{1/2}} e^{-(\ln \frac{B}{B_m})^2 / (2\lambda^2)} \quad B \geq 1$$

$$C_B = 1.419$$

$$B_m = 1.336$$

$$\lambda = 0.5382$$

$$p = P(> 5) = 10^{-2}$$

This defines the size distribution of cracks given that a crack is present. Hence, the conditional crack size distribution is now defined. The remaining piece of information required to completely define the initial crack distribution is the probability of a crack being initially present. This portion of the initial crack distribution will be discussed in the next section of this report.

2.3.4 Crack Existence Probabilities

The remaining portion of the initial crack distribution to be defined is the probability of a crack initially existing in a weldment. As mentioned in earlier discussions, attention is focussed in this investigation on cracks located on the interior surface of the pipe. Even though surface cracks are considered, the probability of a crack being present will be taken to be controlled by the weld volume. Other parameters, such as length of weld or surface area of weld and heat affected zone could be considered, but will not be included in the present work. Which of these are taken will not have a large affect on the results, unless large variations in thickness are encountered. Such is not the case here.

The weld volume, V , will be taken to also include the heat affected zone which will be taken to be two wall thicknesses wide. The weld volume V is then equal to

$$V = \pi D_1 h (2h) = 2\pi D_1 h^2 \quad (2-23)$$

The rate of cracks per unit volume will be denoted as p_v^* , and the number of cracks in a body of volume V will be taken to be Poisson distributed. There are theoretical reasons for making such an assumption (see for instance page 59 of Mood 50). The following expression for the probability of having N cracks in a body of volume V is therefore applicable (Hahn 67).

$$P(N) = (Vp_v^*)^N \frac{e^{-Vp_v^*}}{N!} \quad (2-24)$$

The probability of having a crack in a body of volume V is one minus the probability of having no cracks, which is given by the following expression

$$\begin{aligned} &\text{probability of having a crack in } V \\ &= p^* = 1 - e^{-Vp_v^*} \sim Vp_v^* \end{aligned} \quad (2-25)$$

The probability of having exactly 1 crack is

$$P(1) = Vp_v^* e^{-Vp_v^*} \sim Vp_v^* \quad (2-26)$$

The above approximations hold if $Vp_v^* \ll 1$. This shows that the probability of having a crack is approximately equal to the probability of having exactly 1 crack, and that p^* varies linearly with p_v^* (for $Vp_v^* \ll 1$).

The remaining part of the problem is to estimate the parameter, p_v^* . Not a great deal of information is available in this regard. Cramond 74 surveys results from a number of sources, with his results for cracks summarized in Table 2-2. The frequency of cracks per unit of weld length varies in this table from 1.1×10^{-4} to 9.4×10^{-2} per inch. Such results could be cast in a unit volume basis by dividing by $2h^2$ (h = plate thickness). Hence, the thickness would be required to estimate p_v^* from the data of Table 2-2.

Table 2-2

Summary of Value of Crack Frequencies
From Cramond 74

Page 95, HSST flaws in base plate

$$D_V^a = 7.1 \times 10^{-6} / \text{in}^3$$

Table 4.10

$$4 \times 10^{-6} - 7.1 \times 10^{-6} / \text{in}^2$$

Table 4.12, flaws in butt welds, Japanese ship data

$$3.1 \times 10^{-4} / \text{in} \quad \text{automatic weld}$$

$$2.0 \times 10^{-4} / \text{in} \quad \text{manual weld}$$

Table 4.15 A, multilayer circumferential arc welds

$$9.4 \times 10^{-2} / \text{in} \quad \text{welds on bottom section}$$

$$7.8 \times 10^{-3} / \text{in} \quad \text{welds on section}$$

$$1.8 \times 10^{-2} / \text{in} \quad \text{field welds}$$

Table 4.15 B, electrosity welds (ultrasonic inspection)

$$1.0 \times 10^{-3} \text{ to } 6.6 \times 10^{-3} / \text{in} \quad \text{various components exclusive of bottom and cover rings}$$

$$6.6 \times 10^{-2} / \text{in} \quad \text{bottom \& cover rings}$$

Table 4.18, pressure vessel butt welds, cracks only

$$1.7 \times 10^{-4} - 2.9 \times 10^{-4} / \text{in} \quad \text{automatic weld}$$

$$1.1 \times 10^{-4} - 1.9 \times 10^{-4} / \text{in} \quad \text{manual welds}$$

The Marshall report (Marshall 76) also contains some relevant information. Page 85 of Marshall, states a frequency of one weld repair per 56 ft. of weld run in high quality welds. This translates to $1.5 \times 10^{-3}/\text{in}$. On page 126 of the Marshall report, it is stated that U.S. and U.K. sources indicate that 12 defects were found with depths between 0.5 and 1 inch in 44 vessels. This is then used to estimate the number of cracks in a vessel as a function of their size. In accordance with the Marshall initial crack size distribution, which is on a per vessel basis, the number of as-fabricated cracks in a vessel is given by (using the notation of Marshall, 76)

$$\text{no. of cracks} = \int_0^{\infty} A(x) dx = \int_0^{\infty} A_0 e^{-\lambda x} dx = \frac{A}{\lambda} = \frac{14.8}{4.06} = 3.65$$

($A = 14.8/\text{in}$, $\lambda = 4.06/\text{in}$ as given on page 125 of Marshall 76). This can be put on a unit volume basis by dividing by the weld volume in a vessel, which can be estimated from information in Marshall 76. Figure 2.3a of Marshall shows the welding layout employed in fabricating a pressure vessel for a typical pressurized water reactor (PWR). Estimating that one-tenth of the completed vessel is composed of weld and heat affected zone, and knowing that the weight of the vessel is 428 tons (Marshall 76, page 18), there are some $3 \times 10^6 \text{ in}^3$ of material in a typical vessel. Therefore, there are about $3 \times 10^6 \text{ in}^3$ of weld and heat affected zones, from which the following value of p_v^* is estimated

$$p_v^* = 3.64/V \sim 3.64/3 \times 10^6 \text{ in}^3 = 1.2 \times 10^{-6}/\text{in}^3$$

Another estimate of crack existence frequencies can be obtained by noting that there are some 420 ft. of welds in a typical PWR vessel (Figure 16 of Marshall 76). This would provide the following estimate of the number of cracks between 1/2 and 1 inch deep on a per inch of weld basis

$$\frac{12 \text{ defects between } 1/2 \text{ and } 1 \text{ inch}}{44 \text{ vessels} \times 420 \text{ ft/vessel}} = 5.4 \times 10^{-5}/\text{in}$$

This falls well below corresponding values in Table 2-2, which is undoubtedly due to the consideration of only cracks between 0.5 and 1.0 inches in depth in the above number.

Another set of useful results is presented by Nichols 75, which states that in 2336 m of welds in pressure main seams 153 planar effects (cracks or lack of penetration) were found that had to be repaired by present rules. He did not discuss how this data was collected, or what the present rules were. If the data was obtained by nondestructive examination (as it probably was), then the number of defects found is a function of the inspection procedure. Nichols result translates to

$$\frac{153 \text{ defects}}{2336 \text{ m of weld}} = 6.6 \times 10^{-2} / \text{m} = 1.7 \times 10^{-3} / \text{in.}$$

This value is also within the range of values summarized in Table 2-2. This result can be transformed to a unit volume basis by dividing by $2h^2$. This provides the following estimates

$$p_v^*(\text{in}^{-3}) \sim \begin{cases} 2.2 \times 10^{-4} & h=2 \text{ in.} \\ 5.5 \times 10^{-5} & h=4 \text{ in.} \\ 1.4 \times 10^{-5} & h=8 \text{ in.} \end{cases}$$

Since not all defects were found, these numbers could be quite low. Alternatively, since some of the defects were not actually cracks, these numbers could be somewhat high.

In summary, the results discussed above reveal a large range of values of p_v^* . The MSST density of flaws in base plates was $7 \times 10^{-5} / \text{in}^3$, Nichols values were in the range of $0.1 - 2 \times 10^{-4} / \text{in}^3$, and the corresponding estimate from Marshall 76, was $1.2 \times 10^{-5} / \text{in}^3$. Overall, it appears that a value of about $10^{-4} / \text{in}^3$ is a reasonable estimate in that it falls pretty much in the midrange of available values. This is the value that will be used in succeeding portions of this investigation. A good case could be made for this being a conservative value, because it is well above

the value resulting from the Marshall data. In the end, if p_v^* exceeds $10^{-4}/\text{in}^3$, this would not have much influence on the calculated failure probabilities, because the probability of having a crack in a typical weld joint already exceeds 0.1 for this value of p_v^* . Hence, increases in p_v^* could increase the calculated failure probabilities by at most, an order of magnitude. For the weld volume being considered ($V = 1139 \text{ in}^3$ for a joint in the hot leg), the calculated failure probabilities would vary roughly linearly with p_v^* as the value of this parameter decreased below $10^{-4}/\text{in}^3$.

Certain results obtained from the fracture mechanics analysis will be virtually independent of the value of p_v^* . This will be true of certain relative results, such as the percentage of LOCA s that are seismic induced, or the ratio of leaks to LOCA s.

As another sidelight, using $V = 1139 \text{ in}^3$ and p_v^* of $10^{-4}/\text{in}^3$, the probability of one cr * and a crack are given exactly as follows:

$$\text{probability of a crack} = 0.1077$$

$$\text{probability of 1 crack} = 0.1016$$

Hence, the distinction of one crack versus a crack is largely lost for the values of p_v^* and V employed in this investigation.

Harris 76, 77b employed a value of p_v^* of $10^{-6}/\text{in}^3$, which is well below the value suggested here. However, only cracks that were very long relative to their depth ($\beta > 5$), and with an initial surface length exceeding a certain value (typically 4 in) were considered in the population. Figure 2-7 shows about 1% of the cracks will have $2b_0 > 4 \text{ in}$. for the crack size distribution employed in the investigation. Therefore, the two order of magnitude difference between p_v^* employed here, and Harris's earlier value is felt to be consistent.

The initial crack size distribution is now completely defined. This as-fabricated distribution must be combined with the probability of detecting a defect as a function of its size in order to provide the post-

inspection distribution which, in turn, forms the initial conditions for the fracture mechanics analysis. The detection probability will be presented in the next section.

2.4 Inspection Detection Probabilities

Failures in nuclear plant piping are caused by unchecked propagation of defects until an intolerable crack size has been reached. A periodic inspection is often used in attempts to detect these flaws before they reach critical size (ASME 80). Ultrasonics is the most often used method of non-destructive inspection of nuclear plant pipes. The probability of detecting a flaw P_D with ultrasonics, or with any other non-destructive testing method, is a function of the size of the flaw. The probability of detecting a very small flaw is near zero, whereas the probability of detecting a very large one is nearly one. The probability of not detecting a flaw (P_{ND}) is equal to $(1 - P_D)$, and will be the parameter concentrated upon here.

2.4.1 Review of Past Results

Data on probability of non-detection for ultrasonic inspection have been extensively reviewed by Harris (Harris 76, 77b, 79) and relevant features of these reviews are summarized here. Harris 77b includes data for fatigue cracks in a 0.66 or 0.2 inch thick 2219-T8 aluminium plate (Rummel 74) and also data for ultrasonic inspection of 3 inch OD, 0.25 inch thick aluminium tubes (Tang 73). Based on these data, a lognormal relation of the type

$$P_{ND}(a) = \frac{1}{2} \operatorname{erfc}(\sqrt{\ln a/a^*}) \quad (2-27)$$

was found quite adequate to mathematically characterize P_{ND} . In the above equation, a^* is the crack depth that has a 50% chance of being detected and v is the parameter that controls the slope of the $P_{ND} - a$ curve when plotted on lognormal probability paper. For the probabilistic rupture analysis (Harris 77b) of ferritic piping, $a^* = 0.25$ in. and $v = 1.33$ were chosen. This model is graphically shown in Figure 2-8 along with the data of Rummel, Tang, and other investigators.

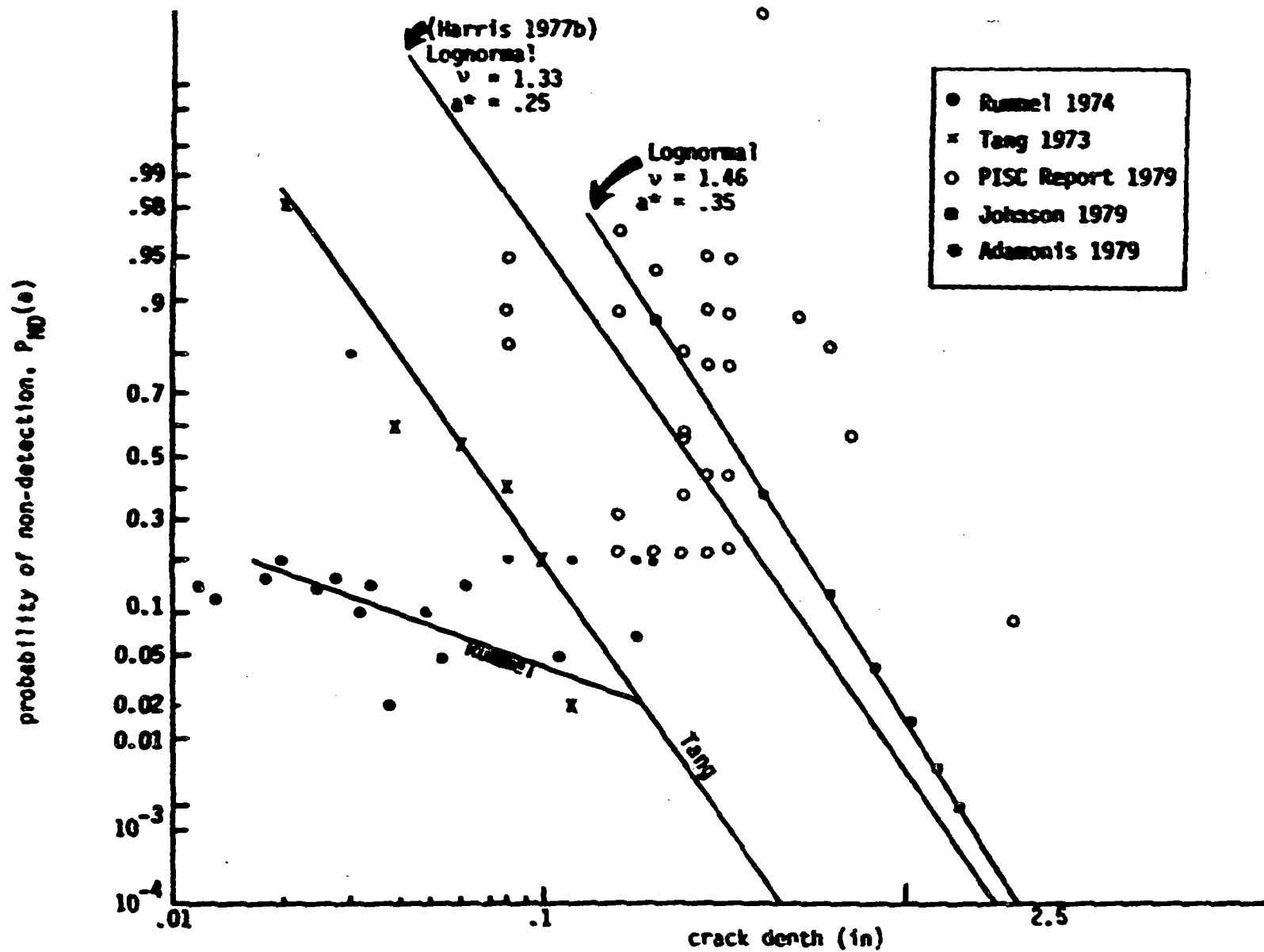


Figure 2-8. Probability of Non-Detection of a Crack as a Function of its Depth for an Ultrasonic Inspection--Data From Literature.

In addition to these, data on ultrasonic inspection of stress corrosion cracks in austenitic pipes (Kuppermann 78) were reviewed by Harris. (Harris 79) and again a lognormal relation between P_{ND} and defect depth was found appropriate. The value of $\nu = 3$ was found most reasonable and two values of a^* (0.1 and 0.2 inch) were considered for the probabilistic piping analysis.

Since the publication of the above mentioned reviews, additional information on probability of detection of flaws by ultrasonic inspection has become available. The results from a PVRC Industry Cooperative Program on heavy section steels for nuclear reactor pressure vessels were analysed (Johnson 79). These results consisted of detection probabilities for ultrasonic inspection of welds made on 8.25 inch thick A533B low alloy steel plates. Small internal imperfections were implanted in the weldment, and the specimen was subject to ultrasonic inspection by five different teams. Later, the specimen was metallurgically sectioned to reveal the locations and dimensions of these flaws. Assuming that the ultrasonic inspection was carried out according to ASME Section XI Code (ASME 80) Johnson et. al. obtained best estimates for $P_{ND}(a)$ (Table 2-3) using "inspection uncertainty analysis." Their data of Table 2-3 could be described by (Figure 2-8) Equation 2-27 with $\nu = 1.46$ and $a^* = 0.35$ in.

Table 2-4 shows non-detection probabilities of ultrasonic inspections made on 8 to 12 inch thick welded plates. These data were obtained from a preliminary report by the Plate Inspection Steering Committee (PISC 79). This study consisted of round robin ultrasonic inspection of the plates and the detection probability for each flaw was evaluated by the fraction of the inspectors detecting that particular flaw--the existence of flaw being verified by a later destructive examination. The data listed in Table 2-4 are for only those flaws that were later verified to be crack-like defects. These data are plotted in Figure 2-8 which shows a large scatter but generally centered around a lognormal model with $\nu = 1.46$ and $a^* = 0.35$, which was based on the analysis by Johnson et al.

Table 2-3

The Probability of Non-Detection of a Defect
of Depth 'a' as a Function of 'a' For
Ultrasonic Inspection

<u>flaw depth, a (in)</u>	<u>$P_{ND}^{(a)}$ (best estimate)</u>
.2	.88
.4	.39
.6	.13
.8	.044
1.0	.015
1.2	.0054
1.4	.002
1.6	< .001
1.8	< .001
2.0	< .001

Ref: Johnson, 1979.

Table 2-4
The Probability of Non-Detection of a Defect
of Depth 'a' as a Function of 'a' For
Ultrasonic Inspection

<u>a (in)</u>	<u>P_{ND} (a)</u>
.08	.83
.08	.87
.08	.95
.16	.22
.16	.32
.16	.89
.16	.92
.16	.95
.16	.97
.20	.23
.20	.87
.20	.94
.24	.23
.24	.38
.24	.56
.24	.55
.24	.80
.28	.68
.28	.85
.32	.23
.32	.44
.32	.77
.32	.88
.32	.95
.40	1.0
.50	.88
.60	.82
.70	.58
2.0	.09

Ref: PISC Report, 1979.

2.4.2 Model for Influence of Surface Length

The fracture mechanics analysis in the current study includes a two-dimensional model of crack growth of semi-elliptical cracks, that is, at any stage during its existence, a crack is defined by a and b (Figure 2-2). The probability of detection of a crack by ultrasonic inspection is dependent not only by its depth (a), but also its length ($2b$), and to a certain extent on the crack area. The P_D should also depend on the diameter (D_B) of the ultrasonic beam used for inspection. Assuming P_{ND} to be a function of crack area (A), the lognormal relation for P_{ND} (Equation 2-27) can be generalized in terms of A ,

$$P_{ND} = \frac{1}{2} \operatorname{erfc} \left(\sqrt{\ln \frac{A}{A^*}} \right) \quad (2-28)$$

As shown in Figure 2-9, there are three distinct cases for evaluation of A :

- (i) If both a and $2b$ are less than D_B , then the P_{ND} should depend only on the total crack area.
- (ii) If a is less than D_B and if $2b$ is greater than D_B , then the ' a ' dimension would have a predominant effect on P_{ND} .

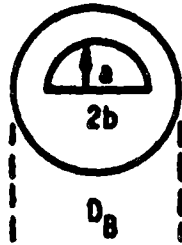
$$\therefore A = \frac{\pi}{4} a D_B$$

- (iii) If both a and $2b$ are greater than the diameter of the beam, then P_{ND} would still be a function of the defect depth.

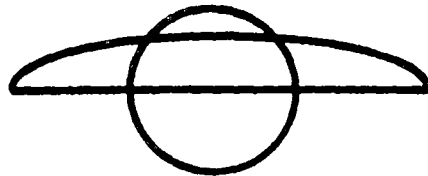
$$\therefore A = \frac{\pi}{4} a D_B$$

As was the case in the one dimensional model, there are still two parameters, ν and A^* , which characterize the model. A^* in the two-dimensional model is defined in such a manner that when the defect length ($2b$) is greater than the beam diameter (D_B), P_{ND} for a defect of depth a^* is equal to 0.5.

Case (i) $a < D_B$, $2b < D_B$.



Case (ii) $a < D_B$, $2b > D_B$.



Case (iii) $a > D_B$, $2b > D_B$.

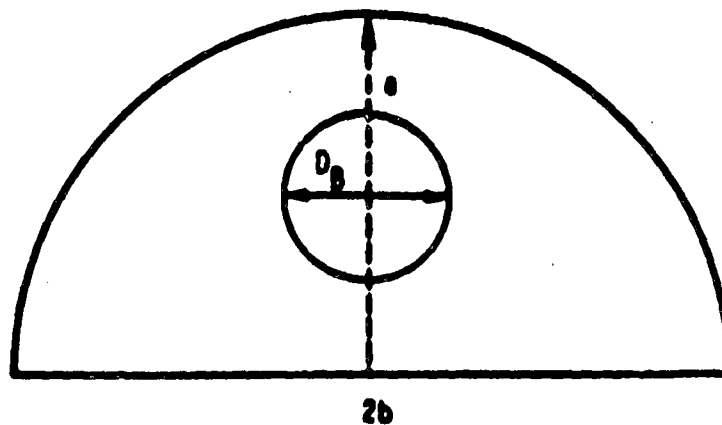


Figure 2-9. Crack Geometry Versus Beam Diameter for the Two Dimensional Model of Probability of Non-Detection Based on Crack Area.

$$A^* = \frac{\pi}{4} D_B a^*$$

For $a^* = 0.25$ in. and $v = 1.33$, and for a beam diameter of 1 inch, the two dimensional model for P_{ND} is shown in Figures 2-10 and 2-11 as a function of defect depth for various aspect ratios. For $2b/a = \infty$, the two dimensional model degenerates to one dimensional model with the same a^* and v . The P_{ND} versus a curves for any aspect ratio merge into the one-dimensional model when $2b$ becomes larger than the beam diameter. For a defect of given depth, the probability of non-detection decreases with increasing aspect ratio, until the length of the defect exceeds the beam diameter.

2.4.3 Specialization to Austenitic Weldments

All the data on detection probabilities reviewed in Section 2.4.1 were based on either wrought or welded ferritic steels or aluminium. As discussed in Section 1.2, the primary piping at Zion is fabricated from centrifugally cast austenitic stainless steel. The large columnar grains resulting from the casting process makes the ultrasonic inspection very difficult. The value of a^* of 0.35 in. estimated in Section 2.4.1 is fairly conservative for the data presented, but is overly optimistic for cast austenitic stainless steel. The functional form of P_{ND} given in Equation 2-27 will be assumed to be also applicable to cast austenitic materials, and the values of a^* and v will be altered. Becker 80 suggests that a crack would have to be half way through the wall thickness to have a 50% chance of being found. Using a typical wall thickness of 2.50 in, this results in a value of a^* of 1.25 in. The value of v can be evaluated from the assumption that a through-wall crack would be detected with a probability of 0.95. This results in a value of v of 1.60. In summary, the nondetection probability used in the investigation is given by the following expression:

$$P_{ND}(A) = \frac{1}{2} \operatorname{erfc} \left(v \ln \frac{A}{A^*} \right) \quad (2-29)$$

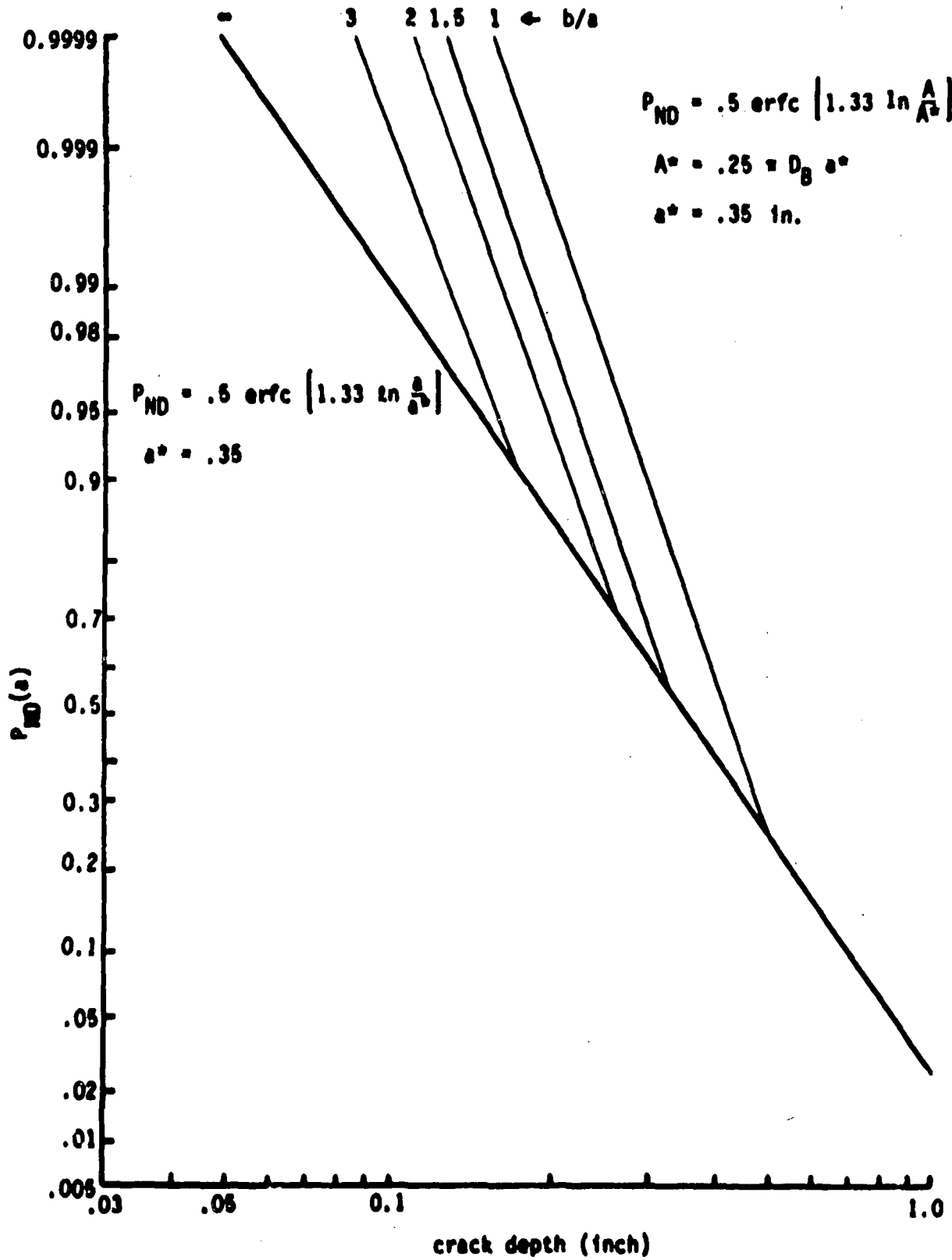


Figure 2-10. Two Dimensional Lognormal Model of Probability of Non-Detection of a Crack Based on Crack Area Plotted on Lognormal Probability Paper.

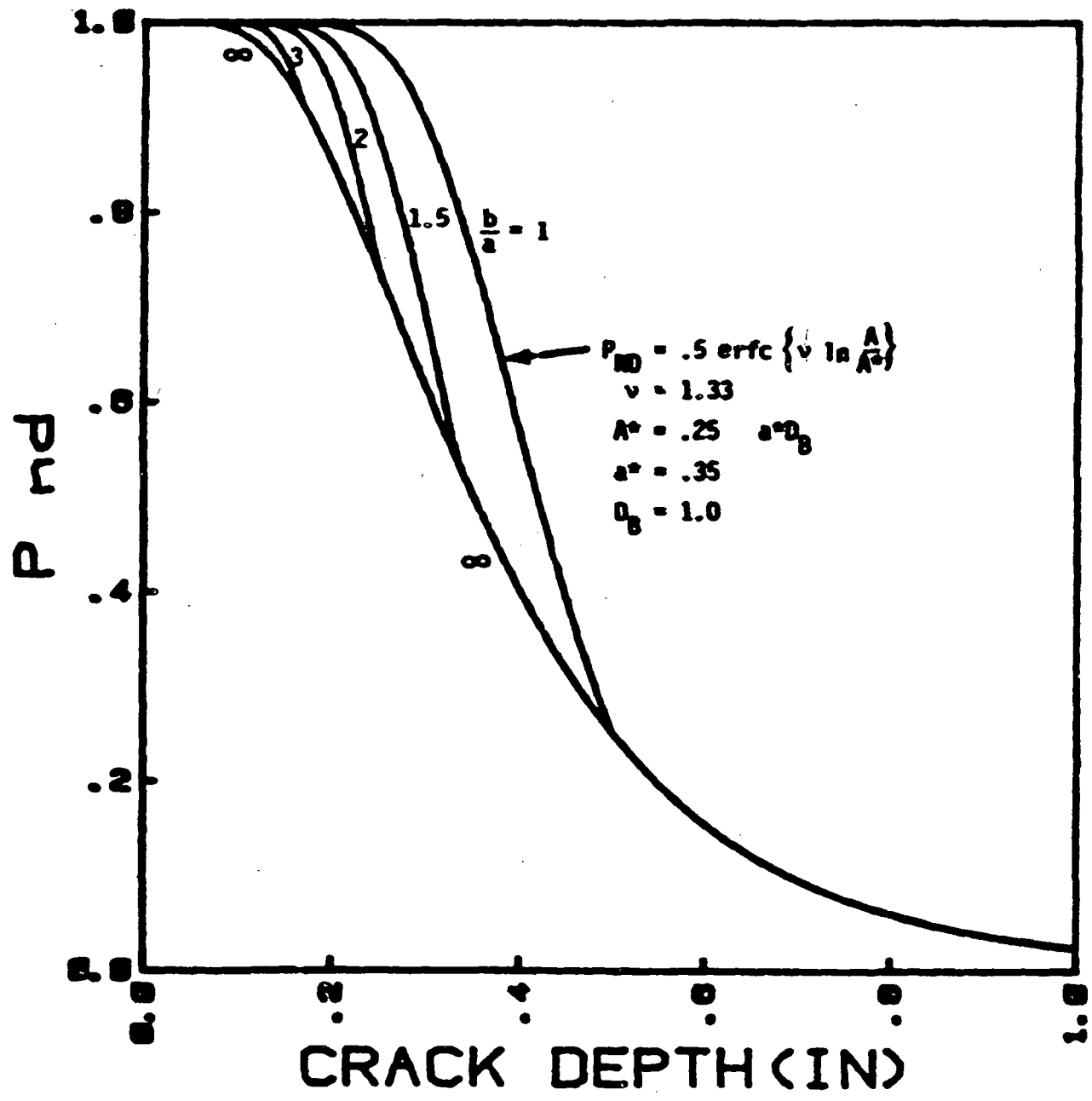


Figure 2-11. Two Dimensional Lognormal Model of Probability of Non-Detection for Crack Based on Crack Area Plotted on Linear Scales.

$$\begin{aligned}
 v &= 1.60 \\
 A^* &= \frac{\pi}{4} a^* D_B \\
 a^* &= 1.25 \text{ in.}
 \end{aligned}$$

The expression to be used for A is discussed in Section 2.4.2, and a value of D_B of 1 inch will be used in succeeding portions of this work.

The two-dimensional results for P_{ND} from Equation 2-29 is presented in Figure 2-12 along with data from the literature reviewed in Section 2.4.1. The P_{ND} result from Equation 2-29 is well above the data from the literature, which reflects the "corrections" made to account for the difficulty of detecting cracks in cast austenitic materials. The results of Figure 2-12 show that the value of v is not too critical, since the slopes for $v = 1.33, 1.46$ and 1.60 all appear quite similar.

Results obtained by the use of Equation 2-29 and the model for the influence of surface length discussed in Section 2.4.2 are summarized in Figure 2-13. The influence of the surface length is seen to not be very strong. The nondetection probabilities shown in Figure 2-13 will be used in succeeding portions of this investigation. These detection probabilities are combined with the as-fabricated crack size distribution (discussed in Section 2.3) to provide the post-inspection crack size distribution which then serves as the initial conditions for the fracture mechanics calculations. Such calculations require the crack growth and failure characteristics of the material. These will be reviewed in the next sections.

2.5 Material Fracture Characteristics

The fracture characteristics of the material are required in order to perform the fracture mechanics calculations of subcritical and fast crack growth. The subcritical crack growth will be taken to occur as a result of fatigue crack growth which may be accelerated by environmental influences--such as the presence of cooling water in the crack.

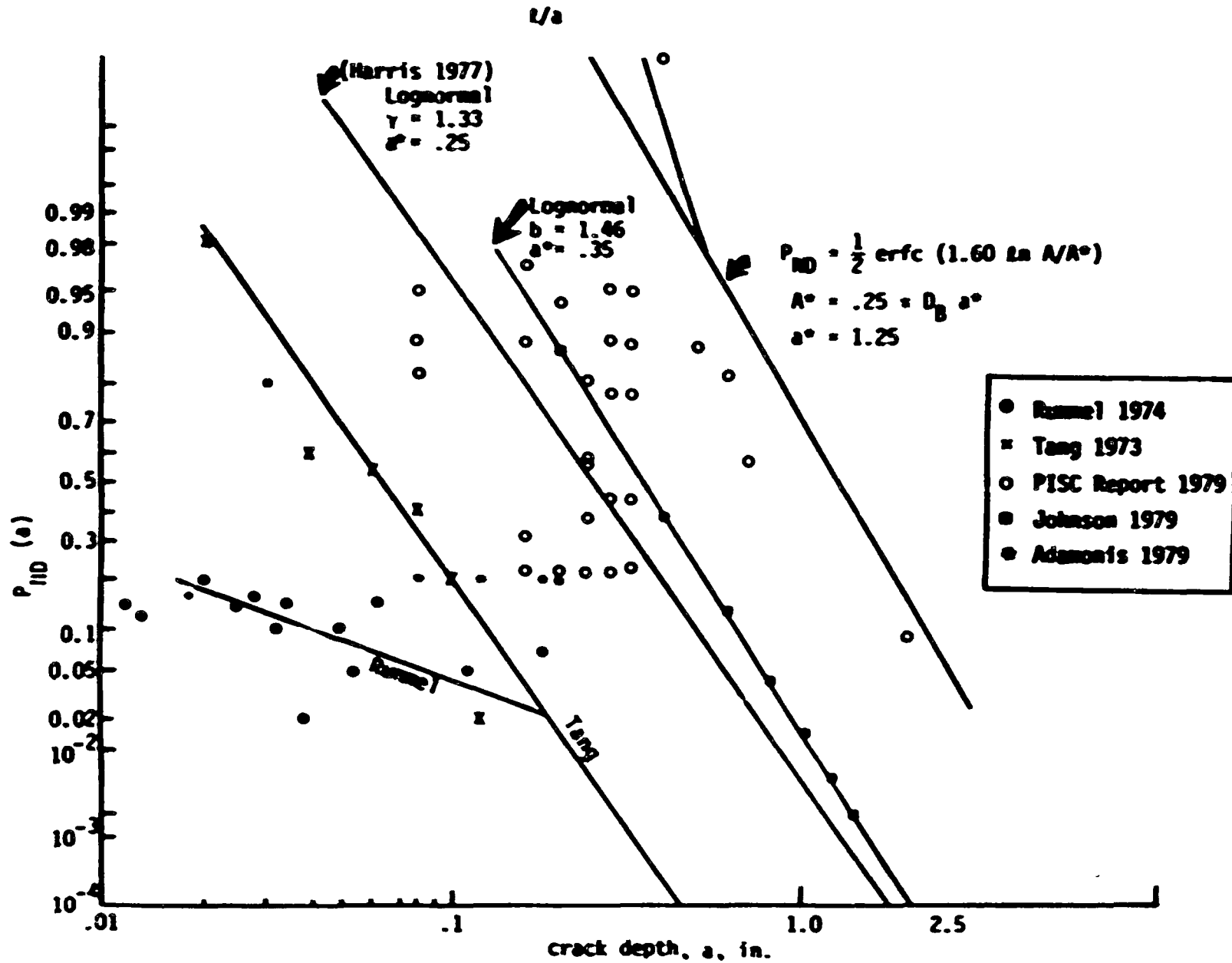


Figure 2-12. P_{ID} Data for Wrought Materials (Same as Figure 2-8) and

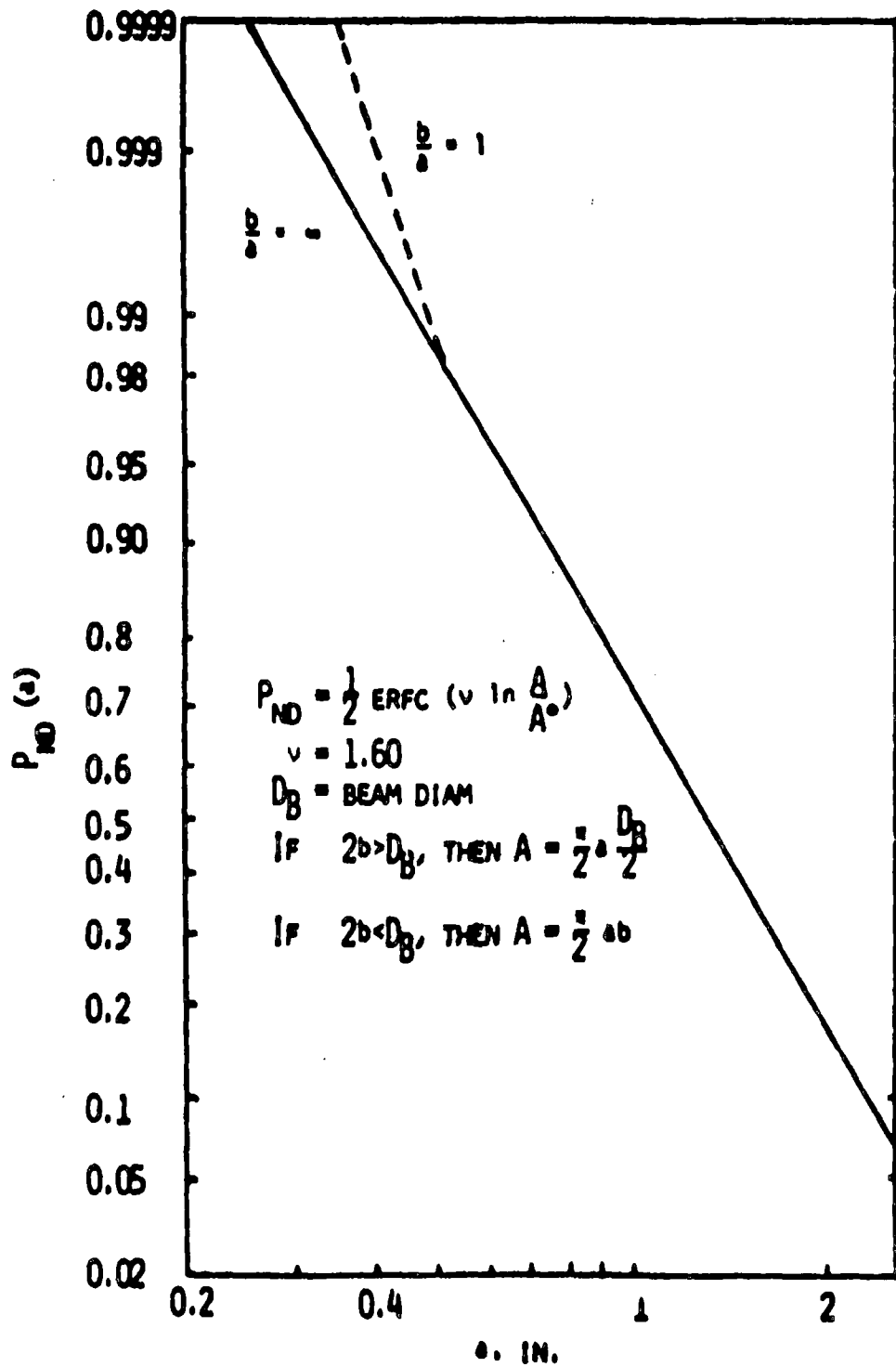


Figure 2-13. Two Dimensional Lognormal Model for Probability of Non-Detection of a Crack in Cast Austenitic Material.

Stress corrosion cracking will not be considered, because such cracking has not been observed in the primary piping of a PWR. Fatigue crack growth under nominally elastic conditions will be considered. Elastic-plastic failure criteria will be employed in treatment of the onset of fast fracture. The fracture characteristics of the material will be reviewed in the following sections.

2.5.1 Fatigue Crack Growth

The subcritical crack growth characteristics of the piping material is an important input to the piping reliability analysis. As mentioned in Section 1.2, the material used in the primary piping at Zion 1 is basically 316 type austenitic stainless steel. This material has never been observed to be susceptible to stress corrosion cracking in PWR primary piping. Attention will therefore be concentrated on fatigue crack growth, and possible environmental influences. Hence, corrosion fatigue is included in the analysis.

Crack Growth "Law"

The presence of water in growing fatigue cracks is widely known to accelerate crack growth. It also increases the influence of loading rate and mean stress (related to R ratio). Additionally, mean stress effects seem to be more important as temperature is increased. Hence, in addition to the cyclic stress intensity factor, $\Delta K (= K_{max} - K_{min})$ the load ratio $R (K_{min}/K_{max})$ may also be important. Bamford 79a, Hale 78, and James 75 indicate that the influence of R can be accounted for by considering the "effective stress intensity factor" K_{eff} , which equals $K_{max} (1-R)^m$, and that da/dn (crack growth per cycle) is a function of K_{eff} , rather than just ΔK . Further, they show that $m = \frac{1}{2}$ is a good value to use for the steels and environments under consideration. The notation of K_{eff} is rather awkward and will be replaced by

$$K' = K_{max} (1-R)^{\frac{1}{2}} = \Delta K / (1-R)^{\frac{1}{2}} \quad (2-30)$$

Results reviewed here will concentrate on the use of K' .

Bamford 79a provides data that shows that the environmentally enhanced fatigue crack growth (corrosion-fatigue) characteristics of 304 and 316 stainless steel are virtually identical, and are independent of whether the material is cast, forged, or welded. Michel 78 also indicates that welding has no influence--nor does irradiation. The lack of effects due to fabrication history, composition, and irradiation are not surprising, and are consistent with observations drawn from the much larger data base for ferritic pressure vessel and piping steels for nuclear applications (such as A533B, A508, A517, etc.). The similarity of results from 304 and 316 stainless steel suggests that information on 304 can be used to estimate the subcritical crack growth characteristics of 316.

The fatigue crack growth rate of most materials is a strong function of cyclic stress intensity factor, and the crack growth rate can be adequately characterized by the following empirical relation (Bamford 79a, James 75).

$$\frac{da}{dn} = C \left[\frac{\Delta K}{(1-R)^{1/2}} \right]^m = C(K')^m \quad (2-31)$$

where $\frac{da}{dn}$ = fatigue crack growth rate (inches/cycle)
 ΔK = cyclic stress intensity factor = $K_{max} - K_{min}$ (ksi-in^{1/2})
 R = load ratio = K_{min}/K_{max}
 C, m = empirical constants

K' is the effective stress intensity factor expressed in Equation 2-30, that accounts for the effect of cyclic stress intensity (ΔK) as well as the load ratio (R) on fatigue crack growth rate. It is necessary to obtain the numerical values of the constants C and m to compute the fatigue crack growth as a function of stress intensity and load ratio for the materials and environment under consideration.

Sufficient data on fatigue crack growth rates of 304 and 316 type stainless steels in simulated LWR environment are available for a range of stress intensity, various load ratios, test frequencies and specimen orientations. Crack growth rate data most relevant to this study are available in Bamford 79a which were obtained from tests conducted in a simulated PWR environment. These data were obtained for a range of stress intensity and for various load ratios, test frequencies and specimen orientations. These data, along with other data available in the literature (Hale 78, 79, Shahinian 75, Ford 80, FCFMS 79) were pooled together and the crack growth rate (da/dn) were plotted as a function of effective stress intensity (K') on log paper. As seen in Figure 2-14, all these data fall within a fairly narrow band. By a least-square regression analysis of these data, the values of C and m were obtained as

$$C = 7.19 \times 10^{-12}$$

$$m = 4.071$$

The value of m obtained is very close to 4, and will be rounded off to 4 for convenience. The value of C will be altered somewhat by this procedure, and a least-squares regression analysis using $m = 4$ provides a new value of C of 9.14×10^{-12} (da/dn is inches per cycle, K is $\text{ksi-in}^{1/2}$). Figure 2-14 shows the fatigue crack growth data along with the results for $m = 4$ and 4.071. It is seen that the two curve fits are not significantly different, and a value of 4 for m will be used in this investigation.

The data points on Figure 2-14 from Ford 80 are for furnace sensitized 304 stainless steel tested in water at 97C with 1.5 ppm oxygen. Such sensitization is known to be responsible for the intergranular stress corrosion cracking (IGSCC) that has been troublesome in some piping in BWR's (Vieperfer 75, PCSO 75, 79, Giannuzzi 78). The sensitized steels may be more susceptible to environmental acceleration of fatigue crack growth although data in Hale 78 suggests that this is not the case--at least for crack growth rates above 10^{-6} in/cycles. The Ford data points are for different rise-times of the loading, which consisted of variable ramp loading followed by unloading in 0.05s and no load for 0.05s.

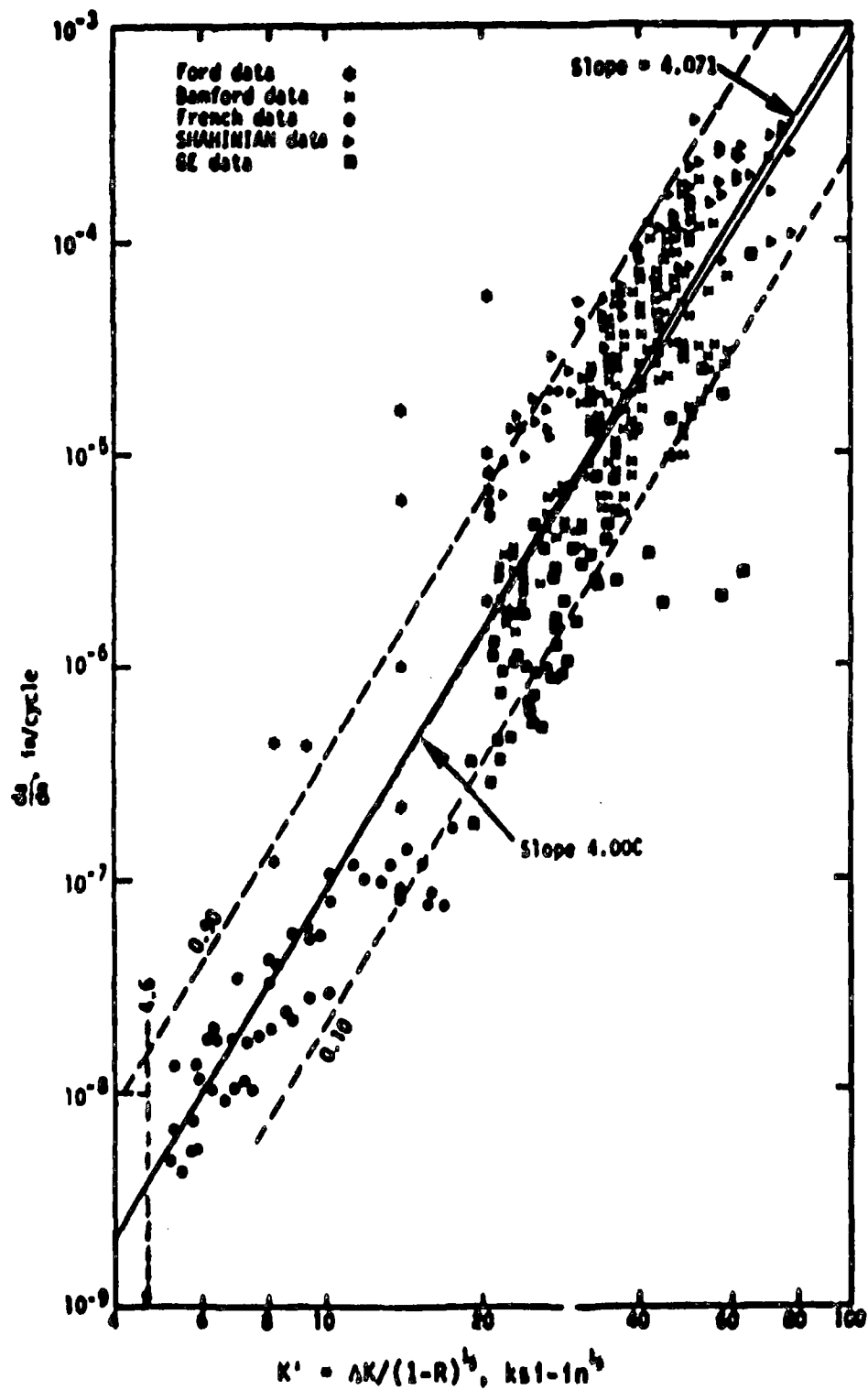


Figure 2-14. Fatigue Crack Growth Rate Data as a Function of Effective Stress Intensity Shown Along with the Least Square Curve-Fit.

Oxygen content of the water is known to influence the failure times and rate of growth of stress corrosion cracks in sensitized 304 stainless steel (Klepfer 75, Clarke 73), and could also have some effect on corrosion-fatigue crack growth rates. The data of Bamford 79a is generally applicable to PWR water, which contains less than 0.1 ppm of oxygen (Table 4.2-2 of Zion FSAR). The data of Hale 79 is for BWR operating conditions, which are typically 0.2 - 0.4 ppm (Hale 79, Klepfer 75). The data of Ford 80 is for 1.5 ppm water at 97C. A comparison of the results obtained at these different oxygen levels suggest that oxygen content is not influential within the ranges of oxygen content, loading frequencies and crack growth rates considered.

Crack Growth Threshold

Another important aspect of the fatigue crack growth relation is the threshold conditions below which crack growth will not occur. The existence of such a threshold has now been firmly established (Ritchie 77a, 77b, Vanderglass 79, Shahinian 75, Paris 72, Vosikovsky 75, Cooke 75). The presence of this threshold may be important in the analysis of fatigue crack growth of reactor piping, and should be considered. This is especially true if the small but numerous steady state fluctuations in coolant pressure and temperature are considered. The value of the threshold has been found to be independent of the environment, but dependent on R. Additionally, Ritchie 77a, 77b has found it to be dependent on the tensile properties and microstructure of the material.

Considering first the influence of R, it seems reasonable to assume that K' would provide a useful parameter to account for R. As mentioned above, environment generally does not effect the threshold, although Cooke 75 shows a difference between air and vacuum in that R does not have an effect in a vacuum. Cooke 75 found that the parameter $\Delta K_0 / (1-R)^{0.53}$ was independent of R (ΔK_0 is the measured threshold ΔK). This suggests the use of $K'_0 (= \Delta K_0 / (1-R)^{0.53})$ to characterize the threshold. This provides the added convenience of being a single fixed value on the x-axis of Figure 2-14, and interfaces nicely with the da/dn relation for higher K' . Additional information on the influence of R on the fatigue threshold is provided in Paris 72 and Ritchie 77b. Their results show that the

parameters K'_0 for a given material, heat treatment and temperature is not as dependent on R as the parameter ΔK_0 , and therefore provides a better measure of the threshold than ΔK_0 . The value of m is the expression $\Delta K_0/(1-R)^m$ could be adjusted to provide results even less dependent on R , but this seems to be an unnecessary refinement at this time.

The use of the parameter $\Delta K_0/(1-R)^{1/2}$ to characterize the threshold provides good agreement with experimental results for small R . However, care must be taken to adequately account for R values as R approaches 1 (Schmidt 73). The use of this parameter becomes questionable above $R = 0.9$. However, its use is conservative in that it predicts a higher ΔK threshold than is actually observed.

The threshold value σ : the effective stress intensity factor, K'_0 , can be estimated from information generated by the French Metallurgical Society (FCFMS 79), in which the threshold conditions for fatigue crack growth in austenitic stainless steel were specifically investigated. The data points in Figure 2-14 include their results, from which it is seen that a threshold value of 4.6 ksi-in^{1/2} provides a reasonable and somewhat conservative value of the effective threshold stress intensity factor.

Distribution of C

The data presented in Figure 2-14 exhibits an appreciable amount of scatter, which is typical of fatigue crack growth rate data. The scatter is seen to be present in the results from each investigator, rather than from investigator-to-investigator. Various means of accounting for each scatter have been suggested (Bamford 77, Basuner 77a), and the procedure of Basuner 77a will be followed. In this case, the value of the exponent, m , in Equation 2-31 is taken to be fixed, and statistical variations of da/dn for a given cyclic stress intensity factor are accounted for by considering the coefficient C to be randomly distributed. This is also the procedure used by Harris 77b.

The numerous data points in Figure 2-14 each have a value of C associated with them, once m has been fixed at a value of 4 ($C_i = (da/dn)_i / K_i^4$ where $(da/dn)_i$ and K_i are the original data point). A histogram of the resulting values of $\ln C$ is shown in Figure 2-15, from which it is seen that some skewness of the distribution exists, but a normal distribution of $\ln C$ would provide a reasonable approximation. This would imply that C is lognormally distributed.

The cumulative distribution of C can also be obtained from this data, and is plotted on lognormal probability paper in Figure 2-16. The data falls nearly on a straight line, with some deviations at large C. This further supports the contention that C is lognormally distributed. A chi-squared test was performed, which showed that the observed data do not contradict the assumption of a normal distribution of $\ln C$ at 0.05 significance level. Therefore, C will be taken to be lognormally distributed.

The mean value and standard deviation of $\ln C$ were calculated from the data points by standard procedures [i.e., $(\overline{\ln C}) = (1/N \sum (\ln C_i))$, etc.]. The following values were obtained

$$(\overline{\ln C}) = -25.418$$

$$(\ln C)_{sd} = 1.042 = s$$

The median value and standard deviation of C can be evaluated as follows (Hastings 74)

$$C_{50} = e^{(\overline{\ln C})} = 9.14 \times 10^{-12}$$

$$C_{sd} = C_{50} (e^{2s^2} - e^{-s^2})^{1/2} = 2.20 \times 10^{-11}$$

Since C is lognormally distributed, it will have the following probability density function and complementary cumulative distribution (Hahn 67, Hastings 74)

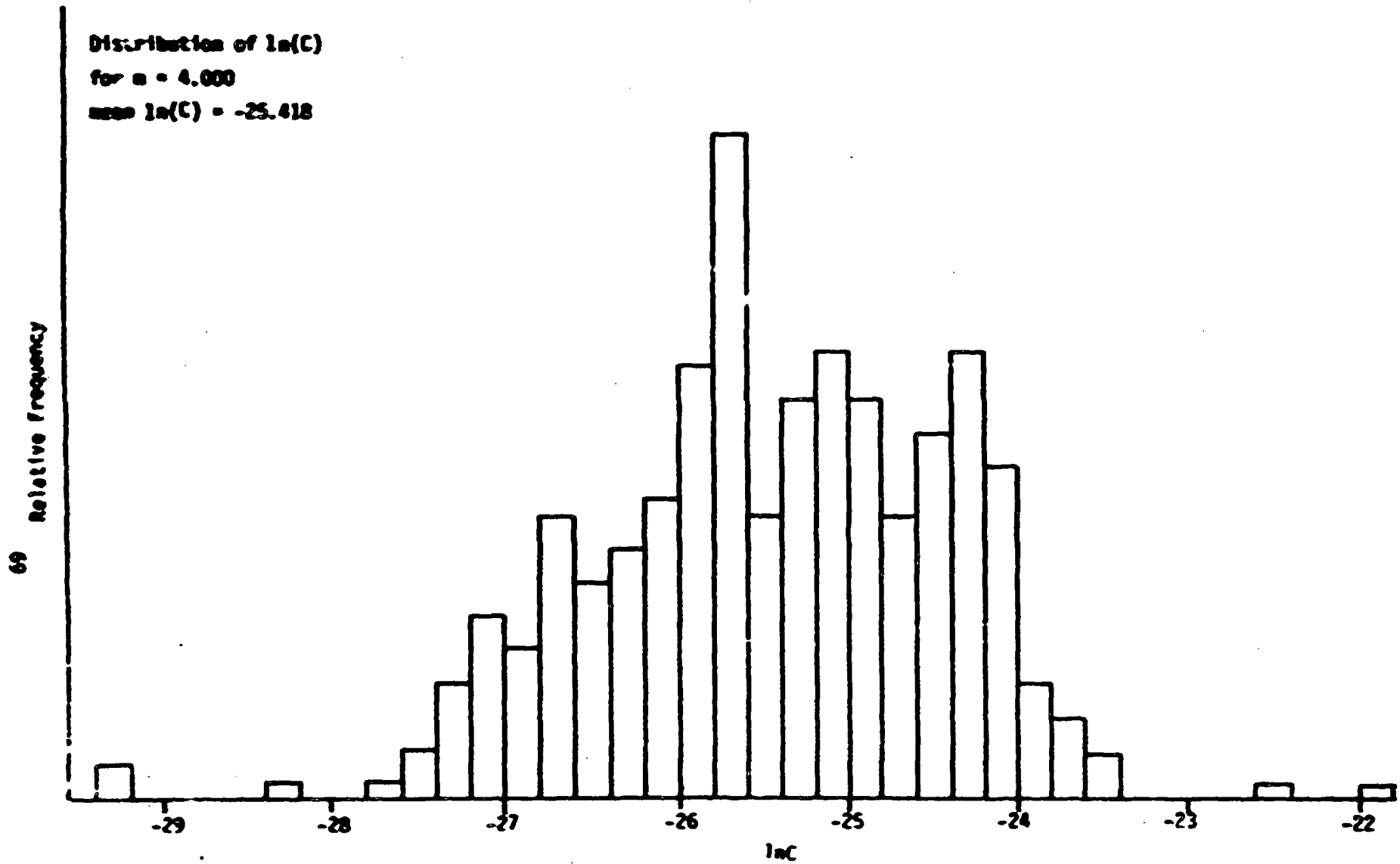


Figure 2-15. Frequency Histogram of $\ln(C)$ for $n = 4.0$.

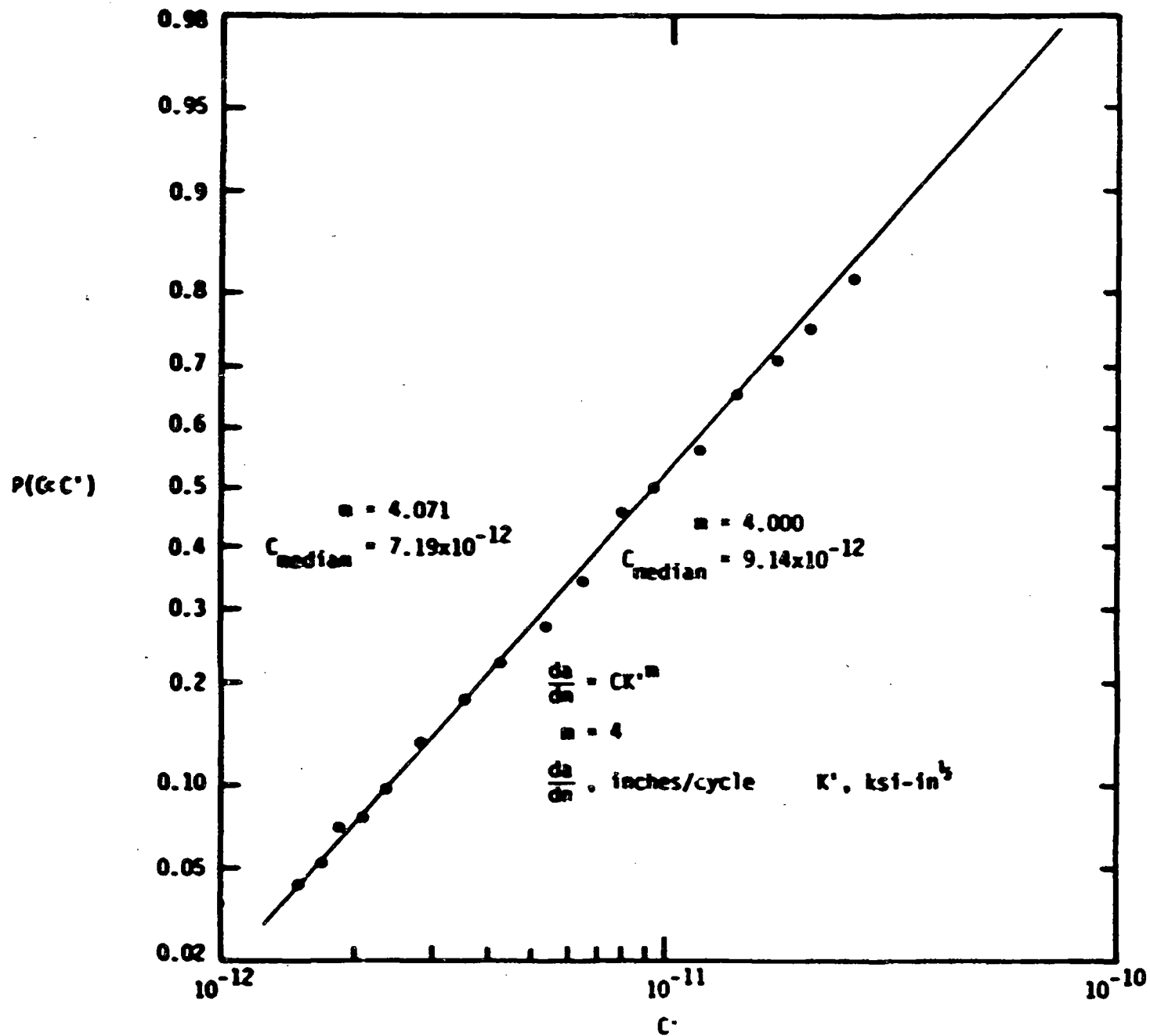


Figure 2-16. Cumulative Distribution of C Plotted on a Lognormal Probability Paper.

$$p(C) = \frac{1}{n C (2\pi)^{1/2}} e^{-\frac{1}{2n^2} (\ln C/C_{50})^2}$$

$$p(<C) = \frac{1}{2} \left[1 + \operatorname{erf} \left(\frac{1}{n^{1/2}} \ln \frac{C}{C_{50}} \right) \right] \quad (2-32)$$

The mean value of C follows from the result for C_{50} and n , as follows (Hastings 74)

$$\bar{C} = C_{50} e^{1/n^2} = 1.57 \times 10^{-11}$$

The 10th and 90th percentiles of C are obtainable from the second of Equation 32, with the following results

$$C_{10} = 2.4 \times 10^{-12}$$

$$C_{90} = 3.5 \times 10^{-11}$$

The lines on the $da/dn-K'$ plot corresponding to these values of C are shown in Figure 2-14, from which it is seen that the bulk of the data falls between these two lines--as it should. There is a factor of 14 between the 10th and 90th percentiles, which is a fairly "tight" distribution for fatigue crack growth rate results.

The lognormal distribution of C has intuitive appeal, because such a distribution results in symmetrical distributions of da/dn for a given K' on log-log plots such as shown in Figure 2-14. Basuner 77a and Harris 77b assumed C to be lognormally distributed. Such an assumption appears justified for the fatigue crack growth data considered here.

In summary, the fatigue crack growth rate will be given by the following expression

$$\frac{da}{dn} = \begin{cases} 0 & K' < K'_0 \\ CK'^4 & K' > K'_0 \end{cases} \quad (2-33)$$

$$K' = \Delta K / (1 - R)^{1/2}$$

$$K'_0 = 4.6 \text{ ksi-in}^{1/2}$$

C lognormally distributed with

median = 9.14×10^{-12}

standard deviation = 2.20×10^{-11}

$\frac{da}{dn}$: inches/cycle

K: ksi-in^{3/2}

Results reviewed above indicate that this is applicable to base material, weld material and heat affected zone material for coolant water being present or absent. This relation will be used in this investigation for all piping materials and conditions considered.

2.5.2 Final Fracture

The subcritical crack growth characteristics of the piping material were reviewed in the previous section, and provide information required to calculate the growth of cracks up to the point of unstable final fracture. Criteria employed in calculation of conditions for fast fracture are reviewed in this section. Since current state-of-the-art can treat elastic-plastic behavior, such criteria will be employed.

There are basically two types of elastic-plastic criteria that are applicable to the case under consideration: (i) exceedance of J_{IC} and T_{mat} ; and (ii) exceedance of a critical net section stress. The governing criterion is the one that predicts the smallest unstable crack size.

The exceedance of J_{IC} and T_{mat} is a fracture criterion based on the use of Rice's J-integral (Rice 68), which provides a generalization of earlier energy release considerations to the case of nonlinear elasticity. The use of the J-integral as a failure criterion was first suggested by Begley and Landes (Begley 72, Landes 72), and has been subjected to numerous experimental confirmations since then. The exceedance of critical value of J_{IC} is a necessary requirement for failure. However, the use of such a criterion as a sufficient condition is conservative, because it does not take credit for the increased "driving force" required

to grow a crack once J_{IC} is exceeded. An overly conservative failure criterion is not desired in this work, because "best estimate" results are sought. Therefore, in order to take credit for the increased driving force to grow a crack beyond J_{IC} , the tearing instability analysis of Paris and his coworkers will be employed (Paris 79, Hutchinson 79). Figure 2-17 schematically shows a J-resistance curve. From this it is seen that if the applied value of J exceeds J_{IC} , an amount of crack extension can occur that will elevate the material resistance to the applied J level. However, the applied value of J also increases with increasing crack length, and an instability will occur if $(dJ/da)_{mat} < (dJ/da)_{app}$. This is the essence of the tearing instability criterion. Paris 79 suggests the use of a dimensionless "tearing modulus" for the material. This is denoted as T_{mat} and is given by the following expression

$$T_{mat} = \frac{E}{\sigma_{f10}^2} \left(\frac{dJ}{da} \right)_{mat} \quad (2-34)$$

σ_{f10} is the flow stress of the material (commonly taken as $\frac{1}{2}(\sigma_{ys} + \sigma_{ult})$) and E is Young's modulus. The tearing instability criterion is stated as failure will occur if the applied value of T [$T_{app} = (E/\sigma_o^2)(dJ/da)_{app}$] exceeds T_{mat} .

$$\text{for instability: } T_{app} > T_{mat} \text{ and } J_{app} > J_{IC} \quad (2-35)$$

Values of J_{IC} and T_{mat} for austenitic reactor piping steels are available from a number of sources (Bamford 79b, Wilkowski 80). Bamford and Bush (Bamford 79b) present results for 304 and 316 austenitic stainless steel specimens that were cast, forged and rolled plate, oriented in axial and circumferential directions with temperatures of 70 and 600F. They found values of J_{IC} ranging from 1500 - 4400 in-lb/in². The corresponding values of T_{mat} varied from 190 - 700. It will be shown in Section 2.9 that the tearing instability does not govern in the reactor piping considered here. Therefore no attempts will be made to estimate the statistical distributions of J_{IC} and T_{mat} . The work reported in Nilsson 78 would prove useful if it was desired to estimate such distributions.

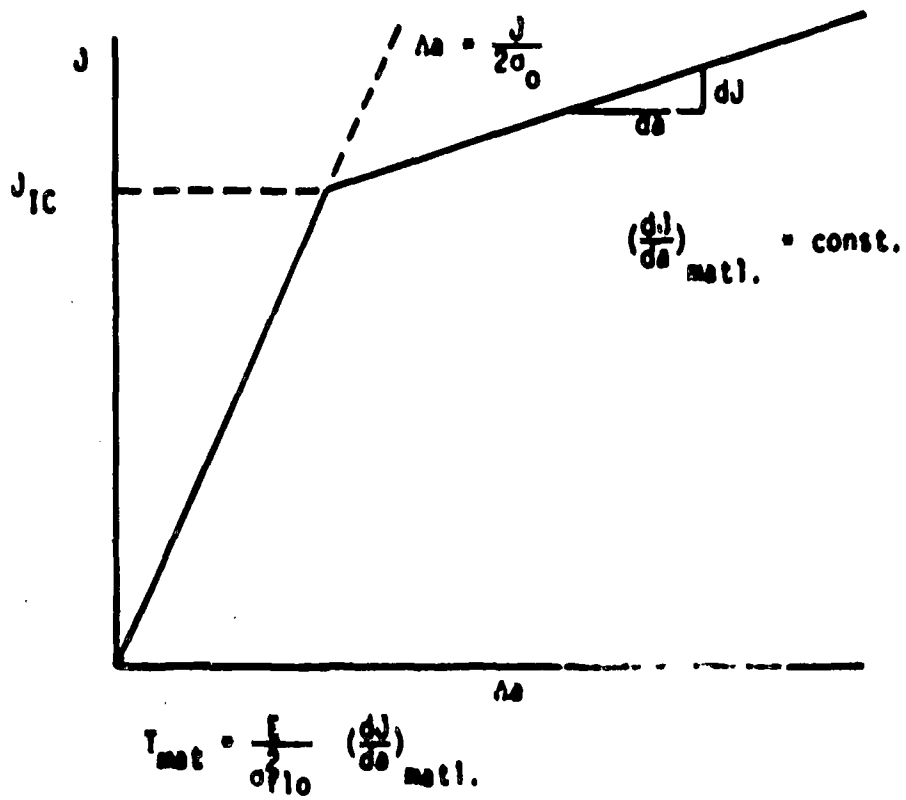


Figure 2-17. Schematic Representation of J-Integral R Curve.

In the event that the tearing instability theory predicts that cracks would never go unstable, complete and sudden failures could still occur if the remaining pipe cross-section was not sufficient to support the applied loads. This forms the basis of the net section stress criterion suggested by Kanninen, and subjected to experimental confirmation (Kanninen 78, Horn 79). The "load controlled stresses," σ_{LC} , will be used as the applied stress in this criterion. Such stresses can not be relaxed by the presence of cracks or deformation of the pipe, and must be supported by any remaining ligament. Axial components of such stress are of relevance here, because attention has been focussed on circumferential cracks. The critical value of the net section stress is observed to be equal to the flow stress, σ_{f10} , which is equal to $(\sigma_{ys} + \sigma_{ult})/2$ (Kanninen 78). The failure criterion can be stated as follows: failure will occur if

$$\sigma_{LC} A_p > \sigma_{f10} (A_p - A_{crack}) \quad (2-36)$$

where σ_{LC} is the axial component of the load controlled stress, A_p is the cross-sectional area of the pipe wall, and A_{crack} is the cross-sectional area of the crack. This criterion will be applied to the cases of interest here in Section 2.9.

The value of σ_{f10} is required in order to use this failure criterion. From above

$$\sigma_{f10} = \frac{1}{2} (\sigma_{ys} + \sigma_{ult}) \quad (2-37)$$

Hence, σ_{f10} is determinable from the values of the yield and ultimate strength. In actuality, these tensile properties are not deterministic values, but are random variables.* Hence, σ_{f10} is also a random variable.

* The following discussion of the statistical distribution of tensile properties and related results was contributed by Dr. R.O. Streit of Lawrence Livermore National Laboratory.

and its distribution can be estimated from information in the literature. Results for temperatures close to reactor operating values of about 550F are desired.

Information on the tensile properties of 316 stainless steel in the range 400 - 800F (200 - 430C) indicates that the tensile strength is not influenced strongly by temperature, and that the yield strength varies slightly in this range (Kadlecek 73, Lyman 74, Simmons 65, Smith 69). Since this temperature range covers the reactor operating range, data at these temperatures will be considered in estimating the statistical distribution of the relevant tensile properties.

The nature of the variability of tensile properties has been discussed by various investigators (Kadlecek 73, Lyman 74, Swindeman 77, Goepfert 77, Mansour 73, Stiansen 79). A normal distribution of tensile properties is generally assumed, although lower values often appear to have been truncated. The elimination of lower values is often associated with meeting minimum strength requirements of material specifications. Inclusion of the lower tail of the distribution, as is done here, is somewhat conservative.

The distribution of the yield and ultimate strength of 316 stainless steel at reactor operating temperatures was assumed to be normal, with means and variances estimated from a variety of sources (Kadlecek 73, Simmons 65, Smith 69). The flow stress is then also normally distributed, with mean and standard deviation obtainable from the corresponding values for the yield and ultimate strength (Hahn 67). The following are the resulting mean and standard deviation of the flow stress

$$\bar{\sigma}_{f10} = 44.9 \text{ ksi}$$

$$\sigma_{f10}(\text{sd}) = 1.9 \text{ ksi}$$

These values will be used in subsequent calculations of pipe failure probabilities. As shown in Section 2.9, this failure criterion will be the one applicable to the pipes under consideration.

A comparison of the above results with σ_{f10} derived from Section III of the ASME Boiler and Pressure Vessel Code (ASME 80) is of interest. Code minimum values at 600°F for SA376TP316 provide a σ_{f10} of 45.3 ksi. This is close to the value determined above. Thus, the above distribution suggests an approximately 50% chance that σ_{f10} does not meet code requirements. This indicates that the above assumed distribution is conservative.

2.6 Fatigue Crack Growth Calculation Procedures

Details of the procedures for calculating fatigue crack growth will be provided in this section. Two aspects of the problem will be covered: the relevant stress intensity factors for the crack growth analysis, and the manner of treating cycles with varying stress amplitudes.

2.6.1 Relevant Stress Intensity Factors for Part-Through Cracks

The crack geometry considered in this investigation is a part-circumferential interior surface crack, as shown schematically in Figure 2-2. Such cracks require two length dimensions for their characterization, a and b . In spite of the numerous investigations of the manner in which such cracks grow due to fatigue (for extensive review see references such as Swedlow 72, Chang 79, and JWES 77), such growth is not well understood. In reality, cracks can change shape as they grow, that is, as b and a increase, the value of β ($\equiv b/a$) changes. The manner in which β changes will depend on the initial crack shape, and the applied stress distribution. In all cases, it appears that the aspect ratio will tend towards the value that produces a constant K along the crack periphery. However, this "equilibrium" value of β will depend on the nature of the applied stress. For uniform stress, the equilibrium value is about 3.

The rate at which a and b extend will depend on the (cyclic) values of K along the crack front, as well as the fatigue crack growth characteristics of the material. The growth characteristics for cases where K is uniform along the crack front for the materials under consideration here were reviewed in Section 2.5.1, and was summarized in Equation 2-33.

This growth law will be assumed to also be applicable to part-through cracks but the stress intensity factor to be employed must be carefully defined, because K varies along the crack front. Consideration of a local growth rate controlled by the local value of K would be analytically prohibitive, and probably unrealistic. Semi-elliptical cracks would not necessarily remain semi-elliptical, and stress intensity factor solutions for non-elliptical cracks would be required. Therefore, it will be assumed that the growth of a and b need only be considered, with appropriate selection of the controlling stress intensity factors. Candidates are (Cruse 75b, Besuner 76, 77b, 78, Nair 78)

- (i) The growth of a is controlled by the cyclic value of K at the point of maximum crack penetration, and the growth of b is controlled by the cyclic K at the surface. This will be called the local K approach.
- (ii) The growth of a and b are controlled separately by some averaged stress intensity along the crack front that is associated with growth in each of these directions, or "degrees-of-freedom."

Suggested averaged values are the "RMS-average" associated with each degree of freedom (Cruse 75b, Besuner 76, 77b, 78). This seems to be a more realistic assumption than the use of simply the local values. Therefore, these RMS-averaged values associated with each degree of freedom will be assumed to govern the rate of growth of a and b. Details and additional discussion are provided in Section C.1. Basically, the RMS-averaged values are denoted with a "bar" over the K, and are defined as follows:

$$\bar{K}_a^2 = \frac{1}{\Delta A_a} \int_0^{\pi} \frac{1}{2} K^2(\phi) d[\Delta A_a(\phi)]$$

$$\bar{K}_b^2 = \frac{1}{\Delta A_b} \int_0^{\pi} \frac{1}{2} K^2(\phi) d[\Delta A_b(\phi)]$$

(2-38)

These equations are discussed in detail in Section C.1. An added advantage of this formulation is that \bar{K}_a and \bar{K}_b can be evaluated for arbitrary stresses on the crack plane by the use of influence functions. These functions can be evaluated from information on the opening displacements on the crack surface for an arbitrary (non-zero) state of stress. This is fully explained in Appendix C, which also develops and applies the relevant influence functions. Thus, values of \bar{K}_a and \bar{K}_b can be obtained for arbitrary stresses. The use of local values of K would require considerably more numerical stress analysis for each stress system of interest.

In accordance with the above consideration, the fatigue crack growth rates will be taken to be governed by the following equations:

$$\frac{da}{dn} = \begin{cases} 0 & \bar{K}'_a < K'_0 \\ C\bar{K}'_a{}^4 & \bar{K}'_a > K'_0 \end{cases} \quad (2-39)$$

$$\frac{db}{dn} = \begin{cases} 0 & \bar{K}'_b < K'_0 \\ C\bar{K}'_b{}^4 & \bar{K}'_b > K'_0 \end{cases}$$

$$K' = \Delta K / (1 - R)^{1/2}$$

As discussed in Appendices C and D, and Section 2.7, \bar{K}_a and \bar{K}_b depend on the aspect ratio (among other things) so that the growth in the depth and length dimensions is still "coupled". Additionally, the values of \bar{K}_a and \bar{K}_b depend on the magnitude and distribution of the applied stress, and changes in the aspect ratio can be accounted for.

The suitability of using the RMS-averaged stress intensity factors for calculating fatigue crack growth can be judged from experimental evidence. Cruse, et al. (Cruse 75b, 77) provides comparisons of theoretical and experimental results which suggests that such procedures are reasonable. Alternative approaches are suggested in the papers included in Chang 79 and Swedlow 72. One approach that has been taken is to use different crack growth "laws" for cracks growing along a

surface versus growth in the depth direction (Engle 79, Hodulak 79). However, the R approach embodied in Equations 2-38 and 2-39 have intuitive appeal, and are applicable to complex stress systems in a straightforward manner. This approach will therefore be used throughout this investigation.

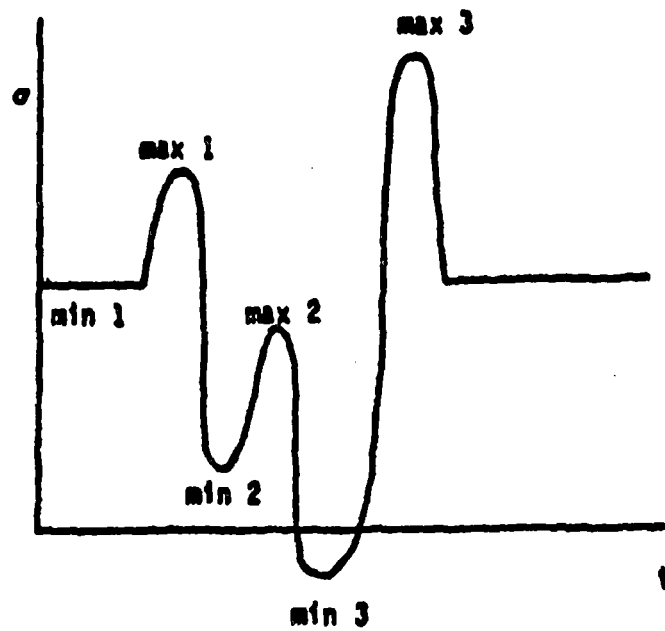
2.6.2 Cycle Counting and Load Interactions

The other aspect of fatigue crack growth analysis requiring discussion is the manner in which stress cycles are counted. For particularly simple stress histories, such as constant amplitude sinusoidal loading, such matters are trivial. This is the type of loading commonly used in laboratory testing to produce $da/dn-\Delta K$ results such as those included in Figure 2-14. In actual structural applications, including reactor piping, the cyclic loads are seldom as simple as this. Two complicating factors arise: (i) the influence of overloads on crack retardation, and (ii) what constitutes a stress cycle. Occasional high stress cycles have been observed to retard crack growth during subsequent cycles (Hertzberg 76, Broek 78, Wei 76). However, no generally applicable means of treating such phenomena are available. It will therefore be assumed that no "load interactions" occur, that is, the growth of a crack during a given cycle is controlled by the conditions during that cycle so that a crack growth "law" such as Equation 2-33 is always applicable. This is equivalent to assuming that "history" effects are not present. This assumption greatly simplifies the fatigue crack growth analysis, and is conservative (Hertzberg 76, Broek 78) but realistic within the context of the current state-of-the-art of fracture mechanics.

An alternative procedure to the cycle-by-cycle computation of fatigue crack growth employed in this investigation, is to consider the "RMS" time-averaged value of K . This RMS value is then related to crack growth rates (Barsom 73, 76, Rolfe 75), and good correlations are generally observed. However, such techniques are generally considered applicable only to ΔK probability density functions that are unimodal, whereas it is desired to treat multi-modal ΔK histories. Such multiple modes could arise from different cyclic stress contributors in reactor piping, such as normal heat up and cool down, versus seismic events, versus radial gradient thermal stresses.

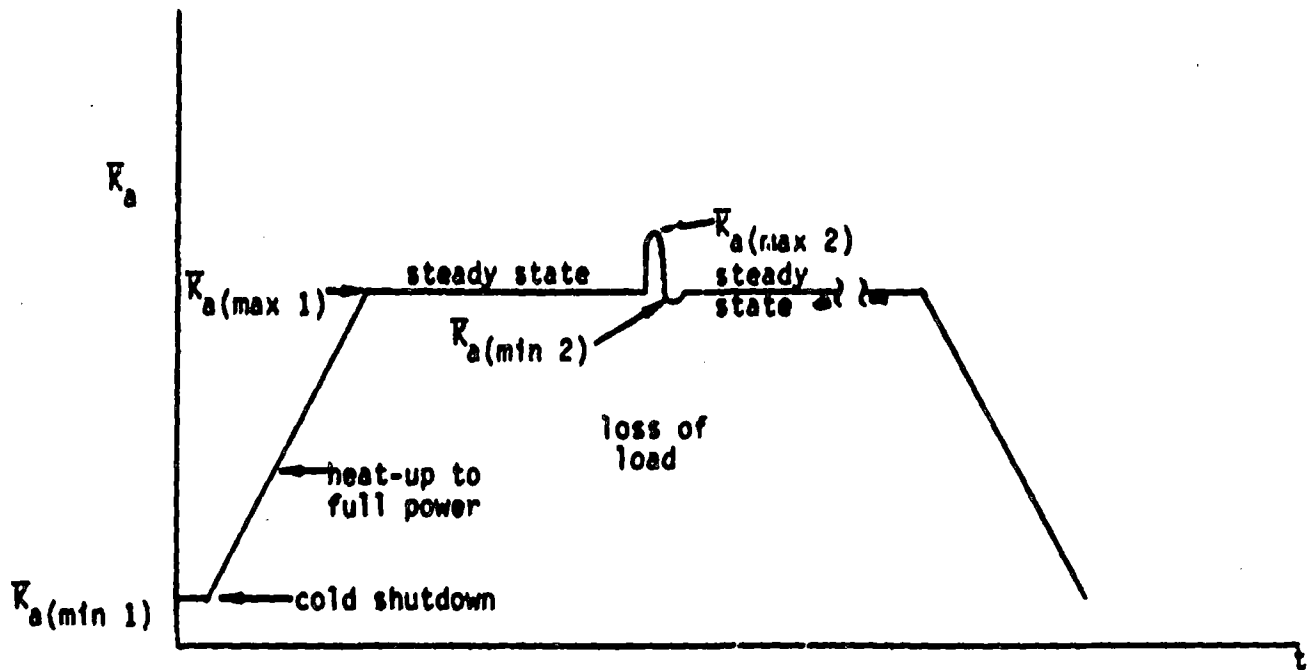
The remaining aspect of fatigue crack growth analysis to be considered is how a stress cycle is defined. Various techniques have been suggested (Wei 76, Dowling 72, Tsao 75, Nelson 75), with the range-pair and rain-flow counting techniques being widely used. Dowling 72 provides an especially informative discussion of the various proposed techniques. The method that will be employed here is closely related to the range-pair procedure. Since fatigue crack growth is generally considered to occur during the rising-load portion of a cycle, attention will be focussed on such portions of the stress (or K) history. The technique employed is shown schematically in Figure 2-18, which shows a stress history for a transient (such as a seismic event) that produces uniform stress through the pipe wall thickness.

This procedure will be slightly altered in the case of transients that produce radial gradient thermal stresses in the piping (see Sections 1.3.3 and D.4). As an example, consider the loss of load from full power discussed in Appendix D, Section D.4. Consider the sequence of events that includes this transient to be heat-up from cold shut down, steady state operation, with a loss of load and return to steady state, followed (eventually) by a shutdown to cold conditions. For a given initial crack size, K_a as a function of time would be as shown schematically in Figure 2-19. An analogous figure could be drawn for the time variation of \bar{K}_b . The procedure employed in Figure 2-19 is a slight variation of that shown in Figure 2-18, and each of these procedures could possibly be improved--such as by the use of the "rain-flow" method (Dowling 72). However, the above procedure is particularly simple for the problem at hand, and is felt to be reasonable for the present purposes. It also simplifies the "bookkeeping" involved in the numerical calculation which will be discussed in Section 3. It will be seen in Section 4 that transients producing radial gradient thermal stresses have only a small influence on the calculated probability of failure of the piping welds. Hence, the counting procedure employed is not particularly influential in the present problem.



3 cycles: $\Delta\sigma_1 = \sigma_{\max 1} - \sigma_{\min 1}$
 $\Delta\sigma_2 = \sigma_{\max 2} - \sigma_{\min 2}$
 $\Delta\sigma_3 = \sigma_{\max 3} - \sigma_{\min 3}$

Figure 2-18. Schematic Representation of a Stress-Time History Showing Means of Counting Stress Cycles and Corresponding $\Delta\sigma_1$.



$$\begin{aligned}
 2 \text{ cycles: } \Delta K_a(1) &= K_a(\text{max } 1) - K_a(\text{min } 1) \\
 \Delta K_a(2) &= K_a(\text{max } 2) - K_a(\text{min } 2)
 \end{aligned}$$

Figure 2-19. Schematic Representation of a Time History for Stress Intensity Factor for a Transient That Produces Radial Gradient Thermal Stresses During Steady State Plant Operation.

As a final topic, a means of "condensing" stress histories such as shown schematically in Figure 2-18 will be presented. The actual stress-time histories during seismic events will be quite complex, and it would be more difficult and unnecessary to perform cycle-by-cycle calculations. Instead, the following procedure, alluded to in Section 1.3.2, is employed.

The following are the governing relevant equations for growth in the a direction. (A completely analogous set of equations is applicable to the other degree-of-freedom; growth in the b direction.) Stress cycles below the threshold will also be counted as if the threshold does not exist, which will be conservative. Recall that only cases of uniform stress through the pipe wall thickness are considered in the following formulation.

$$\frac{da}{dn} = C \bar{K}_a'^4 \quad \bar{K}_a' = \Delta \bar{K}_a / (1-R)^{1/2}$$

$$\Delta \bar{K}_a = \bar{K}_a(\max) - \bar{K}_a(\min) \quad R = \frac{\bar{K}_a(\min)}{\bar{K}_a(\max)}$$

$$\bar{K}_a = \sigma a^{3/2} Y_a(\alpha, \beta) \quad [\text{uniform stress (discussed in Section 2.7)}]$$

$$\frac{da}{dn} = C \bar{K}_a'^4 = C \left[\frac{(\sigma_{\max} - \sigma_{\min})^4}{\left(1 - \frac{\sigma_{\min}}{\sigma_{\max}}\right)^2} \right] a^2 Y_a^4 \left(\frac{a}{h}, \frac{b}{a}\right)$$

$$= C a^2 Y_a^4 \sigma_{\max}^2 (\sigma_{\max} - \sigma_{\min})^2$$

$$\frac{da}{a^2 Y_a^4 \left(\frac{a}{h}, \frac{b}{a}\right)} = C \sigma_{\max}^2 (\sigma_{\max} - \sigma_{\min})^2 dn$$

$$\begin{aligned}
 \int_{a_1}^{a_f} \frac{dx}{x^2 Y^4 \left(\frac{x}{h}, \frac{b}{x} \right)} &= C \int_0^n [\sigma_{\max}(n)]^2 [\sigma_{\max}(n) - \sigma_{\min}(n)]^2 dn \\
 &= C \sum_{i=1}^n [\sigma_{\max}(i)]^2 [\sigma_{\max}(i) - \sigma_{\min}(i)]^2 \\
 &= CS^4
 \end{aligned}
 \tag{2-40}$$

This shows that all the information required for calculating the growth during the stress history considered is the value of the parameter, S. This same parameter also enters into the analysis of growth in the b direction. Hence, only the value of S is required for a seismic event rather than details of the time history of the stress. Values of S were determined for a variety of seismic events for each of the weld joints considered. Results are presented in Section 1.3.2.

The parameter S, defined in Equation 2-40, is employed for stresses that are uniform through the wall thickness, have many cycles, and are generally above the fatigue limit. For transients that are relatively few in number and/or have stresses that vary through the wall thickness, calculations of fatigue crack growth are made on a cycle-by-cycle basis with both a and b updated each cycle, or block of few cycles.

Once a part-circumferential crack has broken through the pipe wall to become a through-wall crack, its length will be taken to be equal to the length on the inside surface at the moment of break through. More detailed fracture mechanics analysis would require the generation of considerably more new stress intensity factor solutions, which is not warranted at this time. Once the crack is through the wall, the growth rate during succeeding transients will be taken as

$$\frac{db}{dn} = \begin{cases} 0 & K_b^i < K_b^t \\ CK_b^4 & K_b^i > K_b^t \end{cases}$$

where now K_b^t is the value associated with a through-wall crack. Such values of K_b^t will be discussed in the following section, along with the values of \bar{K}_a and \bar{K}_b used for the analysis of the growth of part-through cracks.

2.7 Stress Intensity Factors

Considerable detail on the stress intensity factors employed for the fatigue crack growth analysis are presented elsewhere. The motivations for using RMS-averaged values of K along the crack front (\bar{K}_j) were discussed in Section 2.6.1, and in more detail in Section C.1. The use of influence functions to calculate \bar{K}_j is also discussed elsewhere (Section 2.6.1 and Appendix C), and is demonstrated for stresses with strong thickness variations in Appendix D--where tabulations of \bar{K}_j for the transients of interest are included. Comparison of results generated as part of this investigation with previously existing solutions demonstrated the accuracy of the present approach. Hence, the majority of information on \bar{K}_j is included elsewhere. The purpose of this section is to present an additional result that remains to be discussed and are of particular importance. These are the values of \bar{K}_j for part-through cracks with uniform stress on the crack plane, and the stress intensity factor solution employed for through-wall cracks.

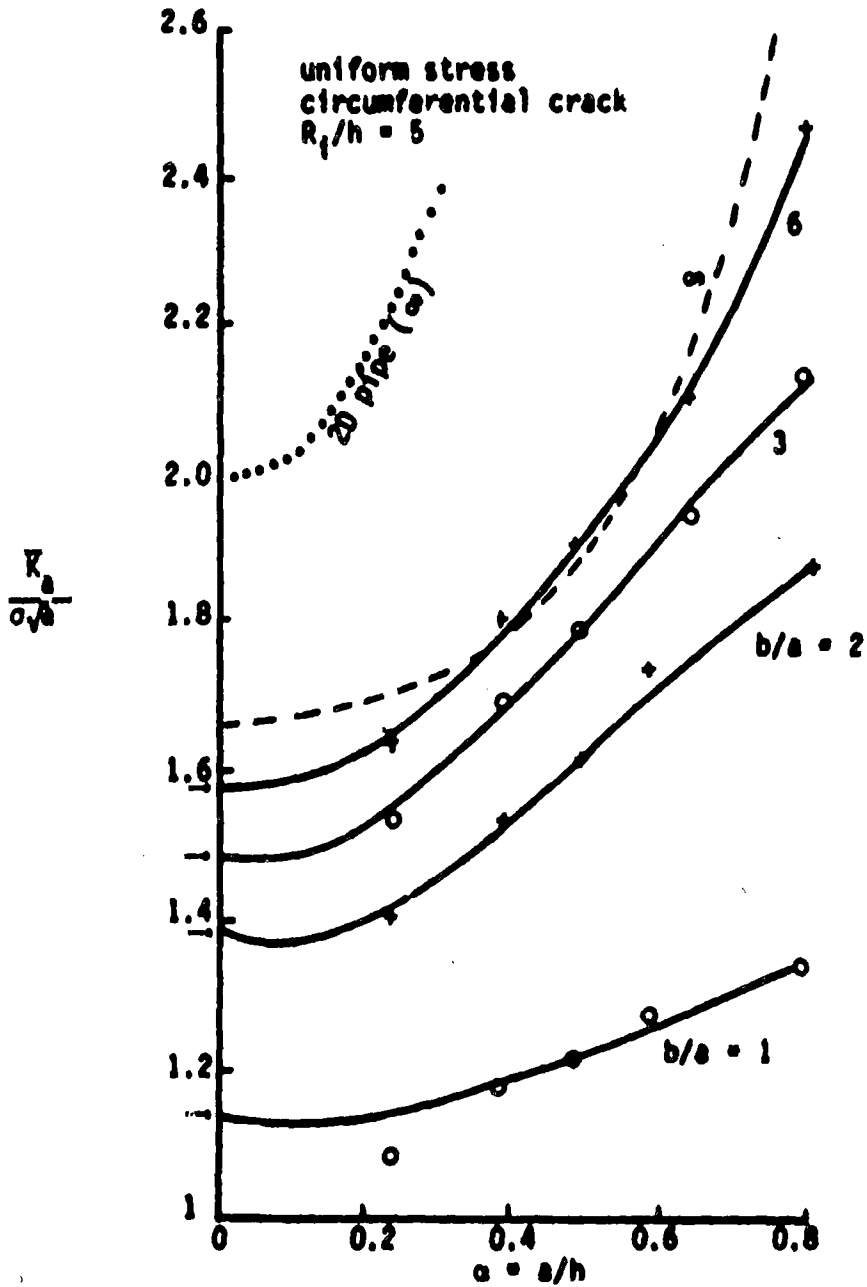
The stress intensity factor for a part-circumferential semi-elliptical interior surface crack with uniform applied stresses will vary along the crack front, as discussed in Section B.3 and shown in Figures B-11 and B-12. The values of \bar{K}_a and \bar{K}_b are actually of more interest in the fatigue crack growth analysis. These parameters can be evaluated from information such as that in Figure B-11 by the use of Equations C-2 through C-4. That is, the RMS-averaged values of \bar{K}_j are evaluated from knowledge of the variation of K along the crack front. Such calculations were performed by numerical integration for a variety of crack sizes that were analyzed by BIE procedures. Values of $\alpha = a/h$ less than 0.2 were not included in the BIE calculations and are therefore not available here. It was decided to curve fit the results for \bar{K}_j with a polynomial that would also be applicable for very shallow cracks. Therefore, values of \bar{K}_a and \bar{K}_b for $\alpha \rightarrow 0$ obtained for an embedded defect (Besuner 77b, see Section D.2.1) were also included in the linear regression analysis at $\alpha = 0.1$. The use of the embedded solutions for small α will result in, at most, 12%

error due to the presence of the free surface. It was desired to accurately and conveniently express K_a and K_b for uniform stress through the pipe wall, because the majority of the important transients (including seismic events) have uniform stresses. Results of the numerical calculations of K_a and K_b are presented as data points in Figures 2-20 and 2-21. Also shown are curves from the linear regression analysis. Good agreement between the numerical results and the regression analysis is observed. Listings of the curve-fitted functions for $K_a (a/h, b/a)/\sigma a^{\frac{1}{2}}$ and $K_b (a/h, b/a)/\sigma a^{\frac{1}{2}}$ follow. The 1.15 correction term mentioned in Section B.2 has been applied.

```

FUNCTION SIFBARA(AH,BA)
C  UNIFORM STRESS, RIN/H=6,CIRCUMFERENTIAL INTERIOR SURFACE CRACK
C
C  A=CRACK DEPTH
C  B=HALF SURFACE LENGTH
C  H=WALL THICKNESS
C  AH=A/H
C  BA=B/A
C
C  MARCH 4,1980
      A1=AH
      A2=A1*A1
      A3=A1*A2
      A4=1./BA
      B1=AB
      B2=B1*B1
      B3=B2*B1
      B4=1.4401
      B5=.34296
      B6=.40410
      B7=.22273
      B8=.68199
      B9=.42320
      B10=.49806
      B11=.98951
      B12=.036574
      B13=11.798
      B14=.20.734
      B15=9.6933
      B16=.42962
      B17=.15.827
      B18=.29.838
      B19=.16.884
      B=(B4+B1*B1)+B2*B2+B3*B3+A1*(B10+B1*B11+B2*B2+B3*B3)+A2*(B12+B1*B13)
      S=(B2*B2+B3*B3)+A1*(B4+B1*B1+B2*B2+B3*B3)/SQRT(1.-A1)
      SIFBARA=1.15*S
      RETURN
      END

```



lines are least squares fit
data are BIE results

Figure 2-20. $K_a/\sigma \sqrt{a}$ for a Part-Circumferential Crack in a Pipe With Uniform Stress in the Pipe Wall.

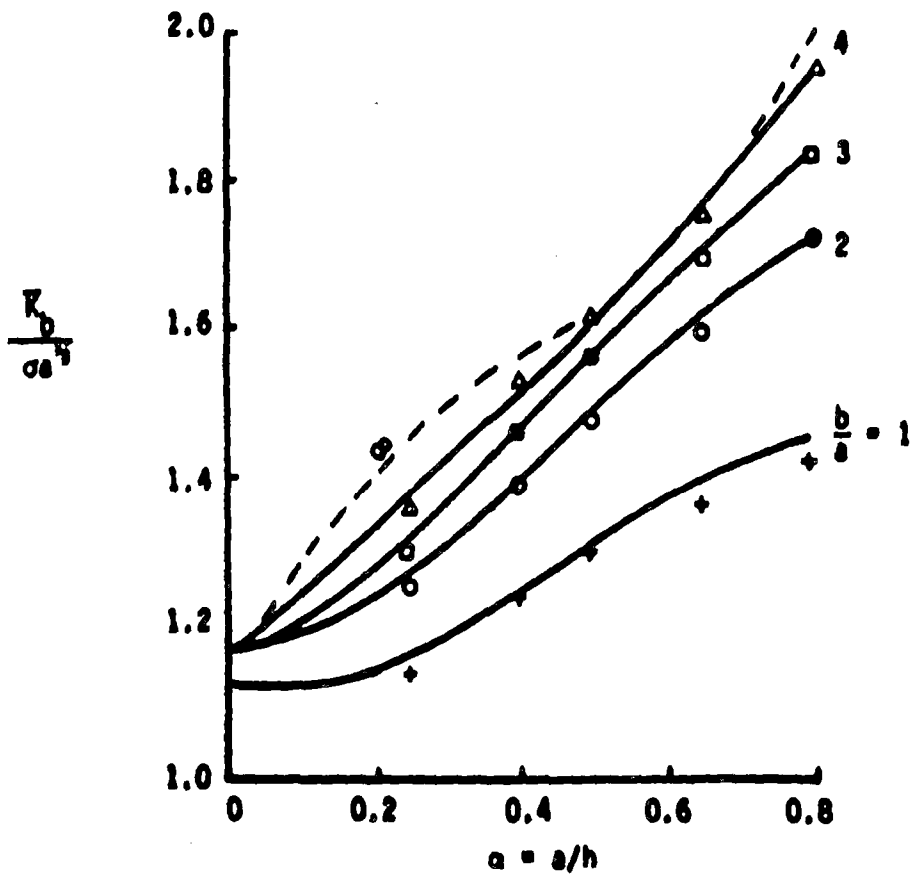


Figure 2-21. $K_I / (\sigma_0 \sqrt{\pi a})$ for a Part-Circumferential Crack in a Pipe With Uniform Stress in the Pipe Wall.

```

FUNCTION STFBAR(BA,BA)
C  UNIFORM STRESS, RIN/H=B,CIRCUMFERENTIAL INTERIOR SURFACE CRACK
C  STFBAR=KBAR/SIGMA SORT(A)
C
C  A=CRACK DEPTH
C  B=HALF SURFACE LENGTH
C  H=WALL THICKNESS
C  AH=A/H
C  BA=B/A
C
C      MARCH 6, 1960
C      A1=AH
C      A2=A1*A1
C      A3=A1*A2
C      AB=1./BA
C      B1=AB
C      B2=B1*B1
C      B3=B2*B1
C      D0=.97917
C      D1=.20174
C      D2=.24769
C      D3=.09483
C      E0=1.0621
C      E1=-6.6890
C      E2=9.2182
C      E3=-4.2890
C      F0=-2.7479
C      F1=21.818
C      F2=-36.218
C      F3=18.606
C      G0=1.4244
C      G1=-17.706
C      G2=31.190
C      G3=-16.477
C      S=(D0+D1*B1+D2*B2+D3*B3+A1*(E0+E1*B1+E2*B2+E3*B3)+A2*(F0+F1*B1
C      S +F2*B2+F3*B3)+A3*(G0+G1*B1+G2*B2+G3*B3))/SQRT(1.-A1)
C      STFBAR=1.18*S
C      RETURN
C      END

```

Figures 2-20 and 2-21 also show the value of the stress intensity factors calculated from the curve fits for $\beta \rightarrow \infty$. Geometrically, this would correspond to a complete circumferential crack. Also shown in figure 2-20 is the result from Labbens 76 for a complete circumferential crack. It is seen that the extrapolated curve fit results are some 30% below the complete circumferential crack. This is somewhat disappointing, but it is perhaps too much to ask of a curve fit to data in the range from 1-6 to be suitable for extrapolation to ∞ . Rice and Levy (Rice 72a) show that K_{max} for a surface crack in a flat plate only slowly approaches the edge crack results as β increases, and that results for $\beta = 6$ are far from the edge crack results. Another contributor to the disagreement between the \bar{K}_a and 2D results has to do with the definition of \bar{K}_a , and the behavior of $\beta \rightarrow \infty$. The limiting case of an embedded elliptical crack is a tunnel crack, in which case $b \rightarrow \infty$ as $2a$ remains constant. The stress intensity factor for this configuration is (Tada 73)

$$K = \sigma(\pi a)^{1/2}$$

It would be expected that this is \bar{K}_a , and \bar{K}_b would be zero. The applicable equations for \bar{K}_a and \bar{K}_b are obtained from the general solution for an embedded elliptical crack subjected to uniform tension (Green 50, Irwin 62). These equations are given in Section D.2.1. For $\beta \rightarrow \infty$, they reduce to the following

$$\frac{\bar{K}_a}{\sigma(\pi a)^{1/2}} = \left(\frac{8}{3\pi}\right)^{1/2} = 0.9213$$

$$\frac{\bar{K}_b}{\sigma(\pi a)^{1/2}} = \frac{2}{(3\pi)^{1/2}} = 0.6515$$

Hence, \bar{K}_a is not equal to $\sigma(\pi a)^{1/2}$ and \bar{K}_b is not equal to zero for $\beta \rightarrow \infty$. This is undoubtedly due to the definitions of $d[\Delta A_j(\phi)]$ which are developed using ellipses. The point is that \bar{K}_i for limiting two-dimensional

cases do not necessarily reduce to the 2D case. This could partially account for the $\beta \rightarrow \infty$ result in Figure 2-20 being somewhat below the corresponding two-dimensional result.

K_a will have a singularity as $\alpha \rightarrow 1$, as may also K_b . The nature of the singularity in K_a can be obtained from Tada's results (Tada 73) for an internal circular crack in a solid circular cylindrical bar. The singularity is of the form $(1 - \alpha)^{1/2}$, which has been included in the above curve fit. This was done in order to increase the confidence in values of K_a and K_b calculated from the curve fit for $\alpha > 0.8$. Such deep cracks may be part of the population required to be considered in the fatigue crack growth analysis.

The value of K for a through-wall crack will be required for the fatigue crack growth analysis of cracks that have broken through the wall, but are not long enough to result in a complete pipe severance. A reasonable approximation for a through-crack of length $2b$ is

$$K = \sigma(\pi b)^{1/2} \quad (2-41)$$

which is the expression for a through crack in an infinite plate (Tada 73). This is certainly a rough approximation, especially for cracks that are an appreciable fraction of the circumference in length. This estimate could be easily improved by the use of results that consider the curvature of the pipe (Folias 67). However, such refinements are not warranted at this time for this problem, because, as will be seen in Section 2.8, the current model for flow rates for through-wall cracks, in conjunction with the current criterion for leak detection, results in all through-wall defects being immediately detected and repaired.* Hence, calculations of fatigue crack growth of through-wall defects are not necessary in the current problem.

* Cracks that become through-wall during a seismic event are not considered to be detected until after the seismic event is over.

2.8 Leak Models

A defect that grows to become a through-wall crack, but that is of insufficient length to result in a complete pipe severance, will be a leak. This will constitute a leak-before-break situation. If the leak is sufficiently large, it will produce a detectable leak, and the plant can be shut down in an orderly manner and the leak repaired. In order to include such considerations, the flow rate through cracks must be estimated, which, in turn, requires estimates of crack opening. The probability of detecting the leak depends on its size, and estimates of detection probabilities must be made. These various aspects of the leak detection problem will be covered in this section.

2.8.1 Prediction of Flashing Water Flow Through PWR Pipe-Wall Cracks*

Leak rates for steam/water mixtures through fine cracks through the walls of LWR piping systems are a complex function of crack geometry, crack surface roughness, and inlet fluid thermodynamic state. Analytical predictions of crack flows are hampered by phenomenological uncertainties which are incurred by the wide spectrum of admissible crack configurations. Appreciable meander, as well as local changes in (flow) cross-section, are often observed for naturally occurring cracks; additionally, detailed knowledge of surface roughness characteristics would likely be unavailable.

Even for a fully specified configuration, however, the analytical task is difficult, involving consideration of highly complex interactions between (non-equilibrium) two-phase flow regimes. This is illustrated in Figure 2-22 where generally accepted features of the flow process are seen to include the formation of an initial liquid jet, an interim transition region wherein the jet breaks up owing to Taylor instabilities and vapor nucleation, and a thoroughly dispersed two-phase flow mixture thereafter.

* The following analysis of two-phase flow through cracks was contributed by Dr. V. Denny of Science Applications, Inc., Palo Alto, California.

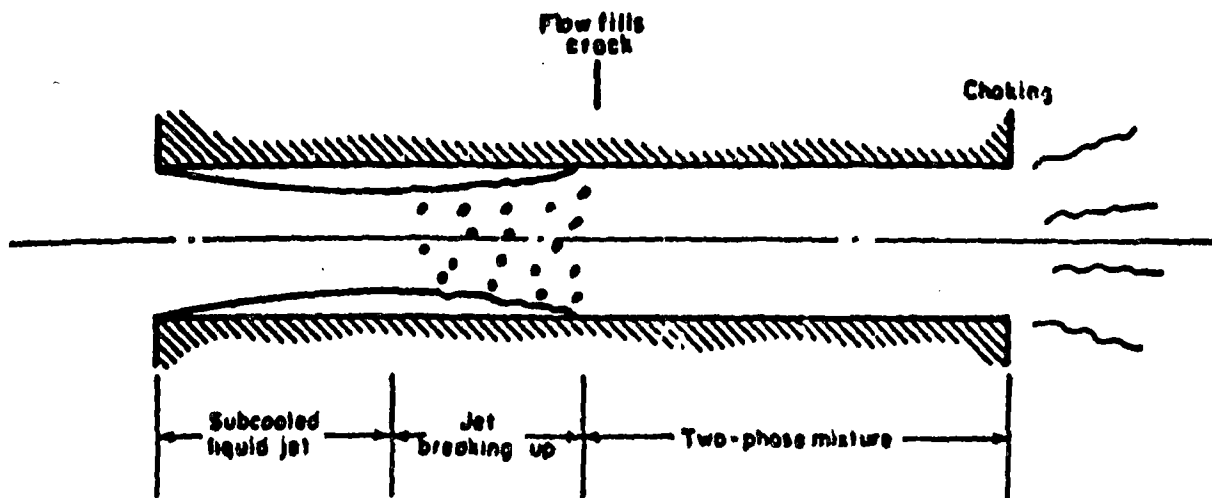


Figure 2-22. Two-Phase Flow Through a Long, Narrow Crack (From Wallis 80).

experimental portion of the study considered the effects of initial fluid state (stagnation pressure and temperature), crack geometry (L/D_h), and crack surface roughness. The crack length (w) and depth (L) were fixed at 2.5 in. and 2.25 in., respectively. Various crack openings were established to give ratios of L/D_h ranging from 27 to 128. RMS surface roughness ranged from 0.32 μm to 10.16 μm , with p_0 and $\Delta T_{\text{sub-cooling}}$ ranging from 1000 to 2250 psia and 11 to 111 $^{\circ}\text{C}$, respectively. Critical flow measurements were compared with predictions from their extension of the Henry model, accounting for wall friction. Measured values of mass flux (G) tended to lie below predicted values, with discrepancies as large as 30-40% in some cases, as shown in Table 2-5, which is produced from Collier 80.

As will be discussed more fully in Section 2.8.3, leaks with more than a few gallons per minute are expected to be detected with a high probability. Therefore, attention will be focussed here on the estimation of leaks through crack sizes in PWR piping for which leak flow rates are less than about 6 gal/min. Likely crack lengths ($2b$) are estimated to range from 1-50 in., with 1-10 in. being most probable. Crack depths ($h = R_0 - R_1$) are established by the range of pipe wall thicknesses, say 1.4 to 2.7 in. Crack opening displacements are estimated to be on the order of 1-10 mils as will be discussed more fully in Section 2.8.2. The crack opening will be taken to be rectangular, with a constant opening, δ , and a constant length $2b$. Tortuosity of typical naturally occurring cracks is uncertain, as is surface roughness. The peculiar conditions under study in the present work (i.e., fatigue cracks) suggest relatively straight cracks (in-depth direction); i.e., relatively insignificant meander. RMS roughness of up to 10% of the crack opening displacement are believed to be reasonable. Initial conditions for the leak flow are taken at typical PWR operating conditions in the primary system piping, giving a fixed value of $p_0 = 2250$ psia and $550 < T_0 < 650^{\circ}\text{F}$. The effects of in-depth reductions in flow cross section were not considered; nor, were the effects of discharge resistance as posed by the possible presence of external insulation.

Owing to considerable phenomenological uncertainty in the geometrical configuration of naturally occurring cracks, an elaborate model of critical two-phase flow is not warranted. Agostinelli et. al. (Agostinelli 58)

Table 2-5

Summary of Flow Rate Experiment Data (From Collier 80)

Test No.	P_o MPa	T_o C	ΔT C	W (meas) $\frac{kg}{s}$	W (calc) kg/s	P_e (meas) MPa	P_e (calc) MPa	r mm	δ mm	G_c (meas) $10^4 kg/m^2-s$	G_c (calc) $10^4 kg/m^2-s$
1	8.36	265.86	32.98	2.03	3.10	3.97	4.59	.3	1.12	2.86	4.37
2	9.27	186.19	119.35	.94	.88	2.28	1.11	.3	.25	5.21	5.47
3	9.88	197.20	106.10	.82	.84	2.66	1.41	.3	.25	5.06	5.23
4	8.35	188.12	117.85	.90	.55	1.55	.96	6.2	.23	6.21	3.80
5	8.77	199.14	102.31	.74	1.04	1.58	1.46	6.2	.36	3.26	4.62
6	8.51	261.96	37.74	3.60	3.87	4.27	4.36	6.2	1.09	5.19	4.42
7	11.53	251.23	78.37	1.93	4.33	3.81	3.79	6.2	1.09	5.67	6.25
8	5.81	199.17	74.25	.43	.80	1.30	1.45	6.2	.36	1.91	3.53
9	5.80	178.88	85.48	.40	.41	1.17	.92	6.2	.23	2.79	2.81
10	3.96	199.97	49.78	.46	.59	1.31	1.44	6.2	.36	2.05	2.62
11	3.26	227.79	18.64	1.35	1.40	1.97	2.23	6.2	1.09	1.95	2.02
12	10.88	234.19	82.49	.52	.54	3.04	2.73	6.2	.23	3.60	3.72
13	10.65	249.81	66.62	.48	.49	3.69	3.41	6.2	.23	3.30	3.34
14	9.91	212.46	97.81	.62	.97	1.93	1.89	6.2	.33	2.95	4.63
15	8.68	217.92	82.82	.49	.87	1.84	2.09	6.2	.33	2.34	4.16
16	9.33	234.88	71.13	.52	.85	2.34	2.80	6.2	.33	2.50	4.03
17	8.88	285.88	95.88	.51	.53	2.17	1.64	6.2	.23	3.53	3.65
18	8.89	238.88	72.38	.49	.48	3.02	2.52	6.2	.23	3.35	3.27
19	8.52	236.85	63.35	.46	.44	3.19	2.75	6.2	.23	3.16	3.02
20	8.65	192.14	108.32	.71	.95	1.47	1.26	6.2	.33	3.38	4.52
21	8.94	286.98	96.26	.86	.93	1.92	1.69	6.2	.33	4.10	4.42
22	4.72	195.32	65.85	2.16	2.53	1.78	2.30	6.2	1.09	3.11	3.64
23	8.98	285.97	96.58	.39	.41	2.01	1.63	10.2	.20	3.03	3.16
24	9.82	218.85	84.61	.40	.39	2.35	2.05	10.2	.20	3.11	3.00
25	8.92	223.73	78.92	.39	.37	2.56	2.22	10.2	.20	3.03	2.89
26	9.46	267.83	39.12	3.14	3.73	4.69	4.80	6.2	1.09	4.53	4.66
27	10.31	256.14	57.89	1.03	3.85	4.20	4.08	6.2	1.09	4.37	5.55

suggested a straight-forward recipe wherein critical flow of initially subcooled liquid, for simple flow geometries, is taken as the arithmetic average of upper and lower bounds of the actual flow. The upper bound ($G = G'_c$) is the intersection of the "sonic" ray, as calculated using the well known compressible critical flow expression

$$G_c = \left[-(\partial P / \partial \hat{v})_s \right] \quad (2-42)$$

and extrapolation of the usual relation for liquid flow between pressure-drop and mass-velocity,

$$G^2 = \frac{2\rho P_{in}}{fL/D_h} (1 - P/P_{in}) \quad (2-43)$$

for back pressures P below P_{sat} . The lower bound is just that given by Equation 2-43 at $P = P_{sat}$; i.e., $G = G_s$. Clearly, the procedure incurs increasing uncertainty as the degree of subcooling of the inlet flow approaches zero; i.e., as saturation conditions are approached.

However, for the range of conditions treated in Agostinelli 58, agreement between the predicted results and experimentally measured values is exceptionally good, as shown in Table 2-6, which is reproduced directly from Agostinelli 58. For the maximum error reported (-11.4%), the degree of subcooling is 28°F, or only about 16°C; thus, the procedure appears to remain satisfactory even for very small subcooling. More to the point, the application of more "rigorous" models, such as two-fluid models with interfacial slip, or even the extended Henry model suffer from the lack of a comprehensive experimental data base for assigning such parameters as slip ratio, two-phase friction factors, and inter-phase dis-equilibrium constants.

For given $D_h = \delta$, $L = h$, c_s/D_h (where c_s is the equivalent sand grain roughness), and inlet conditions (P_{in} , T_{in}), Equations 2-42 and 2-43 were solved graphically, as illustrated in Figure 2-23, to determine $G_c = (G'_c + G_s)/2$. For given P/P_{in} , $(\partial P / \partial \hat{v})_s$ was calculated from steam table data, assuming isenthalpic flow along the crack. Equation 2-43 was solved using liquid properties at inlet conditions (isenthalpic pro-

Table 2-6
Comparison of Experimental Critical Values with Pre-
dicted Limits (from Agostinelli 58).

Diametral clearance, in...	0.006	0.012	0.006	0.012	0.006	0.012	0.006
Temperature, deg F.....	398	400	455	455	470	470	600
P_{10}	800	400	800	600	800	670	2500
P_{50}	227	232.6	444.3	444.3	514.7	514.7	1542
P_{90}	220	216	285	258	320	308	830
P_{95}	212	182	253	278	310	308	880
Q_c (lower limit).....	2120	1660	1610	1710	1500	1580	3560
Q_c (experimental).....	2140	1600	1820	2040	1720	2190	4800
Q_c (upper limit).....	2160	1710	2000	2230	2200	2300	5300
Per cent error.....	0	+1.5	+0.83	-3.4	+9.3	-11.4	-4.8

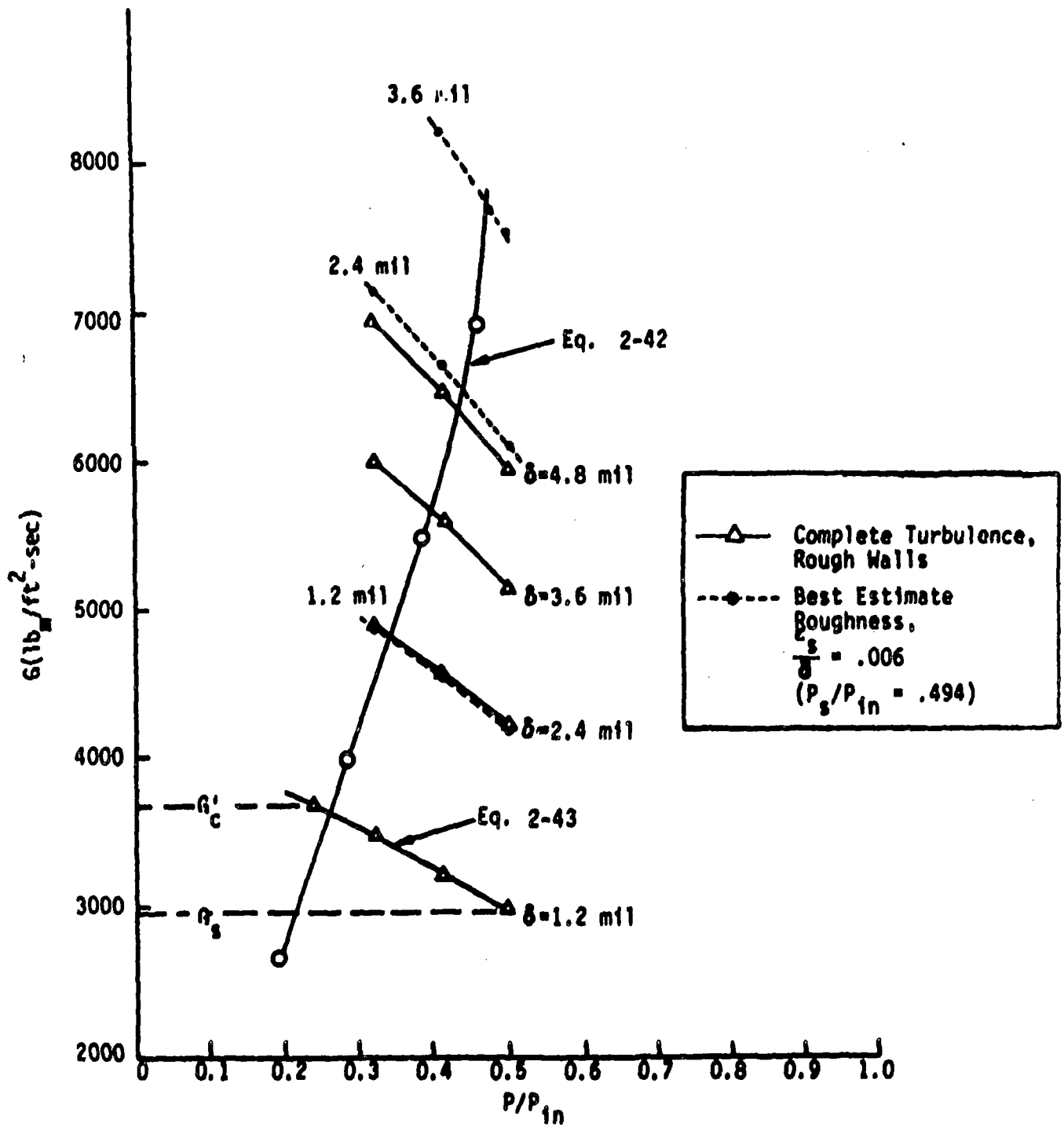


Figure 2-23. Solution Method. HEM Model/Isentropic Flow
 $P_{in} = 2250$ psia, $T_{in} = 550^\circ$ F, $R_2 - R_1 = 1.8$.

cess is also nearly isothermal) and employing conventional friction-factor versus Reynolds number plots. Results for G_c were then converted to volumetric flow (gpm) per foot of crack length, i.e., \dot{Q}' .

For a typical fixed PWR operating pressure (2250 psia), the effects of the problem parameters, are summarized in Table 2-7. Results for best estimate roughness ratios ($\epsilon_s/D_h = .006$) are listed above those for fully turbulent conditions ($f \sim 0.072$), the latter results being placed in parentheses. Typical trends for a wall thickness of 1.8 in. are shown in Figure 2-24. Results such as these, and in Table 2-7 will be used in subsequent portions of the investigation.

Preliminary comparison of the results in Table 2-7 with the results of Collier 80 (as summarized in Table 2-5), indicate some discrepancies between the two sets of results. A careful study is necessary before it would be possible to find the source of any disagreement. Such studies are left for future efforts.

2.8.2 Crack Opening Displacements

The crack opening displacement, δ , is required to estimate the flow rate through cracks (see for instance Figure 2-24). Such opening displacements are influenced by plastic deformation at the crack tip, and the cylindrical nature of the pipe. Pipe bulging due to shell effects can significantly increase opening displacements above corresponding results for a flat plate in tension (Folias 67). Elastic-Plastic estimates of opening displacements could be obtained by use of relations between J-integral values and opening displacements (Paris 79), but elastic results will be used in the present case. A lower bound on the opening displacement for a through-wall crack of length $2b$ in a pipe subjected to a uniform stress, σ , can be obtained from the following result for an infinite plate in tension (Tada 73)

$$\delta = \frac{4\sigma b (1-\nu^2)}{E} \quad (2-44)$$

Table 2-7
Crack Flows Q' (gal/min-ft)

$T_{in} = 550^{\circ}\text{F}$, $P_{in} = 2250$ psia

h (in.)	δ (mils)			
	1.2	2.4	3.6	4.8
1.41	4.90 (3.62)	13.72 (9.90)	-- (17.74)	-- (26.84)
1.8	4.38 (3.24)	12.29 (8.8)	22.33 (15.86)	-- (24)
2.38	3.82 (2.84)	10.85 (7.82)	19.70 (14.07)	-- (21.31)
2.50	3.73 (2.78)	10.62 (7.65)	19.24 (13.79)	-- (20.88)
2.66	3.62 (2.69)	10.31 (7.42)	18.72 (13.37)	-- (20.14)

$T_m = 620^{\circ}\text{F}$, $P_{in} = 2250$ psia

h (in.)	δ (mils)			
	1.2	2.4	3.6	4.8
1.41	4.08 (3.08)	11.24 (8.32)	19.96 (14.76)	--
1.8	3.66 (2.68)	10.14 (7.34)	18.12 (13.1)	27.2 (19.66)
2.38	3.21 (2.44)	9.03 (6.64)	16.19 (11.88)	24.38 (17.87)
2.50	3.14	8.84	15.84	23.94
2.66	3.04 (2.35)	8.60 (6.32)	15.44 (11.34)	23.30 (17.02)

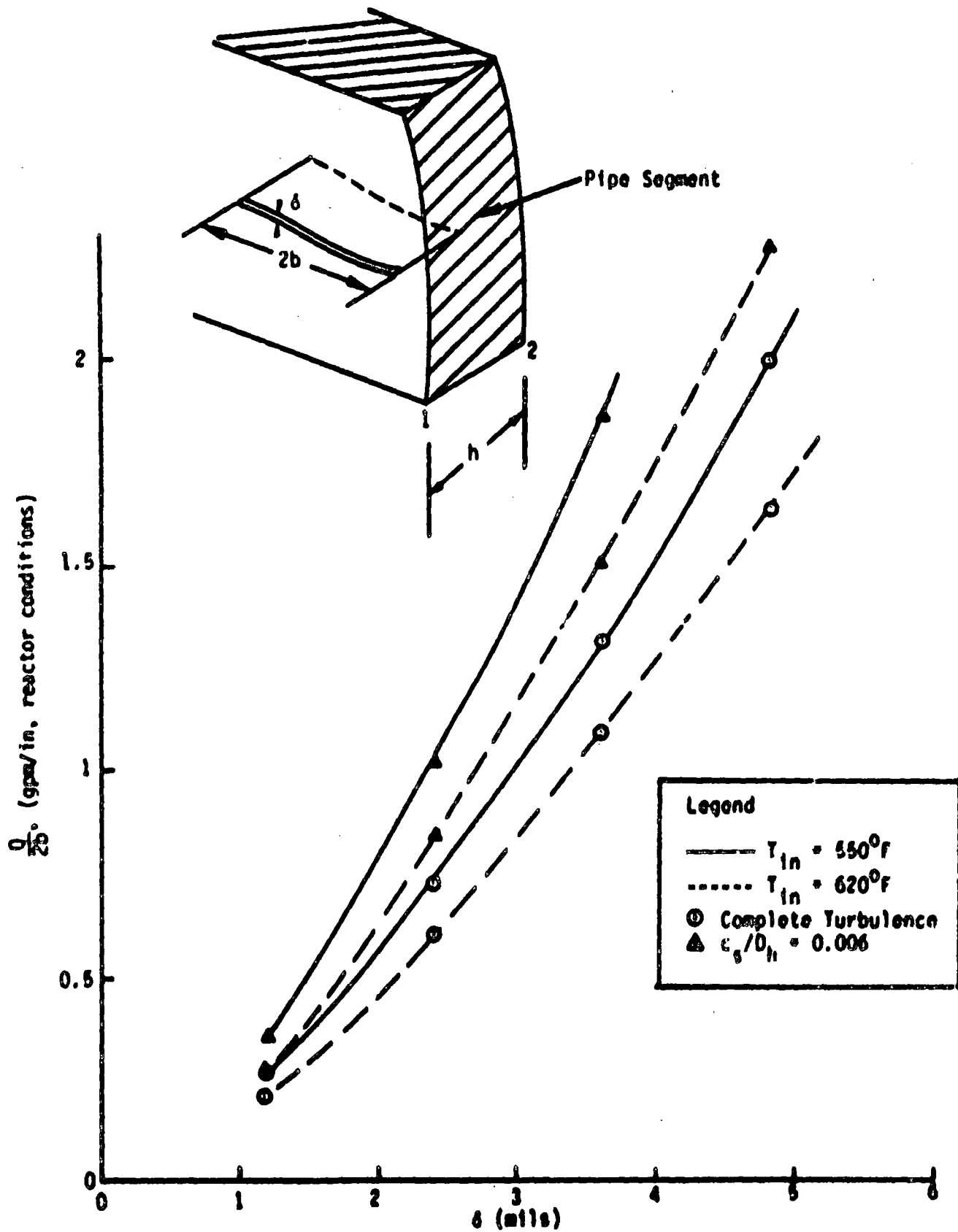


Figure 2-24. Crack Flows. $P_{in} = 2250$ psia, $h = 1.8$ in., $T_{sat} = 652^\circ F$.

The minimum value of b is h (the wall thickness) in accordance with discussions in Section 2.2. The value of σ to be used is the load controlled stress, σ_{LC} , which (for non-seismic conditions is equal to $(\sigma_U + \sigma_{DM})$). From Table 1-2, a lower value of this parameter is about 4.3 ksi. Taking $h = 2.5$ in., Equation 2-44 along with the above parameters, predicts the following lower bound estimate of the opening displacement, and corresponding leak rate from the results in Table 2-7.

$$\delta > \frac{4(4.3)(2.5)(.91)}{28 \times 10^3} = 1.4 \text{ mils}$$

$$\dot{Q}' \sim (3 \text{ gpm/ft})(2 \times 2.5/12)$$

$$\dot{Q} \sim 3 \frac{\text{gpm}}{\text{ft}} \frac{2 \times 2.5 \text{ in.}}{12 \text{ in/ft}} \sim 1.3 \text{ gpm}$$

Recall that this is a conservative lower bound on \dot{Q} . As will be seen in the next section, leak rates greater than 1 gpm will be considered to be detected. Hence, refinements in estimates of the opening displacements are not felt to be warranted at the present time.

2.8.3 Leak Detection Probabilities

Commercial nuclear power reactors are required to use sensitive, sophisticated, and redundant leak detection systems. Currently employed techniques include the following (Frank 77, Wise 77, Harris 80b)

- sump level and flow monitoring
- airborne particulate radioactivity monitoring
- airborne gaseous radioactivity monitoring
- containment air cooler condensate flow rate monitoring.

Three methods of leak detection must be employed (RG 45), which provides redundancy in the leak detection systems. Additionally, sensitivities of less than 1 gpm are generally obtainable (Frank 77, Harris 80b).

The technical specification for Zion I (TS, no date) requires the plant to be shut down if an identified leakage of greater than 1 gpm is measured. This is well within the sensitivities of current leak detection

systems, which, in conjunction with the redundancies mentioned above, provides a high assurance that leaks in excess of 1 gpm will be detected and remedial action taken. Therefore, the probability of detecting a leak of rate greater than 1 gpm will be taken as 1. Correspondingly, the probability of detecting (and repairing) a leak of rate less than 1 gpm will be taken to be zero. Mathematically this is stated as

$$P_{D(\text{leak})}(\dot{Q}) = \begin{cases} 0 & \dot{Q} < 1 \text{ gpm} \\ 1 & \dot{Q} > 1 \text{ gpm} \end{cases} \quad (2-45)$$

and this will be used for leak detection probabilities in this investigation. This, in conjunction with the lower bound calculation of \dot{Q} included in Section 2.8.2, reveals that all through-wall cracks are predicted to be immediately detected and repaired (unless they should initially be large enough to produce a complete pipe severance). Hence, refined estimates of both the crack opening displacements (Section 2.8.2) and stress intensity factors for fatigue crack growth analysis of through-wall cracks (Section 2.7) are not warranted at the present time. This was briefly mentioned in the earlier sections.

This concludes the discussion of leak rate and detection models, which turns out to be particularly simple for the cases of crack opening displacement and leak detection probability estimates employed in this report.

2.9 Failure Criteria

Failure criteria applicable to reactor piping materials were reviewed in Section 2.5.2, which also presented results for the relevant material fracture properties -- such as J_{IC} , T_{mat} and σ_{f10} . In this section, the candidate criteria will be applied to the primary piping of Zion I, and the most suitable criterion for the present case selected. This selection will be based on which criterion results in the smallest critical crack sizes for given applied stresses.

No attempt will be made to provide a comprehensive review of applications

of J_{IC} and tearing instability criteria to reactor piping. Basically, Tada, Paris and Gamble (Tada 79) have demonstrated that circumferential cracks in reactor piping will not be subject to any tearing instability for length-to-diameter ratios representative of primary reactor piping in LHRs. Figure 1-2 shows that the longest straight run of piping in the large main coolant piping at Zion I is the cold leg; running from the isolation valve to the reactor inlet. However, it would perhaps be more appropriate (and certainly more conservative) to include the sum of the length of the cross-over leg, pump casing, isolation valve and cold leg. This constitutes some 60 ft. (720 in.) of piping, with a nominal outside diameter of 32 in. This results in L/R of 45. Tada, et al. (Tada 79) provides the following estimate for T_{app1} . (their Equation 28).

$$T_{app1} = F_1(\theta, \bar{a}, P) \frac{1}{R} + F_2(\theta, \bar{a}, P) \frac{JE}{\sigma_{f10}^2 R}$$

Considering the case of no crack closure, the largest value of F_1 is about 1.2 (Tada Figure 10), and largest value of F_2 is 0.5 (Tada Figure 12). Using $J = 4000 \text{ in-lb/in}^2$ (as in Tada 79), $E = 28 \times 10^6 \text{ psi}$, $\sigma_{f10} = 45 \times 10^3 \text{ psi}$, $R = 16 \text{ in.}$, the following upper bound on T_{app1} is obtained

$$T_{app1} < 1.2 \frac{1}{R} + 1.73$$

For L/R of 45, this results in $T_{app1} < 56$. From Section 2.5.2, the value of T_{mat} is 190 - 700. It can therefore be concluded that a tearing instability will never occur for the piping system under consideration.

The other failure criterion that could come into play is the critical net section stress criterion, which was discussed in Section 2.5.2. This criterion will come into play for very large cracks that reduce the pipe cross-sectional area to the point where the loads that cannot be relaxed by extensive deformation are sufficient to break the remaining area. Such loads are considered to be the "load controlled" components of stress, and are the deadweight stress and axial component of the pressure stress. Additionally, seismic loads will be assumed to be load controlled. The

exceedance of a critical net section stress will be considered to result in a sudden and complete pipe severance (LOCA). In accordance with Section 2.5.2 (Equation 2-36), LOCA will occur if the following condition is met

$$\sigma_{LC} A_p > \sigma_{f10} (A_p - A_{crack})$$

A_p is the cross sectional area of the pipe. σ_{f10} was discussed in Section 2.5.2, where it was found that this parameter is normally distributed. The crack geometry considered for calculation of the critical crack area is shown in Figure 2-25. This is an alteration of the semi-elliptical defect shown in Figures 2-2 and A-1. This modification is necessary, because as will be seen, very large flaws are required for complete pipe severance. The standard geometrical definition of ellipses can not be used for the large semi-"elliptical" cracks necessary for LOCA, and geometric refinements are not felt to be worthwhile at this time. For example, if the crack area was taken to be $\frac{\pi}{2} ab$, with $a = h$ and $b = \pi R_1$, the largest possible crack area is $\frac{1}{2} \frac{\pi}{2} h \pi R_1 = \frac{1}{4} \pi^2 h R_1$. The total pipe cross-sectional area is $\sim 2\pi R_1 h$. Therefore, a complete circumferential crack all the way through the thickness has an $A_{crack}/A_p = \frac{1}{4} \pi^2 h R_1 / (2\pi h R_1) = \pi/4 = 0.79$. It would be preferable to have a complete circumferential crack all the way through the wall thickness to have an area equal to the pipe cross-sectional area. The crack geometry of Figure 2-25 satisfies this condition. This is the crack geometry employed in many of the General Electric Studies of crack stability in BWRs, such as in Horn 79. The area of the crack shown in Figure 2-25 is given by the following expression

$$A_{crack} = ab \left(2 + \frac{a}{R_1} \right) \quad (2-46)$$

Any crack with an area insufficient to result in a sudden pipe severance, i.e., not big enough to satisfy the criterion of Equation 2-36, will be considered to grow only as a fatigue crack. This includes the growth of part-through cracks to become through cracks. That is, as $a \rightarrow h$, the crack does not become unstable, but continues to grow only as a fatigue crack. This is a reasonable approximation that is within the spirit of the tearing instability approach discussed above.

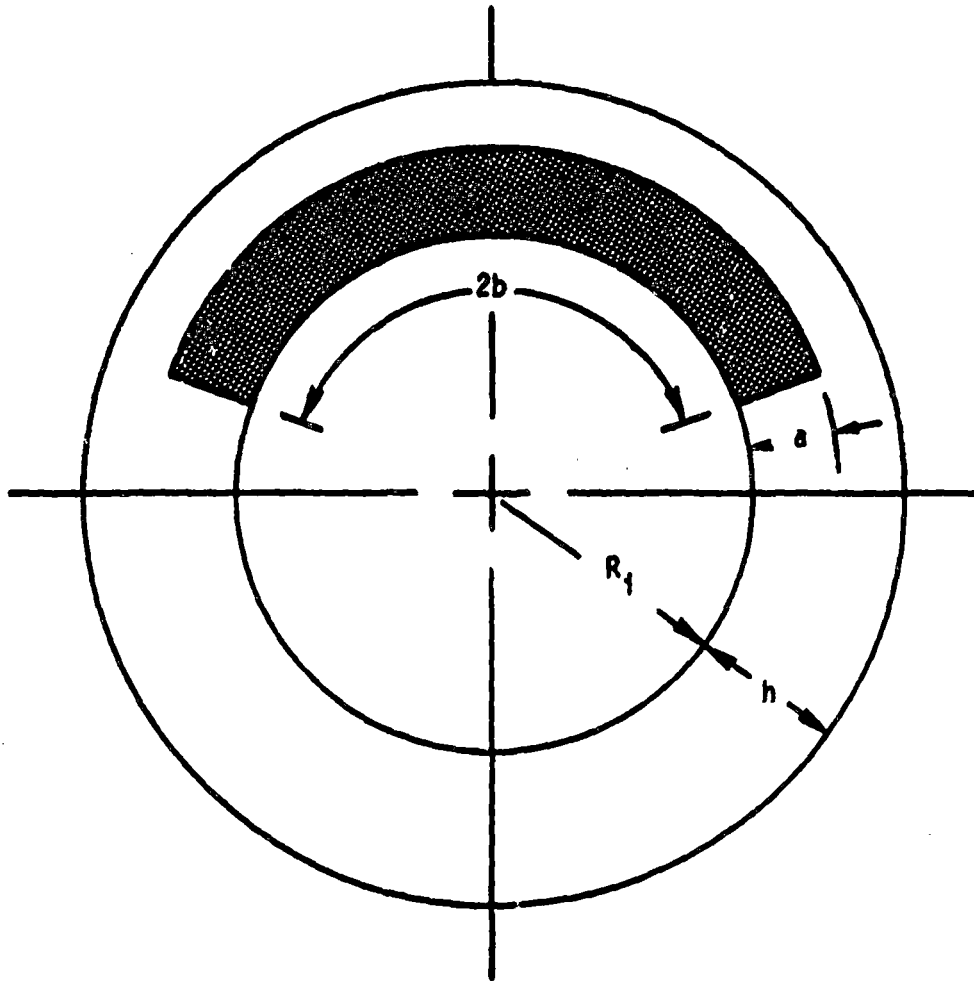


Figure 2-25. Geometry of Part-Circumferential Interior Surface Crack Used for Calculation of Critical Crack Area.

This concludes the discussion of the fracture mechanics model of piping reliability. Section 3 will present the numerical procedures developed to obtain results from this model. The combination of a bivariate crack size distribution with statistically distributed values of flow stress and fatigue crack growth characteristics precludes an analytical approach to this problem.

3.0 NUMERICAL SIMULATION PROCEDURES

The basic tools for the evaluation of the reliability of a circumferential girth butt weld in a reactor pipe were presented and discussed in Section 2.0. Basically, the probability of a leak or complete pipe severance occurring is equal to the probability of cracks larger than the critical size for each type of failure being present. The crack size distribution changes in time due to fatigue crack growth resulting from cyclic stresses induced during operation of the plant. In principle, such calculations are quite straightforward. However, in the present case, numerical techniques must be resorted to. This is because of the complexities involved in treating the bivariate crack size distribution, as well as the complicated nature of the stress history. However, the need to employ numerical techniques is even more acute when various input parameters are random. In the present case, the flow stress and fatigue crack growth characteristics are random variables. Hence, some numerical scheme is required in order to obtain actual results for the piping reliability.

One such numerical technique that is of general applicability is the "Monte Carlo" technique, which will be utilized here. Extensive literature on Monte Carlo techniques exists, with Hahn 67, Mann 74, Schreider 66, Hammersley 64 and Naylor 66 providing discussions of the procedures involved. In the present context, a Monte Carlo simulation can be illustrated by the following situation. Suppose that an estimate for the failure probability of a specific weld joint in the primary coolant system is required. In theory, a simple experiment could be performed. A set of N weld joints, each of which is representative of the joint that is actually in the system is fabricated. Even though these welds would have the same specifications as the joint actually in the system, they will not be identical to that joint or amongst themselves because of manufacturing tolerances, variations between batches of materials, and differences in welding conditions. Suppose next that each joint is subjected to a stress

history typical of the actual joint. Normal operations, anticipated transients, and earthquakes are included. The stress histories are not identical but are equally likely to occur during the plant lifetime. Two pieces of data are recorded for each of the samples:

- (1) the time the joint failed, and
- (2) whether the failure was induced by an earthquake.

The probability that a joint has failed at or before time t can be estimated by randomly selecting a crack. The probability of selecting a given crack size is controlled by the initial crack size distribution and detection probability (which was covered in Sections 2.3 and 2.4 respectively). The crack is then grown through a stress history, which can be either deterministic or stochastic. The fatigue crack relation is used in these calculations. This relation can be statistical, such as the lognormal distribution of C discussed in Section 2.5.1. A value of C is randomly selected from the distribution, and used in the crack growth calculation. The current crack size is then compared with the critical crack size at that time. A random value of u_{f10} is selected from the normal distribution of this parameter that was discussed in Section 2.5.2 in order to determine the critical crack size. In this way, the time-to-failure is evaluated if failure occurs before the end of the 40 year plant lifetime. If failure does not occur within 40 years, this fact is noted. This sampling is performed a large number of times on a computer, with statistics being gathered on the number of simulations that predict failure prior to time t , along with the total number of simulations performed. Let N be the total number of simulations, and $N_F^*(t)$ be the corresponding number of simulations that predict failure at or prior to t . Then, the probability that failure occurs at or before t is simply given by

$$P(t_F \leq t) = \frac{N_F^*(t)}{N} \quad (3-1)$$

The probability of an earthquake and failure occurring simultaneously is then simply the number of failures induced directly by an earthquake divided by the number of samples, or

$$P(\text{FAIL/EQ}) = \frac{N_{\text{EQ-FAIL}}}{N} \quad (3-2)$$

where $N_{\text{EQ-FAIL}}$ is the number of times the failure of the weld was induced by the earthquake. Although this experiment may never be performed with real joints and real stresses, an equivalent numerical experiment can be performed by modeling joints and stress histories on a computer.

In order to increase the computational efficiency, several simplifying assumptions are employed. The basis for the first assumption can be seen by expanding $p(t_F \leq t)$ in terms of conditional probabilities on the number of cracks in the weld joint, or

$$p(t_F \leq t) = \sum_{n=0}^{\infty} p(t_F \leq t|n)p(n) \quad (3-3)$$

where

$p(t_F \leq t|n)$ is the probability that a weld joint with n as-fabricated defects will fail at or before time t ,

and

$p(n)$ is the probability that n cracks will exist in the weld initially. This parameter was discussed in Section 2.3.4.

If crack initiation can be ignored, i.e., no cracks will form during the plant lifetime. Equation (3-3) then becomes

$$p(t_F \leq t) = \sum_{n=1}^{\infty} p(t_F \leq t|n)p(n) \quad (3-4)$$

where the summation index begins with $n=1$ rather than $n=0$, because

$$p(t_F \leq t | \bar{Eq}) = \frac{N_F(t)}{N} \quad (3-7)$$

and

$$p(t_F \leq t | Eq(g,t)) = \frac{N_F(g,t)}{N} \quad (3-8)$$

In Equation 3-7 the samples are subjected to stress histories which have no seismic events. $N_F(t)$ is the number of those samples which fail at or before time t . In Equation 3-8, the samples are subjected to an earthquake of magnitude g at time t . $N_F(g,t)$ is the number of those samples which fail at or before time t .

In principle, either empirical or tabulated functions could be derived which express $p(t_F \leq t | Eq(g,t))$ in terms of both the earthquake magnitude and the time. If the frequency of magnitude g earthquakes is available in the form of a conditional $G(g)$, the $p(t_F \leq t | Eq(g,t))$ can be weighted by $G(g)$ and integrated over all earthquake magnitudes to give the probability that an earthquake at time t will induce a piping failure, or

$$\begin{aligned} & p(\text{FAIL} | \text{Eq at } t | Eq(t)) \\ &= \int_0^{\infty} (p(t_F \leq t | Eq(g,t)) - p(t_F \leq t | \bar{Eq})) G(g) dg \end{aligned} \quad (3-9)$$

If Equation 3-9 is multiplied by the probability of earthquake per unit time and integrated over time, the result is the probability of a simultaneous earthquake and piping failure over the plant lifetime under the assumption that one earthquake occurs during the plant lifetime, or

$$\begin{aligned} p(\text{FAIL} | \text{Eq} | Eq) &= \int_0^T p(\text{FAIL} | \text{Eq} | Eq(t)) p(Eq(t)) dt \\ &= \int_0^T \frac{dt}{T} \int_0^{\infty} dg (p(t_F \leq t | Eq(g,t)) - p(t_F \leq t | \bar{Eq})) G(g) \end{aligned} \quad (3-10)$$

A computer program was specially written to implement Monte Carlo techniques for evaluation of structural reliability. The program concentrated on reactor piping weldments, and was tailored to include the facets of the fracture mechanics model outlined in Section 2.0. The resulting code is called PRAISE, which stands for "Piping Reliability Analysis Including Seismic Events." Details of the code, and its use, are presented by Lim 81, and additional relevant features will be summarized in the following sections.

3.1 Monte Carlo Simulation

The PRAISE computer code (Lim 81) uses Monte Carlo simulation techniques to estimate the distribution of time to first failure for a girth butt weld joint in nuclear reactor piping that is subjected to normal operating conditions, anticipated transients, and seismic events of various magnitude. PRAISE provides a numerical tool for obtaining results from the fracture mechanics model described in Section 2.0. The code is subject to the limitations and assumptions enumerated for the fracture mechanics model, and (as discussed above) is presently limited to analyzing welds having a single as-fabricated crack. Equations 3-1 and 3-2 are the basic equations in the PRAISE simulation. Succeeding portions of Section 3 describe in detail the algorithm that is used to obtain numerical values for the piping failure probabilities (right hand side of Equations 3-1 and 3-2).

A simplified flowchart of the PRAISE algorithm is shown in Figure 3-1. As shown on the right side of the chart, the six basic steps are:

- (1) sample space definition and stratification,
- (2) initial crack size selection,
- (3) next event simulation,
- (4) crack growth calculation,
- (5) leak detection or LOCA event, and
- (6) estimate of failure probabilities and associated confidence intervals.

Corresponding to each of these steps are various user-supplied inputs. The calculational steps and inputs are described in the following sections.

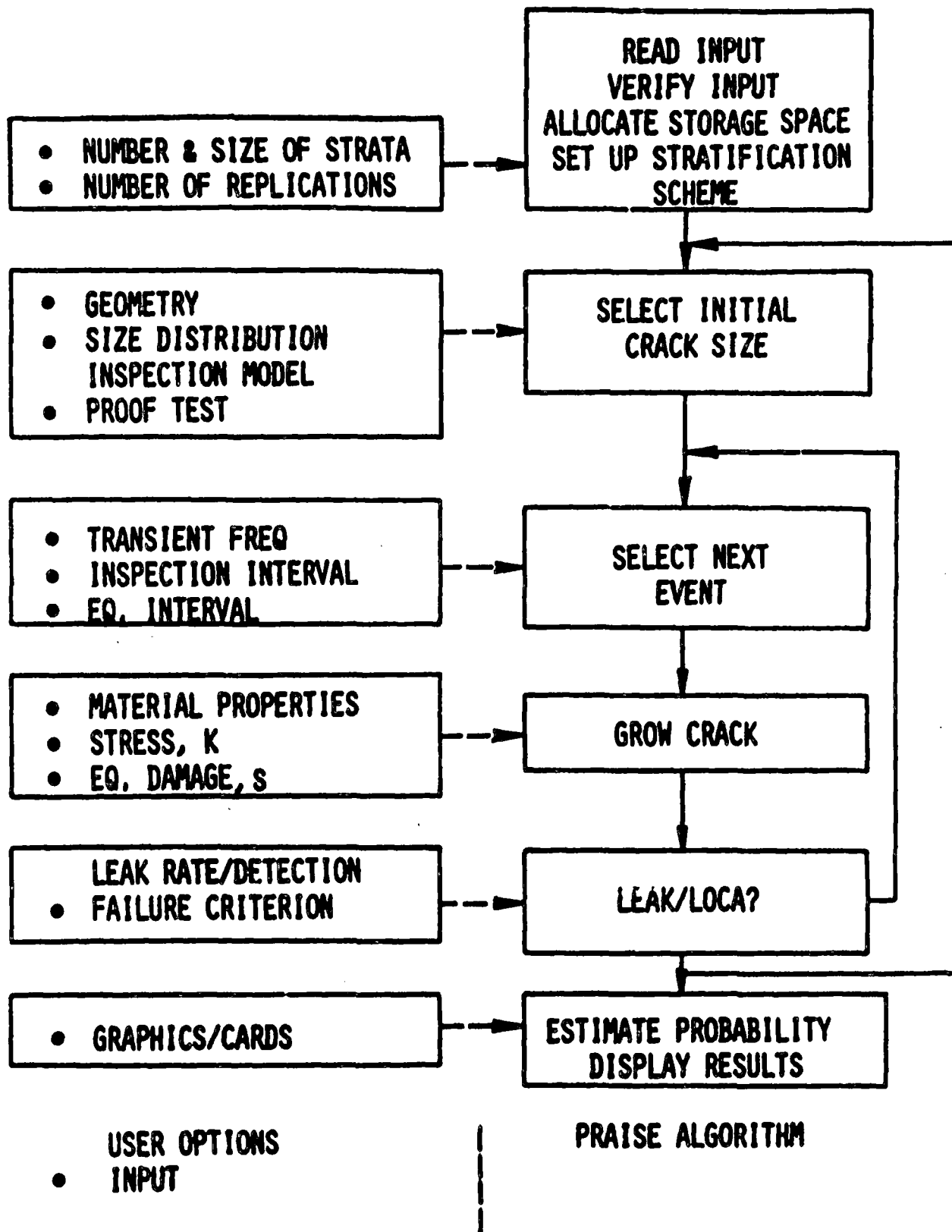


Figure 3-1. Simplified Praise Flowchart.

3.2 Sample Space Definition

A key ingredient in the PRAISE algorithm is the sample space representation of the Monte Carlo simulation. Several possibilities exist. The final choice was motivated largely by computational convenience. From a physical standpoint, the most natural choice for the sample space is a two-dimensional representation with surface crack length ($2b$) and crack depth (a) as the coordinates (see Figure 2-2 for crack geometry). Another possibility is to use crack depth and aspect ratio as the coordinates. These are also the variables that define the initial crack size distribution. The crack depth would lie between zero and the pipe wall thickness, while the aspect ratio is permitted to take values between one and infinity (values less than 1 are omitted from consideration, see Sections 2.2 and 2.3.2). Unfortunately, it is likely that the large value of aspect ratio could lead to some troublesome computational problems. A reasonable compromise is to use the reciprocal of the aspect ratio or $\beta^{-1} = a/b$ as one coordinate. The limits on β^{-1} become zero and one. The crack depth coordinate can be normalized by dividing by the wall thickness so that it also lies between zero and one. This representation of the sample space is displayed in Figure 3-2. Any crack with an (a/h) coordinate equal to one would be a through-wall defect and would cause a leak. Cracks with $(a/b) = 1$ are semi-circular defects. A small wedged-shaped portion adjacent to the $(a/b) = 0$ axis is infeasible because any crack located in this region would have lengths greater than the circumference of the pipe. The infeasible points satisfy

$$(a/b) < \frac{h}{2\pi R_1} (a/b) \quad (3-11)$$

The loci of all cracks that would cause a double-ended guillotine break is also shown in Figure 3-2. The following result is obtainable from the critical net section stress failure criterion discussed in Sections 2.5.2 and 2.9, using the relation for crack area in Section 2.9.

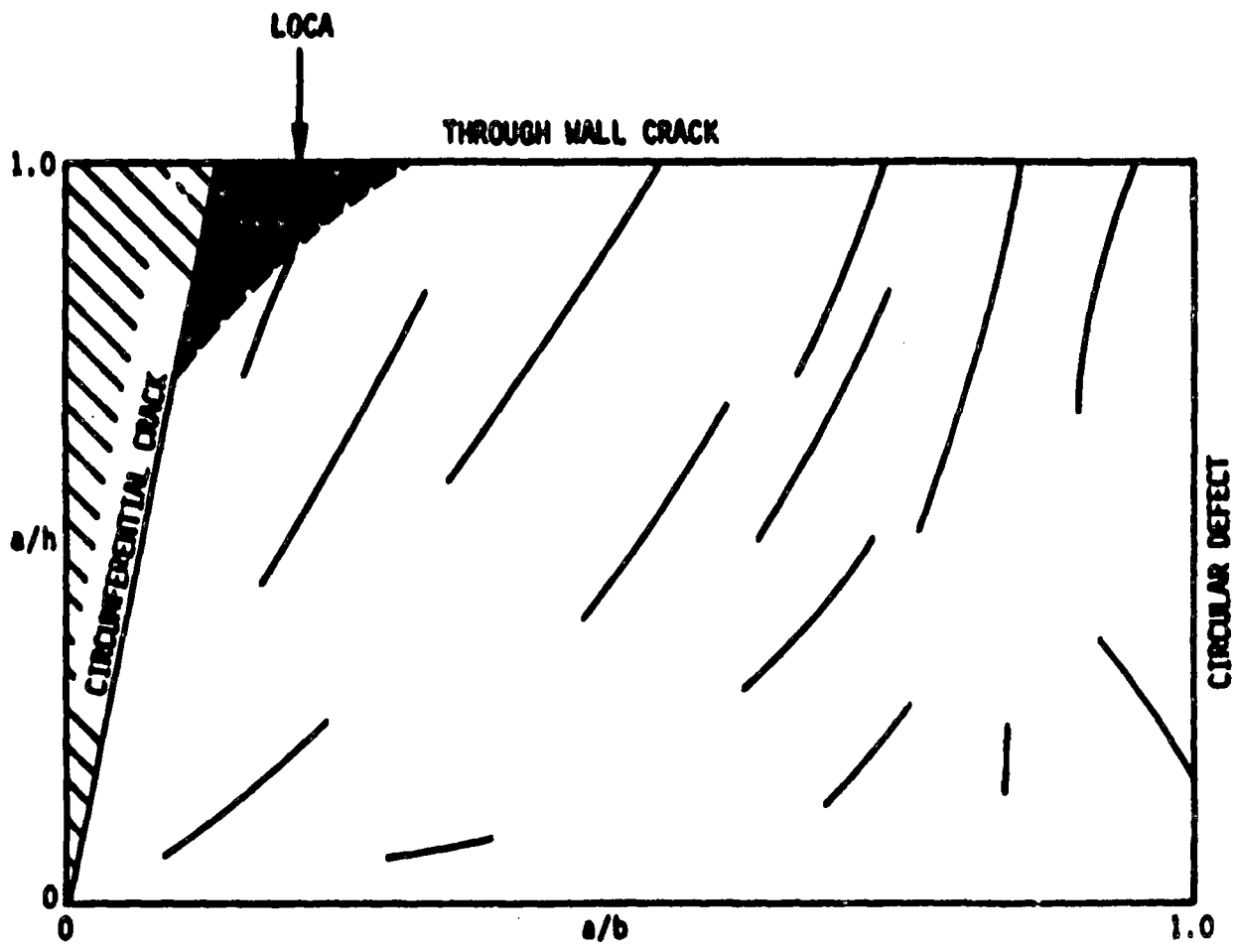


Figure 3-2 Sample Space for PRAISE Code.

$$B^{-1} = (a/b) \leq (1 - \frac{\sigma_{LC}}{\sigma_{f10}}) (\frac{A_{pipe}}{h^2}) \frac{1}{(a/h)^2 \left[2 + \left(\frac{a}{h} \right) \frac{h}{R_i} \right]} \quad (3-12)$$

As suggested by intuition, such cracks are both deep and long.

Typical crack growth trajectories are shown displayed on Figure 3-2. The trajectories are the loci of points showing the variation of crack dimensions with time as the crack grows under the cyclic loads. The crack depth variable is monotonically increasing, while the value of (a/b) is free to either increase or decrease during the crack propagation process, depending on the current aspect ratio and nature of applied stress. These trajectories are a vivid demonstration of the two-degree-of-freedom model discussed in Sections 2.6.1 and C.1, which is being used to represent crack growth in PRAISE. As discussed earlier (Section 2.1) many of the previous models either assumed a complete circumferential defect (cracks which satisfy the equality in Equation 3-11) or a constant aspect ratio [vertical lines in the (a/h) vs. (a/b) space]

If any of the cracks in the sample space were subjected to cyclic loads of sufficient magnitude for a long enough time, they would eventually cause a failure, either as a through-wall leak or a catastrophic complete pipe severance. Figure 3-2 shows that many of the failures would occur as part-through defects that would develop into a leak. If these leaks are not detected, the length of the crack would continue to increase (a/b decreasing) and ultimately reach the large LOCA region. Cracks which exhibit this sequence of leak and LOCA are said to have experienced "leak before break." On the other hand, it is possible to have combinations of initial crack size and stress histories that lead to a large LOCA without first undergoing a leak. Although PRAISE routinely handles both situations, it is not presently equipped to differentiate and display the fraction of LOCAs which experience the "leak before break" phenomena.

3.3 Stratified Sampling

A direct evaluation of Equation 3-1 and 3-2 using simple random sampling in which the initial crack dimensions are selected in accordance with their postulated frequencies of physically occurring is computationally inefficient. For example, suppose that a relatively large defect must exist before failure occurs. However, if the probability of obtaining a large initial defect is small, a very large number of simple random samples may be required before a statistically significant number of failures is obtained. Furthermore, since the quantity of interest is the probability of failure rather than the time-dependent crack size distribution, simulation of cracks which do not eventually lead to failure is, in some sense, a wasted effort. For the initial crack size distribution discussed in Section 2.3, the overwhelming majority of the cracks that exist would not lead to a failure within the plant lifetime.

A variety of well-established techniques exist for increasing the accuracy and computational efficiency of Monte Carlo simulations. These techniques are known by a variety of names, e.g., variance reduction methods, stratified sampling, biased sampling, or importance sampling (Mazumdar 75, McGrath 73, Naylor 66). For convenience in discussion, this report shall refer to the sampling scheme incorporated in PRAISE as the stratified sampling scheme. The basic idea is to partition the sample space into a set of mutually exhaustive cells or strata. A pre-determined number of samples are then selected from each cell. Within each cell, the individual crack dimensions are still selected according to the postulated initial crack size distribution. The distribution of time to first failure is then obtained by use of the following equations, which are modifications of Equations 3-1 and 3-2 to account for the conditional probability of a crack existing in a given cell.

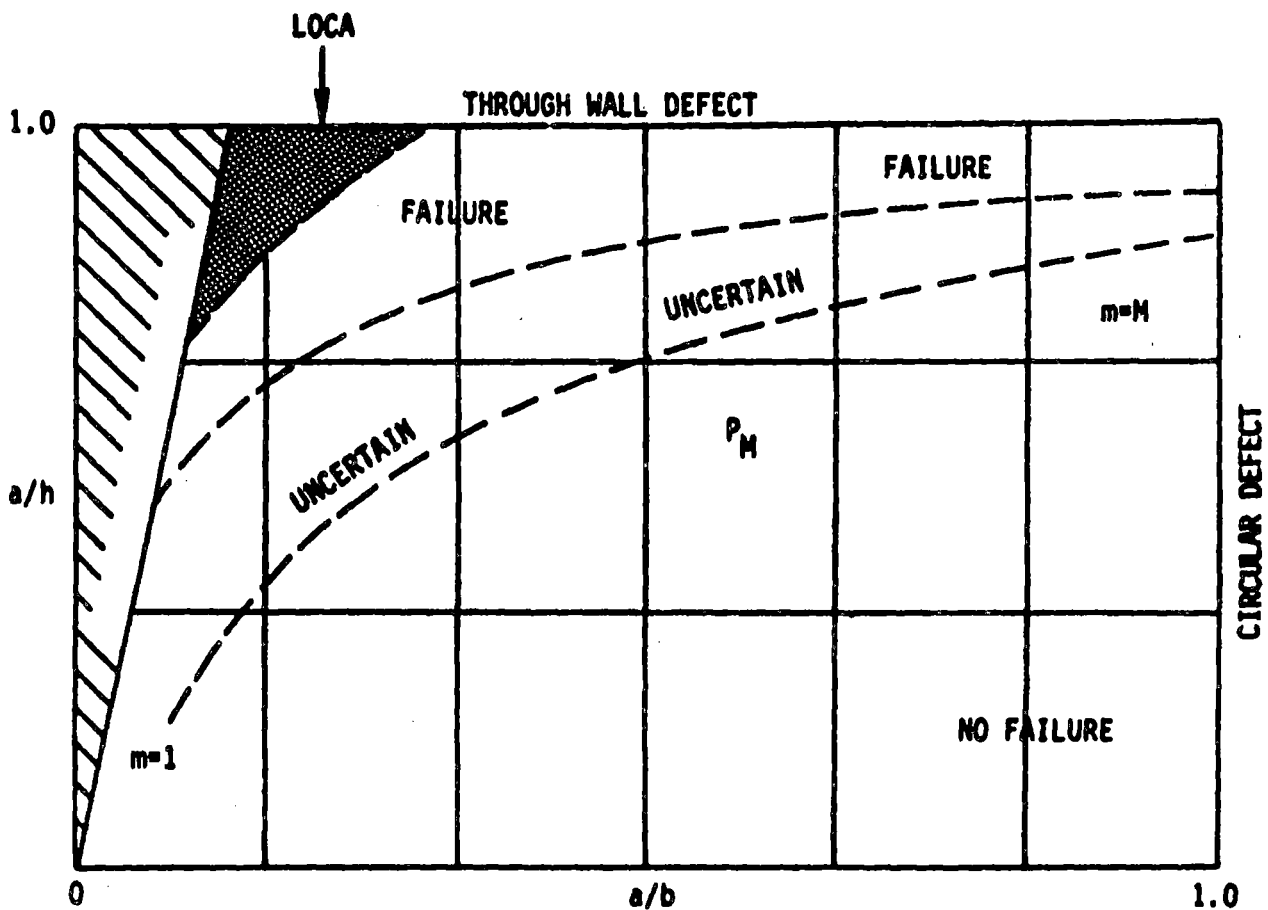
$$P(t_F \leq t | Eq) = \sum_{m=1}^M \frac{N_{F,m}(t)}{N_m} P_m \quad (3-13)$$

and

$$P(t_F \leq t | Eq(g, t)) = \sum_{m=1}^M \frac{N_{F,m}(g, t)}{N_m} P_m \quad (3-14)$$

where M is the total number of cells,
 N_m is the number of samples drawn from the m -th cell,
 $N_{F,m}(t)$ is the number of samples drawn from the m -th cell which have failed at or before time t ,
 $N_{F,m}(g, t)$ is the number of samples drawn from the m -th cell which experience failure at time t when subjected to an earthquake of magnitude g at t .
 P_m is the probability of an initial defect having coordinates within the boundaries of the m -th cell (given that a crack exists in the weld),
and

A typical stratification of the a/h , a/b sample space is illustrated in Figure 3-3. For illustrative purposes, three regions have been schematically identified. Points located in the upper portions of the sample space (near the LOCA or leak regions) are obviously more likely to result in failures than points near the lower portions of the sample space. A region of uncertainty exists between these fail and no-fail regions. In many cases computational experience with similar problems would allow one to draw with a high degree of confidence boundaries on the no-fail region. Since samples drawn from these regions would never lead to failure, a considerable computational improvement can be obtained by ignoring these cells in the sampling plan. In terms of Equations 3-13 and 3-14 the summation would be performed only over cells where there is failure or uncertainty regarding potential failure. Furthermore, a more efficient allocation of the total number of samples selected can be obtained by placing more of the samples into the uncertain region.



P_m = PROBABILITY OF INITIAL CRACK LYING IN CELL m

$$P(t_F \leq t) = \sum_{m=1}^M \frac{N_F(m,t)}{N_m} P_m$$

$N_F(m,t)$ = NUMBER OF REPLICATIONS FROM m -TH CELL IN WHICH FAILURE HAS OCCURRED BY TIME

N_m = NUMBER OF REPLICATIONS FROM m -TH CELL

Figure 3-3. Schematic Representation of Typical Stratification Employed in PRAISE Calculations.

3.4 Initial Crack Size Distribution

The initial crack size distribution described in Section 2.3 is defined in terms of the crack depth and the crack aspect ratio. The coordinates of the PRAISE sample space are normalized crack depth and the inverse aspect ratio, as was discussed in Section 3.2. This section describes the transformation of crack size variables required to obtain the PRAISE formulation. The algorithm used to select initial crack sizes from their respective cells is also discussed.

3.4.1 Transformation of Variables

Suppose that a two-dimensional joint probability density function is defined as $f(x_1, x_2)$ where x_1 and x_2 are the random variables. If new variables are defined by the functions g_1 and g_2^* such that

$$y_1 = g_1(x_1, x_2) \quad (3-15)$$

$$y_2 = g_2(x_1, x_2) \quad (3-16)$$

or

$$\underline{y} = G(x_1, x_2) = G(\underline{x}) \quad (3-17)$$

where \underline{x} and \underline{y} are vectors

$$\underline{x} = \begin{pmatrix} x_1 \\ x_2 \end{pmatrix} \quad (3-18)$$

$$\underline{y} = \begin{pmatrix} y_1 \\ y_2 \end{pmatrix} \quad (3-19)$$

and G is a generalized function

$$G = \begin{pmatrix} g_1(x_1, x_2) \\ g_2(x_1, x_2) \end{pmatrix} \quad (3-20)$$

* These g_1 functions are not to be confused with g_1 used in the influence functions of Appendix C.

how does one obtain the joint probability density function $p(y_1, y_2)$ for the transformed variables y_1 and y_2 ? Elegant formulations and solutions for this problem are presented in several intermediate probability texts (Hogg 70, Walpole72). Only the results are presented here.

Suppose that Equations 3-15 and 3-16 can be solved for the original variables x_1 and x_2 , i.e., an inverse function to $G(\underline{x})$ exists. If this inverse function is denoted by H , or

$$\underline{x} = H(\underline{y}) = \begin{pmatrix} h_1(y_1, y_2) \\ h_2(y_1, y_2) \end{pmatrix} \quad (3-21)$$

the transformed pdf is given by

$$p(\underline{y}) = f(H(\underline{y})) \left| \frac{\partial H}{\partial \underline{y}} \right| \quad (3-22)$$

where $\frac{\partial H}{\partial \underline{y}}$ is the Jacobian of the inverse transformation, or

$$\frac{\partial H}{\partial \underline{y}} = \begin{bmatrix} \frac{\partial h_1}{\partial y_1} & \frac{\partial h_1}{\partial y_2} \\ \frac{\partial h_2}{\partial y_1} & \frac{\partial h_2}{\partial y_2} \end{bmatrix} \quad (3-23)$$

and $\left| \frac{\partial H}{\partial \underline{y}} \right|$ is the absolute value of the determinant of that Jacobian.

For the PRAISE algorithm, the following associations can be made:

- $x_1 = a =$ crack depth
- $x_2 = b/a =$ aspect ratio
- $y_1 = a/h =$ normalized crack depth
- $y_2 = a/b =$ inverse aspect ratio

$$y_1 = x_1/h = g_1(x_1, x_2) \quad (3-24)$$

$$y_2 = 1/x_2 = g_2(x_1, x_2) \quad (3-25)$$

$$x_1 = hy_1 = h_1(x_1, x_2) \quad (3-26)$$

$$x_2 = 1/y_2 = h_2(x_1, x_2) \quad (3-27)$$

Note that h is the wall thickness and is not directly related to the inverse functions h_1 and h_2 . By taking the derivatives of h_1 and h_2 as defined in Equation 3-26 and 3-27, the Jacobian is

$$\frac{\partial H}{\partial \underline{y}} = \begin{bmatrix} h & 0 \\ 0 & -\frac{1}{y_2^2} \end{bmatrix} \quad (3-28)$$

and

$$\left| \frac{\partial H}{\partial \underline{y}} \right| = h/y_2^2 \quad (3-29)$$

Equation 3-14 can now be written as

$$p(\underline{y}) = f(hy_1, 1/y_2)(h/y_2^2) \quad (3-30)$$

Recall that the original random variables were assumed to be independent (see Section 2.3). This means that the

$$p(a, \beta) = f(x_1, x_2) = f_1(x_1)f_2(x_2) = p_a(a)p_\beta(\beta) \quad (3-31)$$

The joint pdf is simply the product of the marginal density functions $f_1(x_1)$ and $f_2(x_2)$. Under the assumption of independence, Equation 3-30 becomes

$$p(\underline{y}) = f_1(hy_1) f_2(1/y_2)(h/y_2^2) \quad (3-32)$$

$$p(y) = p_1(y_1) p_2(y_2) \quad (3-33)$$

where

$$p_1(y_1) = hf_1(hy_1) = hf_1\left[h(a/h)\right] \quad (3-34)$$

$$p_2(y_2) = f_2(1/y_2)(1/y_2^2) = f_2\left(\frac{1}{a/b}\right) \frac{1}{(a/b)^2} \quad (3-35)$$

Hence, the joint pdf for the new variables (a/h) and (a/b) is the product of the marginal density functions of these variables.

In order to be consistent with the formulation of the fracture mechanics model in Section 2, the PRAISE code is designed to accept as inputs the parameters which define the crack depth and aspect ratio probability density functions. PRAISE is capable of treating crack depth and aspect ratio as being either exponential or lognormal distributions. These distributions are then transformed according to the procedures outlined above. The formulas used by PRAISE are given below:*

(1) For crack depth exponentially distributed (see Equation 2-5)

$$p_a(a) = \frac{1}{\mu(1-e^{-h/\mu})} e^{-a/\mu} \quad 0 < a < h \quad (3-36)$$

$$p_1(a/h) = p_1(\alpha) = h p_a(h\alpha) = \frac{h}{\mu(1-e^{-h/\mu})} e^{-ah/\mu}$$

$$p_1(\alpha) = \frac{1}{\mu'(1-e^{-h/\mu})} e^{-\alpha/\mu'} \quad (3-37)$$

* The equations in the succeeding sections are in the notation used in Section 2, which is not directly the same as that employed by Lim 81. Use caution in directly comparing parameters here with those in Lim 81.

$$\text{where } \mu' = \mu/h \quad (3-38)$$

(2) For crack depth lognormally distributed.

In order to make PRAISE more generally applicable, a lognormal distribution of crack depths will also be considered, even though such a distribution will not be employed in this particular investigation. In the following expressions, corrections for the impossibility of having $a > h$ will be omitted. Such "corrections" are small if the predicted probability that $a > h$ is very small. In this case (Hahn 67, Hasting 74)

$$f_1(a) = \frac{1}{\sigma a (2\pi)^{1/2}} e^{-\frac{1}{2\sigma^2} (\ln a/a_{50})^2} \quad (3-39)$$

$$\begin{aligned} p_1(a/h) &= p_1(\alpha) = h f_1(\alpha h) \\ &= \frac{1}{\alpha \sigma (2\pi)^{1/2}} e^{-\frac{1}{2\sigma^2} (\ln \alpha/\alpha_{50})^2} \end{aligned} \quad (3-40)$$

$$\text{where } \alpha_{50} = a_{50}/h. \quad (3-41)$$

In Equation 3-39, a_{50} is the median of the distribution while σ is the standard deviation of $\ln a$ (not the standard deviation of a).

For both the exponential and lognormal distributions, the new pdf has the same form as the old pdf, but with slightly modified parameters. The new rate parameter in the exponential is h times the old rate parameter, while the median in the new lognormal is $1/h$ times the old median.

(3) Aspect ratio is exponentially distributed (see Equations 2-7 and 2-9

$$f_2(b/a) = p_\beta(\beta) = \frac{1}{\lambda} e^{-(\beta-1)/\lambda} \quad \beta > 1 \quad (3-42)$$

$$p_2(a/b) = p_2(\beta^{-1}) = f_2\left(\frac{1}{\beta/b}\right)/(a/b)^2$$

$$\frac{1}{\lambda(\beta^{-1})^2} e^{-\left(\frac{1}{\beta^{-1}} - 1\right)/\lambda} \quad \beta^{-1} < 1 \quad (3-43)$$

(4) Aspect ratio is lognormally distributed (see Equations 2-11 to 2-13).

$$f_2(b/a) = p_\beta(A) = \frac{C_\beta}{\lambda\beta(2\pi)^{1/2}} e^{-(\ln \beta/\beta_m)^2/(2\lambda^2)} \quad (\beta > 1)$$

(3-44)

$$p_2(a/b) = p_2(\beta^{-1}) = f_2(1/\beta^{-1})/(\beta^{-1})^2$$

$$= \frac{C_\beta}{\lambda\beta^{-1}(2\pi)^{1/2}} e^{-[\ln 1/(\beta^{-1}\beta_m)]^2/(2\lambda^2)} \quad (\beta^{-1} < 1) \quad (3-45)$$

In the two cases of the aspect ratio considered above, the new probability density function (for a/b) does not have the same functional form as the old probability density function. On the other hand, the parameters which describe the new distributions have the same numerical values as in the old distributions.

3.4.2 Pre-Service Inspection and Hydrostatic Proof Test

Prior to its first start-up, the primary coolant system of a nuclear reactor undergoes several pre-service inspections designed to detect as-fabricated defects. Such defects are found with a probability depending on their size. The estimated applicable detection probabilities for an ultrasonic inspection were reviewed in Section 2.4. In accordance with the assumptions enumerated in Section 2.2, all detected defects are assumed to be repaired, with such repairs not inducing any additional defects or other detrimental factors. Hence, the pre-service inspection, as well as any in-service inspection will have an influence on the crack

size distribution. Additionally, the piping is subjected to a hydrostatic proof test to pressures higher than will be encountered under service conditions. The fact that a pipe survived the proof test allows the crack size distribution to be truncated at the critical size corresponding to the proof conditions. If cracks larger than that size had existed prior to the proof, then the pipe would not have survived the proof. Hence, the initial crack size distribution employed is altered by the proof test.

The criterion for failure during the hydrostatic proof test is the same as that employed for a complete pipe severance during normal plant operation. The latter was discussed in Section 2.9, and can be stated as follows (see Equation 2-36)

$$(A_p - A_{\text{crack}}) \sigma_{f10} > A_p \sigma_{LC} \quad (3-46)$$

where the load-controlled stress consists of the deadweight and hydrostatic pressure stress contributions,

For a thin-walled cylinder ($h \ll R_1$), the following approximation can be made for σ_{PH}

$$\sigma_{PH} \sim \frac{(\text{Pressure})R_1}{2h} \quad (3-47)$$

Two general approaches exist for incorporating the influence of pre-service inspections on the estimates of failure probability. Suppose that the non-detection probability in an ultrasonic test is given by $P_{ND}(a,b)$ where a and b are the crack depth and crack length, respectively. One approach is to simulate the test explicitly. For example, an initial crack is selected according to the postulated crack size distribution. A random number r that is uniformly distributed between 0 and 1 is then selected and compared to $P_{ND}(a,b)$. If $r > P_{ND}(a,b)$, the crack is assumed to be detected and corrective action is taken. Otherwise crack growth is simulated. Each selection of an initial crack size is treated as one of the samples included in the N and N_m that appear in the denominator of Equations 3-1, 3-2, 3-13, and 3-14. Cracks that are detected do not contribute to the samples which fail. Although this scheme is straight-

forward it may in fact be computationally inefficient. When the probability of non-detection is small, the majority of the defects that lead to failure will be rejected. Hence, only a relatively small number of cracks is actually simulated through the lifetime of the plant. This would result in large variances and large confidence intervals.

Another approach is to grow each crack that is sampled, but to correct the summation in Equations 3-1, 3-2, 3-13, and 3-14 to reflect the influence of non-detection. Rather than adding the number of failures that are observed, this approach would add the P_{ND} associated with the cracks that failed. This procedure can be illustrated by referring to Table 3.1. For simplicity consider first the case of simple random sampling. Suppose that N as-fabricated defects have been selected. The P_{ND} column gives the probability that the crack was not detected. The F_n column presents results from a hypothetical simulation in which random numbers are selected and compared with P_{ND} . A zero indicates that the crack was detected (failed to escape detection i.e., $r > P_{ND}$). Otherwise $r \leq P_{ND}$ and a one is recorded. If N_E is the number of samples that escape detection, the ratio $\frac{N_E}{N}$ asymptotically approaches P_{ND} . The failed column gives results from a simulation in which crack growth is simulated, regardless of whether it is detected. A one in the F_n column indicates that the n -th sample would lead to failure if not detected, while a zero indicates no failure over the lifetime of the plant. N_f is the number of failures in N samples without crack detection. In the direct approach, the only failures would be cracks that escaped the detection in the pre-service inspection ($E_n = 1$) and then grew to failure within the plant lifetime ($F_n = 1$). N_{EF} is the number of cracks in N samples that escape detection and also fail. The failure probability is estimated by the ratio

$$P_F = \frac{N_{FE}}{N} \quad (3-48)$$

In the second approach, each failure is weighted by the probability of non-detection or

$$P_F = \frac{1}{N} \sum_{n=1}^N P_{ND,n} F_n \quad (3-49)$$

Table 3-1

Illustration of Procedure Used in Monte Carlo Simulation to Account for Influence of Pre-Service Inspection.

Sample	P_{ND}	E Spaced Detection	F_n	Product
1	.02	0	1	0
2	.06	0	1	0
3	.15	1	1	1
4	.04	0	0	
5	.10	0	0	
.				
.				
.				
N	.09	$\frac{1}{N_E}$	$\frac{1}{N_F}$	$\frac{1}{N_{EF}}$

Since $F_n = 0$ when there is no failure, Equation 3-48 is equivalent to adding the P_{ND} of the cracks that fail.

A third and more sophisticated approach is to combine the postulated crack size distribution with the non-detection probability and hydrostatic proof test to create a post-inspection joint pdf. The initial crack sizes would then be drawn from this post-inspection joint pdf.

The second approach is presently being used in PRAISE. Computationally speaking, it is more efficient than the direct approach. It requires a minimal change in coding. On the other hand, an application of the third approach requires either that the post-inspection pdf be input by the user or that a specialized procedure be developed to combine the initial crack size distribution with the non-detection probabilities. These requirements would impose unnecessary additional calculations.

The analysis of a hydrostatic proof test is slightly less involved than the ultrasonic inspections. All three approaches are identical because the hydrostatic test is assumed to give perfect results. P_{ND} is exactly one if the conditions of Equation 3-46 are satisfied. Hence, cracks in the failure region corresponding to proof test conditions have absolutely no chance of causing a failure under service conditions unless crack growth occurs, or higher stresses are imposed. The present assumption is that cracks in the failure region would be removed and a new initial crack size selected.

3.5 Arrival Time for Events

The PRAISE algorithm may be broadly classified as a next event simulation in which the calculation proceeds from event to event during the reactor lifetime. Thus, it is necessary for the simulation to model the arrival of various events. From an operational point of view, each point in time at which some calculation is performed is signaled by an event. According to this definition, events include the following:

The PRAISE algorithm may be broadly classified as a next event simulation in which the calculation proceeds from event to event during the reactor lifetime. Thus, it is necessary for the simulation to model the arrival of various events. From an operational point of view, each point in time at which some calculation is performed is signaled by an event. According to this definition, events include the following:

3.5 Arrival Time for Events

The analysis of a hydrostatic proof test is slightly less involved than the ultrasonic inspections. All three approaches are identical because the hydrostatic test is assumed to give perfect results. P_{ND} is exactly one if the conditions of Equation 3-46 are satisfied. Hence, cracks in the failure region corresponding to proof test conditions have absolutely no chance of causing a failure under service conditions unless crack growth occurs, or higher stresses are imposed. The present assumption is that cracks in the failure region would be removed and a new initial crack size selected.

A third and more sophisticated approach is to combine the postulated crack size distribution with the non-detection probability and hydrostatic proof test to create a post-inspection joint pdf. The initial crack sizes would then be drawn from this post-inspection joint pdf. Computational approach is presently being used in PRAISE. Computationally speaking, it is more efficient than the direct approach. It requires a minimal change in coding. On the other hand, an application of the third approach requires either the post-inspection pdf be input by the user or that a specialized procedure be developed to combine the initial crack size distribution with the non-detection probabilities. These requirements would impose unnecessary additional calculations.

Since $F_{ND} = 0$ when there is no failure, Equation 3-48 is equivalent to adding the P_{ND} of the cracks that fail.

- (a) startup or shutdown,
- (b) occurrence of anticipated transients,
- (c) pre-service and in-service inspection time, and
- (d) earthquake evaluation times.

The frequency of arrival for these events is controlled by the user. Additional discussions related specifically to Zion I will be presented in Section 4.

The times at which startup/shutdown and anticipated transients occur can be uniformly spaced throughout the plant lifetime or appear randomly in the plant lifetime. In the stochastic case, the events are assumed to be part of a Poisson process. Each transient type will be governed by a separate intensity λ_i . The distribution of inter-arrival times is exponential, or for the i -th transient type

$$f_i(t) = \lambda_i \exp(-\lambda_i t) \quad (3-50)$$

The intensity λ_i represents the average number of events in a unit time. The reciprocal ($= \lambda_i^{-1}$) is the mean time between arrivals of the i -th transient.

If the user desires to model pre-service inspections, they will naturally occur at the beginning of each replication. In-service inspections and earthquake evaluation times are determined inputs supplied by the user. These can occur either uniformly spaced (with input time interval) or arbitrarily specified (though still deterministic) throughout the plant lifetime.

Additional discussion relevant specifically to reactor piping will be included in Section 4.

3.6 Crack Growth Calculation

The two-degree-of-freedom fatigue crack growth model in PRAISE consists of the following four basic steps:

- (1) identify the condition causing the crack growth (heatup/cooldown or anticipated transient),
- (2) calculate the corresponding values of the effective RMS stress intensity factor,
- (3) evaluate the increase in crack depth and crack length, and
- (4) determine whether the expanded crack will lead to pipe failure.

A flowchart of the PRAISE crack growth algorithm is shown in Figure 3-4. The equations representing the crack growth characteristics were extensively discussed in Section 2.6.1 and related sections. The equations employed were summarized as Equation 2-39. The parameter C in the growth relation can be treated in PRAISE either as a user input constant, or as a lognormally distributed random variable which changes from replication to replication. The appropriate distribution of C for austenitic piping materials was presented in Section 2.5.1.

For purposes of calculating K_{min} and K_{max} , the loading conditions may be classified either as

- (a) uniform through-the-wall stresses, or
- (b) non-uniformly distributed through-the-wall stresses, such as radial gradient thermal stresses and welding residual stresses.

For uniform through-the-wall stresses, the present model assumes that

$$K_{max}(1) = \sigma_{max} a^h Y_1\left(\frac{a}{h}, \frac{b}{a}\right)$$

$$K_{min}(1) = \sigma_{min} a^h Y_1\left(\frac{a}{h}, \frac{b}{a}\right)$$

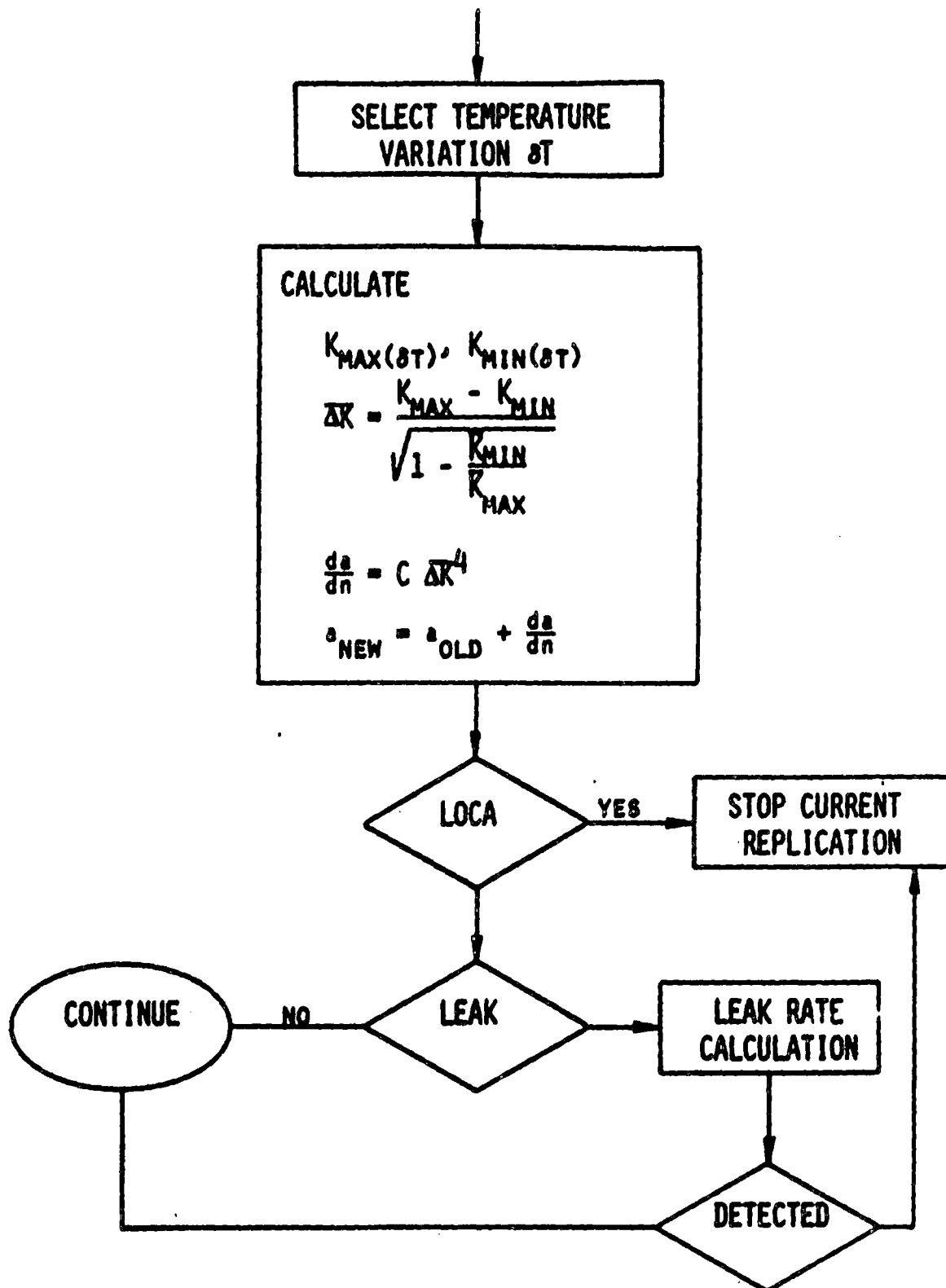


Figure 3-4 Algorithm for Crack Growth Calculations.

where

σ_{\min} and σ_{\max} are the minimum and maximum values of the uniform through-the-wall stresses, a is the crack depth, and

$$Y_1\left(\frac{a}{h}, \frac{b}{a}\right)$$

is a function that relates σ to K_1 (i being associated with the "degree of freedom," a or b). In the cold shutdown condition, the only contribution to the uniform stress is the deadweight. On the other hand, in the hot operating condition there are contributions from the deadweight, pressure, and thermal expansion. For the specific case of a heatup/cooldown cycle,

$$\sigma_{\min} = \sigma_{DW}$$

$$\sigma_{\max} = \sigma_{DW} + \sigma_p + \sigma_{TE}$$

PRAISE currently assumes that radial gradient thermal stresses are the only contributors to non-uniform through wall stresses. Since these stresses are associated with temperature transients, they will be superimposed onto the normal operating stresses. Hence $K_{\min}(i)$ and $K_{\max}(i)$ consist of contributions from both the uniform through the wall operating stress and the transient-dependent non-uniform through-wall stresses, or

$$K_{\min}(i) = K_{op}(i) + \Delta K_{\min}\left(j, \frac{a}{h}, \frac{a}{b}, \Delta T_j\right)$$

$$K_{\max}(i) = K_{op}(i) + \Delta K_{\max}\left(j, \frac{a}{h}, \frac{a}{b}, \Delta T_j\right)$$

where j denotes the transient type, and

ΔT is the temperature variation during the transient.

$K_{op}(i)$ is the normal operating $K_1(i)$. See Section 2.6.2 for additional discussion.

The temperature variation is displayed explicitly in $K_{min(i)}$ and $K_{max(i)}$ because it might not be the same in each occurrence of a particular transient type. PRAISE accomodates these differences in temperature variation by treating ΔT as a random variable. The PRAISE formulations for K_i for transients producing radial gradient thermal stresses can be expressed as follows

$$K_{max(i)} = \Delta T a^{1/2} g_{max(i)} \left(\frac{a}{h}, \frac{b}{a} \right)$$

$$K_{min(i)} = \Delta T a^{1/2} g_{min(i)} \left(\frac{a}{h}, \frac{b}{a} \right)$$

This is consistent with the treatment of the stress intensity factors due to radial gradient thermal stresses presented in Section D.4.

In general, a pdf will be supplied by the user to describe the distribution of ΔT for each transient type. The coding used by PRAISE to evaluate the above g functions is included in Chapter 5 of Lim 81.

The preceding equations are applicable as long as the crack depth is less than the wall thickness. When $a > h$, the crack growth relationship is modified in accordance with discussions in Section 2.6.2.

After each increment of crack growth, the crack is examined to determine whether it has reached a depth equal to the pipe wall thickness, or will lead to a double-ended guillotine break. As shown in Section 2.9, this failure criterion for a double-ended break is based on the exceedance of a critical net section stress, or

$$(A_p - A_{crack})\sigma_{f10} \geq A_p \sigma_{LC} \quad (3-51)$$

The user has the option of treating σ_{f10} either as a constant to be used throughout the calculation or a normally distributed random variable that varies from replication to replication. In the latter case, the user specifies the mean and standard deviation of the normal distribution.

The relevant distribution for austenitic piping materials was discussed in Section 2.5.2. The load controlled stress is defined by

$$\sigma_{LC} = \sigma_{DW} + \sigma_p \quad (3-52)$$

If the crack is a through-wall defect (but does not produce a large LOCA), a leak rate calculation is performed using procedures outlined in Section 2.8. PRAISE is designed to maintain statistics on the number of "small" leaks and the number of "big" leaks. The user is expected to provide a value of leak rate which represents the threshold between small and big leaks.

The leakrate is also used in conjunction with a leak detection model to determine whether a given leak can be detected. The current leak detection model has a user-specified leak detection threshold. Any leak with a rate greater than this threshold is assumed to be detected and lead to a plant shutdown with subsequent corrective maintenance.

3.7 Influence of Earthquakes on Crack Growth

Seismic events occur at random times and with random magnitudes. It would be inefficient to simulate earthquakes as stochastic processes in the PRAISE code. The probability of a significant earthquake within a 40 year period is generally low, so that many plant life times would have to be simulated in order to generate a sufficiently large sample to confidently estimate the influence of seismic events on piping reliability. This is somewhat analagous to the problem discussed earlier associated with randomly sampling the crack size distribution. That problem was circumvented by using stratified sampling. In the case of seismic events another approach will be taken. In this case, the influence of specified earthquakes of a given magnitude and times of occurrence will be evaluated. For example, the influence of a safe shutdown earthquake (SSE) occurring 20 years into the plant lifetime can be considered. Such results can then be used in conjunction with information on the probability of such an event occurring at that time to provide estimates of the probability of a seismically induced piping failure.

Within each replication, PRAISE periodically evaluates the instantaneous effect of seismic events on the crack growth. The times at which these evaluations take place are known as "evaluation" times, and are provided by the user. These times may be either placed at regularly spaced intervals or arbitrarily specified throughout the plant lifetime. Since earthquakes have a continuum of magnitudes and stress-time histories, the "evaluation" earthquake is actually a series of earthquakes. It is envisioned that several earthquake magnitude categories, spanning the credible values at a given site will be included. Within each magnitude category, several earthquakes will be examined. These will be treated as representative and equally likely to occur at that magnitude. At each "evaluation" time, the current crack is subjected to each of the postulated earthquakes. The earthquake evaluation algorithm is shown in Figure 3-5. The case of only one earthquake occurring during the life at the plant will be considered here.

The treatment of crack growth during seismic events is somewhat different than crack growth under normal operation or anticipated transients. Fatigue crack growth due to non-seismic events can be characterized by a single loading cycle of known magnitude. Relationships of the form

$$a_{\text{new}} = a_{\text{old}} + CR_a^4 \quad (3-53)$$

are very convenient for predicting the crack growth under single cycle loadings. An analogous equation for b also exists. Seismic events characteristically have many cycles, each of which may have a different amplitude. A cycle-by-cycle crack growth analysis would require repeated applications of the above equation, and consequently repeated evaluation of R_f' . This approach is time consuming. A reasonable compromise is the approach discussed in Section 2.6.2, which employs the S-factor. Assuming that a does not change much during the cycling considered, the following relation is obtained from the expression immediately above Equation 2-40 along with the definition of S given in Equation 2-40.

$$a_{\text{new}} = a_{\text{old}} + C S^4 \gamma_a^4 a_{\text{old}}^2 \quad (3-54)$$

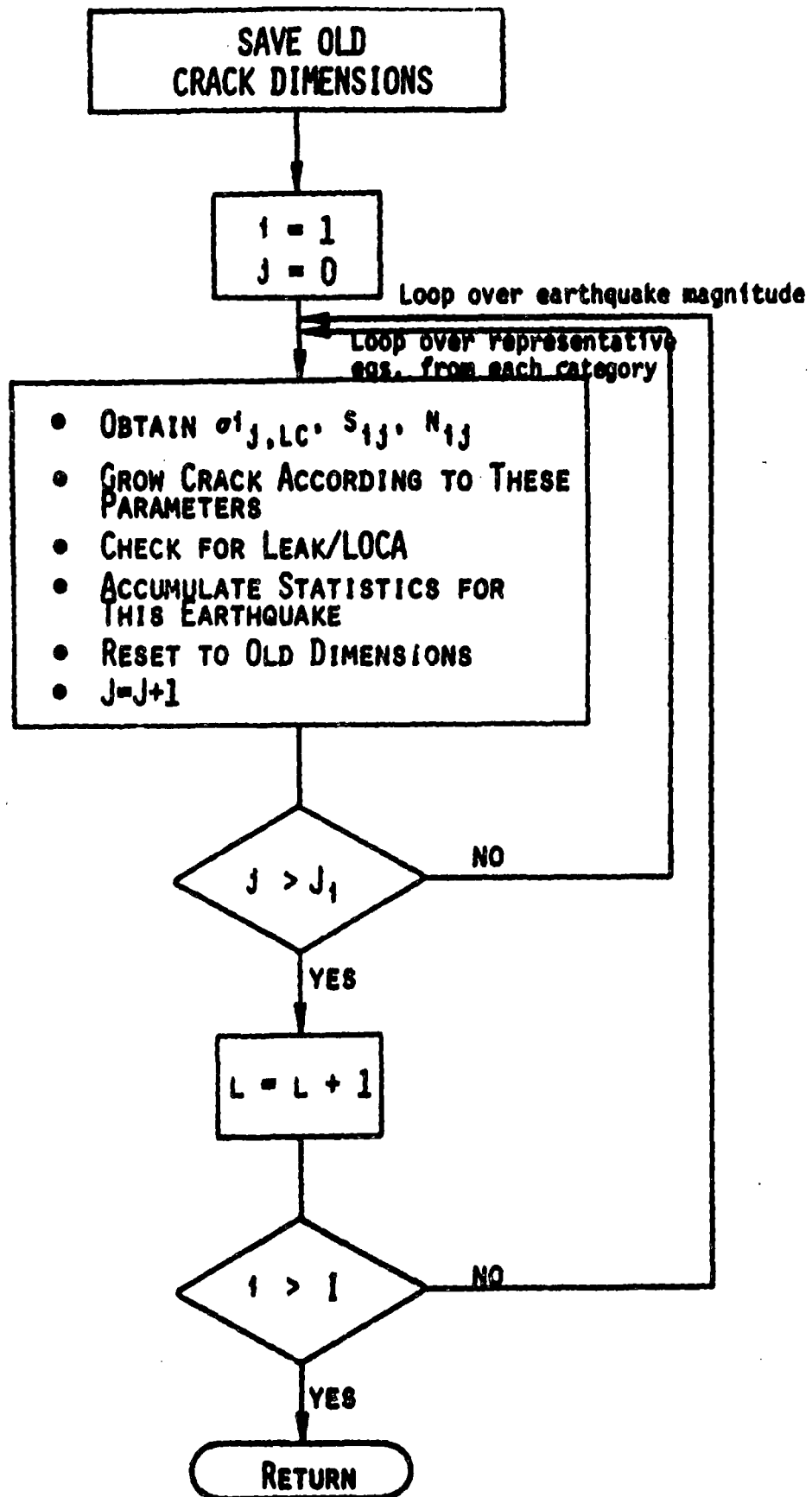


Figure 3-5 Algorithm for "Evaluation" Earthquakes.

In the case of seismic events, a_{old} and a_{new} are the crack depths before and after the seismic event. An expression analogous to 3-54 is applicable to growth in the b direction (which is the other "degree-of-freedom"). After each "evaluation" earthquake and corresponding increment of crack growth, the crack is examined for leak or LOCA. The appropriate load controlled stress to be used in the failure criterion is

$$\sigma_{LC} = \sigma_{DM} + \sigma_p + \sigma_{EQ}$$

where σ_{EQ} is the maximum stress experienced by the joint during the earthquake. Values of σ_{LC} applicable to seismic events are presented in Table 1-3. This is a conservative approach because the worst load controlled stress is applied to the maximum crack size. Within a single seismic event, it is conceivable that a crack can proceed from a safe condition to a leak and ultimately a LOCA. Since the temporal extent of the earthquake is very short, leak detection will be ineffective in shutting down the plant if a leak should occur during the earthquake. Hence, all comparisons for leak and LOCA are performed after the earthquake has occurred.

The effects of the evaluation earthquake are removed, i.e., the crack dimensions are reset to their pre-evaluation values, after each application of the evaluation earthquake. In order to further clarify this point, consider the sample space shown in Figure 3-6. The line $a_1 a_2 a_3 a_4$ is the so-called crack trajectory in the absence of the earthquake. Suppose that "evaluation" earthquakes are desired at times corresponding to points a_1 , a_2 and a_3 . The resulting crack dimensions are schematically represented by the points a_1' , a_2' , a_3' . Since a_1' and a_2' have a/h have values less than 1.0 and are not in the LOCA region, earthquakes at times t_1 and t_2 would not lead to failure. On the other hand, an earthquake at time t_3 would cause a through wall defect. PRAISE records at each evaluation time the number of leaks and LOCAs that result from a single earthquake at that time. It is important to recognize that once the "evaluation" is performed, the crack size is returned to its pre-evaluation value and the simulation proceeds. In other words, points on the crack trajectory are not influenced by the "evaluation" earthquakes.

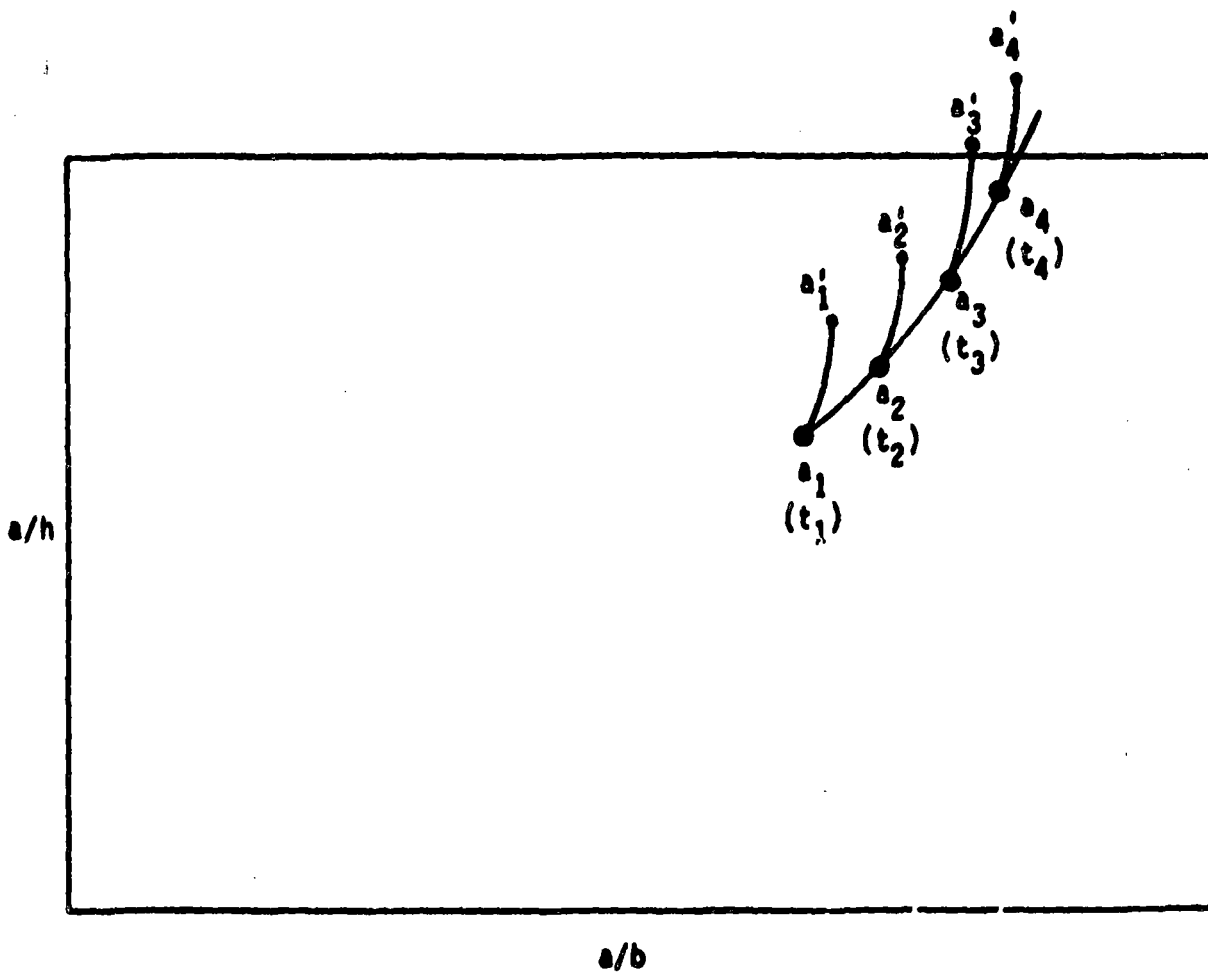


Figure 3-6. Schematic Representation of Crack Growth Trajectories Including Influence of "Evaluation" Earthquakes.

3.8 Probability Estimates and Their Sampling Errors

Since a Monte Carlo technique has been used to estimate the failure probabilities, these estimates will have some sampling errors. Therefore PRAISE also calculates the variance of these probabilities. The variances can be used to construct confidence intervals for the estimated probabilities. In order to derive the appropriate relationships, consider first the case of simple random sampling and no earthquakes. In accordance with Equation 3-1, $F(t)$, the estimator for the probability of failure at or before time t , is given by

$$F(t) = \frac{N_F(t)}{N} \sim P(t_F \leq t) \quad (3-55)$$

where

N is the total number of replications

$N_F(t)$ is the number of replications which have grown to failure at or before time t , and

$P(t_F \leq t)$ is the true, but unknown, probability that the weld has failed at or before time t .

The estimator $F(t)$ is simply the proportion of the samples which have failed at or before time t . At any time during a given replication, the weld joint is in one of two mutually exclusive states; namely failed or not failed. Suppose that a Bernoulli random variable $I_n(t)$ is defined by

$$I_n(t) = \begin{cases} 1 & \text{if the weld is failed at time } t, \\ 0 & \text{if the weld is not failed at time } t. \end{cases} \quad (3-56)$$

The subscript n indicates the particular replication.

In terms of $I_n(t)$, the number of failures is given by

$$N_F(t) = \sum_{n=1}^N I_n(t). \quad (3-57)$$

while the proportion of failures is estimated by

$$F(t) = \frac{1}{N} \sum_{n=1}^N I_n(t) \quad (3-58)$$

It can be easily shown (Lim 81) that an unbiased estimator for the variance of $F(t)$ is

$$\begin{aligned} s^2(t) &= \frac{1}{N-1} F(t) [1-F(t)] \\ &= \frac{1}{N-1} [F(t) - F^2(t)] \end{aligned} \quad (3-59)$$

$$s^2(t) = \frac{1}{N(N-1)} \left[\left(\sum_{n=1}^N I_n(t) \right) - \frac{1}{N} \left(\sum_{n=1}^N I_n(t) \right)^2 \right] \quad (3-60)$$

When stratification is used, these relationships have to be modified to accommodate the stratification. The proportion of cracks drawn from the m -th cell that fail at or before time t is given by

$$F_m(t) = \frac{N_{F,m}(t)}{N_m} \quad (3-61)$$

where N_m is the number of samples from the m -th stratum and $N_{F,m}(t)$ is the number of samples from the m -th stratum which have failed at or before time t .

If, in analogy to Equation 3-56, Bernoulli random variables for initial cracks drawn from the m -th cell are defined as

$$I_{m,n}(t) = \begin{cases} 1 & \text{if the weld with an initial defect from the} \\ & \text{m-th cell is failed at time } t, \text{ and} \\ 0 & \text{if the weld with an initial defect from the} \\ & \text{m-th cell is not failed at time } t \end{cases} \quad (3-62)$$

then

$$H_{F,m}(t) = \sum_{n=1}^{N_m} I_{m,n}(t) \quad (3-63)$$

and

$$F_m(t) = \frac{1}{N_m} \sum_{n=1}^{N_m} I_{m,n}(t) \quad (3-64)$$

where n is an index for the cracks from the m -th stratum and $F_m(t)$ is an unbiased estimator for $P_m(t_F \leq t)$, the probability that cracks from the m -th stratum will fail at or before time t .

In a manner similar to Equation 3-59, an unbiased estimator for the variance of $F_m(t)$ is

$$s_m^2 = \frac{1}{N_m - 1} F_m(t) [1 - F_m(t)] \quad (3-65)$$

$$s_m^2 = \frac{1}{N_m(N_m - 1)} \left[\sum_{n=1}^{N_m} I_{m,n}(t) - \frac{1}{N_m} \left(\sum_{n=1}^{N_m} I_{m,n}(t) \right)^2 \right] \quad (3-66)$$

It can be shown (Lim 81) that $F_{st}(t)$ and s_{st}^2 are unbiased estimators for the overall failure probability and the variance of the overall failure probability, respectively, where

$$F_{st}(t) = \sum_{m=1}^M F_m(t) P_m \quad (3-67)$$

and

$$s_{st}^2(t) = \sum_{m=1}^M s_m^2(t) P_m^2 \quad (3-68)$$

Additional considerations with regard to computational efficiency suggest that Equation 3-62 should be modified to accommodate the pre-service and in-service inspection test. The random variables are redefined so that

$$I_{m,n}(t) = \begin{cases} P_{ND,n} & \text{if the weld has failed by time } t, \\ 0 & \text{if the weld has not failed by time } t \end{cases} \quad (3-69)$$

Equations 3-63 and 3-64 are then evaluated using $I_{m,n}(t)$ as defined in Equation 3-69.

When the influence of earthquakes is to be evaluated, separate random variables are constructed for each earthquake category, or

$$I_{m,n}(g,t) = \begin{cases} P_{ND,n} & \text{if a category } g \text{ earthquake occurs at} \\ & \text{time } t \text{ and the weld with a crack from} \\ & \text{the } m\text{-th stratum has failed at or before} \\ & \text{time } t \\ 0 & \text{if a category } g \text{ earthquake occurs at} \\ & \text{time } t \text{ and the weld with a crack from} \\ & \text{the } m\text{-th stratum has not failed at or} \\ & \text{before time } t. \end{cases} \quad (3-70)$$

The corresponding estimators are:

(1) stratum proportion

$$F_m(g,t) = \frac{1}{R_m} \sum_{n=1}^{N_m} I_{m,n}(g,t) \quad (3-71)$$

(2) variance of the stratum proportion

$$s_m^2 (q,t) = \frac{1}{N_m-1} F_m(q,t) [1 - F_m(q,t)] \quad (3-72)$$

(3) overall failure probability

$$F_{st} (q,t) = \sum_{m=1}^M P_m F_m(q,t) \quad (3-73)$$

(4) variance of the overall failure probability

$$s_{st}^2 (q,t) = \sum_{m=1}^M P_m^2 s_m^2 (q,t) \quad (3-74)$$

The above equations provide values of the standard deviation of the estimates of the failure probabilities. These standard deviations are printed out by the PRAISE code (Lim 81), and are useful in estimating confidence intervals on the failure probabilities. However, no additional use of these results will be made in this report.

4.0 APPLICATIONS TO REACTOR PIPING

Previous sections of this report have been devoted to a description of the fracture mechanics model of component reliability (Section 2), and the procedures developed for generation of numerical results (Section 3). These descriptions were fairly general, and the model and the numerical scheme employed could, with appropriate material properties, be applied to a wide variety of structural components. This section will provide details of the specific application of the described procedures to reactor piping. Introductory comments that set the framework for description of the model were included in Section 1. The primary piping at Zion I was described, and the weld joints considered are shown in Figure 1-2. Additionally, the relevant stresses to be employed in the fracture mechanics analysis were reviewed in Section 1.3.

Basically, it is desired to evaluate the influence of seismic events on the probability of failure of the large primary piping at Zion I. The probability of failure in the absence of seismic events forms an integral portion of the results. Calculations were performed for each of the girth butt welds shown in Figure 1-2 to determine the probability of failure as a function of time for no seismic events. In conjunction with these calculations, seismic events of specified magnitude were imposed at specified times, and the increase in the probability of failure at each weld location was determined for each of the seismic magnitudes considered. The difference in the failure probability before and after the seismic event is the contribution of the seismic event to the failure probability. Results such as shown schematically in Figure 4-1 were generated. This figure clearly shows the increase in the failure probability due to the specified seismic event. Failure probabilities for times following the seismic event were not part of this investigation. The failure probabilities changed with time prior to the seismic event because of the fatigue crack growth that occurs due to cyclic stresses imposed during normal plant operation.

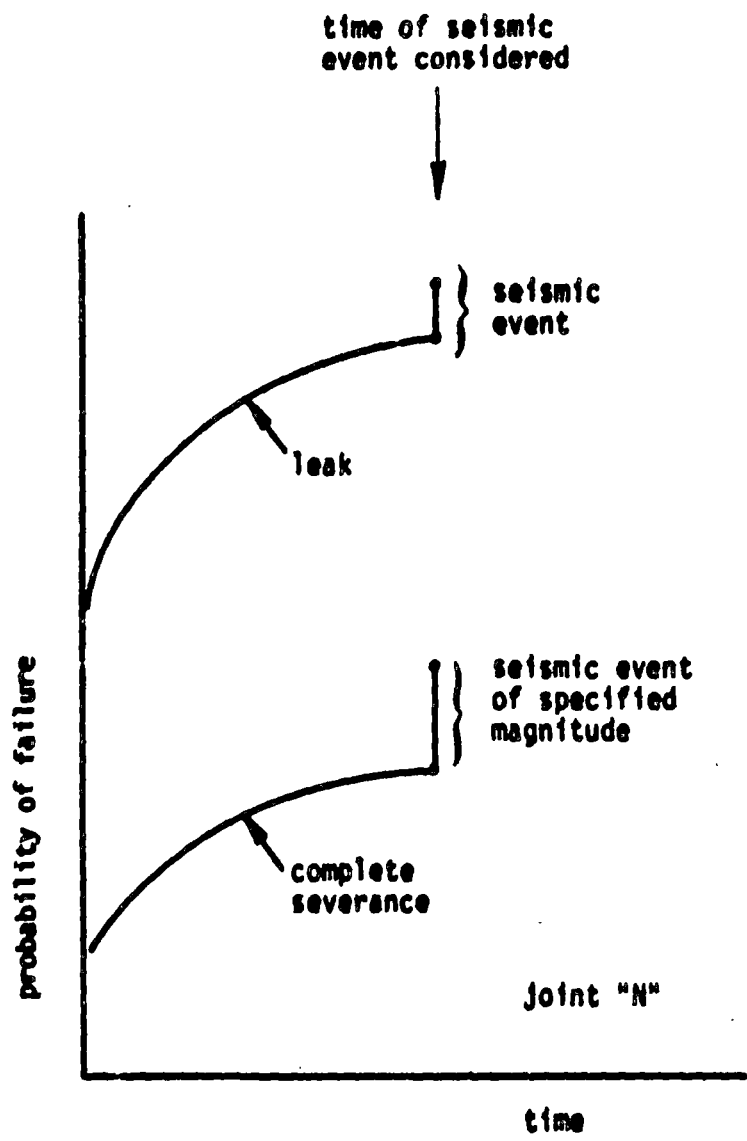


Figure 4-1. Schematic Representation of Type of Basic Results Generated to Ascertain Influence of Seismic Events on Piping Weld Joint Reliability.

In actuality, calculations were performed for seismic events of various imposed magnitudes at a variety of times. Results for a given magnitude event are combined as a function of time as shown schematically as dashed lines in Figure 4-2. These dashed lines are not intended to represent the failure probability as a function of time following a seismic event.

The time history of transients is required in order to perform the calculations of failure probability, in addition to the many other inputs discussed in earlier sections.

4.1 Transient Frequencies

The various transients postulated to occur during the plant lifetime have been briefly discussed elsewhere (see Sections 3.5 and D.4), and the resulting stresses and/or cyclic stress intensity factors have been provided (see Tables 1-2, 1-3, and Appendix D). The remaining information required is the frequency with which the various (non-seismic) transients occur. These are summarized in Table 4-1 (FSAR). This list of transients, and their frequencies agree well with previous results employed in fracture mechanics analysis of reactor piping and pressure vessels (Ricardella 72, Marshall 76, Mayfield 80, Harris 76, 77b, Griesbach 80). The number of transients in 40 years given in Table 4-1 is generally considered to be conservative. In the case of Zion I, this has been verified to be the case by comparing the frequency of transients in the Zion logbook (Zion) with results from Table 4-1. The transients of Table 4-1 could be considered to be distributed in time in a variety of ways--the simplest one being a uniform distribution in time. As an alternative, a Poisson distribution could be utilized, as was discussed in Section 3.5. An additional sophistication could employ aspects of the time variation of transient frequencies associated with early portions of the plant life (Leverenz 78). However, as will be seen in Section 4.3.1, most of the transients in Table 4-1 have only a small influence on crack growth in the piping considered. They therefore have only a small influence on the failure probabilities. Hence, details of their time-distribution of occurrence are not important in the present context and additional sophistication in this area is not warranted.

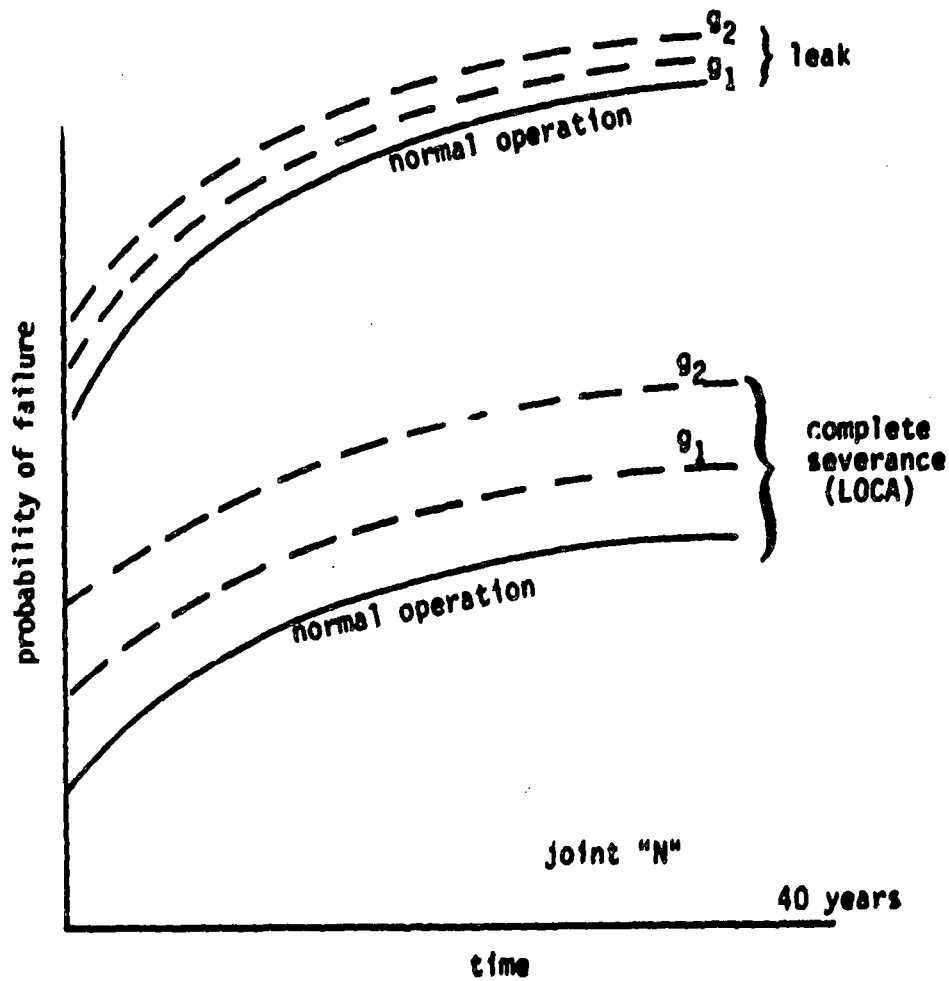


Figure 4-2. Schematic Representation of Type of Results Generated to Show the Influence of Time on the Weld Joint Reliability.

Table 4-1

List of Transients and Postulated Number of Occurrences in 40 Years

Heatup and Cooldown (at 100 F/hr)	200 (each)
Unit Loading and Unloading (at 5% of full power/min)	18,300 (each)
Step Load Increase and Decrease (10% of full power)	2,000 (each)
Large Step Load Decrease	200
Loss of Load	80
Loss of Power	40
Loss of Flow (partial loss)	80
Reactor Trip From Full Power	400
Steam Line Break	1
Turbine Roll Test	10
Hydrostatic Test Condition	5

4.2 Joint and System Reliability

The various factors contributing to the reliability of a given weld joint have been thoroughly discussed in earlier sections of this report. Basically, the weld joints are subjected to a given set of transients whose frequency was discussed in the previous section. Results such as shown schematically in Figure 4-2 are generated for each joint. Hence, the probability of leak or LOCA for each joint is obtained as a function of time, and the influence of a specified seismic event on each joint is determined. Each joint in a given pipe section (such as hot leg, cold leg, etc.) will see the same coolant temperature history. They will therefore see the same radial gradient stress history, but different seismic and normal operating stresses.

The probability of failure in the primary piping system under consideration at Zion I will be governed by the probability of failure of the various joints in each of the four loops. If the failure probability of each of the joints is independent of all the other joints, the following relation will hold for the probability of failure anywhere in the four loops.

$$P_f(\text{sys})(t,g) = 1 - \left\{ \prod_{k=1}^{14} \left[1 - P_f(\text{joint } k)(t,g) \right] \right\}^4 \quad (4-1)$$

The 4th power is present because there are four loops. The use of the same failure probabilities for corresponding joints in each of the four loops is inconsistent with the joints all being independent of one another. Additionally, the failure probabilities for joints in a given loop may not be independent, because they all see the same transient history. Therefore, Equation 4-1 is only approximate. However, it can serve as an upper bound on the loop failure probability. Time, t , and seismic event magnitude, g , are carried along in the calculation.

A lower bound on the system (or loop) failure probability would be the probability of failure of the joint with the highest failure probability.

This can be expressed as

$$P_{f(\text{sys})}(t, g) = \max_{k=1,14} [P_{f(\text{Joint } k)}] \quad (4-2)$$

If all of the joints were perfectly correlated this would provide the exact system failure probability.

The seismic hazard curve must be known before it is possible to directly calculate the probability of a seismic-induced LOCA (or leak). Results generated in this investigation are concerned with the probability of a LOCA (or leak) given that a seismic event of a given magnitude occurred at a given time during the life of the plant. Section 3.0 briefly discussed a procedure for combining the seismic hazard curve with the results generated herein.

The inputs necessary for the numerical generation of the probability of failure at each of the weld joints have now been presented, and actual results can be obtained. Such results are presented in the next section.

4.3 Results and Discussion

Numerical results for pipe joint failure probabilities will now be presented and discussed. Unless otherwise stated, the following conditions will be applicable to all results

- pre-service hydrostatic proof test is performed.
- pre-service inspection is performed, but no in-service inspection.
- C and σ_{f10} are random variables.
- the Marshall distribution on crack depth is used (Equation 2-6).
- the modified lognormal distribution on aspect ratio is used (Equation 2-11) with $\rho=10^{-2}$, and
- occurrences of non-seismic transients are uniform over plant lifetime (see Table 4-1).

4.3.1 Results for All Transients

Calculations were performed for the hot leg-to-pressure vessel joint (number 1 in Figure 1-2) for the case of a transient history based on Table 4-1. The maximum temperature and pressure excursion for each transient were taken to be deterministic with values as specified in Appendix D. The results are presented in Figure 4-3. Also shown in this figure are corresponding results generated by considering the heatup - cooldown transient to be the only nonseismic transient, and the event is taken to occur 5 times per year (200 times in the life of the plant). It is seen that the two sets of results are quite close to one another. This is not too surprising. The heatup-cooldown transient results in a stress that is uniform through the wall thickness, and the cyclic stress is relatively large. Therefore, the cyclic stress intensity factor will also be relatively large. The majority of transients other than heatup-cooldown (HU-CD) produce primarily radial gradient thermal stresses. As shown in Appendix D, these stress contributions produce relatively small cyclic stress intensity factors. In fact, K_I often actually passes through a peak at intermediate crack depths, and decreases as the depths get larger. Therefore, the cyclic stress intensities are not large, and these transients have only a small influence on the large cracks that can produce complete pipe severances.

The inclusion of the radial gradient thermal stresses could be important — especially to LOCAs, because these stresses are highest at the inner wall, and would therefore tend to grow cracks in the circumferential direction (where they could grow to cause LOCAs) rather than through the thickness (where they could grow to cause leaks). It was not known a priori what the influence of radial gradient stresses would be. In the present case, they are seen to not be influential. It will be seen shortly that the influence on leak probabilities is even less than the influence on LOCA probabilities.

The cost of running the PRAISE code increases almost linearly with the number of transients considered. Since the results of Figure 4-3 show that the heatup-cooldown cycle dominates the stress history, subsequent

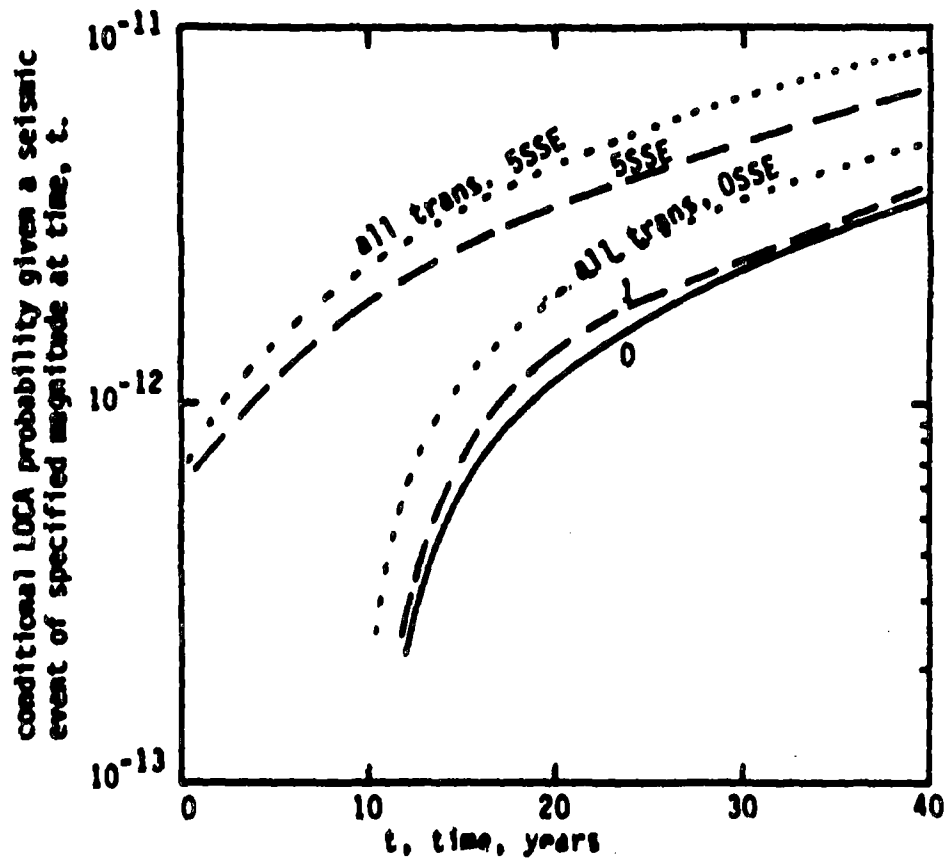


Figure 4-3. Conditional LOCA Probabilities for Joint 1 for Various Magnitude Seismic Events Showing Differences Between Conditions for all Transients Being Considered and Only Heat up-Cool Down Included.

calculations were performed with this being the only nonseismic transient occurring during the plant life. This results in considerable savings in computer costs, and (as indicated in Figure 4-3), will not significantly alter the results obtained. Hence, unless otherwise specified, all remaining results to be presented here are for the heatup-cooldown transients only, along with the other conditions specified at the beginning of this section (4.3). These will be taken to be the base case conditions.

4.3.2 Results for Base Case Conditions

Calculations for the base case conditions were performed for each of the fourteen weld joints. The results for LOCAs and leaks are included in Tables 4-2 and 4-3. The results in these tables form the bulk of the results obtained in the course of this investigation. Selected results extracted from these tables will now be discussed.

The probability of failure is a strong function of weld location, as shown in Tables 4-2 and 4-3. This is because of the strong variation in applied stresses with weld location, which are shown in Tables 1-2 and 1-3. Selected results for joints 1 and 13 are presented in Figure 4-4. As mentioned above, these results are for the base case conditions. All of the LOCA probabilities are very low. This is because of the large tolerable cracks in the tough piping material, and the fairly benign stress history these pipes are subjected to. The observance of very low LOCA probabilities means that cracks that can produce LOCAs are initially very large.

It is seen in Figures 4-3 and 4-4 that seismic events have only a small influence on the LOCA probabilities for joint 1. In contrast to this, Figure 4-4 shows that seismic events have a large influence at joint 13. The relative influence of seismic events is governed by the relative magnitudes of the seismic and normal operating stresses. In Tables 1-2 and 1-3 joint 13 is seen to have a large seismic stress and relatively small normal operating stress. This accounts for the relatively large

Table 4-2

Tabulation of Values of $P\{t_{LOCA} < t | E_q(g,t)\}$ for Weld Joints
 Considered—Results Conditional on a Crack Being Initially Present

RESULTS FOR JOINT 1 LOCATED AT FE NODE 1
 INSIDE RADIUS EQUALS 10.500 THICKNESS EQUALS 2.5000
 CONDITIONAL PLOCAT(G), VARIOUS T AND G

TIME	G = 0.0	.085	.170	.510	.850
0.	0.	0.	0.	2.54598E-13	5.66964E-13
2.0	0.	0.	0.	4.00126E-13	7.87733E-13
4.0	1.34904E-13	1.34994E-13	1.34904E-13	5.82885E-13	9.93012E-13
5.0	1.42912E-13	1.42912E-13	1.42912E-13	1.01867E-12	1.29825E-12
8.0	1.58965E-13	1.55965E-13	1.67663E-13	1.26095E-12	1.60429E-12
10.0	1.58955E-13	1.58965E-13	1.55965E-13	1.61833E-12	2.00544E-12
12.0	2.15568E-13	2.21817E-13	2.21817E-13	2.02592E-12	2.27268E-12
14.0	4.65371E-13	4.92947E-13	5.52242E-13	2.34008E-12	2.59981E-12
16.0	6.04287E-13	7.76593E-13	8.55515E-13	2.35084E-12	2.68586E-12
18.0	9.38163E-13	9.46297E-13	1.12825E-12	2.47701E-12	2.70849E-12
20.0	1.21071E-12	1.33961E-12	1.43427E-12	2.96629E-12	3.19722E-12
22.0	1.49489E-12	1.50851E-12	1.51484E-12	3.21254E-12	3.42947E-12
24.0	1.66713E-12	1.60713E-12	1.63772E-12	3.39955E-12	3.74447E-12
25.0	1.70193E-12	1.70713E-12	1.70461E-12	3.79013E-12	4.09656E-12
26.0	1.59457E-12	2.00537E-12	2.02594E-12	4.00488E-12	4.39610E-12
30.0	2.07544E-12	2.13686E-12	2.29930E-12	4.49154E-12	4.83533E-12
32.0	2.32603E-12	2.41037E-12	2.55274E-12	4.97861E-12	5.50864E-12
34.0	2.61196E-12	2.62117E-12	2.74319E-12	5.36668E-12	5.70717E-12
36.0	2.91215E-12	2.91215E-12	3.037167E-12	5.85879E-12	6.15933E-12
38.0	3.03518E-12	3.66144E-12	3.30708E-12	5.91602E-12	6.10511E-12
40.0	3.46135E-12	3.49163E-12	3.61804E-12	6.00545E-12	6.10670E-12

Table 4-2 (cont.)

RESULTS FOR JOINT 2 LOCATED AT FE NODE 5
 INSIDE RADIUS EQUALS 14.700 THICKNESS EQUALS 2.5009
 CONDITIONAL PLACEMENT, VARIOUS T AND G

TIME	G = 0.0	.085	.170	.510	.850
0.	0.	0.	0.	0.	0.
2.0	0.	0.	0.	0.	0.
4.0	0.	0.	0.	0.	0.
6.0	0.	0.	0.	0.	0.
8.0	6.09856E-15	6.09856E-15	6.09856E-15	6.09856E-15	6.09856E-15
10.0	6.09856E-15	6.09856E-15	6.09856E-15	6.09856E-15	6.09856E-15
12.0	6.09856E-15	6.09856E-15	6.09856E-15	6.09856E-15	6.09856E-15
14.0	6.09856E-15	6.09856E-15	6.09856E-15	6.09856E-15	6.09856E-15
16.0	6.09856E-15	6.09856E-15	6.09856E-15	6.09856E-15	6.09856E-15
18.0	1.38545E-14	1.38545E-14	1.38545E-14	1.38545E-14	1.38545E-14
20.0	1.38545E-14	1.38545E-14	1.98318E-14	1.98318E-14	1.98318E-14
22.0	1.98318E-14	1.98318E-14	1.98318E-14	1.98318E-14	1.98318E-14
24.0	1.98318E-14	1.98318E-14	1.98318E-14	1.98318E-14	1.98318E-14
26.0	1.98318E-14	1.98318E-14	1.98318E-14	2.76672E-14	1.98318E-14
28.0	1.98318E-14	1.98318E-14	2.76672E-14	2.76672E-14	2.76672E-14
30.0	2.76672E-14	2.76672E-14	3.59219E-14	4.19748E-14	3.59219E-14
32.0	4.19748E-14	4.19748E-14	4.19748E-14	4.19748E-14	4.19748E-14
34.0	5.07180E-14	5.07180E-14	5.07180E-14	5.07180E-14	5.07180E-14
36.0	5.07180E-14	5.07180E-14	5.07180E-14	5.07180E-14	5.07180E-14
38.0	5.85324E-14	5.85324E-14	5.85324E-14	5.85324E-14	5.85324E-14
40.0	5.85324E-14	5.85324E-14	5.85324E-14	5.85324E-14	5.85324E-14

Table 4-2 (cont.)

RESULTS FOR JOINT 3 LOCATED AT FE NODE 7
 INSIDE RADIUS EQUALS 15.000 THICKNESS EQUALS 3.2809
 CONDITIONAL PLOCAT(G), VARIOUS T AND G

TIME	G = 0.0	.085	.170	.510	.850
0.	0.	0.	0.	1.71207E-15	2.97419E-16
2.0	0.	0.	0.	2.98799E-15	1.63213E-15
4.0	0.	0.	2.05116E-16	3.96463E-15	2.63141E-15
6.0	0.	0.	0.	6.13923E-15	2.74071E-15
8.0	0.	0.	2.46244E-16	6.21719E-15	4.52426E-15
10.0	2.46244E-16	2.46244E-16	7.16046E-16	7.02451E-15	4.12924E-15
12.0	2.46244E-16	5.42687E-16	5.42009E-16	9.37271E-15	4.90457E-15
14.0	8.19474E-16	8.19474E-16	1.05962E-15	8.21241E-15	3.91803E-15
16.0	1.05962E-15	1.05962E-15	1.30431E-15	1.30431E-14	4.71033E-15
18.0	1.30431E-15	1.30431E-15	1.30431E-15	1.63181E-14	6.45059E-15
20.0	1.62509E-15	1.62509E-15	1.98198E-15	1.63674E-14	9.20028E-15
22.0	1.62509E-15	1.98198E-15	1.98198E-15	2.00865E-14	1.03079E-14
24.0	1.98198E-15	1.98198E-15	1.98198E-15	2.32043E-14	1.40841E-14
26.0	2.22306E-15	2.22306E-15	3.96466E-15	2.30444E-14	1.24226E-14
28.0	4.35464E-15	4.35464E-15	5.67823E-15	2.79257E-14	1.70367E-14
30.0	4.35464E-15	4.35464E-15	5.67823E-15	3.02769E-14	1.57904E-14
32.0	6.50623E-15	6.50623E-15	6.50623E-15	3.29429E-14	1.58107E-14
34.0	6.50623E-15	6.50623E-15	6.50623E-15	3.40085E-14	1.69922E-14
36.0	7.10570E-15	7.10570E-15	8.39424E-15	3.76386E-14	2.17966E-14
38.0	8.15050E-15	8.40363E-15	9.46631E-15	3.99380E-14	2.77911E-14
40.0	9.22627E-15	9.46646E-15	1.03931E-14	3.91563E-14	2.67730E-14

Table 4-2 (cont.)

RESULTS FOR JOINT 4 LOCATED AT FE NODE 9
 INSIDE RADIUS EQUALS 15.000 THICKNESS EQUALS 3.2000
 CONDITIONAL PLGCZ(T.G), VARIOUS T AND G

TIME	G = 3.0	.065	.170	.510	.850
0.0	3.	0.	0.	1.32195E-13	1.60903E-13
2.0	6.	3.	2.95114E-16	1.32986E-13	1.58721E-13
4.0	9.	2.46284E-16	5.47570E-16	1.44754E-13	1.67161E-13
6.0	2.46254E-16	5.42869E-16	1.95962E-15	1.55285E-13	1.82478E-13
8.0	6.19474E-16	1.65963E-15	1.74129E-15	1.62349E-13	1.88398E-13
10.0	1.39431E-15	1.90194E-15	2.33807E-15	1.73404E-13	1.96994E-13
12.0	1.98104E-15	1.52194E-15	4.19945E-15	1.80953E-13	2.02662E-13
14.0	2.55074E-15	4.52704E-15	6.13918E-15	1.86640E-13	2.05847E-13
16.0	5.42496E-15	6.12475E-15	7.47767E-15	1.92455E-13	2.12484E-13
18.0	6.42512E-15	6.72611E-15	8.73939E-15	1.99503E-13	2.20869E-13
20.0	7.30979E-15	6.71795E-15	1.27671E-14	2.07176E-13	2.27414E-13
22.0	9.18541E-15	1.02523E-14	1.45354E-14	2.10370E-13	2.29090E-13
24.0	1.03121E-14	1.59864E-14	1.98235E-14	2.13095E-13	2.31145E-13
26.0	1.45401E-14	1.67866E-14	2.10836E-14	2.23598E-13	2.42008E-13
28.0	1.62934E-14	2.05405E-14	2.42104E-14	2.31876E-13	2.48938E-13
30.0	1.81762E-14	2.14494E-14	2.60430E-14	2.41323E-13	2.54489E-13
32.0	2.26232E-14	2.46304E-14	3.31726E-14	2.41994E-13	2.57124E-13
34.0	2.47543E-14	3.66304E-14	3.85330E-14	2.47572E-13	2.61039E-13
36.0	3.11244E-14	3.47809E-14	4.19736E-14	2.53295E-13	2.66221E-13
38.0	3.49461E-14	3.92344E-14	4.34862E-14	2.51913E-13	2.69716E-13
40.0	3.75740E-14	4.11264E-14	4.56639E-14	2.59617E-13	2.71061E-13

Table 4-2 (cont.)

RESULTS FOR JOINT 5 LOCATED AT FE NODE 26
 INSIDE RADIUS EQUALS 15.500 THICKNESS EQUALS 3.3120
 CONDITIONAL PLOTTING, VARIOUS T AND S

TIME	6 = 0.0	.065	.170	.510	.850
0.0	0.	0.	0.	1.82443E-13	1.21280E-14
2.0	0.	0.	0.	1.74466E-13	1.22656E-14
4.0	0.	0.	1.00659E-16	1.74541E-13	1.37052E-14
6.0	1.45509E-16	1.02500E-16	3.76425E-16	1.80937E-13	1.45908E-14
8.0	3.92272E-16	3.02227E-16	3.92222E-16	1.82691E-13	1.46447E-14
10.0	3.92222E-16	5.01725E-16	5.01725E-16	1.85747E-13	1.62374E-14
12.0	5.01725E-16	5.01725E-16	5.01735E-16	1.88769E-13	1.63245E-14
14.0	7.00602E-16	7.00602E-16	9.04936E-16	1.90058E-13	2.12917E-14
16.0	9.00036E-16	1.02062E-15	1.35063E-15	1.93246E-13	2.35230E-14
18.0	1.04400E-15	1.07060E-15	2.03734E-15	1.95271E-13	2.77713E-14
20.0	2.14043E-15	2.14043E-15	2.10043E-15	1.99109E-13	3.11034E-14
22.0	2.30006E-15	2.24604E-15	2.50350E-15	1.99670E-13	3.33151E-14
24.0	2.70007E-15	2.07014E-15	5.30140E-15	1.99675E-13	3.37607E-14
26.0	5.71151E-15	5.71151E-15	5.91901E-15	2.02792E-13	3.80232E-14
28.0	5.91001E-15	5.91001E-15	6.12075E-15	2.03540E-13	3.96064E-14
30.0	6.01013E-15	6.01013E-15	6.60921E-15	2.05112E-13	4.15876E-14
32.0	6.91536E-15	7.11100E-15	7.56055E-15	2.13241E-13	4.54511E-14
34.0	7.11137E-15	7.11137E-15	7.71330E-15	2.10527E-13	4.84836E-14
36.0	8.04215E-15	6.49215E-15	8.77650E-15	2.14629E-13	4.76363E-14
38.0	8.00597E-15	8.00597E-15	6.89597E-15	2.17001E-13	4.83620E-14
40.0	9.09060E-15	9.09060E-15	9.00864E-15	2.20119E-13	5.12293E-14

Table 4-2 (cont.)

RESULTS FOR JOINT 6 LOCATED AT FE NODE 27
 INSIDE RADIUS EQUALS 15.500 THICKNESS EQUALS 2.6600
 CONDITIONAL FLOC(T.G), VARIOUS T AND G

TIME	G = 0.0	.300	.170	.510	.650
0.	0.	0.	0.	6.57376E-16	0.
2.0	0.	0.	0.	8.22055E-15	3.35157E-15
4.0	1.74753E-15	1.74753E-15	1.74753E-15	9.21426E-15	5.03063E-15
6.0	1.74753E-15	1.74753E-15	1.74753E-15	9.64470E-15	5.15167E-15
8.0	3.23497E-15	3.23487E-15	3.23467E-15	1.76548E-14	7.27147E-15
10.0	4.66228E-15	4.69228E-15	4.69228E-15	3.34521E-14	2.39669E-14
12.0	4.39197E-15	4.39197E-15	4.39197E-15	3.36616E-14	2.50979E-14
14.0	1.39595E-14	1.39595E-14	1.39595E-14	3.76126E-14	2.39679E-14
16.0	1.57437E-14	1.57437E-14	1.57437E-14	5.56964E-14	3.37647E-14
18.0	1.44169E-14	1.44169E-14	1.44169E-14	5.14536E-14	3.62788E-14
20.0	2.33637E-14	2.33637E-14	2.33637E-14	5.12513E-14	3.45905E-14
22.0	2.39796E-14	2.39796E-14	2.39796E-14	5.85399E-14	3.50473E-14
24.0	2.46386E-14	2.46386E-14	2.46386E-14	8.48332E-14	6.35824E-14
26.0	3.17947E-14	3.17947E-14	3.27569E-14	8.33131E-14	5.57291E-14
28.0	3.76548E-14	3.76548E-14	3.76548E-14	9.04556E-14	5.88438E-14
30.0	3.76548E-14	3.76548E-14	3.76548E-14	9.68971E-14	6.49212E-14
32.0	3.98295E-14	3.98295E-14	4.05982E-14	1.09069E-13	7.72442E-14
34.0	4.76235E-14	4.76235E-14	5.13292E-14	1.15198E-13	8.46555E-14
36.0	5.45204E-14	5.45264E-14	5.81912E-14	1.38229E-13	9.58419E-14
38.0	5.88537E-14	5.95845E-14	5.95885E-14	1.55011E-13	9.47602E-14
40.0	6.52499E-14	6.62451E-14	6.62451E-14	1.64687E-13	1.12229E-13

Table 4-2 (cont.)

RESULTS FOR JOINT 7 LOCATED AT FE NODE 28
 INSIDE RADIUS EQUALS 15.500 THICKNESS EQUALS 2.6600
 CONDITIONAL PLOCAT(6), VARIOUS T AND G

TIME	G = 0.0	.085	.170	.510	.850
6.0	0.	0.	0.	0.	0.
2.0	0.	0.	0.	0.	1.67972E-15
4.0	1.74753E-15	1.74753E-15	1.74753E-15	1.74753E-15	1.74753E-15
6.0	1.74753E-15	1.74753E-15	1.74753E-15	1.74753E-15	2.39049E-15
8.0	3.03487E-15	3.03487E-15	3.03487E-15	3.03487E-15	3.03487E-15
10.0	3.03487E-15	3.03487E-15	3.03487E-15	3.03487E-15	4.80901E-15
12.0	4.62092E-15	4.62092E-15	4.62092E-15	6.62457E-15	1.39644E-14
14.0	1.21921E-14	1.21921E-14	1.21921E-14	1.21921E-14	1.54191E-14
16.0	1.40163E-14	1.40163E-14	1.40163E-14	1.56023E-14	1.58023E-14
18.0	1.84354E-14	1.84354E-14	1.84354E-14	1.84354E-14	1.91033E-14
20.0	2.09046E-14	2.09046E-14	2.15804E-14	2.33273E-14	2.39892E-14
22.0	2.39592E-14	2.39892E-14	2.39892E-14	2.39892E-14	2.46572E-14
24.0	2.46572E-14	2.46572E-14	2.64411E-14	2.64411E-14	2.81596E-14
26.0	3.00948E-14	3.00948E-14	3.12173E-14	3.52061E-14	3.83527E-14
28.0	3.41556E-14	3.59007E-14	3.59007E-14	3.76519E-14	4.03456E-14
30.0	3.59007E-14	3.59007E-14	3.59007E-14	3.59007E-14	3.82071E-14
32.0	3.59257E-14	3.59007E-14	3.65848E-14	3.89338E-14	4.64046E-14
34.0	4.12575E-14	4.12575E-14	4.12575E-14	4.53962E-14	5.75778E-14
36.0	4.72448E-14	4.72448E-14	4.75268E-14	5.33579E-14	5.74536E-14
38.0	4.96932E-14	4.96932E-14	5.33579E-14	5.73633E-14	5.82983E-14
40.0	5.46752E-14	5.46752E-14	5.56684E-14	6.14098E-14	6.95009E-14

Table 4-2 (cont.)

RESULTS FOR JOINT " LOCATED AT FE NODE 31
 INSIDE RADIUS EQUALS 15.530 THICKNESS EQUALS 2.6600
 CONDITIONAL FLOCAL(T,G), VARIOUS T AND G

TIME	G = 0.0	.085	.170	.510	.850
0.	0.	0.	0.	0.	0.
2.0	0.	0.	0.	0.	0.
4.0	0.	0.	0.	0.	0.
6.0	0.	0.	0.	0.	0.
8.0	0.	0.	0.	0.	0.
10.0	5.92358E-15	5.92358E-15	5.92358E-15	5.92358E-15	5.92358E-15
12.0	5.92358E-15	5.92358E-15	5.92358E-15	5.92358E-15	5.92358E-15
14.0	7.33550E-15	7.33550E-15	7.33550E-15	7.33550E-15	7.33550E-15
16.0	7.33550E-15	7.33550E-15	7.33550E-15	7.33550E-15	7.33550E-15
18.0	7.33550E-15	7.33550E-15	7.33550E-15	7.33550E-15	7.33550E-15
20.0	9.67295E-15	9.67295E-15	9.67295E-15	1.00006E-14	1.00006E-14
22.0	1.00006E-14	1.00006E-14	1.00006E-14	1.14136E-14	1.14136E-14
24.0	1.00006E-14	1.00006E-14	1.00006E-14	1.00006E-14	1.00006E-14
26.0	1.00006E-14	1.00006E-14	1.00006E-14	1.00006E-14	1.00006E-14
28.0	1.00006E-14	1.00006E-14	1.00006E-14	1.00006E-14	1.00006E-14
30.0	1.00006E-14	1.00006E-14	1.00006E-14	1.00006E-14	1.00006E-14
32.0	1.00006E-14	1.00006E-14	1.00006E-14	1.00006E-14	1.00006E-14
34.0	1.00006E-14	1.00006E-14	1.00006E-14	1.00006E-14	1.00006E-14
36.0	1.00006E-14	1.00006E-14	1.00006E-14	1.00006E-14	1.00006E-14
38.0	1.35937E-14	1.35937E-14	1.35937E-14	1.49040E-14	1.49040E-14
40.0	1.49040E-14	1.49040E-14	1.49040E-14	1.62662E-14	1.62662E-14

Table 4-2 (cont.)

RESULTS FOR JOINT 9 LOCATED AT FE NODE 35
 INSIDE RADIUS EQUALS 15.500 THICKNESS EQUALS 2.6600
 CONDITIONAL PLOC(T,G), VARIOUS T AND G

TIME	G = 0.0	.065	.170	.510	.850
0.	0.	0.	0.	5.37917E-14	3.96343E-14
2.0	0.	0.	0.	5.80035E-14	4.70871E-14
4.0	0.	0.	0.	7.33026E-14	4.57365E-14
6.0	1.74753E-15	1.74753E-15	1.74753E-15	8.80711E-14	5.56335E-14
8.0	1.74753E-15	1.74753E-15	1.74753E-15	1.07090E-13	6.07703E-14
10.0	2.39049E-15	2.39049E-15	2.39049E-15	1.25271E-13	7.92631E-14
12.0	2.39049E-15	2.39049E-15	3.02271E-15	1.50963E-13	8.69311E-14
14.0	3.02271E-15	3.02271E-15	3.02271E-15	1.79840E-13	1.01378E-13
15.0	3.69550E-15	3.69550E-15	3.69550E-15	1.86376E-13	1.10340E-13
18.0	5.47074E-15	5.47074E-15	7.96916E-15	1.93153E-13	1.12865E-13
20.0	6.60620E-15	1.41737E-14	1.41737E-14	2.13425E-13	1.29936E-13
22.0	1.66535E-14	1.66535E-14	1.72966E-14	2.23709E-13	1.49647E-13
24.0	1.72966E-14	1.72966E-14	1.72966E-14	2.36035E-13	1.52633E-13
26.0	1.72966E-14	1.72966E-14	1.79694E-14	2.54457E-13	1.64910E-13
28.0	1.86136E-14	1.86136E-14	1.9215E-14	2.53642E-13	1.56062E-13
30.0	2.17547E-14	2.17547E-14	2.2439E-14	2.61132E-13	1.61761E-13
32.0	2.37411E-14	2.37411E-14	2.37411E-14	2.61806E-13	1.71692E-13
34.0	2.37411E-14	2.55169E-14	2.55169E-14	2.73593E-13	1.83980E-13
36.0	2.55169E-14	2.55169E-14	2.55169E-14	2.92166E-13	2.02188E-13
38.0	3.09565E-14	3.09565E-14	3.26779E-14	2.94235E-13	2.06330E-13
40.0	3.43286E-14	3.43286E-14	3.49552E-14	3.05971E-13	2.18696E-13

Table 4-2 (cont.)

RESULTS FOR JOINT 10 LOCATED AT FE NODE 37
 INSIDE RADIUS EQUALS 15.599 THICKNESS EQUALS 3.3120
 CONDITIONAL FLOC=(T,G), VARIOUS T AND G

TIME	G = 0.0	.045	.170	.510	.850
0.	0.	0.	0.	3.51515E-14	7.76331E-14
2.0	0.	0.	0.	4.01623E-14	7.98302E-14
4.0	1.83599E-16	1.83599E-16	3.76423E-16	4.49186E-14	8.56844E-14
6.0	3.92222E-16	3.92222E-16	3.92222E-16	4.90411E-14	8.92258E-14
8.0	5.81725E-16	5.81725E-16	5.81725E-16	5.34241E-14	9.26226E-14
10.0	9.98936E-16	9.98936E-16	9.98936E-16	6.22435E-14	9.93641E-14
12.0	1.69712E-15	1.69810E-15	2.23796E-15	6.88331E-14	1.02421E-13
14.0	1.98101E-15	1.98101E-15	2.77533E-15	7.36882E-14	1.07799E-13
16.0	2.58445E-15	2.58445E-15	5.53214E-15	8.03890E-14	1.09364E-13
18.0	5.51336E-15	5.51336E-15	5.51336E-15	8.22904E-14	1.11250E-13
20.0	6.00447E-15	6.00447E-15	6.57491E-15	8.51027E-14	1.16143E-13
22.0	6.58954E-15	6.78571E-15	7.29776E-15	9.12568E-14	1.21151E-13
24.0	8.68649E-15	8.68649E-15	8.75417E-15	9.22958E-14	1.22308E-13
26.0	8.29716E-15	8.49962E-15	8.89830E-15	9.39265E-14	1.28161E-13
28.0	6.77558E-15	6.98454E-15	9.38111E-15	9.63967E-14	1.28572E-13
30.0	9.96313E-15	1.08419E-14	1.12314E-14	1.11056E-13	1.38515E-13
32.0	1.36433E-14	1.13215E-14	1.17936E-14	1.06907E-13	1.38412E-13
34.0	1.20750E-14	1.24747E-14	1.34624E-14	1.10746E-13	1.38217E-13
36.0	1.26757E-14	1.35877E-14	1.73397E-14	1.17436E-13	1.43785E-13
38.0	1.40949E-14	1.51859E-14	1.34876E-14	1.19122E-13	1.46820E-13
40.0	1.53941E-14	1.6365E-14	1.66993E-14	1.22528E-13	1.50121E-13

Table 4-2 (cont.)

RESULTS FOR JOINT 11 LOCATED AT FE NODE 4A
 INSIDE RADIUS EQUALS 14.599 THICKNESS EQUALS 4.0060
 CONDITIONAL PLOC(T,G), VARIOUS T AND G

TIME	G =	0.0	.005	.170	.510	.850
3.0	0.	0.	0.	2.01293E-17	1.59194E-13	1.05144E-13
2.0	0.	0.	0.	0.41620E-17	1.56647E-13	1.03723E-13
4.0	0.	0.	0.	4.74335E-17	1.55803E-13	1.03127E-13
6.0	0.	0.	0.	1.06063E-16	1.55370E-13	1.02594E-13
8.0	0.	0.	1.15809E-17	4.53119E-17	1.54570E-13	1.02110E-13
10.0	3.	0.	0.	6.61072E-17	1.54409E-13	1.02029E-13
12.0	6.	0.	0.	1.12133E-16	1.53970E-13	1.01773E-13
14.0	0.	0.	0.	1.07944E-16	1.53391E-13	1.01641E-13
16.0	0.	0.	0.	9.94863E-17	1.52752E-13	1.01147E-13
18.0	0.	0.	0.	1.15606E-16	1.52602E-13	1.01166E-13
20.0	0.	0.	2.50665E-17	1.57121E-16	1.52217E-13	1.01128E-13
22.0	0.	0.	1.71616E-17	1.14333E-16	1.51940E-13	1.01628E-13
24.0	0.	0.	0.	2.01425E-16	1.51558E-13	1.01607E-13
26.0	0.	0.	0.	2.17903E-16	1.51301E-13	1.02171E-13
28.0	0.	0.	1.42549E-17	1.31237E-16	1.50952E-13	1.01475E-13
30.0	0.	0.	0.	1.99111E-16	1.50499E-13	1.01763E-13
32.0	0.	0.	0.	2.65386E-16	1.50076E-13	1.01619E-13
34.0	0.	0.	2.79455E-17	3.69079E-16	1.50675E-13	1.01501E-13
36.0	0.	0.	2.73453E-17	4.93157E-16	1.50371E-13	1.01376E-13
38.0	0.	0.	1.34174E-17	4.19364E-16	1.50203E-13	1.01273E-13
40.0	0.	0.	2.69026E-17	4.03515E-16	1.50179E-13	1.01204E-13

100

Table 4-2 (cont.)

RESULTS FOR JOINT 12 LOCATED AT FE NODE 51
 INSIDE RADIUS EQUALS 13.746 THICKNESS EQUALS 2.3836
 CONDITIONAL PLACEMENT, VARIOUS T AND G

TIME	G = 0.0	.685	.170	.510	.650
0.	0.	0.	0.	4.76946E-11	3.29918E-11
2.0	0.	0.	0.	4.51399E-11	3.10384E-11
4.0	0.	0.	1.17822E-14	4.30676E-11	3.03785E-11
5.0	0.	0.	5.9498E-14	4.20895E-11	3.00020E-11
8.0	0.	0.	2.63548E-14	4.21338E-11	2.96340E-11
10.0	0.	2.72463E-14	2.72463E-14	4.20648E-11	2.95567E-11
12.0	1.11669E-14	1.11669E-14	4.27519E-14	4.99295E-11	2.86521E-11
14.0	1.11669E-14	1.11669E-14	3.65554E-14	4.32637E-11	2.83707E-11
16.0	1.11669E-14	1.11669E-14	1.11669E-14	3.96746E-11	2.78496E-11
18.0	1.11669E-14	1.11669E-14	3.74302E-14	3.93127E-11	2.76325E-11
24.0	1.11669E-14	1.11669E-14	9.33845E-14	3.96675E-11	2.77029E-11
22.0	1.11669E-14	1.11669E-14	7.55144E-14	3.94234E-11	2.74896E-11
24.0	1.11669E-14	2.52949E-14	5.17903E-14	3.92415E-11	2.73419E-11
25.0	2.52049E-14	2.52049E-14	7.55023E-14	3.90446E-11	2.72406E-11
26.0	2.52049E-14	2.52049E-14	6.67784E-14	3.86619E-11	2.70499E-11
30.0	3.61636E-14	3.61606E-14	9.06395E-14	3.85205E-11	2.67773E-11
32.0	3.61636E-14	3.61606E-14	9.06979E-14	3.85701E-11	2.68797E-11
34.0	3.61636E-14	3.61606E-14	7.86406E-14	3.86348E-11	2.69647E-11
36.0	3.61636E-14	3.61636E-14	9.39435E-14	3.84461E-11	2.67878E-11
38.0	3.61636E-14	3.61606E-14	1.07361E-13	3.81581E-11	2.65109E-11
46.0	3.61606E-14	3.76604E-14	9.97463E-14	3.79593E-11	2.63558E-11

Table 4-2 (cont.)

RESULTS FOR JOINT 13 LOCATED AT FE NODE 50
 INSIDE RADIUS EQUALS 13.743 THICKNESS EQUALS 2.3A00
 CONDITIGNAL PLOCX(T.G). VARIOUS T AND G

TIME	G = 0.0	.085	.170	.510	.850
0.	0.	0.	0.	3.28722E-11	1.10050E-11
2.0	0.	0.	0.	3.11609E-11	1.04205E-11
4.0	0.	0.	0.	3.05137E-11	1.01476E-11
6.0	0.	0.	0.	2.99090E-11	1.01747E-11
8.0	0.	0.	1.11667E-14	2.99307E-11	1.01448E-11
10.0	1.11669E-14	1.11660E-14	1.11669E-14	2.95705E-11	1.00919E-11
12.0	1.11645E-14	1.11453E-14	2.72945E-14	2.87287E-11	9.99013E-12
14.0	1.11609E-14	1.11653E-14	1.11669E-14	2.83561E-11	9.93417E-12
16.0	1.11669E-14	1.11669E-14	1.11669E-14	2.81392E-11	1.02713E-11
18.0	1.11659E-14	1.11669E-14	1.11669E-14	2.80186E-11	1.01401E-11
20.0	1.11669E-14	1.11669E-14	2.73515E-14	2.77752E-11	1.01065E-11
22.0	2.73516E-14	2.73518E-14	2.73519E-14	2.75950E-11	1.01498E-11
24.0	2.73518E-14	2.73519E-14	2.73514E-14	2.76555E-11	1.01112E-11
26.0	2.73510E-14	2.73514E-14	2.73510E-14	2.75162E-11	1.00206E-11
28.0	2.73510E-14	2.73510E-14	2.73510E-14	2.69739E-11	9.94615E-12
30.0	2.73510E-14	2.73510E-14	2.73510E-14	2.66971E-11	9.99774E-12
32.0	2.73510E-14	2.73514E-14	2.73510E-14	2.67805E-11	9.98765E-12
34.0	2.73514E-14	2.73510E-14	2.73510E-14	2.66411E-11	9.93473E-12
36.0	2.73516E-14	2.73510E-14	2.73510E-14	2.65790E-11	9.87793E-12
38.0	2.73510E-14	2.73510E-14	5.91270E-14	2.65465E-11	9.90332E-12
40.0	2.73510E-14	2.73510E-14	3.04575E-14	2.70960E-11	9.86135E-12

170

Table 4-7 (cont.)

RESULTS FOR JOINT 14 LOCATED AT FE NODE 59
 INSIDE RADIUS EQUALS 13.750 THICKNESS EQUALS 3.0300
 CONDITIONAL BLOCK(T,G), VARIOUS T AND G

TIME	G = 0.0	.005	.170	.510	.850
0.	0.	0.	0.	1.31452E-12	4.35005E-14
2.0	0.	0.	0.	1.25143E-12	4.61770E-14
4.0	0.	0.	0.	1.23561E-12	3.65496E-14
6.0	0.	0.	0.	1.23763E-12	4.49594E-14
8.0	0.	0.	0.	1.25027E-12	5.26505E-14
10.0	0.	0.	0.	1.24431E-12	5.62253E-14
12.0	0.	0.	0.	1.25594E-12	5.24309E-14
14.0	0.	0.	0.	1.26137E-12	5.89470E-14
16.0	0.	0.	0.	1.25919E-12	7.46630E-14
18.0	0.	0.	0.	1.25972E-12	6.46674E-14
20.0	0.	0.	0.	1.24417E-12	9.32575E-14
22.0	0.	0.	0.	1.24174E-12	8.93014E-14
24.0	0.	0.	2.30794E-15	1.23109E-12	4.03740E-14
26.0	0.	0.	0.	1.23240E-12	4.52424E-14
28.0	0.	0.	0.	1.23075E-12	4.05477E-14
30.0	0.	0.	0.	1.23151E-12	1.03615E-13
32.0	0.	0.	0.	1.22494E-12	1.09591E-13
34.0	0.	0.	1.03523E-15	1.21277E-12	1.07763E-13
36.0	0.	0.	3.41596E-15	1.21819E-12	1.16472E-13
38.0	0.	3.41596E-15	6.97744E-15	1.22108E-12	1.25072E-13
40.0	1.74072E-15	3.41596E-15	3.41596E-15	1.23563E-12	1.21142E-13

Table 4-3
 Tabulation of Values of $P|t_{leak} < t|Eq.(9,t)|$ For Weld Joints
 Considered-Results Conditional on a Crack Being Initially Present

RESULTS FOR JOINT 1 LOCATED AT FE NODE 1

CONDITIONAL PLEAK(T,G), VARIOUS T AND G

TIME	$\delta = 6.0$.885	.170	.510	.850
0.	7.17789E-08	7.94792E-08	8.43995E-08	1.32816E-07	1.69116E-07
2.6	2.36272E-07	2.38499E-07	2.39828E-07	2.57411E-07	2.69928E-07
4.0	2.99167E-07	3.06163E-07	3.01456E-07	3.15095E-07	3.27433E-07
6.0	3.60988E-07	3.61180E-07	3.65850E-07	3.78176E-07	3.82684E-07
8.0	4.06879E-07	4.06936E-07	4.08329E-07	4.14562E-07	4.19895E-07
10.0	4.52267E-07	4.52267E-07	4.52267E-07	4.58425E-07	4.64399E-07
12.6	4.92510E-07	4.94269E-07	4.94269E-07	4.99343E-07	5.06220E-07
14.0	5.25294E-07	5.27342E-07	5.24326E-07	5.31370E-07	5.32826E-07
16.0	5.45340E-07	5.45340E-07	5.45340E-07	5.51159E-07	5.55510E-07
18.0	5.75356E-07	5.76051E-07	5.78948E-07	5.81130E-07	5.86454E-07
20.0	6.06636E-07	6.06037E-07	6.00037E-07	6.00120E-07	6.06578E-07
22.0	6.19441E-07	6.19441E-07	6.19441E-07	6.21684E-07	6.26780E-07
24.0	6.39623E-07	6.39623E-07	6.39789E-07	6.41121E-07	6.43980E-07
26.0	6.59836E-07	6.59836E-07	6.59865E-07	6.61369E-07	6.62738E-07
28.0	6.79426E-07	6.79427E-07	6.79427E-07	6.87558E-07	6.94860E-07
30.0	7.12168E-07	7.12168E-07	7.14163E-07	7.14720E-07	7.23899E-07
32.0	7.47205E-07	7.47205E-07	7.48695E-07	7.48790E-07	7.53584E-07
34.0	7.66627E-07	7.66627E-07	7.66627E-07	7.68999E-07	7.73824E-07
36.0	7.81262E-07	7.81262E-07	7.81372E-07	7.85824E-07	7.88349E-07
38.0	7.95934E-07	7.95934E-07	7.98446E-07	8.02623E-07	8.06487E-07
40.0	8.18901E-07	8.18901E-07	8.19345E-07	8.23835E-07	8.26610E-07

Table 4-3 (cont.)

RESULTS FOR JOINT 2 LOCATED AT FE NO. 5

CONDITIONAL PLEAK(T.G), VARIOUS T AND G

TIME	G = 0.8	.085	.170	.510	.850
0.	2.64735E-08	2.92691E-08	2.96861E-08	3.63977E-08	3.81070E-08
2.0	7.39530E-08	7.69530E-08	7.18005E-08	7.36933E-08	7.50702E-08
4.0	9.44335E-08	9.44036E-08	9.44036E-08	9.60383E-08	9.60640E-08
6.0	1.10707E-07	1.10707E-07	1.10707E-07	1.10814E-07	1.12065E-07
8.0	1.23360E-07	1.23060E-07	1.23509E-07	1.24449E-07	1.26077E-07
10.0	1.37217E-07	1.37217E-07	1.37217E-07	1.37649E-07	1.37649E-07
12.0	1.47398E-07	1.47398E-07	1.47398E-07	1.47398E-07	1.47444E-07
14.0	1.55651E-07	1.55651E-07	1.55651E-07	1.55652E-07	1.56062E-07
16.0	1.62391E-07	1.63348E-07	1.63348E-07	1.63348E-07	1.66240E-07
18.0	1.73367E-07	1.73367E-07	1.73367E-07	1.73367E-07	1.73394E-07
20.0	1.79832E-07	1.79832E-07	1.79832E-07	1.79832E-07	1.81043E-07
22.0	1.90093E-07	1.90093E-07	1.90093E-07	1.90093E-07	1.90093E-07
24.0	1.92464E-07	1.92464E-07	1.92464E-07	1.92464E-07	1.92465E-07
26.0	2.02225E-07	2.02225E-07	2.02225E-07	2.02655E-07	2.02655E-07
28.0	2.08374E-07	2.08374E-07	2.08374E-07	2.08374E-07	2.08374E-07
30.0	2.11933E-07	2.11933E-07	2.11933E-07	2.11933E-07	2.12375E-07
32.0	2.15066E-07	2.15066E-07	2.15066E-07	2.15066E-07	2.16029E-07
34.0	2.20971E-07	2.20971E-07	2.20971E-07	2.20971E-07	2.20972E-07
36.0	2.21982E-07	2.21982E-07	2.21982E-07	2.23001E-07	2.23001E-07
38.0	2.29623E-07	2.29623E-07	2.29623E-07	2.29623E-07	2.29623E-07
40.0	2.33120E-07	2.33120E-07	2.33120E-07	2.33120E-07	2.33178E-07

Table 4-3 (cont.)

RESULTS FOR JOINT 3 LOCATED AT FE NODE 7

CONDITIONAL CLEARCY.G), VARIOUS T AND G

TIME	G = 0.0	.025	.170	.510	.850
0.	4.56546E-10	4.63743E-10	5.81863E-10	4.96293E-10	1.09322E-09
2.0	1.15779E-09	1.17635E-09	1.18650E-09	1.31996E-09	1.52173E-09
4.0	1.57237E-09	1.60473E-09	1.61467E-09	1.70180E-09	1.78521E-09
6.0	1.82522E-09	1.82523E-09	1.84020E-09	1.91936E-09	1.99351E-09
8.0	2.05500E-09	2.05537E-09	2.07117E-09	2.12959E-09	2.15743E-09
10.0	2.19099E-09	2.25913E-09	2.21863E-09	2.25988E-09	2.29162E-09
12.0	2.32163E-09	2.32142E-09	2.32183E-09	2.34830E-09	2.37565E-09
14.0	2.41509E-09	2.41529E-09	2.41897E-09	2.44936E-09	2.47417E-09
16.0	2.50216E-09	2.51132E-09	2.51177E-09	2.54904E-09	2.60512E-09
18.0	2.61026E-09	2.61392E-09	2.61392E-09	2.68051E-09	2.75301E-09
20.0	2.70990E-09	2.79817E-09	2.79037E-09	2.81710E-09	2.85806E-09
22.0	2.75540E-09	2.85711E-09	2.86649E-09	2.89183E-09	2.93072E-09
24.0	2.87553E-09	2.98020E-09	2.99233E-09	3.02576E-09	3.03562E-09
26.0	3.26139E-09	3.07710E-09	3.08429E-09	3.12227E-09	3.16654E-09
28.0	3.17297E-09	3.17980E-09	3.18026E-09	3.18728E-09	3.24562E-09
30.0	3.25677E-09	3.25677E-09	3.26597E-09	3.28313E-09	3.29465E-09
32.0	3.29106E-09	3.30870E-09	3.30769E-09	3.32958E-09	3.36396E-09
34.0	3.36050E-09	3.36858E-09	3.36858E-09	3.38097E-09	3.39521E-09
36.0	3.41211E-09	3.42209E-09	3.43164E-09	3.44635E-09	3.49104E-09
38.0	3.52770E-09	3.53561E-09	3.54889E-09	3.57301E-09	3.59034E-09
40.0	3.61326E-09	3.61756E-09	3.62455E-09	3.65626E-09	3.66332E-09

Table 4-3 (cont.)

RESULTS FOR JOINT 4 LOCATED AT FE NODE 9

CONDITIONAL PLEAK(T,G), VARIOUS T AND G

TIME	G = 0.0	.005	.170	.510	.850
0.	4.82410E-10	6.09595E-10	6.95315E-10	1.09984E-09	1.20615E-09
2.0	1.61600E-09	1.63717E-09	1.69400E-09	1.83565E-09	1.91821E-09
4.0	2.10024E-09	2.11934E-09	2.15272E-09	2.23651E-09	2.26729E-09
6.0	2.39204E-09	2.41177E-09	2.41511E-09	2.48827E-09	2.51586E-09
8.0	2.60191E-09	2.60244E-09	2.61506E-09	2.67574E-09	2.72048E-09
10.0	2.85299E-09	2.86234E-09	2.89264E-09	2.9519E-09	2.98416E-09
12.0	3.05952E-09	3.06844E-09	3.08614E-09	3.16002E-09	3.18672E-09
14.0	3.28719E-09	3.28768E-09	3.31046E-09	3.34758E-09	3.36188E-09
16.0	3.45150E-09	3.46132E-09	3.46133E-09	3.47926E-09	3.50331E-09
18.0	3.57363E-09	3.57392E-09	3.58351E-09	3.61394E-09	3.64368E-09
20.0	3.74405E-09	3.75762E-09	3.76191E-09	3.80603E-09	3.82624E-09
22.0	3.88970E-09	3.91211E-09	3.93516E-09	3.97430E-09	4.00660E-09
24.0	4.07903E-09	4.07904E-09	4.07906E-09	4.12188E-09	4.16375E-09
26.0	4.22295E-09	4.22777E-09	4.23115E-09	4.26129E-09	4.29067E-09
28.0	4.36378E-09	4.37809E-09	4.39209E-09	4.42384E-09	4.46867E-09
30.0	4.53078E-09	4.53078E-09	4.53511E-09	4.56709E-09	4.58788E-09
32.0	4.62582E-09	4.63470E-09	4.63471E-09	4.66729E-09	4.67983E-09
34.0	4.76088E-09	4.76088E-09	4.76118E-09	4.78196E-09	4.81230E-09
36.0	4.87257E-09	4.87257E-09	4.87962E-09	4.92315E-09	4.93807E-09
38.0	5.02236E-09	5.02710E-09	5.02710E-09	5.03775E-09	5.06775E-09
40.0	5.09933E-09	5.09934E-09	5.11780E-09	5.13240E-09	5.13730E-09

Table 4-3 (cont.)

RESULTS FOR JOINT 5 LOCATED AT FE NODE 26

CONDITIONAL PLEAK(T,G), VARIOUS T AND G

TIME	G = 0.0	.085	.170	.510	.850
0.	2.89576E-10	3.53124E-10	4.31564E-10	8.96100E-10	1.04584E-09
2.0	9.75334E-10	9.85340E-10	1.00867E-09	1.24158E-09	1.37375E-09
4.0	1.32774E-09	1.34520E-09	1.36414E-09	1.49232E-09	1.62009E-09
6.0	1.58611E-09	1.59897E-09	1.62035E-09	1.73415E-09	1.81815E-09
8.0	1.79280E-09	1.80065E-09	1.80126E-09	1.89926E-09	1.95990E-09
10.0	1.94662E-09	1.94662E-09	1.95665E-09	2.00408E-09	2.06498E-09
12.0	2.05643E-09	2.06216E-09	2.07255E-09	2.13292E-09	2.19883E-09
14.0	2.18883E-09	2.19881E-09	2.19881E-09	2.27062E-09	2.27431E-09
16.0	2.25752E-09	2.26296E-09	2.26296E-09	2.33716E-09	2.36789E-09
18.0	2.35911E-09	2.36765E-09	2.36804E-09	2.43417E-09	2.46794E-09
20.0	2.45636E-09	2.45637E-09	2.46501E-09	2.52988E-09	2.55340E-09
22.0	2.54764E-09	2.54764E-09	2.55494E-09	2.60125E-09	2.64166E-09
24.0	2.63592E-09	2.63593E-09	2.63618E-09	2.70771E-09	2.73963E-09
26.0	2.73084E-09	2.73348E-09	2.73961E-09	2.78341E-09	2.81478E-09
28.0	2.80314E-09	2.80884E-09	2.81176E-09	2.88627E-09	2.92341E-09
30.0	2.91570E-09	2.92338E-09	2.92940E-09	2.96576E-09	3.01170E-09
32.0	3.00002E-09	3.00025E-09	3.01173E-09	3.04783E-09	3.10012E-09
34.0	3.08555E-09	3.09168E-09	3.09437E-09	3.15302E-09	3.19662E-09
36.0	3.18413E-09	3.19078E-09	3.19078E-09	3.23086E-09	3.24877E-09
38.0	3.24304E-09	3.24304E-09	3.24304E-09	3.26013E-09	3.28719E-09
40.0	3.28715E-09	3.28715E-09	3.28715E-09	3.29320E-09	3.29838E-09

Table 4-3 (cont.)

RESULTS FOR JOINT 6 LOCATED AT FE NODE 27

CONDITIONAL FLEAK(T,G). VARIOUS T AND G

TIME	G = 0.0	.085	.170	.510	.850
0.	1.26188E-08	1.42811E-08	1.59229E-08	2.35490E-08	2.60449E-08
2.0	4.07433E-08	4.09066E-08	4.13863E-08	4.23879E-08	4.32135E-08
4.0	5.31040E-08	5.34153E-08	5.34154E-08	5.46014E-08	5.51014E-08
6.0	6.21107E-08	6.22837E-08	6.24398E-08	6.38927E-08	6.42146E-08
8.0	7.01524E-08	7.01524E-08	7.01575E-08	7.07015E-08	7.08542E-08
10.0	7.54300E-08	7.55864E-08	7.59001E-08	7.64365E-08	7.65927E-08
12.0	8.10609E-08	8.12483E-08	8.12718E-08	8.16181E-08	8.18192E-08
14.0	8.68833E-08	8.68833E-08	8.72133E-08	8.78791E-08	8.80381E-08
16.0	9.13250E-08	9.13300E-08	9.13532E-08	9.15247E-08	9.30117E-08
18.0	9.51038E-08	9.52621E-08	9.52621E-08	9.61503E-08	9.61719E-08
20.0	9.88435E-08	9.88435E-08	9.88436E-08	9.93827E-08	9.97247E-08
22.0	1.01567E-07	1.01572E-07	1.01911E-07	1.01939E-07	1.01946E-07
24.0	1.04017E-07	1.04017E-07	1.04017E-07	1.04236E-07	1.04404E-07
26.0	1.06852E-07	1.06859E-07	1.06859E-07	1.07012E-07	1.07183E-07
28.0	1.10042E-07	1.10046E-07	1.10229E-07	1.10400E-07	1.10423E-07
30.0	1.13259E-07	1.13259E-07	1.13416E-07	1.14146E-07	1.14500E-07
32.0	1.16960E-07	1.16960E-07	1.16960E-07	1.17117E-07	1.17143E-07
34.0	1.19876E-07	1.19893E-07	1.20081E-07	1.20759E-07	1.20776E-07
36.0	1.22046E-07	1.22053E-07	1.22070E-07	1.22405E-07	1.22567E-07
38.0	1.24939E-07	1.24939E-07	1.25095E-07	1.25290E-07	1.25466E-07
40.0	1.26129E-07	1.28129E-07	1.28305E-07	1.28538E-07	1.28538E-07

Table 4-3 (cont.)

RESULTS FOR JOINT 7 LOCATED AT FE NODE 28
 CONDITICNAL PLEAK(T,G), VARIOUS T AND G

TIME	G = 0.0	.085	.170	.510	.850
0.	1.26188E-08	1.39709E-08	1.49502E-08	2.02317E-08	2.38788E-08
2.0	4.07385E-08	4.09172E-08	4.10803E-08	4.20667E-08	4.23839E-08
4.0	5.23609E-08	5.26332E-08	5.30925E-08	5.39150E-08	5.44253E-08
6.0	6.14704E-08	6.15203E-08	6.19519E-08	6.29199E-08	6.33971E-08
8.0	6.96156E-08	6.96205E-08	6.96490E-08	6.99800E-08	7.03235E-08
10.0	7.45807E-08	7.45807E-08	7.45807E-08	7.57226E-08	7.59122E-08
12.0	8.02082E-08	8.02132E-08	8.07003E-08	8.07393E-08	8.09286E-08
14.0	8.58668E-08	8.58668E-08	8.62111E-08	8.65285E-08	8.68653E-08
16.0	8.99293E-08	8.99293E-08	9.03114E-08	9.07991E-08	9.09985E-08
18.0	9.38443E-08	9.38507E-08	9.38508E-08	9.47338E-08	9.50908E-08
20.0	9.74592E-08	9.74592E-08	9.74592E-08	9.84527E-08	9.84888E-08
22.0	1.00891E-07	1.00891E-07	1.00891E-07	1.01208E-07	1.01208E-07
24.0	1.03111E-07	1.03111E-07	1.03111E-07	1.03465E-07	1.03482E-07
26.0	1.05660E-07	1.05660E-07	1.05660E-07	1.05850E-07	1.05851E-07
28.0	1.09112E-07	1.09112E-07	1.09129E-07	1.09152E-07	1.09175E-07
30.0	1.11993E-07	1.11993E-07	1.11993E-07	1.12487E-07	1.12720E-07
32.0	1.15153E-07	1.15153E-07	1.15338E-07	1.16231E-07	1.16412E-07
34.0	1.18817E-07	1.18817E-07	1.18975E-07	1.19162E-07	1.19345E-07
36.0	1.20599E-07	1.20599E-07	1.20599E-07	1.20767E-07	1.20774E-07
38.0	1.23914E-07	1.23918E-07	1.23918E-07	1.23918E-07	1.24077E-07
40.0	1.26448E-07	1.26611E-07	1.26611E-07	1.26931E-07	1.27123E-07

Table 4-3 (cont.)

RESULTS FOR JOINT , LOCATED AT FE NODE 31

CONDITIONAL PLEAK(T,G), VARIOUS T AND G

TIME	G = 0.0	.085	.170	.510	.850
0.	9.33594E-09	1.05855E-08	1.19613E-08	1.52011E-08	1.68063E-08
2.0	2.08541E-08	2.92085E-08	2.92085E-08	3.02813E-08	3.02815E-08
4.0	3.65385E-08	3.65385E-08	3.65485E-08	3.65592E-08	3.65594E-08
6.0	4.25092E-08	4.28254E-08	4.31362E-08	4.31364E-08	4.34511E-08
8.0	4.77536E-08	4.80633E-08	4.80633E-08	4.80735E-08	4.83918E-08
10.0	4.94955E-08	4.98034E-08	4.98034E-08	4.98271E-08	5.01841E-08
12.0	5.39448E-08	5.39448E-08	5.39448E-08	5.43208E-08	5.46293E-08
14.0	5.72718E-08	5.72718E-08	5.72718E-08	5.79178E-08	5.79179E-08
16.0	6.03726E-08	6.06868E-08	6.06868E-08	6.06868E-08	6.07003E-08
18.0	6.17966E-08	6.17966E-08	6.17966E-08	6.17966E-08	6.18306E-08
20.0	6.39137E-08	6.39137E-08	6.39137E-08	6.42518E-08	6.42519E-08
22.0	6.58921E-08	6.58921E-08	6.58921E-08	6.59057E-08	6.59057E-08
24.0	6.75905E-08	6.75005E-08	6.78139E-08	6.78239E-08	6.78239E-08
26.0	7.01597E-08	7.01597E-08	7.01597E-08	7.01597E-08	7.01597E-08
28.0	7.11993E-08	7.11993E-08	7.11993E-08	7.11994E-08	7.11994E-08
30.0	7.26132E-08	7.26132E-08	7.26132E-08	7.26132E-08	7.26132E-08
32.0	7.33768E-08	7.34111E-08	7.34113E-08	7.34113E-08	7.34451E-08
34.0	7.62911E-08	7.62913E-08	7.62913E-08	7.66078E-08	7.66078E-08
36.0	7.70101E-08	7.70101E-08	7.70101E-08	7.70340E-08	7.70340E-08
38.0	7.80541E-08	7.80541E-08	7.80541E-08	7.80541E-08	7.84217E-08
40.0	8.04788E-08	8.04788E-08	8.04788E-08	8.04788E-08	8.04788E-08

Table 4-3 (cont.)

RESULTS FOR JOINT 9 LOCATED AT FE NODE 35

CONDITIONAL PLEAK(T,G), VARIOUS T AND G

TIME	G = 0.0	.085	.170	.510	.850
0.	1.05382E-08	1.29581E-08	1.62687E-08	2.73611E-08	3.21091E-08
2.0	3.37757E-08	3.48992E-08	3.46262E-08	3.88408E-08	4.06721E-08
4.0	4.22086E-08	4.27411E-08	4.35964E-08	4.68596E-08	4.87514E-08
6.0	5.06368E-08	5.08022E-08	5.13135E-08	5.25189E-08	5.49155E-08
8.0	5.58510E-08	5.58512E-08	5.60085E-08	5.78428E-08	6.02666E-08
10.0	6.18725E-08	6.23648E-08	6.23815E-08	6.30836E-08	6.51679E-08
12.0	6.63128E-08	6.64673E-08	6.64776E-08	6.77991E-08	6.89977E-08
14.0	7.07119E-08	7.07171E-08	7.07337E-08	7.09137E-08	7.25919E-08
16.0	7.54235E-08	7.54236E-08	7.56079E-08	7.48242E-08	7.56925E-08
18.0	7.67189E-08	7.67304E-08	7.67305E-08	7.81005E-08	7.92543E-08
20.0	8.01750E-08	8.03281E-08	8.04931E-08	8.21729E-08	8.33270E-08
22.0	8.39338E-08	8.39338E-08	8.40921E-08	8.44608E-08	8.51600E-08
24.0	8.64392E-08	8.66062E-08	8.66064E-08	8.81002E-08	8.86252E-08
26.0	8.88603E-08	8.88605E-08	8.90690E-08	8.99924E-08	9.12376E-08
28.0	9.16188E-08	9.16189E-08	9.16405E-08	9.21834E-08	9.23727E-08
30.0	9.35645E-08	9.35858E-08	9.39403E-08	9.48125E-08	9.52109E-08
32.0	9.54528E-08	9.54528E-08	9.56129E-08	9.60987E-08	9.64751E-08
34.0	9.71564E-08	9.71571E-08	9.73109E-08	9.80029E-08	9.83581E-08
36.0	9.83834E-08	9.83998E-08	9.83998E-08	9.90775E-08	9.96516E-08
38.0	1.00210E-07	1.00210E-07	1.00551E-07	1.01053E-07	1.01538E-07
40.0	1.02579E-07	1.02579E-07	1.02601E-07	1.03626E-07	1.04015E-07

Table 4-3 (cont.)

RESULTS FOR JOINT 10 LOCATED AT FE NODE 37

CONDITIONAL PLEAK(T,G), VARIOUS T AND G

TIME	G = 0.0	.085	.170	.510	.850
0.	3.55984E-10	4.20912E-10	4.81128E-10	8.43870E-10	1.05394E-09
2.0	1.19266E-09	1.20265E-09	1.23317E-09	1.39548E-09	1.51631E-09
4.0	1.63018E-09	1.64320E-09	1.66474E-09	1.76916E-09	1.86245E-09
6.0	1.92074E-09	1.94214E-09	1.94252E-09	2.00219E-09	2.05636E-09
8.0	2.11194E-09	2.11767E-09	2.13078E-09	2.17839E-09	2.25442E-09
10.0	2.26808E-09	2.26808E-09	2.28309E-09	2.32988E-09	2.40392E-09
12.0	2.42022E-09	2.42876E-09	2.42915E-09	2.47877E-09	2.53776E-09
14.0	2.57881E-09	2.59403E-09	2.60233E-09	2.62610E-09	2.67162E-09
16.0	2.72001E-09	2.72002E-09	2.72043E-09	2.76695E-09	2.82379E-09
18.0	2.84850E-09	2.85111E-09	2.86141E-09	2.90167E-09	2.96818E-09
20.0	3.01321E-09	3.01322E-09	3.02309E-09	3.05524E-09	3.10768E-09
22.0	3.14064E-09	3.14064E-09	3.14064E-09	3.19579E-09	3.24262E-09
24.0	3.29221E-09	3.29221E-09	3.30045E-09	3.33216E-09	3.35028E-09
26.0	3.35866E-09	3.35867E-09	3.36135E-09	3.38866E-09	3.39454E-09
28.0	3.39977E-09	3.39977E-09	3.40597E-09	3.45484E-09	3.47644E-09
30.0	3.51501E-09	3.51501E-09	3.51501E-09	3.55435E-09	3.58719E-09
32.0	3.61239E-09	3.61239E-09	3.61493E-09	3.66529E-09	3.73517E-09
34.0	3.72834E-09	3.73206E-09	3.73206E-09	3.76923E-09	3.82814E-09
36.0	3.81850E-09	3.81874E-09	3.81891E-09	3.86365E-09	3.89394E-09
38.0	3.89433E-09	3.89433E-09	3.89696E-09	3.91818E-09	3.93027E-09
40.0	3.96163E-09	3.96185E-09	3.96930E-09	3.99421E-09	4.02126E-09

Table 4-3 (cont.)

RESULTS FOR JOINT 11 LOCATED AT FE NODE 48

CONDITIONAL PLEAK(T,S), VARIOUS T AND G

TIME	G = 0.0	.085	.170	.510	.850
0.	2.87691E-12	4.41626E-12	7.59684E-12	2.16570E-11	2.75456E-11
2.0	9.14158E-12	9.41735E-12	1.05442E-11	2.19513E-11	2.61610E-11
4.0	1.18814E-11	1.21831E-11	1.28219E-11	2.17187E-11	2.62642E-11
6.0	1.35430E-11	1.36477E-11	1.41625E-11	2.19997E-11	2.67997E-11
8.0	1.49053E-11	1.50339E-11	1.54320E-11	2.23657E-11	2.70200E-11
10.0	1.64315E-11	1.65420E-11	1.73921E-11	2.30671E-11	2.73473E-11
12.0	1.79439E-11	1.81172E-11	1.85081E-11	2.38652E-11	2.75046E-11
14.0	1.88772E-11	1.89742E-11	1.93762E-11	2.41168E-11	2.76102E-11
16.0	1.97579E-11	1.98004E-11	2.00654E-11	2.53075E-11	2.79480E-11
18.0	2.05266E-11	2.65768E-11	2.07094E-11	2.57663E-11	2.85255E-11
20.0	2.12763E-11	2.13909E-11	2.16248E-11	2.61031E-11	2.89478E-11
22.0	2.20379E-11	2.21254E-11	2.23010E-11	2.61383E-11	2.91966E-11
24.0	2.26997E-11	2.27706E-11	2.31865E-11	2.66970E-11	2.97800E-11
26.0	2.37019E-11	2.37890E-11	2.39777E-11	2.69784E-11	2.99352E-11
28.0	2.41562E-11	2.41674E-11	2.43914E-11	2.74463E-11	3.03753E-11
30.0	2.45859E-11	2.46449E-11	2.48134E-11	2.80029E-11	3.08177E-11
32.0	2.50157E-11	2.50743E-11	2.52309E-11	2.85257E-11	3.14993E-11
34.0	2.55282E-11	2.55694E-11	2.57950E-11	2.90469E-11	3.19476E-11
36.0	2.60930E-11	2.61867E-11	2.63574E-11	2.96421E-11	3.23748E-11
38.0	2.67065E-11	2.67370E-11	2.68346E-11	3.00760E-11	3.28282E-11
40.0	2.70873E-11	2.71801E-11	2.73229E-11	3.04154E-11	3.31831E-11

Table 4-3 (cont.)

RESULTS FOR JOINT 12 LOCATED AT FE NODE 51

CONDITIONAL PLEAK(T,G), VARIOUS T AND G

TIME	G = 0.0	.085	.170	.510	.850
C.	4.33423E-08	5.48718E-08	8.51381E-08	2.33183E-07	2.92144E-07
2.0	1.22624E-07	1.24962E-07	1.31024E-07	2.24636E-07	2.84526E-07
4.0	1.46709E-07	1.49465E-07	1.54628E-07	2.30558E-07	2.87584E-07
6.0	1.63818E-07	1.63818E-07	1.69736E-07	2.41304E-07	2.80450E-07
8.0	1.87133E-07	1.87133E-07	1.89824E-07	2.53987E-07	2.85879E-07
10.0	2.02357E-07	2.02358E-07	2.05534E-07	2.65372E-07	2.93039E-07
12.0	2.15591E-07	2.16420E-07	2.20517E-07	2.65132E-07	3.06422E-07
14.0	2.34646E-07	2.37974E-07	2.41194E-07	2.75045E-07	3.09209E-07
15.0	2.43113E-07	2.43164E-07	2.45850E-07	2.76757E-07	3.11940E-07
18.0	2.52272E-07	2.52273E-07	2.52273E-07	2.93716E-07	3.24266E-07
20.0	2.59039E-07	2.59040E-07	2.59193E-07	2.99274E-07	3.39958E-07
22.0	2.68527E-07	2.68527E-07	2.70401E-07	3.08306E-07	3.42828E-07
24.0	2.76011E-07	2.60276E-07	2.80380E-07	3.17016E-07	3.46152E-07
26.0	2.81861E-07	2.81964E-07	2.81965E-07	3.25443E-07	3.45276E-07
28.0	2.87247E-07	2.89589E-07	2.91379E-07	3.28336E-07	3.51255E-07
30.0	2.98570E-07	2.98570E-07	3.03994E-07	3.35124E-07	3.57959E-07
32.0	3.07071E-07	3.07071E-07	3.10784E-07	3.34273E-07	3.58271E-07
34.0	3.10282E-07	3.11858E-07	3.13501E-07	3.36574E-07	3.56738E-07
35.0	3.14609E-07	3.14609E-07	3.17265E-07	3.43343E-07	3.62217E-07
38.0	3.23168E-07	3.23168E-07	3.25005E-07	3.49104E-07	3.64684E-07
40.0	3.26493E-07	3.26493E-07	3.27543E-07	3.49412E-07	3.75471E-07

Table 4-3 (cont.)

RESULTS FOR JOINT 13 LOCATED AT FE NODE 58

CONDITIONAL PLEAK(T,G), VARIOUS T AND G

TIME	G = 0.0	.085	.170	.510	.850
0.	4.51572E-08	4.98782E-08	7.12946E-08	1.53473E-07	1.87701E-07
2.0	1.26728E-07	1.26728E-07	1.29879E-07	1.63762E-07	1.88871E-07
4.0	1.53032E-07	1.55672E-07	1.55821E-07	1.78242E-07	2.08759E-07
6.0	1.70999E-07	1.70999E-07	1.75998E-07	2.01618E-07	2.18591E-07
8.0	1.97941E-07	1.97942E-07	2.00580E-07	2.15790E-07	2.34457E-07
10.0	2.13941E-07	2.16239E-07	2.16290E-07	2.35833E-07	2.57766E-07
12.0	2.30405E-07	2.31222E-07	2.31273E-07	2.54788E-07	2.67509E-07
14.0	2.51133E-07	2.51133E-07	2.51950E-07	2.63901E-07	2.72130E-07
16.0	2.54782E-07	2.54782E-07	2.54782E-07	2.63057E-07	2.69959E-07
18.0	2.63029E-07	2.63029E-07	2.63029E-07	2.72344E-07	2.82988E-07
20.0	2.72316E-07	2.72316E-07	2.74786E-07	2.83057E-07	2.98407E-07
22.0	2.79386E-07	2.79386E-07	2.80217E-07	2.96649E-07	3.03613E-07
24.0	2.89388E-07	2.89388E-07	2.91198E-07	2.98197E-07	3.07594E-07
26.0	2.92721E-07	2.92721E-07	2.93665E-07	3.04495E-07	3.16630E-07
28.0	3.04468E-07	3.04520E-07	3.04520E-07	3.18592E-07	3.34371E-07
30.0	3.11165E-07	3.11165E-07	3.11269E-07	3.26988E-07	3.31663E-07
32.0	3.21535E-07	3.21535E-07	3.23402E-07	3.26254E-07	3.34896E-07
34.0	3.24360E-07	3.26165E-07	3.26217E-07	3.33045E-07	3.39522E-07
36.0	3.33018E-07	3.33124E-07	3.35676E-07	3.39590E-07	3.47301E-07
38.0	3.37728E-07	3.37728E-07	3.41869E-07	3.45482E-07	3.54039E-07
40.0	3.43655E-07	3.43655E-07	3.43655E-07	3.52307E-07	3.59895E-07

Table 4-3 (cont.)

RESULTS FOR JOINT 14 LOCATED AT FE NODE 59

CONDITIONAL PLEAK(T,G), VARIOUS T AND G

TIME	G = 0.0	.085	.170	.510	.850
0.	7.60813E-10	9.55400E-10	1.52800E-09	3.04124E-09	3.88487E-09
2.0	2.36768E-09	2.52507E-09	2.72915E-09	3.52771E-09	4.03561E-09
4.0	3.26618E-09	3.31788E-09	3.37025E-09	3.90386E-09	4.22197E-09
6.0	3.72354E-09	3.74685E-09	3.74041E-09	4.20311E-09	4.47934E-09
8.0	4.01422E-09	4.14840E-09	4.17366E-09	4.48154E-09	5.09058E-09
10.0	4.37446E-09	4.37446E-09	4.48000E-09	5.09212E-09	5.29932E-09
12.0	4.93193E-09	4.93196E-09	5.08865E-09	5.19488E-09	5.48954E-09
14.0	5.14109E-09	5.14110E-09	5.25811E-09	5.48640E-09	5.63482E-09
16.0	5.33261E-09	5.38078E-09	5.38080E-09	5.53887E-09	5.83118E-09
18.0	5.52963E-09	5.52963E-09	5.55347E-09	5.83392E-09	6.11383E-09
20.0	5.77798E-09	5.77798E-09	5.88718E-09	6.06104E-09	6.29423E-09
22.0	5.90120E-09	5.90120E-09	5.96888E-09	6.13677E-09	6.35804E-09
24.0	6.02671E-09	6.02871E-09	6.03072E-09	6.29735E-09	6.55411E-09
26.0	6.18941E-09	6.18941E-09	6.24446E-09	6.57299E-09	6.84146E-09
28.0	6.46171E-09	6.46171E-09	6.46669E-09	6.73553E-09	7.02799E-09
30.0	6.62807E-09	6.62808E-09	6.62811E-09	7.05826E-09	7.11132E-09
32.0	6.93662E-09	6.93662E-09	7.00494E-09	7.11345E-09	7.34066E-09
34.0	7.00651E-09	7.00651E-09	7.00651E-09	7.30475E-09	7.42671E-09
36.0	7.12822E-09	7.12822E-09	7.31431E-09	7.32120E-09	7.52955E-09
38.0	7.31999E-09	7.31999E-09	7.32002E-09	7.59770E-09	7.73129E-09
40.0	7.42289E-09	7.48993E-09	7.48993E-09	7.62585E-09	8.11759E-09

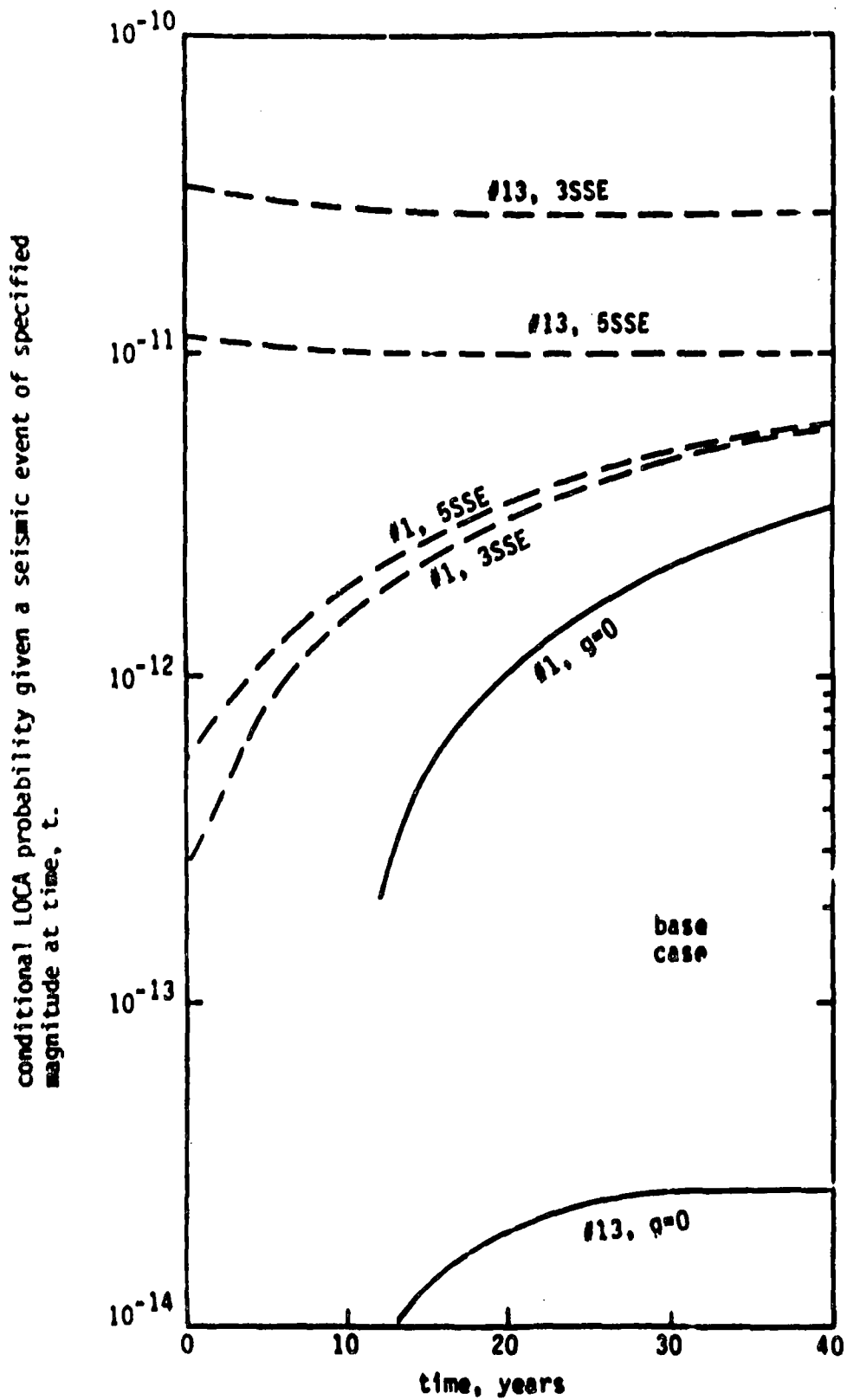


Figure 4-4. Conditional LOCA Probability as a Function of Time for Two Representative Weld Locations Showing Influence of Seismic Events.

sensitivity of joint 13 to seismic events. Additionally, the stresses in joint 13 are seen to be more largely influence by a 3SSE seismic event than a 5SSE event. This is because of the stress values in Table 1-3, which, in turn, has to do with variances in the stresses due to seismic events.

Overall, the results of Table 4-2 and Figures 4-3 and 4-4 show that the probability of a sudden and complete pipe severance (LOCA) is very low (10^{-11} per weld joint per plant lifetime given that a crack is initially present), and that the influence of seismic events is not large. (Joint 13 is somewhat of an exception to this as far as seismic events are concerned.) System failure probabilities will be dominated by the high failure probability locations, which generally show a relatively small influence of seismic events.

Leak probability results were summarized in Table 4-3. Figure 4-5 shows results for joints 1 and 13. From this it is seen that the probability of developing a leak is much higher than the corresponding LOCA probability. This is because very large cracks are required to produce a LOCA, whereas shorter cracks (which occur with a much higher probability) can produce a leak. Figure 4-5 shows that seismic events have a very small influence on the probability of developing a leak. Additionally, calculations were performed for joint 1 that considered all the transients in Table 4-1. The leak probabilities were virtually identical to the corresponding results that included heatup-cooldown only. Hence, the lesser expected influence of radial gradient stresses on leak probabilities that was mentioned above is borne out.

The results of Tables 4-2 and 4-3 can be combined to provide system failure probabilities, and the probability of a seismic induced LOCA. Equations such as 3-9, 3-10, 4-1 and 4-2 would be used. It is important to recall that all results in Tables 4-2 and 4-3 are conditional on a crack being initially present (in each of the weld joints). Hence, the probability of a crack being initially present must be included (see Equation 2-25). As mentioned in Section 2.3.4, the probability of a

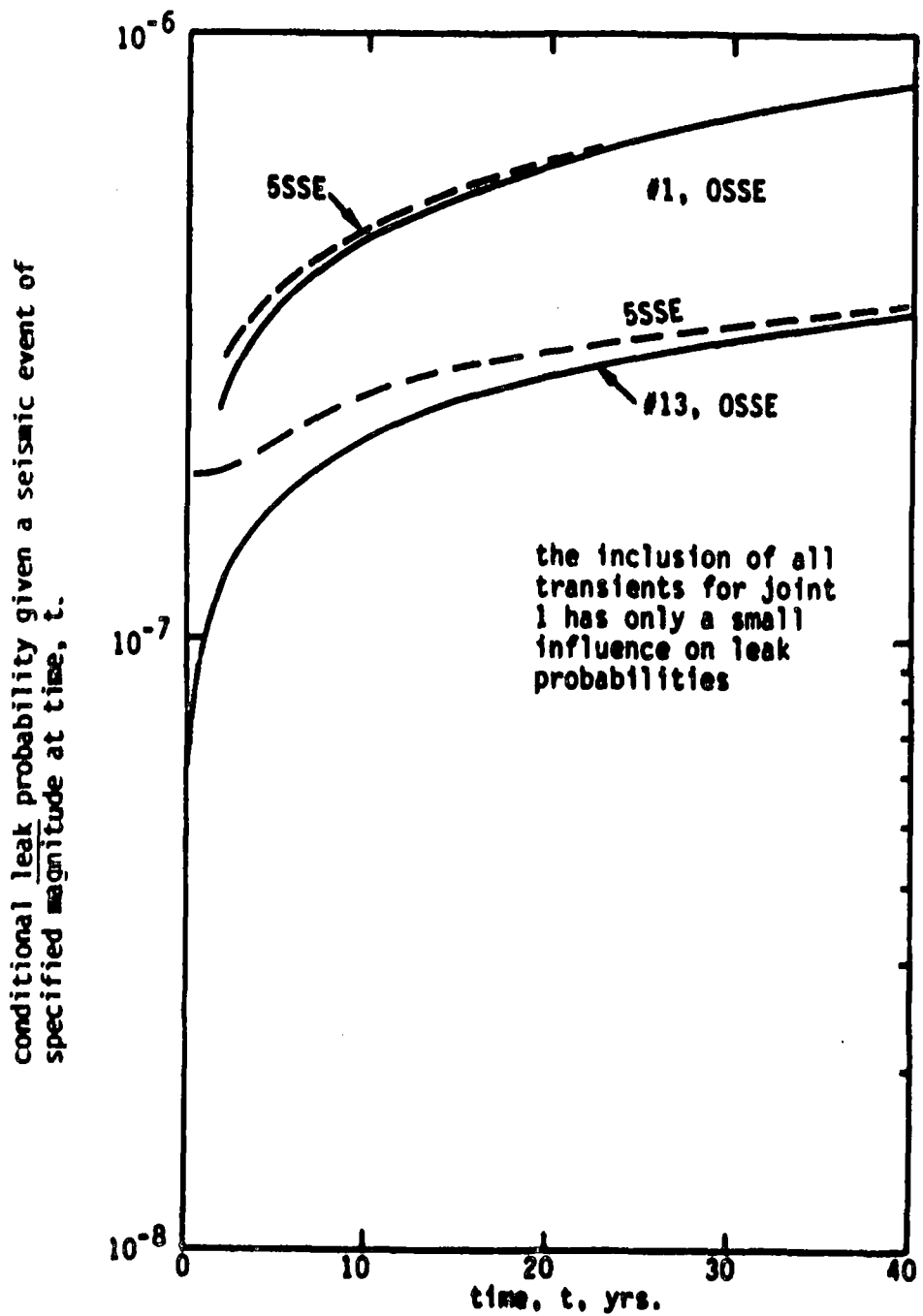


Figure 4-5. Conditional Leak Probabilities as a Function of Time for Two Representative Weld Locations Showing Influence of Seismic Events.

crack being initially present in a weld is about 0.1 for the weld volumes considered. Hence, the absolute failure probabilities will be about an order of magnitude less than the values included in Tables 4-2 and 4-3.

In the case of no seismic events, calculation of the system failure probabilities are particularly simple. The use of Equations 4-1 and 4-2 provide the following results (which include the correction for cracks being initially present).

$$\left\{ \begin{array}{l} \text{cumulative probability of a sudden} \\ \text{and complete pipe severance in} \\ \text{large primary piping (no seismic} \\ \text{events)} \end{array} \right\} = \left\{ \begin{array}{l} 3.7 \times 10^{-13} \text{ (lower bound)*} \\ 1.7 \times 10^{-12} \text{ ("upper bound")} \end{array} \right.$$

$$\left\{ \begin{array}{l} \text{cumulative probability of a leak} \\ \text{in large primary piping (no seismic} \\ \text{events)} \end{array} \right\} = \left\{ \begin{array}{l} 8.8 \times 10^{-8} \text{ (lower bound)*} \\ 9.4 \times 10^{-7} \text{ ("upper bound")} \end{array} \right.$$

Corresponding results that include the influence of seismic events require information on the seismic hazard curve $G(g)$, as shown in Equations 3-9 and 3-10. The consideration of such results is beyond the scope of the current work, and will be generated as part of the Load Combination Program (George 81). However, results presented here on the influence of specified seismic events indicate that the probability of a simultaneous LOCA and seismic event is very low; even when compared to the already small number presented above. Results in Figure 4-5 indicate that the influence of seismic events on leak probabilities is also very small.

The estimates on leak and LOCA probabilities in the primary piping at Zion I that are provided immediately above are quite small. The leak probability in the small subset of piping of $\sim 10^{-6}$ per plant lifetime is somewhat low--but is felt to not be unreasonable. The 6 order of magnitude difference between the leak and LOCA results is somewhat

* Result for joint 1 - highest probability joint.

larger than expected. These results seem to indicate that a sudden and complete pipe severance in the main coolant piping is a very low probability event; bordering on incredible. Additional discussions on this topic follow a discussion of the influence of various input parameters on the calculated failure probability. This forms the topic of the next section.

4.3.3 Influence of Input Parameters on Results

Results for the base case conditions were presented in Section 4.3.2. In order to assess the influence of the values of various input parameters on these results, a series of calculations was performed. The results of such calculations are summarized in this section. Attention is restricted to joint 1, because this joint has the highest failure probability, and therefore tends to dominate the primary loop system failure probability. Additionally, results for joint 13 are generated to provide additional perspectives. All results consider heatup-cooldown as the only non-seismic transient.

The influence of considering the fatigue crack growth characteristics (C) and material failure characteristic (σ_{f10}) as deterministic values rather than random variables is of interest. Calculations were performed that fixed C at its median value, and σ_{f10} at its mean value. The LOCA results are compared in Figure 4-6 with corresponding results considering C and σ_{f10} as random variables. Whether these parameters are taken to be deterministic or random does have an influence on the LOCA probabilities — especially in the absence of seismic events. However, as shown in Figure 4-6, the influence is one-half to one order of magnitude, which, in the present context, is not a large influence.

The effect of random or deterministic C and σ_{f10} on the leak probabilities is even less. This can be seen from the results tabulated below.

t, yrs	Value of $P\{i_{leak} > 1 S_e(0, t)\}$			
	Random C, σ_{f10}		Deterministic C, σ_{f10}	
	$\sigma = 0$	$\sigma = 0.5\sigma$	$\sigma = 0$	$\sigma = 0.5\sigma$
0	7.2×10^{-8}	1.7×10^{-7}	9.2×10^{-8}	1.7×10^{-7}
20	6.6×10^{-7}	6.1×10^{-7}	6.6×10^{-7}	6.6×10^{-7}
10	8.2×10^{-7}	8.2×10^{-7}	7.6×10^{-7}	7.7×10^{-7}

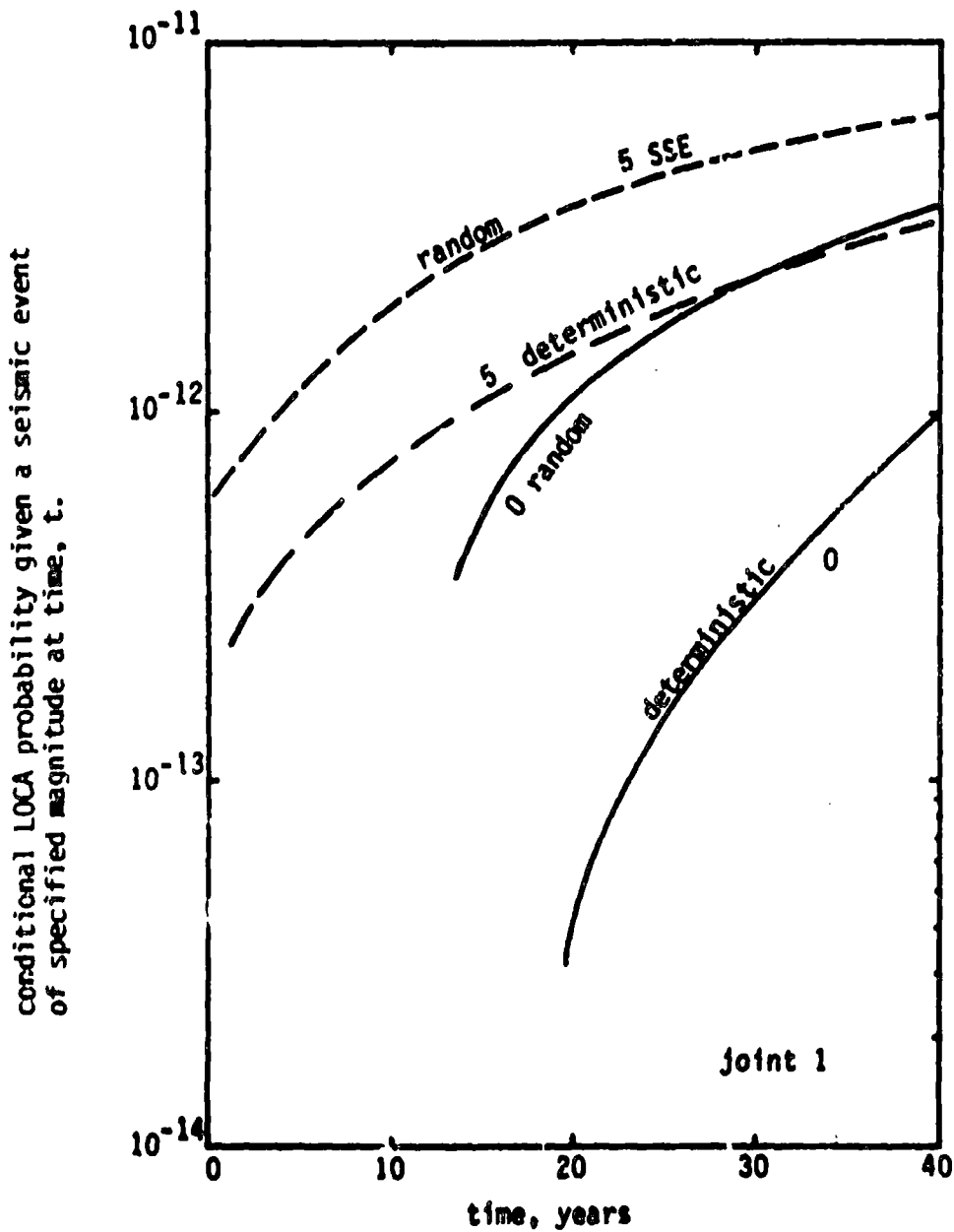


Figure 4-6. Conditional LOCA Probability as a Function of Time Showing Influence of Taking C and σ_{f10} to be Random or Deterministic.

The fairly small influence of considering C and σ_{f10} to be random variables is most likely due to the fairly small variances of these parameters (i.e., small scatter).

The influences of the pre-service inspection and proof test are shown in Figures 4-7 and 4-8. It is seen that both of these procedures have a noticeable influence. The omission of either one raises the failure probability by an order of magnitude. An exception to this is the influence of a proof test on the leak probability. As shown in Figure 4-8, the omission of the proof test has no influence on the leaks. This is because the proof test will not "weed out" the intermediate size cracks that can grow to produce a leak. The proof test does "weed out" a significant portion of the cracks that could grow to produce a LOCA. The difference between an inspection and no inspection on the LOCA probabilities (Figure 4-7) is approximately a factor of 20. This is approximately the value of $(1/P_{ND})$ for large cracks that could grow to produce a LOCA (see Figure 2-13). The influence of inspection on the leak probabilities is somewhat smaller, because P_{ND} for cracks that would grow to produce a leak is somewhat larger (because the relevant cracks are somewhat smaller). These results show that the values of the failure probabilities are influenced by the pre-service inspections and proof test, but that only roughly an order of magnitude is involved. Hence, the calculated failure probabilities remain very low.

In order to gain additional insight into the influence of other factors on the calculated failure probabilities, numerous additional computer runs were made. A comparison of the results was based on the values calculated for a 40 year period (i.e., values at $t = 40$ yrs.). The input parameters were varied from the base case conditions as indicated on Figures 4-9 and 4-10 which show bar graphs of the various results. Conditions were altered from the base case one at a time. The altered conditions are indicated at the bottom of the figures, with the corresponding leak and LOCA probabilities shown in the bar graph. The following observations can be drawn from these figures:

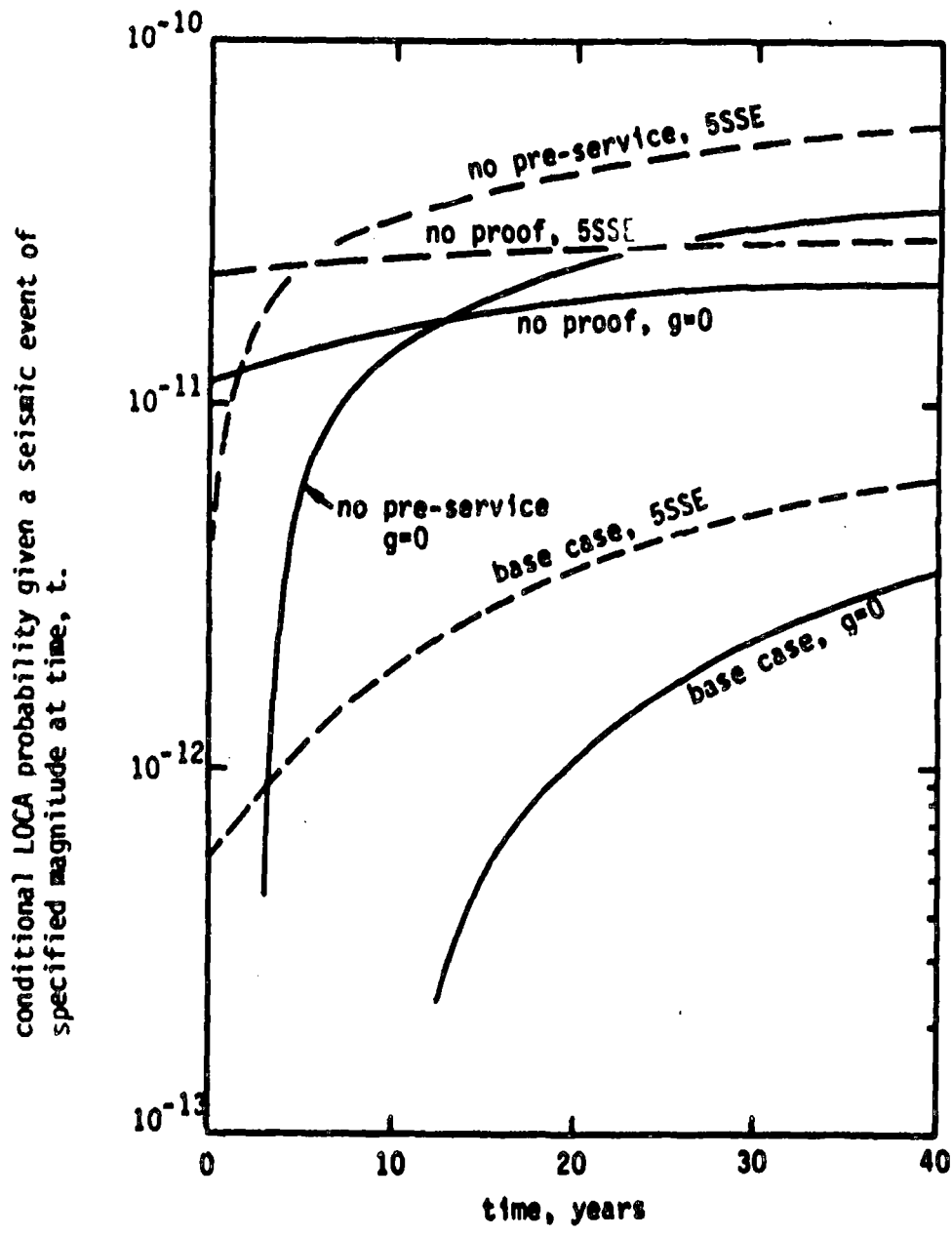


Figure 4-7. Conditional LOCA Probabilities for Joint 1 as a Function of Time for Base Case Conditions and for no Pre-Service Proof Test or no Pre-Service Inspection.

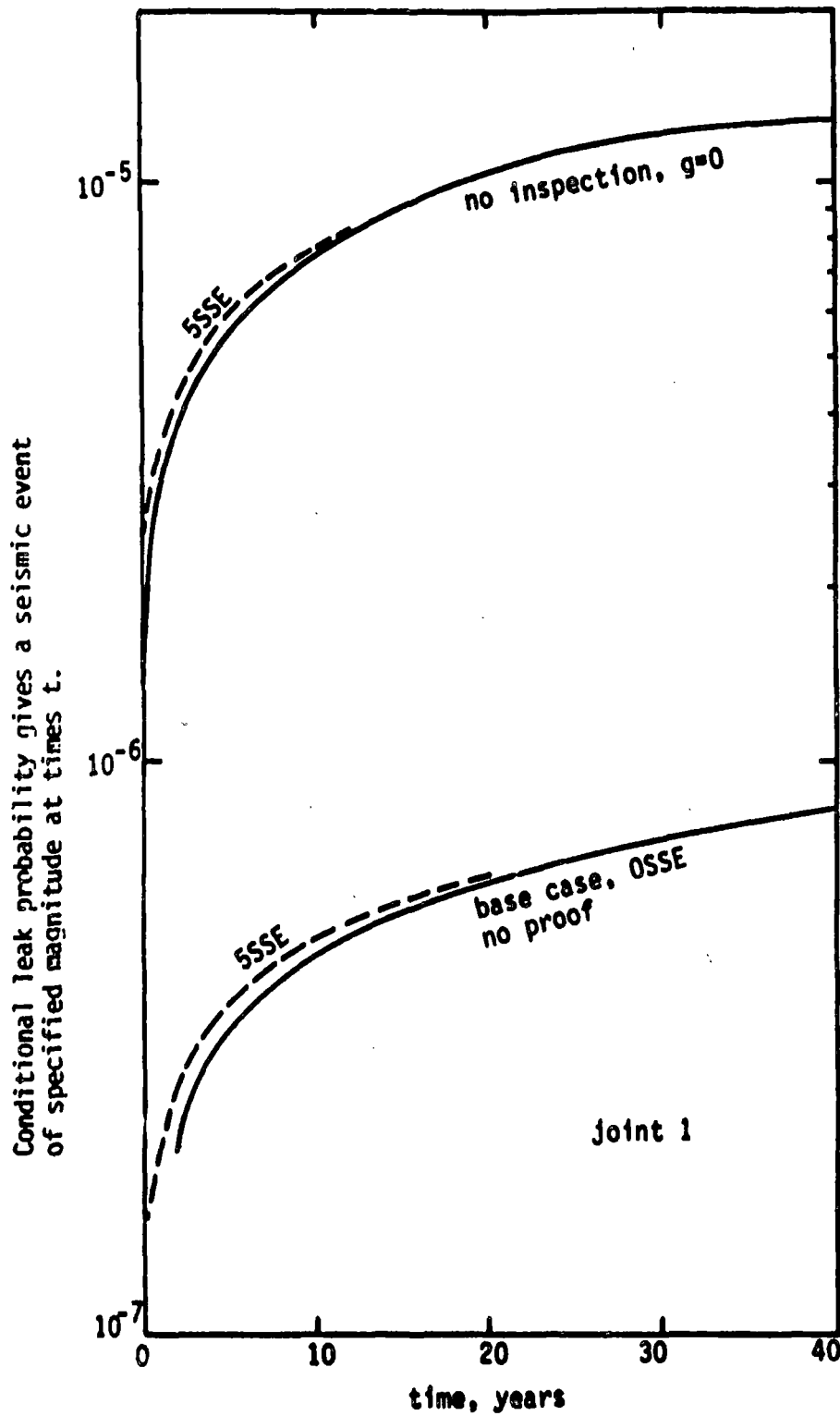


Figure 4-8. Conditional Leak Probabilities as a Function of Time Showing Influence of no Pre-Service Inspection or no Proof Test.

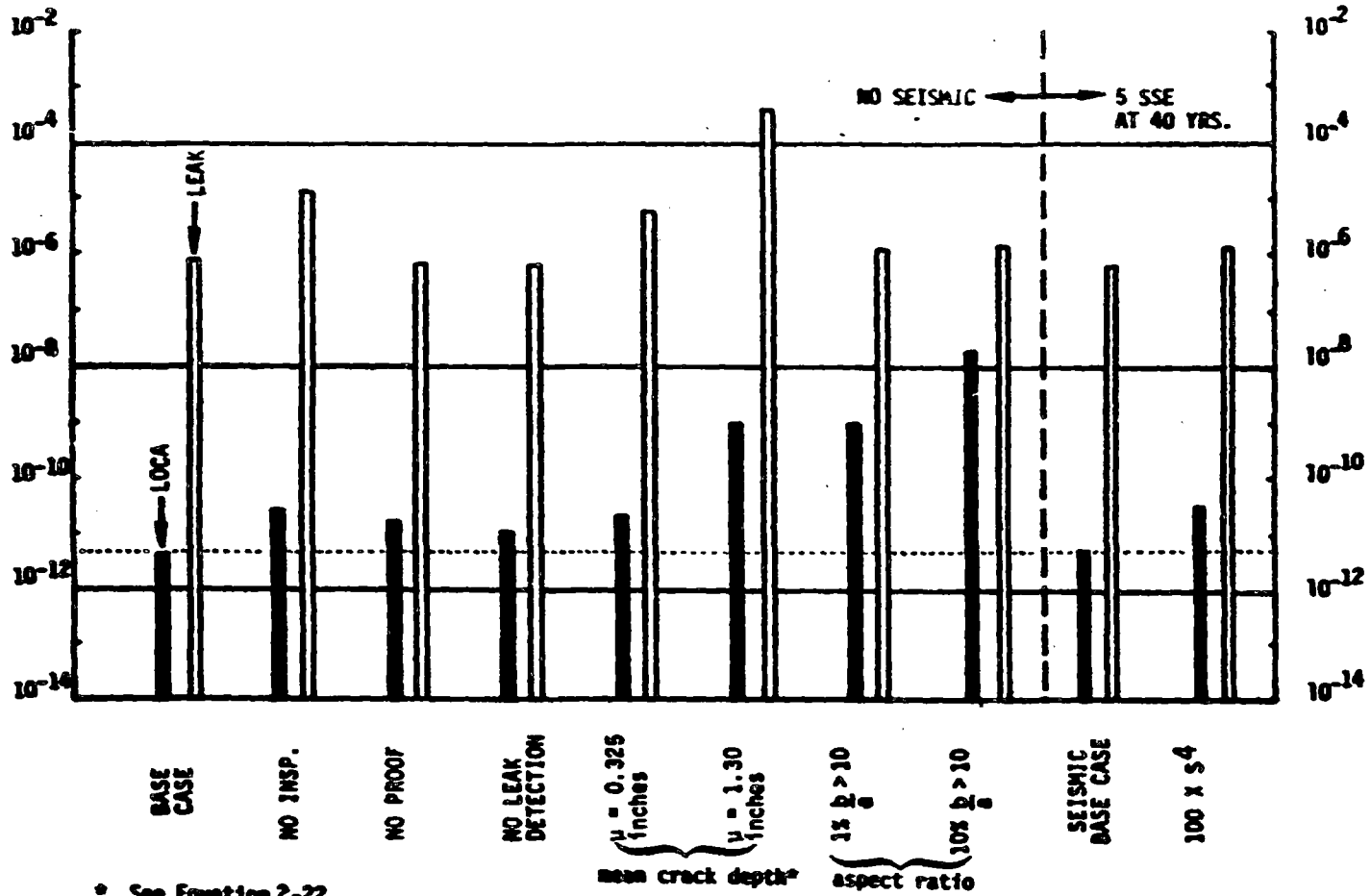


Figure 4-9. Cumulative Probability of Failure at Hot Leg to Pressure Vessel Weld Within 40 Years, Given That a Crack is Initially Present.

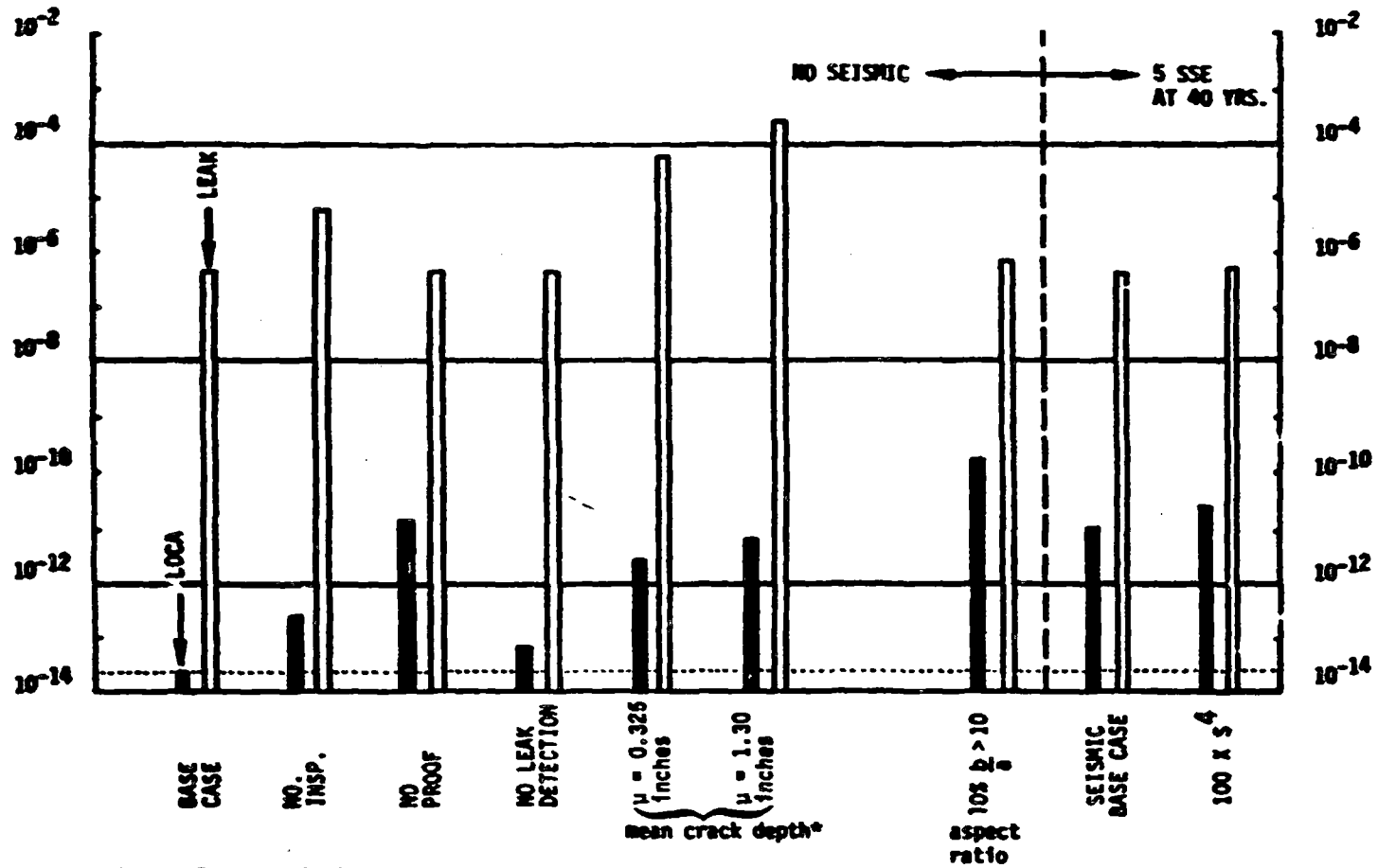


Figure 4-10. Cumulative Probability of Failure at Cold Leg Elbow Weld Within 40 Years, Given that a Crack is Initially Present.

- The proof test can have a large influence on LOCA probabilities, but has little influence on leak probabilities. This is in accordance with earlier observations.
- Inspection has some influence on LOCA probabilities, and leak probabilities.
- The influence of leak detection is small. This is because the majority of cracks that grow to leaks are fairly small, and would have to grow substantially as through-wall cracks before they could result in a LOCA. The stress intensity factor used for through-wall cracks (Equation 2-41) would tend to underestimate the growth of such cracks, but this is not a significant factor.
- Changes in the marginal distribution of crack depth (changes in μ) have more of an influence on leaks than LOCAs. Crack depth distributions bordering on ridiculous are required to raise the LOCA probabilities more than a couple of orders of magnitude.
- Changes in the distribution of aspect ratio have only a small influence on leak probabilities. However, such changes have a large influence on LOCA probabilities. This is an expected result. In fact, changing the aspect ratio distribution so that 1% of the cracks have $b/a > 10$ (rather than 1% with $b/a > 5$) has the same effect as going to the "ridiculous" crack depth distribution. Taking 10% of the cracks to have $b/a > 10$ represents an extreme case that is seen to further increase the calculated failure probability.
- Increasing the S for seismic events by a factor of 100 produces only a minimal increase in the failure probability due to seismic events.

Overall, it is seen that the distribution of aspect ratios is the most influential factor affecting the LOCA probabilities. However, even going to extremes (such as 10% of cracks with $b/a > 10$) produces LOCA probabilities of only 10^{-8} at the location most likely to fail (given that a crack is initially present). These results therefore indicate that a sudden and complete pipe severance in the primary piping at Zion I is an extremely unlikely event. The probability of developing a leak is much higher, but still not likely. An additional parameter to be considered in sensitivity studies is p_v^* . However, as discussed in Section 2.3.4, the calculated failure probabilities vary nearly linearly with p_v^* as the parameter decreases below $10^{-4}/\text{in}^3$, and if this parameter is increased the calculated failure probabilities would increase by at most an order of magnitude. The relative influence of seismic events, if expressed as a ratio of failure probabilities with and without seismic events, would be independent of p_v^* , because this parameter appears in the same form in both factors.

Additional discussions of some of these results will be included in the following section.

4.3.4 Additional Discussion of Results

The results presented in earlier portions of Section 4 can now be used to assess the suitability of some of the assumptions made in this investigation. The low LOCA and leak probabilities obtained reveal that such failures result from cracks that are large at the beginning of the plant life. Hence, within the context of the present work, crack initiation will not contribute to the calculated failure probabilities, and the omission of such initiation from the current model appears justified. However, this may not be true of all piping systems. Additionally, the omission of longitudinal welds will not appreciably alter the estimated system failure probabilities in the present case. This is especially true of the LOCA probabilities. There are relatively fewer longitudinal welds, and their failure is much less likely to lead to a double ended

pipe break than the failure of a circumferential girth butt weld. Stress corrosion cracking has been observed to be a large contributor to failure in piping in boiling water reactors (Klepfer 75, PCSG 75), but has not been observed in the primary side of pressurized water reactors (PCSG 79). Hence, omission of this crack growth mechanism is justified in the present case.

Cyclic stresses due to steady state coolant temperature and pressure fluctuations (FSAR) have not been included in the present analysis. Although such stresses will have many cycles associated with them, their influence will be small, because (except for very large cracks) they are of insufficient magnitude to produce cyclic stress intensity factors above the threshold used for these piping materials. If such a threshold was not present, then these numerous small cyclic stresses could be very important. The same is true for vibratory stresses, which were estimated by Chan, et al., (Chan 81). The inclusion of the welding residual stresses (Chan 81) would not significantly alter the results of this investigation, because they would enter only through their influence on the load ratio, and would not affect the cyclic stresses or critical crack sizes.

Primary piping in a commercial power reactor is required to be inspected during the life of the plant (ASME 80). Such in-service inspections (ISI) will reduce the probability of failure of the piping, and are easily included in the model (see Section 3.5). However, such inspections have not been considered in the results reported here. The influence of in-service inspections is dependent on many factors, including the times of inspection, the time of the first inspection, and the detection probability. An upper bound on the influence of ISI would be the case of all cracks that could result in a subsequent failure being found and removed at the first in-service inspection. This would result in the cumulative failure probability not varying after the first inspection, as shown schematically in Figure 4-11. For simplification, only the case of no seismic events is shown. For base case conditions at location 1 (hot leg to pressure vessel weld), the results shown in Table 4-4 can be obtained from Tables 4-2 and 4-3. It is seen from Table 4-4 that the cumulative failure probability within the plant lifetime is not strongly

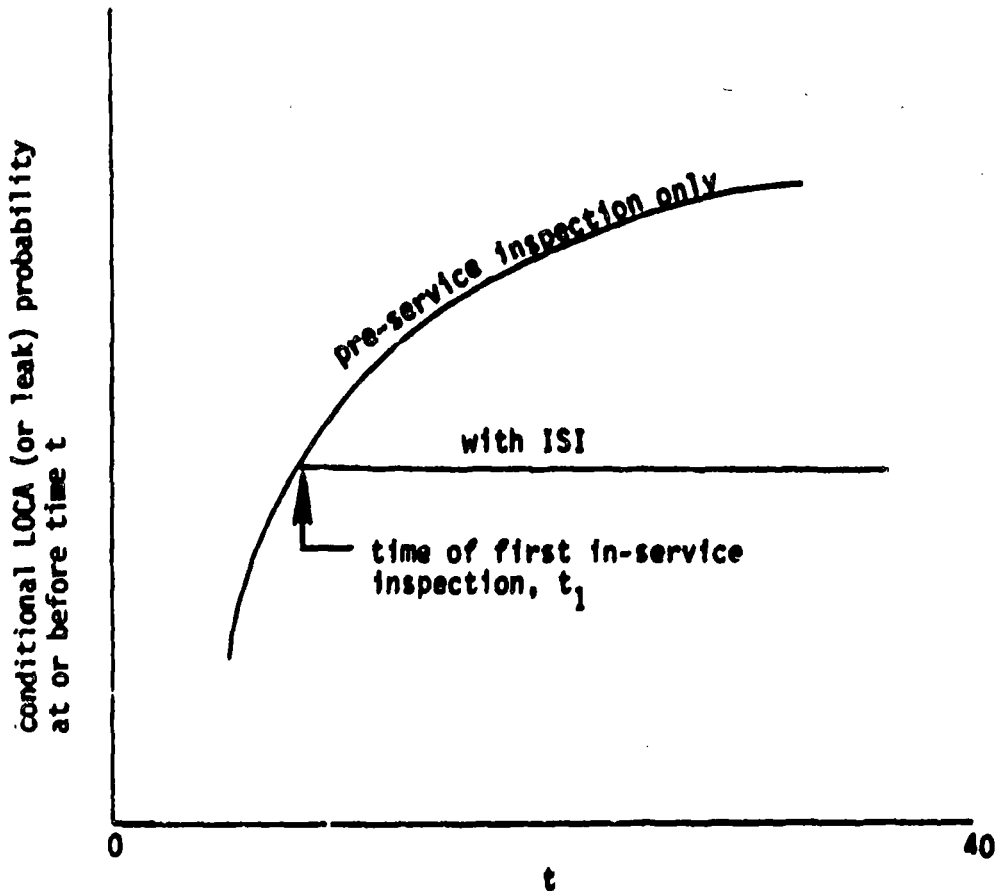


Figure 4-11. Schematic Representation of Cumulative Failure Probability With and Without In-Service Inspection Showing Largest Possible Influence of ISI.

Table 4-4
Estimates of Influence of In-Service Inspection for Various Times of First Inspection

t ₁ , time of first inspection	$\frac{P(t_f < t E_g)}{P(t_f < 40 E_g)}$		$\frac{P(t_f < 40 E_g) \text{ no ISI}}{P(t_f < 40 E_g) \text{ with ISI}}$	
	LOCA	LEAK	LOCA	LEAK
10	1.59x10 ⁻¹³	4.53x10 ⁻⁷	22	1.8
20	1.21x10 ⁻¹²	6.00x10 ⁻⁷	2.9	1.4
30	1.08x10 ⁻¹²	7.12x10 ⁻⁷	1.7	1.2
40	3.48x10 ⁻¹²	8.19x10 ⁻⁷	--	--

influenced by ISI. Thus, it appears that ISI will generally not have a large influence on the results presented here. The ratio of failure rates with and without ISI is independent of the initial crack size distribution for univariate crack depth distributions (Harris 79). Also, the parameter p_y^* cancels out in ratios such as included in the comparison. Thus, this estimate of the influence of ISI is not strongly dependent on the initial crack size and frequencies. It appears that ISI can result in appreciable increases in piping reliability, but in many instances it will not. This is in agreement with earlier results obtained by Harris (Harris 78a, 79).

The leak and LOCA probabilities reported in earlier portions of Section 4 are generally lower than estimates suggested in the literature. The results were approximately 10^{-6} for leaks and 10^{-12} for LOCAs—cumulative within the plant lifetime in large primary piping considered. Before proceeding with a comparison of the above results with estimates from other sources, a reminder is provided that only circumferential welds in the large piping were considered here. Hence, the following items were specifically omitted

- longitudinal welds in elbows (4 per loop)
- dissimilar metal girth butt weld (4 per loop), only the austenitic-to-austenitic portions of these welds were considered
- nozzles and nozzle-to-run pipe welds.

The inclusion of these welds in the analysis could have a significant influence on the failure probability results.

The reactor safety study (RSS 75) contains estimates of pipe failure probabilities based largely on past industrial experience. A summary of values in the reactor safety study is provided in Table III 2-1 of that reference. The values are quoted for a pipe section, which is defined to be a length of 10-100 ft between major discontinuities such as valves and pumps. The following values are given for the rupture of high quality pipe of diameter greater than 3 inches.

$$\begin{aligned}
 p_f &= 8.8 \times 10^{-7} / \text{section-year ("assessment median")} \\
 &2.6 \times 10^{-8} / \text{section-year (lower bound)} \\
 &2.6 \times 10^{-5} / \text{section-year (upper bound)}
 \end{aligned}$$

As shown in Figure 1-2, the primary piping at Zion contains 12 sections. Considering the 40 year plant life, the cumulative failure probability within the lifetime would approximately be

$$40 \times 12 \times 8.8 \times 10^{-7} = 4.2 \times 10^{-4}$$

for the assessed median. This estimate of the rupture probability is some two orders of magnitude above the result obtained here for the leak probability. One source of this discrepancy arises from using data for pipes 3 in. and larger for the 30 in. lines analyzed here.

The reactor safety study estimates the probability of rupture for pipes of diameter less than 3 in. to be an order of magnitude higher. Hence, it is recognized that the probability of failure decreases with increasing pipe size. Wilson 74 also shows that pipe rupture probabilities decrease with increasing pipe diameter.

The reactor safety study (RSS 75) contains another estimate of pipe failure rates in Table III-6-9, where the following LOCA initiating rupture rates are given for pipes with diameter greater than 6 in.

$$\begin{aligned}
 p_f &= 10^{-4} / \text{plant-year (median)} \\
 &10^{-5} \text{ to } 10^{-3} / \text{plant year (90\% range)}
 \end{aligned}$$

It is interesting to note that the immediately above estimates cover a range of 100 (upper bound/lower bound = 100), whereas the values given earlier cover a range of 1000. The differences in these estimates could be due to differences in pipe diameters, mixing of infant and mature data, and data from different class codes.

Phillips and Warwick (Phillips 69) provide a summary of 10^5 pressure vessel years of British experience with fossil fired plants from which they deduce the probability of catastrophic failure in nuclear primary circuits to be $2 \times 10^{-5} / \text{plant-year}$ (p. 8, Phillips 69). Comparisons between countries are difficult because of differences in code require-

ments, but this estimate provides a useful additional piece of information. This value for catastrophic failure is orders of magnitude above the LOCA probabilities obtained here. However, Phillips and Warwick include the entire primary circuit, whereas this analysis considers only a small subset.

Additional discussions of pipe rupture probabilities are provided by Bush 75a, 75b, 76, WASH-1285 (1974), Burns 78, and Basin 77. The estimates contained in these references vary widely, but are invariably considerably larger than even the leak probabilities obtained in this investigation. As mentioned above, one factor that could account for the disagreement is that the estimates from the literature are generally applicable to much smaller pipes than considered here, and the failure probability is generally considered to decrease with increasing pipe size. An additional factor is that the estimates cited above are averaged out over large populations of pipes, which will generally include pipes that are subjected to considerably less quality control, and higher stresses and number of cycles than the primary piping considered here. These factors would tend to result in pipe failure rates well above those applicable to the special small subset of pipes considered in this investigation. Nevertheless, the results obtained here are very small, and the LOCA probabilities are well below any estimate that could be based on observations of actual piping systems. The fact that no leaks have been observed in the large primary piping of PWRs is of some comfort, however.

The very low LOCA probabilities obtained here, along with the observation that alterations bordering on ridiculous are necessary to bring the failure probabilities up to the values based on past observations (see Section 4.3.3), suggest that some factors that could produce a LOCA in actual situations have not been considered in the current model. Such factors would include design errors, fabrication errors, errors in operation of the plant, and mechanisms of accelerated crack growth that are of fairly low probability but could result in much faster growth than the

fatigue mechanism considered here. An example of operator error would be some error that would produce pressure excursions to higher pressure than considered here. Quite high pressure, with resulting high stresses and increased failure probabilities, could be present with a probability much higher than 10^{-12} per plant lifetime.

The quantification of the influence of these various "human factor errors" is quite difficult, and well beyond the scope of this investigation. Sabri 80, Rasmussen 78, and Swain 78, 80, contain discussions of such considerations. Rzevski 78 provides a discussion of design errors. Although the results presented here indicate that human errors are important, results generated by the techniques employed herein for other piping sizes, systems and materials would be very informative in providing additional perspectives on the relative importance of various factors on the reliability of reactor piping systems.

5.0 SUMMARY AND CONCLUSIONS

A fracture mechanics model of structural reliability has been applied to obtain estimates of the influence of seismic events on the probability of failure in the large primary piping of a commercial pressurized water power reactor.* This work forms a portion of the Lawrence Livermore Load Combination Program, and is aimed at assessing the need to design commercial power reactors for simultaneous seismic events and loss-of-coolant-accidents (LOCAs). Zion 1 was analyzed in this project, so that results obtained are representative of realistic situations. However, the applicability of the results obtained here to plants other than Zion remains to be seen. Best estimates of the failure probabilities were desired, rather than upper bound estimates.

Basically, the fracture mechanics model assumes that failures in the primary piping can occur only as the result of the subcritical growth of a pre-existing defect introduced during fabrication of the plant. The growth of such defects is assumed to be predictable using fracture mechanics techniques based on laboratory investigations. Numerous additional assumptions are made which are detailed throughout the report. The as-fabricated defects are considered to be randomly distributed in size, and to be concentrated in piping weldments. The calculated stress history at each circumferential girth butt weld is used in conjunction with the subcritical crack growth characteristics of the material to predict the time variation of the crack size distribution. The crack geometry considered is a semi-elliptical interior surface part-circumferential crack. Therefore, a bivariate crack size distribution is employed. Seismic stresses are considered as part of the stress history, and the influence of such stresses on piping reliability can be ascertained. Cyclic stresses induced during normal plant operation form an important part of the stress history. The probability of failure (leak or LOCA) at a given location and time is simply the probability of having a crack larger than the corresponding critical size. Elastic-plastic failure criteria were employed to estimate critical crack sizes, whereas subcritical crack growth was calculated based on elastic analysis.

* Specifically, 56 girth butt welds were considered — 14 welds in each of the four loops, such as shown in Figure 1-2.

Considerable new information on stress intensity factors for part-circumferential interior surface cracks was generated as a portion of this project in order to adequately treat the desired complex factors involved.

A special computer program was written for generation of numerical results from the fracture mechanics model. This program is called PRAISE (Piping Reliability Analysis Including Seismic Events), and its development was required in order to handle the initial bivariate crack size distribution in conjunction with the complex stress history and statistical distribution of material properties.

The results for LOCA and leak probabilities generated by PRAISE indicated that the stress history for the piping system considered was dominated by the heatup-cooldown cycle. Radial gradient thermal stresses due to temperature excursions of the coolant during various plant operating transients provided only a minimal influence on the calculated failure probabilities. Pre-service inspection and proof test had an appreciable influence on the calculated failure probabilities, but in-service inspection generally would not have a large influence. Results for various weld locations showed differing results depending on the level of applied stresses. The leak and LOCA probabilities were calculated to be quite small, being on the order of 10^{-6} and 10^{-12} per plant lifetime (respectively). Large variations in the input parameters (such as initial crack size distribution) were required before these values were significantly altered. The LOCA probabilities were more strongly influenced by the statistical distribution of initial aspect ratio (ratio of crack surface length to crack depth) than by other input parameters. The results also showed that the influence of seismic events on calculated failure probabilities was not large. Hence, it appears that the probability of a sudden and complete pipe severance in the large primary piping at Zion 1 is very low - bordering on incredible. The probability of a simultaneous LOCA and seismic event (seismic induced LOCA) is even lower. Thus, it appears that the requirement to design commercial power reactors for simultaneous LOCA and seismic events should be reviewed.

The very low LOCA probabilities obtained in this work, along with the observation that extreme alterations of inputs are required before the calculated values are increased to be comparable to current estimates of piping reliability, suggest that some factors that could contribute to a LOCA have been omitted from the model. Such factors could include failures in portions of the primary coolant loop not evaluated herein, design errors, fabrication errors, errors in plant operation, and the presence of crack growth mechanisms that could produce higher crack growth rates (but be present with low probability). Although the results presented here indicate that dominant failure contributors may have been omitted from consideration, it is important to remember that only a very special subset of the piping at Zion 1 was included in this analysis. Additional results generated by the techniques employed herein for other piping sizes, systems and materials would be very informative in gaining additional perspectives on the relative importance of various factors on the reliability of reactor piping systems.

SUMMARY OF MAJOR NOTATION

A	area of crack
A*	crack area having a 50% chance of being found during inspection.
A _p	cross-sectional area of pipe
ΔA _i	increment of crack area for a crack extending in the "i" direction.
a	maximum depth of a semi-elliptical surface crack
a*	crack depth having a 50% chance of being found during inspection.
da/dn	fatigue crack growth rate
b	half surface length of a semi-elliptical surface crack
C	parameter in fatigue crack growth relation
C ₀	constant in distribution of initial crack depth
C _β	constant in distribution of initial crack aspect ratio (β)
c	equals a ²
D _B	diameter of beam of ultrasonic probe used in inspection
D _i	inside pipe diameter
E	modulus of elasticity
erfc(x)	complementary error function of argument x
F	equals $\int_0^{\pi/2} (\sin^2 x + \frac{1}{\beta^2} \cos^2 x)^{1/2} dx$
f _i	correction factor for h _i for surface crack
G	shear modulus (or a function of a/b)
g	peak acceleration (relative to gravity) during a seismic event.
g ₁	a function in influence function (see Eq. C-13)
g ₂	a function in influence function (see Eq. C-14).
H	equals E/(1-ν ²)
h	pipe wall thickness
h _i	influence function associated with K _i (see Eq. C-1)
h _i *	known influence function for a buried elliptical crack

h_i^{**}	nonsingular portion of influence function (see Eq. D-3).
J	value of J-integral
J_{IC}	critical value of J for onset of crack extension
K	stress intensity factor
K'	equals $K_{max}/(1-R)^{1/2}$
K_0'	threshold value of K'
\bar{K}_i	RMS averaged stress intensity factor associated with crack extension in the "i" degree of freedom direction.
K_{max}	maximum K during a stress cycle
K_{min}	minimum K during a stress cycle
ΔK	cyclic stress intensity factor (equals $K_{max}-K_{min}$)
$\delta \bar{K}_i$	stress intensity factor (\bar{K}_i) due only to radial gradient thermal stress.
k	equals $[1-(a/b)^2]^{1/2}$
m	exponent in fatigue crack growth relation
$m(u, \alpha)$	influence function for complete circumferential crack
n	number of stress cycles
$P(t_F < t)$	probability of failure at or before time t given that a crack is initially present
$P(t_F < t \bar{E}_q)$	probability of failure at or before time t in the absence of seismic events (given that a crack is initially present).
$P(t_F < t E_q(g, t))$	probability of failure at or before time t given an earthquake of peak acceleration g at time t (given that a crack is initially present).
$P_D(\text{leak}) (\dot{Q})$	probability of detecting a leak of rate \dot{Q} .
$P_D(a)$	probability of detecting a crack of depth a during inspection.
$P_{ND}(a)$	probability of nondetection of a crack of depth a during inspection.
$P_f(\text{sys})(t, g)$	probability of failure in primary system considered at or before time t given an earthquake of magnitude g occurring at t (given that a crack is initially present).
p	pressure
p_a	marginal density function of initial crack depth
p_β	marginal density function of initial aspect ratio

p^*	frequency of cracks in a weld of volume V
p_V^*	frequency of cracks in a unit volume of weld
$p(n)$	probability that n cracks exist initially in a weld of volume V.
Q	leak rate through a crack
Q'	leak rate through a crack per unit length of crack.
R	load ratio (equals K_{min}/K_{max}) (or radial distance in a polar coordinate system)
R_i	inside radius of pipe
S	parameter associated with influence of stress cycles on fatigue crack growth (see Eq. 2-40).
T	temperature [or tearing modulus $E(dJ/da)/\sigma_{f10}^2$]
T_{appl}	applied value of tearing modulus
T_{mat}	value of material tearing modulus
\bar{T}	average temperature through pipe wall thickness
T_C	temperature in cold leg
T_H	temperature in hot leg
T_{steam}	temperature of steam
t	time
U	strain energy
U^*	exact value of U for a reference problem
\bar{U}	approximate U for a general problem
\hat{U}	approximate U for a reference problem
u	equals x/h
V	weld volume
v	opening displacement of a crack surface
W	crack opening displacement (as a function of crack size and position on crack surface).
W^*	exact value of W for a reference problem
\bar{W}	approximate W for a general problem
\hat{W}	approximate W for a reference problem
x	distance into pipe wall
Y_i	function in expression for \bar{K}_i for uniform stress
y	a Cartesian coordinate

α	equals a/h
α'	coefficient of thermal expansion
β	aspect ratio (equals b/a)
β'	equals $\pi\beta/2$
β_L	largest of 1 or b/h
β_m	parameter in marginal distribution of initial crack aspect ratio
γ	equals R_i/h
δ	maximum total crack opening displacement
n	parameter in distribution of C
θ	a polar coordinate
λ	parameter in marginal distribution of initial crack aspect ratio
λ_i	parameter related to frequency of occurrence of transient type "i" (see Eq. 3-50).
μ	parameter in marginal distribution of initial crack depth
μ'	equals μ/h
ν	parameter in expression for P_{ND}
ν'	Poisson's ratio
ξ	equals $[1-(x/a)^2 - (y/b)^2]$
ρ	fraction of initial cracks with $\beta > 5$
σ	axial stress (or occasionally standard deviation)
σ_{DW}	stress due to dead weight loads
σ_{EQ}	maximum stress due to an earthquake
σ_{f10}	flow stress [equals $(\sigma_{ys} + \sigma_{ult})/2$]
σ_{LC}	load controlled portion of applied stress
σ_{max}	maximum stress during a stress cycle
σ_{min}	minimum stress during a stress cycle
σ_{NO}	normal operating stress
σ_p	axial stress due to pressure
σ_{TE}	stress due to restraint of thermal expansion
σ_{ult}	ultimate tensile strength

σ_{ys} 0.2% of offset yield strength
 ϕ elliptical angle

General Comments

1. A bar over a variable denotes the mean value of the variable.
2. A subscript "sd" denotes the standard deviation of the variable.
3. A numerical subscript (such as "50") denotes the value of the variable at that percentile of its distribution (therefore, a_{50} would be the median value of a).
4. An upper case P generally denotes a cumulative distribution function.
5. A lower case p generally denotes a density function.

REFERENCES*

- Abramowitz 64 M. Abramowitz and A. Stegun, Handbook of Mathematical Functions, National Bureau of Standards, Applied Mathematics Series 55, Washington, D.C., 1964.
- Adamonis 79 D.C. Adamonis and E.T. Hughes, "Ultrasonic Evaluation and Sectioning of PVRC Plate Weld and Specimen 201," Welding Research Council Bulletin No. 252, New York, September 1979.
- Agostinelli 58 A. Agostinelli and V. Salemann, "Prediction of Flashing Water Flow Through Fine Annular Clearances," Transactions of the ASME, Vol. 80, 1958, pp. 1138-1142.
- Ardron 76 K.H. Ardron and R.A. Furness, "Study of the Critical Flow Models Used in Reactor Blowdown Analysis," Nuclear Engineering and Design, Vol. 39, 1976, pp. 257-266.
- Arnett 76 L.M. Arnett, "Optimization of In-Service Inspection of Pressure Vessels," Report DP-1428, E.I. duPont de Nemours and Company, Savannah River Laboratory, Aiken, South Carolina, August 1976.
- ASME 80 Boiler and Pressure Vessel Code, Section XI, Rules for In-Service Inspection of Nuclear Power Plant Components, American Society of Mechanical Engineers, New York, 1980.
- ASTM 80 Annual Book of ASTM Standards, American Society for Testing and Materials, Philadelphia, Pennsylvania, 1980.
- Atluri 77a S.N. Atluri, K. Kathiresan, A.S. Kobayashi, and M. Nakagaki, "Inner Surface Cracks in an Internally Pressurized Cylinder Analyzed by a Three Dimensional Displacement-Hybrid Finite Element Method," Third International Conference on Pressure Vessel Technology, Part II Materials and Fabrication, American Society of Mechanical Engineers, New York, 1977.
- Atluri 77b S.N. Atluri and K. Kathiresan, "Outer and Inner Surface Flaws in Thick-Walled Pressure Vessels," Transactions of the 4th International Conference on Structural Mechanics in Reactor Technology, Vol. G, Paper G 5/4, August 1977.

*The availability of references marked with an asterisk(s) is indicated on page 232.

- Atluri 79 S.N. Atluri and K. Kathiresan, "Influence of Flaw Shapes on Stress Intensity Factors for Pressure Vessel Surface Flaws and Nozzle Corner Cracks", American Society of Mechanical Engineers Paper 79-PVP-65, New York, 1979.
- Bamford 77 W.H. Bamford, D.H. Schaffer and G.M. Jouris, "Statistical Methods for Interpreting Fatigue Crack Growth Data with Applications to Reactor Pressure Vessel Steel," Third International Conference on Pressure Vessel Technology, Part II: Materials and Fabrication, pp. 815-823, American Society of Mechanical Engineers, New York, 1977.
- Bamford 79a W.H. Bamford, "Fatigue Crack Growth of Stainless Steel Piping in a Pressurized Water Reactor Environment," Journal of Pressure Vessel Technology, Vol. 101, No. 1 (February 1979), pp. 73-79.
- Bamford 79b W.H. Bamford and A.J. Bush, "Fracture Behavior of Stainless Steel," Elastic-Plastic Fracture, pp. 553-577, American Society for Testing and Materials, Special Technical Publication No. 668, Philadelphia, Pennsylvania, 1979.
- Basin 77 S.L. Basin and E.T. Burns, "Characteristics of Pipe System Failures in Light Water Reactors," Report EPRI NP-438, Electric Power Research Institute, Palo Alto, California, August 1977.
- Barsom 73 J.M. Barsom, "Fatigue-Crack Growth Under Variable Amplitude Loading in ASTM A514-B Steel," Progress in Flaw Growth and Fracture Toughness Testing, pp. 147-167, American Society for Testing and Materials Special Technical Publication No. 536, Philadelphia, Pennsylvania 1973.
- Barsom 76 J.M. Barsom, "Fatigue Crack Growth Under Variable Amplitude Loading in Various Bridge Steels," Fatigue Crack Growth Under Spectrum Loads, pp. 217-235, American Society for Testing and Materials Special Technical Publication No. 595, Philadelphia, Pennsylvania, 1976.
- Becher P.E. Becher and B. Hansen, "Statistical Evaluation of Defects in Welds and Design Implications," Danish Welding Institute, Danish Atomic Energy Commission, Research Establishment, RISØ, (no date).

- Becher 74 P.E. Becher and A. Pederson, "Application of Statistical Linear Elastic Fracture Mechanics to Pressure Vessel Reliability Analysis," Nuclear Engineering and Design, Vol. 27, No. 3, pp. 413-425, 1974.
- Becker 80 F.L. Becker, Sr., Battelle Pacific Northwest Laboratory, Richland, Washington, private communication, 1980.
- Begley 72 J.A. Begley and J.D. Landes, "The J-Integral as a Failure Criterion," Fracture Toughness, pp. 1-23, American Society for Testing and Materials Special Technical Publication No. 514, Philadelphia, Pennsylvania, 1972.
- Besuner 76 P.M. Besuner, "Residual Life Estimate for Structures with Partial Thickness Cracks," Mechanics of Crack Growth, pp. 403-419, American Society for Testing and Materials Special Technical Publication No. 590, Philadelphia, Pennsylvania 1976.
- Besuner 77a P.M. Besuner and A.S. Tetelman, "Probabilistic Fracture Mechanics," Nuclear Engineering and Design, Vol. 43, No. 1, (August 1977), pp. 99-114.
- Besuner 77b P.M. Besuner, "The Influence Function Method for Fracture Mechanics and Residual Life Analysis of Cracked Components Under Complex Stress Fields," Nuclear Engineering and Design, Vol. 43, No. 1, (August 1977), pp. 115-154.
- Besuner 78 P.M. Besuner, et al., "BIGIF: Fracture Mechanics Code for Structures," Report EPRI NP-838, Electric Power Research Institute, Palo Alto, California, July 1978.
- Blaue1 75 J.G. Blaue1, D. Stahn, and J.F. Kalthoff, "Investigations into Brittle Fracture Behavior of Thick-Walled Hollow Cylinders Subjected to Thermal Shock," U.S. Nuclear Regulatory Commission Translation Series NUREG/TR-0022, R3, NRC publication date January 1978 of original German report BMFT RS 61 dated September 1975.
- Broek 78 D. Broek, Elementary Engineering Fracture Mechanics Sijthoff and Noordhoff, The Netherlands, 1978.
- Buchalet 76 C.B. Buchalet and W.H. Bamford, "Stress Intensity Factor Solutions for Continuous Surface Flaws in Reactor Pressure Vessels," Mechanics of Crack Growth, pp. 385-402, American Society for Testing and Materials Special Technical Publication No. 590, Philadelphia, Pennsylvania, 1976.

- Burns 78 E.T. Burns, D.O. Harris and R.C. Erdmann, "Reliability of Nuclear Piping Systems with Consideration of Cases Where Design Points Have Been Exceeded," Science Applications, Inc., Report SAI-091-79-PA, Palo Alto, California, presented at ASME/CSME Pressure Vessels and Piping Conference, Montreal, June 1978.
- Bush 75a S.H. Bush, "Pressure Vessel Reliability," Journal of Pressure Vessel Technology, Vol. 97, Series H, No. 1, (February 1975), pp. 54-70.
- Bush 75b S.H. Bush, "The Impact of Inservice Inspection on the Reliability of Pressure Vessels and Piping," Reliability Engineering in Pressure Vessels and Piping, pp. 1-13, American Society of Mechanical Engineers, New York, 1975.
- Bush 76 S.H. Bush, "Reliability of Piping in Light-Water Reactors," Nuclear Safety, Vol. 17, No. 5, (Sept-Oct 1976), pp. 568-579.
- Chan 81 A.L. Chan, E.F. Rybicki and D.J. Curtis, "Non-Seismic Stress Analysis", Vol. 3 of "Probability of Pipe Fracture in the Primary Coolant Loop of a PWR", U.S. Nuclear Regulatory Commission Report NUREG/CR-2189, Washington, D.C., August 1981.*
- Chang 79 Part-Through Crack Fatigue Life Prediction, edited by J.B. Chang, American Society for Testing and Materials Special Technical Publication No. 687, Philadelphia, Pennsylvania, 1979.
- Clarke 73 W.L. Clarke and G.M. Gordon, "Investigation of Stress Corrosion Cracking Susceptibility of Fe-Ni-Cr Alloys in Nuclear Reactor Water Environments," Corrosion-NACE, Vol. 29, No. 1, (January 1973), pp. 1-12.
- Collier 77 J.G. Collier and W. Marshall, "How UK Experts Assessed the Integrity of PWR Pressure Vessels," Nuclear Engineering International, Vol. 22, No. 260, July 1977, pp. 41-45.
- Collier 80 R.P. Collier et. al., "Study of Critical Two-Phase Flow Through Simulated Cracks," Interim Report, BCL-EPRI-80-1, Battelle Columbus Laboratories, Columbus, Ohio, 1980.

- Cooke 75 R.J. Cooke, P.E. Irving, G.S. Booth and C.J. Beevers, "The Slow Fatigue Crack Growth and Threshold Behavior of a Medium Carbon Alloy Steel in Air and Vacuum," Journal of Engineering Fracture Mechanics, Vol. 7, (1975), pp. 69-77.
- Cramond 74 R. Cramond, Jr., A Probabilistic Analysis of Structural Reliability Against Fatigue and Failure, Ph.D. Thesis, University of Illinois, at Urbana, Champaign, 1974
- Cruse 69 T.A. Cruse, "Numerical Solutions in Three Dimensional Elastostatics," International Journal of Solids and Structures, Vol. 5, (1969), pp. 1259-1274.
- Cruse 73 T.A. Cruse, "An Improved Boundary - Integral Equation Method for Three Dimensional Elastic Stress Analysis," Report SM-73-19, Department of Mechanical Engineering, Carnegie-Mellon University, Pittsburgh, Pennsylvania, August 1973.
- Cruse 75a Boundary Integral Equation Method: Computational Applications in Applied Mechanics, edited by T.A. Cruse and F.J. Rizzo, American Society of Mechanical Engineers, New York, 1975.
- Cruse 75b T.A. Cruse and P.M. Besuner, "Residual Life Prediction for Surface Cracks in Complex Structural Details," Journal of Aircraft, Vol. 12, No. 4, (April 1975), pp. 369-375.
- Cruse 77 T.A. Cruse, G.J. Meyers and R.B. Wilson "Fatigue Growth of Surface Cracks," Flaw Growth and Fracture, pp. 174-189, American Society for Testing and Materials Special Technical Publication No. 631, Philadelphia, Pennsylvania, 1977.
- Derby 77 S.L. Derby and N.E. Hackford, "Probabilistic Leak Analysis for LMFBR Primary Coolant Piping," General Electric Fast Breeder Reactor Department Report GE FR-00041, UC-79p, Sunnyvale, California, July 1977.
- Dowling 72 N.E. Dowling, "Fatigue Failure Predictions for Complicated Stress-Strain Histories," Journal of Materials, Vol. 7, No. 1, (March 1972), pp. 71-87.
- Dufresne 78 J. Dufresne, et al., "The CEA-Sponsored Research Program on PWR Reactor Vessel Failure Probability Calculation," Probabilistic Analysis of Nuclear Reactor Safety, Vol. 2, Paper III.1, Proceedings of Topical Meeting sponsored by the American Nuclear Society, Los Angeles, California, May 1978.

- Dvorak 72 H.R. Dvorak and E.C. Schwegler, Jr., "Statistical Distribution of Flaw Sizes," International Journal of Fracture Mechanics, Vol. 8, (1972), pp. 110-111.
- Engle 79 R.M. Engle, Jr., "Aspect Ratio Variability in Part-Through Crack Life Analysis," Part-Through Crack Fatigue Life Prediction, pp. 74-88, edited by J.B. Chang, American Society for Testing and Materials Special Technical Publication No. 687, Philadelphia, Pennsylvania, 1979.
- Erdol 78 R. Erdol and F. Erdogan, "A Thick-Walled Cylinder with an Axisymmetric Internal or Edge Crack," Journal of Applied Mechanics, Vol. 45, No. 2, (June 1978), pp. 281-286.
- FCFMS 79 "Influence of Various Parameters on the Determination of the Fatigue Crack Arrest Threshold," Fatigue Commission of the French Metallurgical Society, presented at ASTM Meeting, Pittsburgh, Pennsylvania, October 1979.
- Feldman 68 L.S. Feldman, "Statistical Analysis of the Results of Ultrasonic Monitoring of Large Forged Pieces and Stampings of Aluminum Alloys," Defektoskopija, 1968, pp. 26-32, English translation available from D.O. Harris, Science Applications, Inc., San Jose, California.
- Flugge 62 W. Flugge, Handbook of Engineering Mechanics, McGraw-Hill Book Company, New York, 1962.
- Folias 67 E.S. Folias, "A Circumferential Crack in a Pressurized Cylindrical Shell," International Journal of Fracture Mechanics, Vol. 3, No. 1, (March 1967), pp. 1-11.
- Ford 80 P. Ford, to appear in Second Semi-Annual Progress Report on Electric Power Research Institute Research Project RP-1332, EPRI, Palo Alto, California.
- Frank 77 F.J. Frank and M.J. Asztalos, "Primary Coolant Leak Detection System Evaluation and Development Program: Capability Study of Existing Reactor Coolant Pressure Boundary Leakage Detection Systems," Report WCAP-9173, Westinghouse Electric Company, Pittsburgh, Pennsylvania, September 1977.
- Frost 67 N.E. Frost and K. Denton, "The Fatigue Strength of Butt Welded Joints in Low Alloy Structural Steel," British Welding Journal, Vol. 14, No. 4, (April 1967), pp. 156-161.

- FSAR Final Safety Analysis Report, Zion Station, Unit 1, Commonwealth Edison Company (no date).
- Gallagher 79 Structural Integrity Technology, edited by J.P. Gallagher and T.W. Crooker, American Society of Mechanical Engineers, New York, 1979.
- George 80 Letter from L. George, Lawrence Livermore National Laboratory, to D. Harris, Science Applications, Inc., San Jose, California, dated May 9, 1980.
- George 81 L. George and R. Mensing, "Piping System Fracture Probability Estimation", Vol. 7 of "Probability of Pipe Fracture in the Primary Coolant Loop of a PWR", U.S. Nuclear Regulatory Commission Report NUREG/CR-2189, Washington, D.C. (to be published September 1981).
- Giannuzzi 78 "Studies on AISI Type-304 Stainless Steel Piping Weldments for Use in BWR Applications," Report EPRI NP-944, RP449-2, Electric Power Research Institute, Palo Alto California, December 1978.
- Goepfert 77 W.P. Goepfert, "Statistical Aspects of Mechanical Property Assurance," Reproducibility and Accuracy of Mechanical Tests, pp. 136-144, American Society for Testing and Materials Special Technical Publication No. 626, Philadelphia, Pennsylvania, 1977.
- Graham 74 T.W. Graham and A.S. Tetelman, "The Use of Crack Size Distribution and Crack Detection for Determining the Probability of Fatigue Failure," AIAA Paper No. 74-394, presented at AIAA/ASME/SAE 15th Structure, Structural Dynamics and Materials Conference, Las Vegas, Nevada, April 1974.
- Green 50 A.E. Green and I.N. Sneddon, "The Distribution of Stress in Neighborhood of a Flat Elliptical Crack in an Elastic Solid," Proceedings of the Cambridge Philosophical Society, Vol. 46, 1950, pp. 159-164.
- Griesbach 80 T.J. Griesbach, "Dynamic Elastic-Plastic Behavior of Circumferential Cracks in a Pipe Subject to Seismic Loading Conditions," American Society of Mechanical Engineers Paper No. 80-C2/PVP-151, New York, 1980.
- Hahn 67 G.J. Hahn and S.S. Shapiro, Statistical Models in Engineering, John Wiley and Sons, Inc., New York, 1967.
- Hale 78 D.A. Hale, J. Yuen and T. Gerber, "Fatigue Crack Growth in Piping and RPV Steels in Simulator BWR Water Environment," Report GEAP-24098, NRC-5, Report Prepared by General Electric Company, San Jose, California for the U.S. Nuclear Regulatory Commission, January, 1978.

- Hale 79 D.A. Hale, C.W. Jewett and J.N. Kass, "Fatigue Crack Growth Behavior of Four Structural Alloys in High Temperature High Purity Oxygenated Water," American Society of Mechanical Engineers Paper 79-PVP-104, New York, 1979.
- Hamburg 70 M. Hamburg, Statistical Analysis for Decision Making, Hartcourt, Brace and World, Inc., New York, 1970.
- Hammersley 64 J.M. Hammersley and D.C. Handscomb, Monte Carlo Methods, Fletcher & Son Ltd., Norwich, Great Britain.
- Harris 76 D.O. Harris and R.R. Fullwood, "An Analysis of the Relative Probability of Pipe Rupture at Various Locations in the Primary Cooling Loop of a Pressurized Water Reactor Including the Effects of a Periodic Inspection," Report SAI-001-PA, Science Applications, Inc., Palo Alto, California, June 1976.
- Harris 77a D.O. Harris, "Relative Rupture Probabilities at Various Locations in Reactor Coolant Piping," Transactions of the American Nuclear Society, Vol. 26, p. 404, June 1977.
- Harris 77b D.O. Harris, "An Analysis of the Probability of Pipe Rupture at Various Locations in the Primary Cooling Loop of a Babcock and Wilcox 177 Fuel Assembly Pressurized Water Reactor - Including the Effects of a Periodic Inspection," Science Applications, Inc., Report SAI-050-77-PA, Palo Alto, California, September 1977.
- Harris 77c D.O. Harris, "A Means of Assessing the Effects of NDE on the Reliability of Cyclically Loaded Structures," Materials Evaluation, Vol. 35, No. 7, pp. 57-65, July 1977.
- Harris 78a D.O. Harris, "Probabilistic Analysis of Rupture in Reactor Coolant Piping," Probabilistic Analysis of Nuclear Reactor Safety, Vol. 2, Paper II.7, Proceedings of Topical Meeting sponsored by the American Nuclear Society, Los Angeles, California, May 1978.
- Harris 78b D.O. Harris, "A Means of Assessing the Effects of Periodic Proof Testing and NDE on the Reliability of Cyclically Loaded Structures," Journal of Pressure Vessel Technology, Vol. 100, No. 7, pp. 150-157, May 1978.
- Harris 79 D.O. Harris, "The Influence of Crack Growth Kinetics and Inspection on the Integrity of Sensitized BWR Piping Welds," Report EPRI NP-1163, Electric Power Research Institute, Palo Alto, California, 1979.

- Harris 80a D.O. Harris and E.Y. Lim, "Stress Intensity Factors for Complete Circumferential Interior Surface Cracks in Hollow Cylinders," Report SAI-181-80-PA, Science Applications, Inc., Palo Alto, California, presented at Thirteenth National Symposium on Fracture Mechanics, Philadelphia, Pennsylvania, June 1980, to be published in symposium proceedings.
- Harris 80b D.O. Harris, R.G. Brown, D. Dedhia and D.E. Leaver, "Acoustic Emission Leak Detection and Location Systems Technology Review," Electric Power Research Institute Report NP-80-7-LD, Palo Alto, California, December 1980.
- Harris 81 D.O. Harris and D. Dedhia, "Further Studies of the Influence of Residual Stresses and Crack Growth Kinetics on the Integrity of Sensitized BWR Piping Welds," Science Applications, Inc., Report SAI-002-81-SJ, San Jose, California, January 1981, report on Electric Power Research Institute Research Project T118-6, Palo Alto, California.
- Hartranft 72 R.J. Hartranft and G.C. Sih, "Alternating Method Applied to Edge and Surface Crack Problems," Mechanics of Fracture 1: Methods of Analysis and Solutions of Crack Problems, edited by G.C. Sih, Ch. 4, pp. 179-238, Noordhoff International Publishing, Leyden, The Netherlands, 1972.
- Hastings 77 N.A.J. Hastings and J.B. Peacock, Statistical Distributions, Butterworths, London, 1974.
- Heer 71 E. Heer and J.N. Yang, "Structural Optimization Based on Fracture Mechanics and Reliability Criteria," AIAA Journal, Vol. 9, April 1971, pp. 621-628.
- Helliot 79 J. Helliot, R.C. Labbens and A. Pellisier-Tanon, "Semi-Elliptical Cracks in a Cylinder Subjected to Stress Gradients," Fracture Mechanics, pp. 341-364, American Society for Testing and Materials Special Technical Publication No. 677, Philadelphia, Pennsylvania, 1979.
- Henry 70 R.E. Henry, "The Two-Phase Critical Discharge of Initially Saturated or Sub-cooled Liquid," Nuclear Science and Engineering, Vol. 41, 1970, pp. 336-342.
- Henry 71 R.E. Henry and H.K. Fauske, "The Two-Phase Critical Flow of One-Component Mixtures in Nozzles, Orifices and Short Tubes," Journal of Heat Transfer, Vol. 93, 1971, pp. 179-187.

- Hertzberg 76 R.W. Hertzberg, Deformation and Fracture Mechanics of Engineering Materials, John Wiley and Sons, New York, 1976.
- Hodulak 79 L. Hodulak, H. Kordisch, S. Kunzelmann, and E. Sommer, "Growth of Part-Through Cracks," Fracture Mechanics, pp. 399-410, American Society for Testing and Materials Special Technical Publication No. 677, Philadelphia, Pennsylvania, 1979.
- Hogg 70 R.V. Hogg and A.T. Craig, Introduction to Mathematical Statistics, 3rd Ed., The Macmillan Company, Collier-Macmillan Limited, London, 1970.
- Horn 79 R.M. Horn, "The Growth and Stability of Stress Corrosion Cracks in Large Diameter BWR Piping," Report NEDC-24750-1, General Electric Company, San Jose, California, November 1979.
- Hutchinson 79 J.W. Hutchinson and P.C. Paris, "Stability Analysis of J-Controlled Crack Growth," Elastic-Plastic Fracture, pp. 37-64, American Society for Testing and Materials Special Technical Publication No. 668, Philadelphia, Pennsylvania, 1979.
- Irwin 62 G.R. Irwin, "Crack-Extension Force for a Part-Through Crack in a Plate," Journal of Applied Mechanics, December 1962, pp. 641-654.
- James 75 L.A. James, "Some Questions Regarding the Interaction of Creep and Fatigue," Journal of Engineering Materials and Technology, (ASME paper 75-WA/Mat-6).
- Johnson 79 D.P. Johnson, T.L. Toomay and C.S. Davis, "Estimation of the Defect Detection Probability for Ultrasonic Tests on Thick Section Steel Weldment," Electric Power Research Report EPRI NP-991, Palo Alto, California, February 1979.
- Johnston 78a G.O. Johnston, "What Are the Chances of Failure? Part 1, Material Properties and Design Factors," Welding Institute Research Bulletin, Vol. 19, pp. 36-40, February 1978.
- Johnston 78b G.O. Johnston, "What Are the Chances of Failure? Part 2, NDT, Pressure Vessel Applications and Fatigue," Welding Institute Research Bulletin, Vol. 19, pp. 78-82, March 1978.

- Leverenz 78 F.L. Leyerenz, Jr., J.M. Koren, R.C. Erdmann and G.S. Lellouche, "ATWS: A Reappraisal, Part III: Frequency of Anticipated Transients," Report EPRI NP-801, Electric Power Research Institute, Palo Alto, California, July 1978.
- Lidiard 78 A.B. Lidiard and M. Williams, "The Sensitivity of Pressure Vessel Reliability to Material and Other Factors," Reliability Problems of Reactor Pressure Components, Vol. 1, pp. 233-248, International Atomic Energy Agency, Vienna, 1978.
- Lim 81 E.Y. Lim, "PRAISE Computer Code User's Manual", Vol. 9 of "Probability of Pipe Fracture in the Primary Coolant Loop of a PWR", U.S. Nuclear Regulatory Commission, Report NUREG/CR-2189, Washington, D.C., August 1981.*
- Love 44 A.E.H. Love, A Treatise on the Mathematical Theory of Elasticity, Dover Publications, New York, 1944.
- Lucia 79 A.C. Lucia, R. Brunnhuber and J. Elbat, "A New Computer Code for the Estimation of the Probability of Failure of PWR Pressure Vessels," American Society of Mechanical Engineers Paper 79-PVP-118, New York, 1979.
- Lyman 74 Metals Handbook, Vol. 1, Properties and Selection of Materials, edited by T. Lyman, 8th edition, American Society for Metals, Novelty, Ohio, 1974.
- Lynn 77 E.K. Lynn, "The OCTAVIA Code for Predicting Vessel Performance and Failure Probabilities," presented at the Fifth Water Reactor Safety Meeting, Gaithersburg, Maryland, November 1977.
- Lu 81 S. Lu, M. Ma and R. Larder, "Seismic Response Analysis", Vol. 3 of "Probability of Pipe Fracture in the Primary Coolant Loop of a PWR", U.S. Nuclear Regulatory Commission, Report NUREG/CR-2189, Washington, D.C., August 1981.*
- Mann 74 N.R. Mann, R.E. Schafer and N.D. Singpurwalla, Methods for Statistical Analysis of Reliability and Life Data, John Wiley and Sons, New York, 1974.
- Mansour 73 A.E. Mansour and D. Faulkner, "On Applying the Statistical Approach to Extreme Sea Loads and Ship Hull strength," Transaction of the Royal Institution of Naval Architects, Vol. 115, (1973), p. 277.
- Marshall 76 "An Assessment of the Integrity of PWR Pressure Vessels," Report by a Study Group Chaired by W. Marshall, available from H.M. Stationary Office, London, October 1976.
- Mayfield 80 M.E. Mayfield, T.P. Forte, E.C. Rodabaugh, B.N. Leis and R.J. Eiber, "Cold Leg Integrity Evaluation," Battelle Columbus Laboratories Report to U.S. Nuclear Regulatory Commission NUREG/CR-1319, February 1980.*

- JWES 77 "Study on the Safety Assessment of Fatigue Strength of Pressure Vessels and Piping Systems in Nuclear Plants," Japan Welding Engineering Society Report JWES-AE-7707, December 1977, (NCR Translation No. 351).
- Kadlecek 73 P. Kadlecck, "Mechanical Property Data on Hot-Extruded 304N and 316N Stainless Steel Pipe," Elevated Temperature Properties as Influenced by Nitrogen Additions to Types 304 and 316 Austenitic Stainless Steel, pp. 3-34, American Society for Testing and Materials Special Technical Publication No. 522, Philadelphia, Pennsylvania, 1973.
- Kanninen 78 M.F. Kanninen, et al., "Towards an Elastic - Plastic Fracture Mechanics Capability for Reactor Piping," Nuclear Engineering and Design, Vol. 45, (1978), pp. 117-134.
- Kitagawa 77 H. Kitagawa and T. Hisada, "Reliability Analysis of Structures Under Periodic Inspection," Third International Conference on Pressure Vessel Technology, Part I, Analysis and Design, pp.475-482, American Society of Mechanical Engineers, New York, 1977.
- Klepfer 75 H.H. Klepfer, et al., "Investigation of Cause of Cracking in Austenitic Stainless Steel Weldments," Report NEDO-21000, General Electric Company, Nuclear Energy Division, San Jose, California, July 1975.
- Kobayashi 77 A.S. Kobayashi, N. Polvnicha, A.F. Emery and W.J. Love, "Inner and Outer Cracks in Internally Pressurized Cylinder," Journal of Pressure Vessel Technology, February 1977, pp. 83-89.
- Kupperman 78 D.S. Kupperman, K.J. Reimann and W.A. Ellingson, "Evaluation of Ultrasonic Technique for Detection of Stress Corrosion Cracks in Stainless Steel Piping," Electric Power Research Institute Report EPRI NP-761, Palo Alto, California, June 1978.
- Labbens 76 R. Labbens, A. Pellissier-Tanon and J. Heillot, "Practical Method for Calculating Stress-Intensity Factors Through Weight Functions," Mechanics of Crack Growth, pp. 368-384, American Society for Testing and Materials Special Technical Publication No. 590, Philadelphia, Pennsylvania, 1976.
- Landes 72 J.D. Landes and J.A. Begley, "The Effect of Specimen Geometry on J_{1c} ," Fracture Toughness, pp. 24-39, American Society for Testing and Materials Special Technical Publication No. 514, Philadelphia, Pennsylvania, 1972.

- Mazumdar 75 M. Mazumdar, "Importance Sampling in Reliability Estimation," in Reliability and Fault Tree Analysis Theoretical and Applied Aspects of System Reliability and Safety Assessment SIAM, Philadelphia, 1975, pp. 153-163.
- McGowan 79 J.J. McGowan and M. Raymund, "Stress Intensity Factor Solutions for Internal Longitudinal Semi-Elliptical Surface Flaws in a Cylinder Under Arbitrary Loading," Fracture Mechanics, pp. 365-380, American Society for Testing and Materials Special Technical Publication No. 677, Philadelphia, Pennsylvania, 1979.
- McGrath 73 E.J. McGrath, et al., "Techniques for Efficient Monte-Carlo Simulation," Science Applications, Inc., Report SAI-72-590-LJ, for Office of Naval Research, March 1973.
- Michel 78 D.J. Michel, L.E. Steele and J.R. Hawthorne, "Influence of Irradiation and Other Factors on Fatigue Crack Propagation in Austenitic Stainless Steels," Reliability Problems of Reactor Pressure Components, Vol. 1, pp. 333-343, International Atomic Energy Agency, Vienna, Austria, 1978.
- Mood 50 A.M. Mood, Introduction to the Theory of Statistics McGraw-Hill, New York, 1950.
- Nair 78 P.I. Nair, "Fatigue Crack Growth Model for Part-Through Flaws in Plates and Pipes," American Society of Mechanical Engineers Paper No. 78-Mat-9, New York, 1978, also published in Journal of Engineering Materials and Technology.
- Naylor 66 T.H. Naylor, J.I. Balinty, D.S. Burdick and K. Chu, Computer Simulation Techniques, John Wiley & Sons, Inc., New York, 1966.
- Nelson 75 D.V. Nelson and H.O. Fuchs, "Predictions of Cumulative Damage Using Condensed Load Histories," Paper 750045, presented at SAE Automotive Engineering Congress and Exposition, February 1975.
- Newman 79 J.C. Newman, Jr., "A Review and Assessment of the Stress-Intensity Factors for Surface Cracks," Part-Through Crack Fatigue Life Prediction, pp. 16-42, American Society for Testing and Materials Special Technical Publication No. 687, Philadelphia, Pennsylvania, 1979.

- Nichols 75 R.W. Nichols, "The Uses of Welded Materials in Nuclear Power Engineering," Welding Journal, Vol. 54, No. 12, (December 1975), pp. 417s-432s.
- Nilsson 77 F. Nilsson, "A Model for Fracture Mechanical Estimation of the Failure Probability of Reactor Pressure Vessels," Third International Conference on Pressure Vessel Technology, Part 1, Materials and Fabrication, pp. 593-601, American Society of Mechanical Engineers, New York, 1977.
- Nilsson 78 F. Nilsson and B. Ostensson, "J_{IC}-Testing of A-533B Statistical Evaluation of Some Different Testing Techniques," Engineering Fracture Mechanics, Vol. 10, (1978), pp. 223-232.
- Paris 65 P.C. Paris and G.C. Sih, "Stress Analysis of Cracks," Fracture Toughness Testing and its Applications, pp. 30-81, American Society for Testing and Materials Special Technical Publication No. 381, Philadelphia, Pennsylvania, 1965.
- Paris 72 P.C. Paris, R.J. Bucci, E.T. Wessel, W.G. Clark and T.R. Mager, "Extensive Study of Low Fatigue Crack Growth Rates in A533 and A508 Steels," Stress Analysis and Growth of Cracks, American Society for Testing and Materials Special Technical Publication No. 513, pp. 141-176, Philadelphia, Pennsylvania, 1972.
- Paris 79 P.C. Paris, H. Tada, A. Zahoor and H. Ernst, "The Theory of Instability of the Tearing Mode of Elastic-Plastic Crack Growth," Elastic-Plastic Fracture, pp. 5-36, American Society for Testing and Materials Special Technical Publication No. 668, Philadelphia, Pennsylvania, 1979.
- PCSG 75 "Investigation and Evaluation of Cracking in Austenitic Stainless Steel Piping of Boiling Water Reactor Plants," Report NUREG-75/067 (NTIS No. PB-246 645) Pipe Cracking Study Group, Nuclear Regulatory Commission, Washington, D.C., October 1975.
- PCSG 79 "Investigation and Evaluation of Stress-Corrosion Cracking in Piping of Light Water Reactor Plants," Report NUREG-0531, Pipe Crack Study Group, Nuclear Regulatory Commission, Washington, D.C., February 1979.*
- Phillips 69 C.A.G. Phillips and R.G. Warwick, "A Survey of Defects in Pressure Vessels Built to High Standards of Construction and its Relevance to Nuclear Primary Circuit Envelopes," AHSB(S)R162, AKAEA, 1969.
- PISC 79 "Evaluation of PISC Trials Results," Preprint of Report No. 5, Plate Inspection Steering Committee, May 1979.

- Rasmussen 78 J. Rasmussen, "Notes on Human Error Analysis and Predictions," Synthesis and Analysis Methods for Safety, pp. 357-389, edited by G. Apostolakis, S. Garribba and G. Volta, Plenum Press, New York, 1978.
- Reynen 77 J. Reynen, "Surface Cracks in Cylinders During Thermal Shock," American Society of Mechanical Engineers Paper 77-PVP-5, New York, 1977.
- RG45 Regulatory Guide 1.45, "Reactor Coolant Pressure Boundary Leakage Detection System," Nuclear Regulatory Commission, Washington, D.C.
- Ricardella 72 P.C. Ricardella and T.R. Mager, "Fatigue Crack Growth in Pressurized Water Reactor Vessels," Pressure Vessels and Piping: Design and Analysis, Vol. 1, Analysis, pp. 321-340, American Society of Mechanical Engineers, New York, 1972.
- Rice 68 J.R. Rice, "A Path Independent Integral and the Approximate Analysis of Strain Concentration by Notches and Cracks," Journal of Applied Mechanics, Vol. 35, (1968), pp. 379-386.
- Rice 72a J.R. Rice and N. Levy, "The Part-Through Surface Crack in an Elastic Plate," Journal of Applied Mechanics, Vol. 39, (1972), pp. 185-194.
- Rice 72b J.R. Rice, "Some Remarks on Elastic Crack-Tip Stress Fields," International Journal of Solids and Structures, Vol. 8, (1972), pp. 751-758.
- Ritchie 77a R.O. Ritchie, "Near-Threshold Fatigue Crack Propagation in Ultra-High Strength Steel: Influence of Load Ratio and Cyclic Strength," Journal of Engineering Materials and Technology, (July 1977), pp. 195-204.
- Ritchie 77 R. Ritchie, "Influence of Microstructure on Near-Threshold Fatigue-Crack Propagation in Ultra-High Strength Steel," Metal Science, August/September 1977, pp. 368-381.
- Rizzo 67 F.J. Rizzo, "An Integral Equation Approach to Boundary Value Problems in Classical Elastostatics," Quarterly of Applied Mathematics, Vol. 25, (1967), pp. 83-95.
- Rolfe 75 S.T. Rolfe and J.M. Barsom, Fracture and Fatigue Control in Structures, Applications of Fracture Mechanics, Prentice-Hall, Inc., Englewood Cliffs, New Jersey, 1975.

- RSS75 Reactor Safety Study, An Assessment of Accident Risks in U.S. Commercial Nuclear Power Plants, WASH-1400, (NUREG-75/014), Appendices III and IV, "Failure Data and Common Mode Failures Bounding Techniques and Special Techniques," Nuclear Regulatory Commission, Washington, D.C., October, 1975.
- Rummel 74 W.D. Rummel, P.H. Todd, Jr., R.A. Rathke and W.L. Castner, "The Detection of Fatigue Cracks by Non-Destructive Test Methods," Materials Evaluation, Vol. 32, No. 10, (October 1974), pp. 205-212.
- Rzevski 78 F. Rzevski, "Improving System Reliability by the Elimination of a Class of Design Errors," Synthesis and Analysis Methods for Safety and Reliability Studies, pp. 391-399, edited by G. Apostolakis, S. Garribba and G. Volta, Plenum Press, New York, 1978.
- Sabri 80 Z.A. Sabri and A.A. Hussein, "Human Factors in Nuclear Power Plant Operation," Proceeding of the American Nuclear Society/European Nuclear Society Topical Meeting on Thermal Reactor Safety, Knoxville, Tennessee, April 1980, CONF-800403, Vol. II, pp. 1056-1063.
- Schmidt 73 R.A. Schmidt and P.C. Paris, "Threshold for Fatigue Crack Propagation and the Effects of Load Ratio and Frequency," Progress in Flaw Growth and Fracture Toughness Testing, pp. 79-94, American Society for Testing and Materials Special Technical Publication No. 536, Philadelphia, Pennsylvania, 1973.
- Schmidt 77 W. Schmidt, E. Rohrich and R. Wellein, "Application of Probabilistic Fracture Mechanics to the Reliability Analysis of Pressure Bearing Reactor Components," Paper G 6/2, Transaction of the 4th International Conference on Structural Mechanics in Reactor Technology, San Francisco, August 1977.
- Schmidt 79 W. Schmidt and R. Wellein, "Leakage Probability of Circumferential Defects in Pipes", Nuclear Energy Agency, Steering Committee for Nuclear Energy, Paris, August 30, 1979.
- Shahinian 75 P. Shahinian, "Creep-Fatigue Crack Propagation in Austenitic Stainless Steel," Journal of Pressure Vessel Technology, (ASME Paper 75-WA/PVP-1).
- Shinozuka 69 M. Shinozuka and J.N. Yang, "Optimum Structural Design Based on Reliability and Proof Load Test," Annals of Assurance Science Proceedings of the Reliability and Maintainability Conference, Vol. 8, July 1964, pp. 375-391.
- Shreider 66 Y.A. Shreider, The Monte Carlo Method - The Method of Statistical Trials, Pergamon Press 1966.

- Simmons 65 W.F. Simmons and J.A. Van Echo, Elevated Temperature Properties of Stainless Steels, ASTM Data Series Publication DS5-S1, American Society for Testing and Materials, Philadelphia, Pennsylvania, 1965.
- Simoneau 74 R.J. Simoneau, "Two-Phase Choked Flow of Sub-Cooled Nitrogen Through a Slit," NASA Technical Memorandum, NASA TM X-71516, NASA Lewis Research Center, 1974.
- Smith 72 F.W. Smith, "The Elastic Analysis of the Part-Circular Surface Flaw Problem by the Alternating Method," The Surface Crack: Physical Problems and Computational Solutions, pp. 125-152, American Society of Mechanical Engineers, New York, 1972.
- Smith 69 G.V. Smith, An Evaluation of the Yield, Creep, and Rupture Strengths of Wrought 304, 316, 321, and 347 Stainless Steels at Elevated Temperatures, ASTM Data Series DS 552, American Society for Testing and Materials, Philadelphia, Pennsylvania, 1969.
- Stiansen 79 S.G. Stiansen, A. Mansour, H.Y. Jan and A. Thayamballi, "Reliability Methods in Ship Structures," Paper No. 5, Spring 1979, Meeting of the Royal Institution of Naval Architects, London.
- Swain 78 A.D. Swain and H.E. Guttmann, "Human Reliability Analysis of Dependent Events," Probabilistic Analysis of Nuclear Reactor Safety, Vol. 3, p. x.2-1, topical meeting sponsored by American Nuclear Society at Los Angeles, May 1978.
- Swain 80 A.D. Swain and H.E. Guttman, "Handbook of Human Reliability Analysis with Emphasis on Nuclear Power Plant Applications," U.S. Nuclear Regulatory Commission Report NUREG/CR-1278, Washington, D.C., April 1980.**
- Swedlow 72 The Surface Crack: Physical Problems and Computational Solutions, edited by J.L. Swedlow, American Society of Mechanical Engineers, New York, 1972.
- Swindeman 77 R.W. Swindeman, W.J. McAfee and V.K. Sikka, "Product Form Variability in the Mechanical Behavior of Type 304 Stainless Steel at Room Temperature and 593C (1100F)," Reproducibility and Accuracy of Mechanical Tests, pp. 41-64, American Society for Testing and Materials Special Treatment Publication No. 626, Philadelphia, Pennsylvania, 1977.
- Tada 73 H. Tada, P.C. Paris and G.R. Irwin, The Stress Analysis of Cracks Handbook, Del Research Corporation, Hellertown, Pennsylvania, 1973.
- Tada 79 H. Tada, P. Paris and R. Gamble, "Stability Analysis of Circumferential Cracks in Reactor Piping Systems," NUREG/CR-0838, U.S. Nuclear Regulatory Commission, Washington D.C., June 1979.*

- Tang 73 W.H. Tang, "Probabilistic Updating of Flaw Information," Journal of Testing and Evaluation, Vol. 1, No. 6, (November 1973), pp. 459-467.
- Timoshenko 51 S. Timoshenko and J.N. Goodier, Theory of Elasticity, McGraw-Hill Book Company, Inc., New York, 1951.
- TS Zion Station Technical Specifications, Commonwealth Edison Company, Docket No. 50-304.
- Tsao 75 H.S. Tsao and S.D. Werner, "Determination of Equivalent Response Cycles for Use in Earthquake - Induced Fatigue Analyses," Agbabian Associates, El Segundo, California, Report SAN/1011-106, to Energy Research and Development Administration, May 1975.
- Vanderglass 79 M.L. Vanderglass and B. Mukherjee, "Fatigue Threshold Stress Intensity and Life Estimation of ASTM A-106 Piping Steel", American Society of Mechanical Engineers Paper 79-PVP-86, New York, 1979.
- Vesely 78 W.E. Vesely, E.K. Lynn and F.F. Goldberg, "OCTAVIA: A Computer Code to Calculate the Probability of Pressure Vessel Failure From Pressure-Transient Occurances," Reliability Problems of Reactor Pressure Components, Vol. 1, pp. 105-122, International Atomic Energy Agency, Vienna, 1978.
- Vosikovsky 75 A. Vosikovsky, "Fatigue Crack Growth in an X-65 Line-Pipe Steel at Low Cyclic Frequencies in Aqueous Environments," Journal of Engineering Materials and Technology, (October 1975), pp. 298-304.
- Wallis 80 G.B. Wallis, "Critical Two-Phase Flow," International Journal of Multiphase Flow, Vol. 6, 1980, pp. 97-112.
- Walpole 72 R.E. Walpole and R.H. Myers, Probability and Statistics for Engineers and Scientists, Macmillan Publishing Co. Inc., New York, 1972.
- WASH 74 Report on the Integrity of Reactor Vessels for Light Water Power Reactors, The Advisory Committee on Reactor Safeguards, U.S. A.E.C. Report WASH-1285, Washington, D.C., January 1974, also published in Nuclear Engineering and Design, Vol. 28, (1974), pp. 147-195.

- Wei 76 Fatigue Crack Growth Under Spectrum Loads, edited by R.P. Wei and R.Y. Stephens, American Society for Testing and Materials Special Technical Publication No. 595, Philadelphia, Pennsylvania, 1976.
- Wilkowski 80 G.M. Wilkowski, A. Zahoor and M.F. Kanninen, "A Plastic Fracture Mechanics Prediction of Fracture Instability in a Circumferentially Cracked Pipe in Bending - Part II: Experimental Verification on a Type 304 Stainless Steel Pipe," American Society of Mechanical Engineers Paper 80-WA/PVP-4, New York, 1980.
- Wilson 74 S.A. Wilson, "Estimating the Relative Probability of Pipe Severance by Fault Cause," General Electric Company Report GEAP-20615, Boiling Water Reactor Systems Department, San Jose, California, September 1974.
- Wise 77 M.J. Wise and E.R. Reinhart, "Survey of Recent Operating Experience Using Leak Detection Systems to Improve Plant Operation," Transaction of the American Nuclear Society, Vol. 27, November 1977, p. 936.
- Witt 78 F.J. Witt, W.H. Bamford and T.C. Esselman, "Integrity of the Primary Systems of Westinghouse Nuclear Power Plants During Postulated Seismic Events," Westinghouse Electric Corporation Report WCAP-9283, Pittsburgh, Pennsylvania, March 1978.
- Yagawa 79 G. Yagawa, M. Ichiyama and Y. Ando, "Theoretical and Experimental Analysis of Semi-Elliptical Surface Cracks Subject to Thermal Shock," Fracture Mechanics, pp. 381-398, American Society for Testing and Materials Special Technical Publication No. 677, Philadelphia, Pennsylvania, 1979.
- Yang 74 J.N. Yang and W.J. Trapp, "Reliability Analysis of Aircraft Structures Under Random Loading and Periodic Inspection," AIAA Journal, Vol. 12, pp. 1623-1630, December 1974.
- Zion "Zion Station Thermal Cycle Records," logbook of observed transients maintained by Commonwealth Edison, Zion Generating Station, Zion, Illinois.

*Available for purchase from the NRC/GPO Sales Program, U.S. Nuclear Regulatory Commission, Washington, DC 20555 and/or the National Technical Information Service, Springfield, VA 22161.

**Single copies are available free upon written request to the Division of Technical Information and Document Control, U.S. Nuclear Regulatory Commission, Washington, DC 20555.

APPENDIX A

**INTRODUCTION AND REVIEW OF
STRESS INTENSITY FACTOR ANALYSIS**

APPENDIX A

INTRODUCTION AND REVIEW OF STRESS INTENSITY FACTOR ANALYSIS

Previously existing information on stress intensity factors for semi-elliptical surface cracks in bodies of finite thickness was insufficient to perform an analysis for semi-elliptical cracks of arbitrary size subjected to stresses that vary strongly through the thickness. Such information is necessary in order to adequately treat the bivariate distribution of initial cracks (discussed in Section 2.3), and to allow consideration of stresses that vary strongly through the thickness. Radial gradient thermal stresses have strong thickness variations, as discussed in Section 1.3 and Appendix D. In order to circumvent these shortcomings of previously existing solutions, new information was generated as a part of this research project that will allow inclusion of the above factors in the piping reliability analysis. A considerable amount of new fracture mechanics information was obtained. Details of these results will be presented in the following appendices, with only major highpoints being included in the main body of the report.

A.1 Desired Solutions

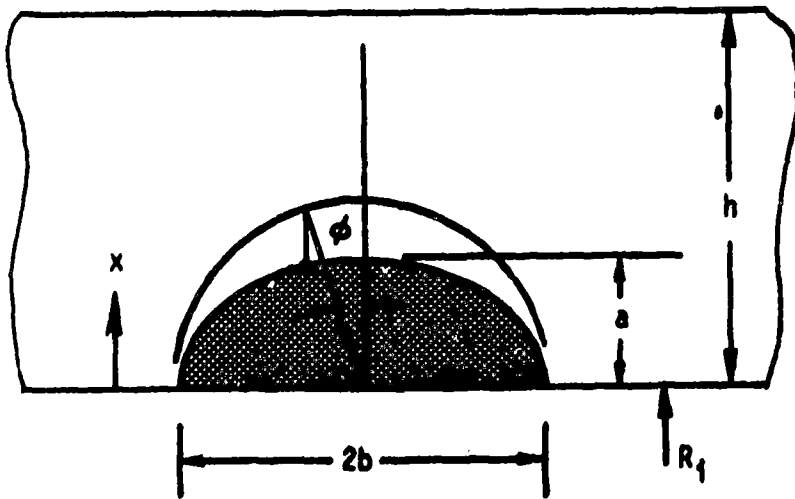
The crack geometry considered in the analysis of piping reliability is a part-circumferential interior surface semi-elliptical crack, which is shown in Figure 2-2. The reasons for considering this crack geometry and orientation were discussed in Section 2.2. The stress intensity factors for cracks of arbitrary aspect ratio, $\beta = b/a$ ($\beta > 1$), and a/h are required. Additionally, it is desired to account for growth in both the depth and length directions, and to allow the aspect ratio to change as the crack grows. Changes in the aspect ratio will depend on the nature of the applied stresses. It is desired to account for stresses with steep thickness gradients, such as radial gradient and residual stresses. Therefore, fairly general results are required, rather than just uniform or linearly varying stresses. Thus, it is seen that a fairly

general stress intensity factor solution for part-circumferential cracks is required. Previously existing stress intensity solutions will be reviewed in the next section, from which it will be seen that these solutions are insufficient for the current purposes. Therefore, new solutions were generated by boundary integral equation (BIE) techniques. Such techniques will be briefly reviewed, and the results obtained presented. Since the results of the fracture mechanics analysis was intended for use in the piping reliability efforts, no efforts were made to attain extreme accuracy in the K solutions. Uncertainties in various input parameters, such as the initial crack size distribution, are large enough that the expense and effort of obtaining highly accurate stress intensity results was not warranted. Hence, the results generated are not of high accuracy, but are felt to be sufficient to adequately treat the desired phenomena. The accuracies attained will be discussed in the following, and were estimated by comparisons with selected previous solutions.

1.2 Review of Previously Existing Stress Intensity Solutions

Previously existing stress intensity factor solutions for crack geometries related to part-circumferential interior surface cracks in pipes will be briefly reviewed in this section. No attempt will be made to provide a complete review of work in this area. Semi-elliptical cracks in flat plates and in longitudinal and circumferential orientations in pipes will be considered. Figure A-1 shows the geometric parameters of interest.

Three limiting cases of elliptical cracks in pipes are of interest: (i) an elliptical crack in an infinite body, (ii) a complete circumferential interior crack, and (iii) a very long interior longitudinal crack. Case i is approachable by classical elasticity, and was solved in 1950 (Green 50). This solution was cast in a stress intensity factor form by Irwin 62, who obtained the following approximate expressions for K for a semi-elliptical surface defect in a flat plate subjected to uniform stress, σ



$$\alpha = a/h$$
$$\beta = b/a$$
$$\gamma = R_1/h$$

Figure A-1. Part-Through Crack in a Pipe (or Plate) of Wall Thickness h .

$$\frac{K}{\sigma a^{1/2}} = \frac{1.12 \pi^{1/2}}{F} \left(\frac{1}{\beta^2} \sin^2 \phi + \cos^2 \phi \right)^{1/4} \quad (\text{A-1})$$

$$F = \int_0^{\pi/2} \left(\sin^2 \psi + \frac{1}{\beta^2} \cos^2 \psi \right)^{1/4} d\psi$$

The notation of Figure A-1 is used in this expression. The F integral is the complete elliptic integral of the second kind, which is tabulated in a variety of places. Newman 79 reports the following convenient approximation for F

$$F = \begin{cases} \left[1 + 1.464 \left(\frac{1}{\beta} \right)^{1.65} \right]^{1/4} & \beta \geq 1 \\ \left[1 + 1.464 (\beta)^{1.65} \right]^{1/4} & \beta < 1 \end{cases} \quad (\text{A-2})$$

The maximum error introduced by use of this approximation for F is reportedly about 0.1%.

Newman 79 provides a review of K solutions for semi-elliptical cracks in flat plates. However, he provides no information on the variation of K along the crack front.

The case of a complete internal circumferential crack (case 11 above) subjected to axisymmetric stresses is an axisymmetric problem. It can therefore be economically solved by finite element techniques. Labbens 76 and Buchalet 76 provide such solutions. Labbens provides results for $\gamma = 5, 10$, and ∞ (flat plate), $\alpha < \sim 0.9$ which are applicable to a completely arbitrary axisymmetric stress distribution. Buchalet and Bamford (Buchalet 76) provide solutions for $\gamma = 10$ with axisymmetric stresses which vary as a third-order polynomial through the wall thickness. Additionally, axisymmetric cracks at pressure vessel nozzles are included in Buchalet 76, which serves to show that the K values are very similar to those for a straight run of pipe.

The Labbens solution (Labbens 76) appears preferable because it includes more values of γ and is capable of treating completely arbitrary axisymmetric stresses. Stress intensity factors for complex stress conditions are very economically obtained by numerical integration of Labbens' results. Figure A-2 (from Labbens 76) provides an example of Labbens' solution. K for an arbitrary axial stress distribution $\sigma(x/h)$ can be obtained from the equation

$$K = (2a/\pi)^{1/2} \int_0^1 \frac{\gamma+au}{\gamma+a} \frac{m(u,\alpha) \sigma(au) du}{(1-u)^{1/2}} \quad (A-3)$$

$m(u,\alpha)$ is obtainable directly from Labbens, et al., with m for $\gamma = 10$ and a circumferential crack shown in Figure A-2.

Figure A-3 summarizes a variety of results for interior complete circumferential cracks in pipes subjected to uniform axial stress. This figure shows that γ as large as 10 still is far from a flat plate, and γ does not have an overly strong influence for values less than 10. These results are of interest because they are a limiting case for circumferential interior surface defects.

The case of a very long longitudinal crack in a pipe (case iii above) is also a two-dimensional problem which can be economically solved by finite element techniques. Labbens 76 and Buchalet 76 provide such results, and give influence functions for this geometry in a form analogous to those discussed above for circumferential cracks. Figure A-4 presents results for uniform stress, and provides a direct comparison between longitudinal and circumferential cracks in a pipe and the corresponding flat plate solution. This figure shows large differences between long longitudinal and complete circumferential cracks which are especially noteworthy as a/h exceeds about $1/2$. These results would suggest that large differences would be expected between part-circumferential semi-elliptical surface cracks and semi-elliptical longitudinal surface cracks. The degree to which these differences exist can not be assessed from information currently in the literature.

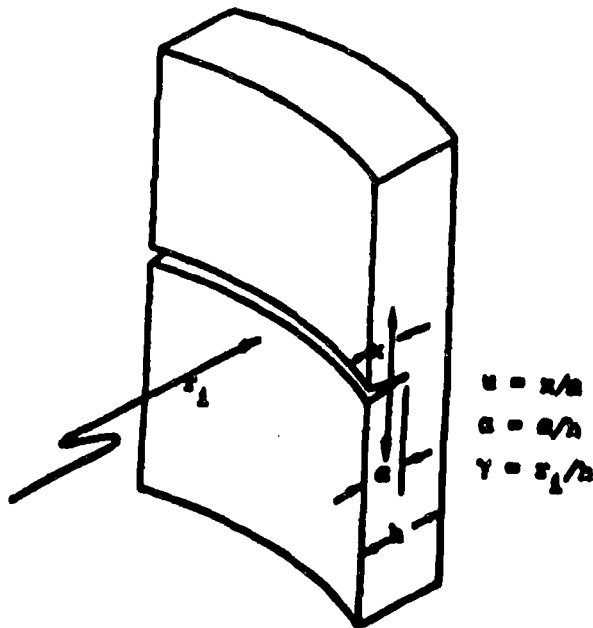
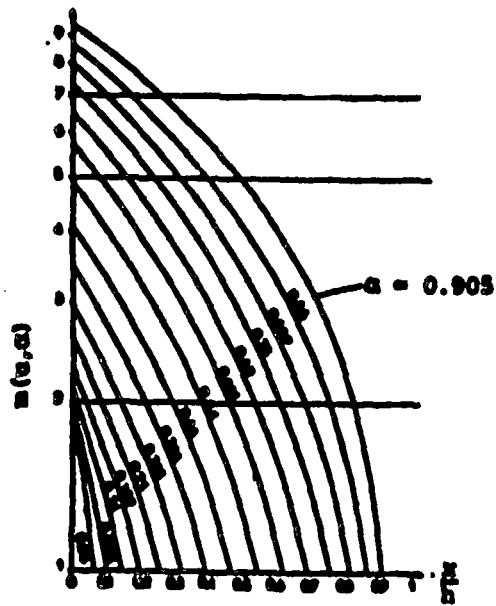


Figure A-2. Weight Function for an Internal Circumferential Surface Crack in a Section of Straight Pipe (from Labbens 76).

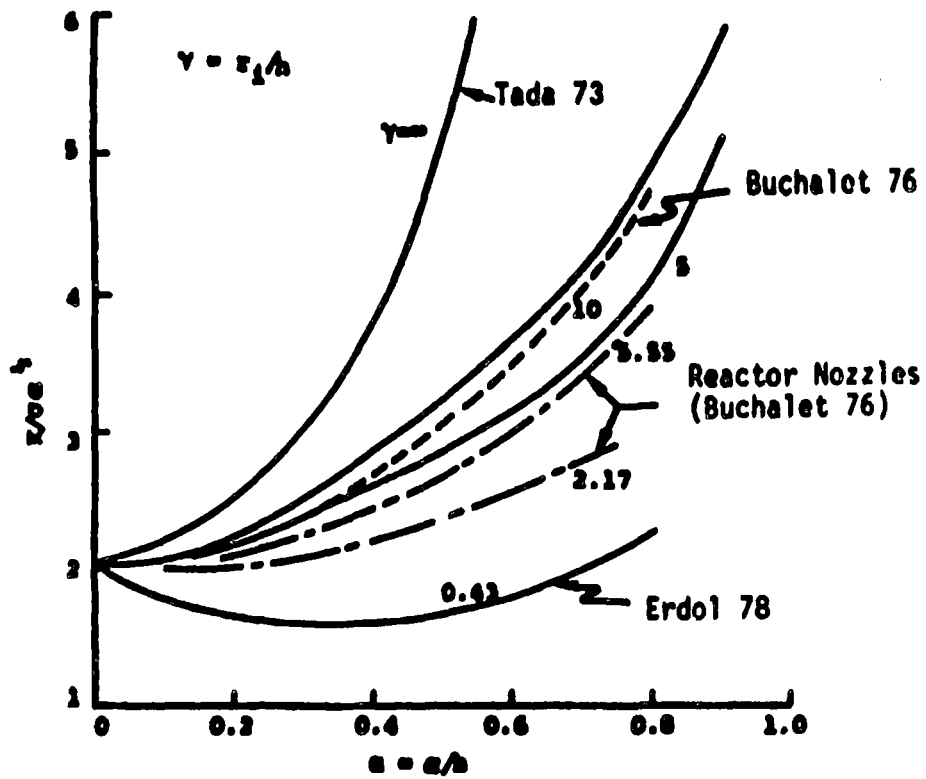


Figure A-3. A Comparison of K for Internal Surface Circumferential Cracks in Pipes Subjected to Uniform Axial Stress. Results are from Labbens 76 and are for straight pipe runs unless otherwise noted.

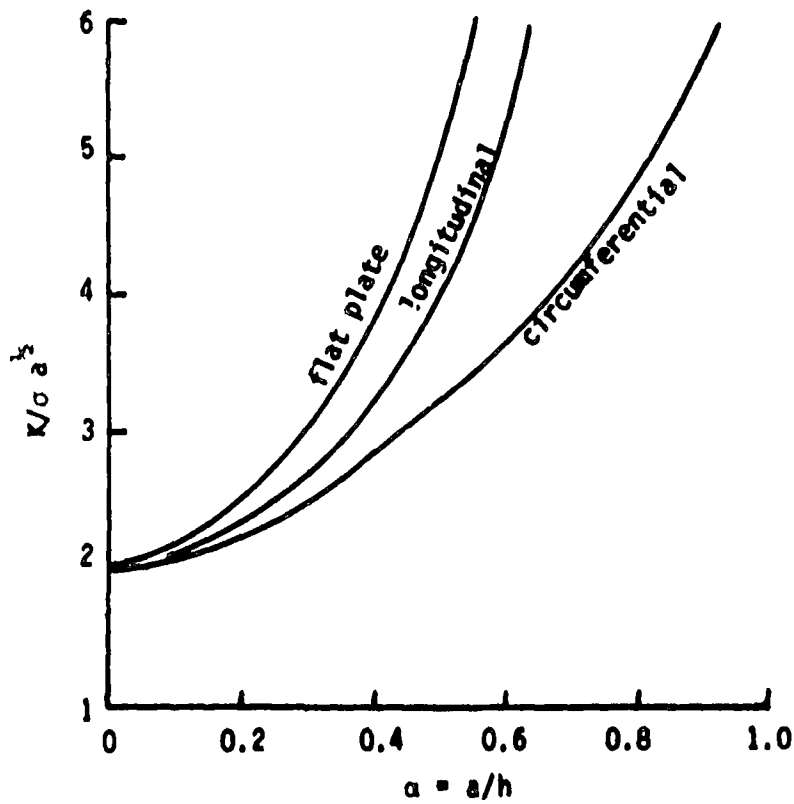


Figure A-4. Stress Intensity Factor for Edge Crack in a Flat Plate and for Long Longitudinal and Complete Circumferential crack in a Pipe with $R_1/h = 10$. Pipe results are from Labbens 76.

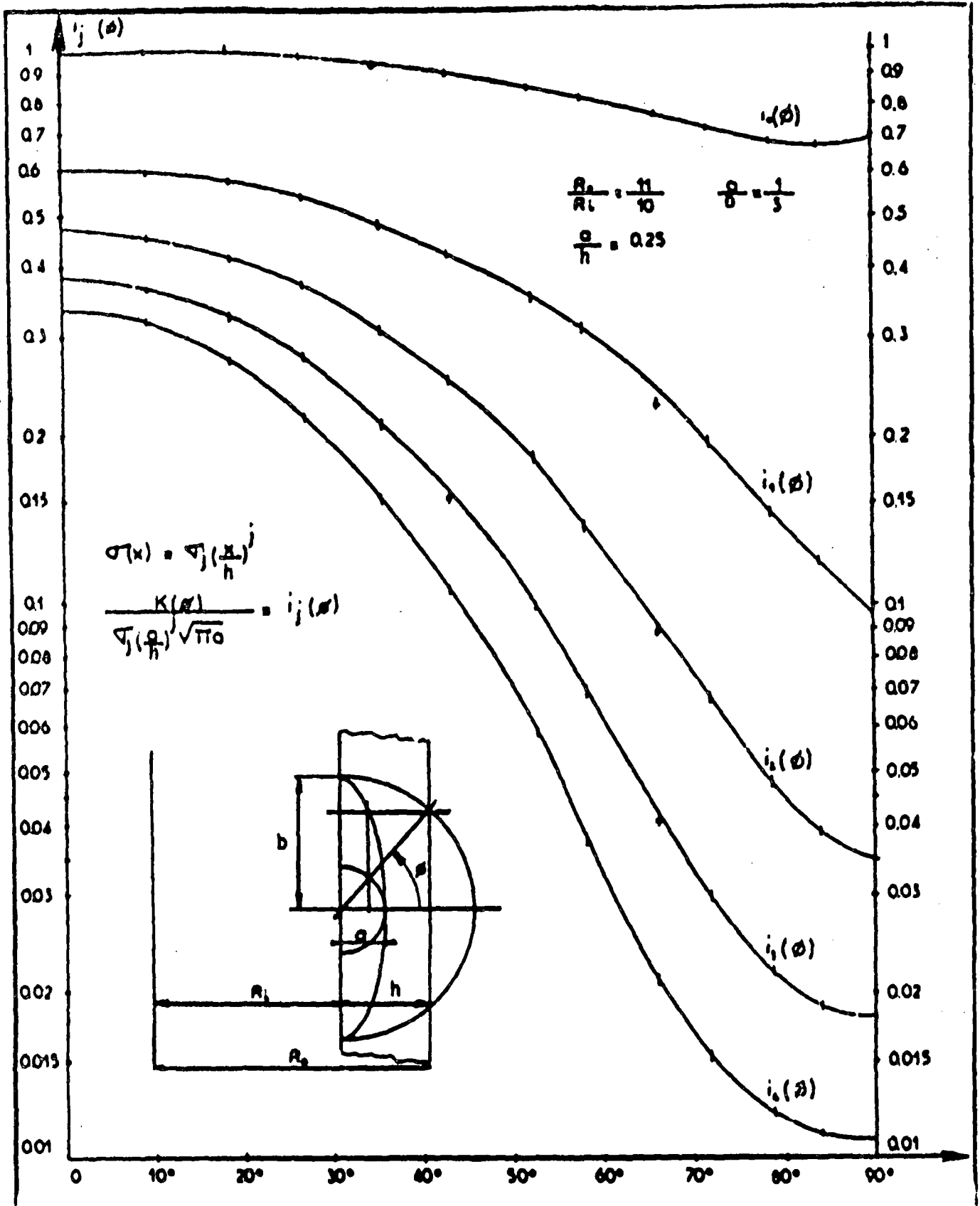


Figure A-5. Function $i_j(\phi)$ for $\frac{a}{h} = 0.25$ (from Hellot 79).

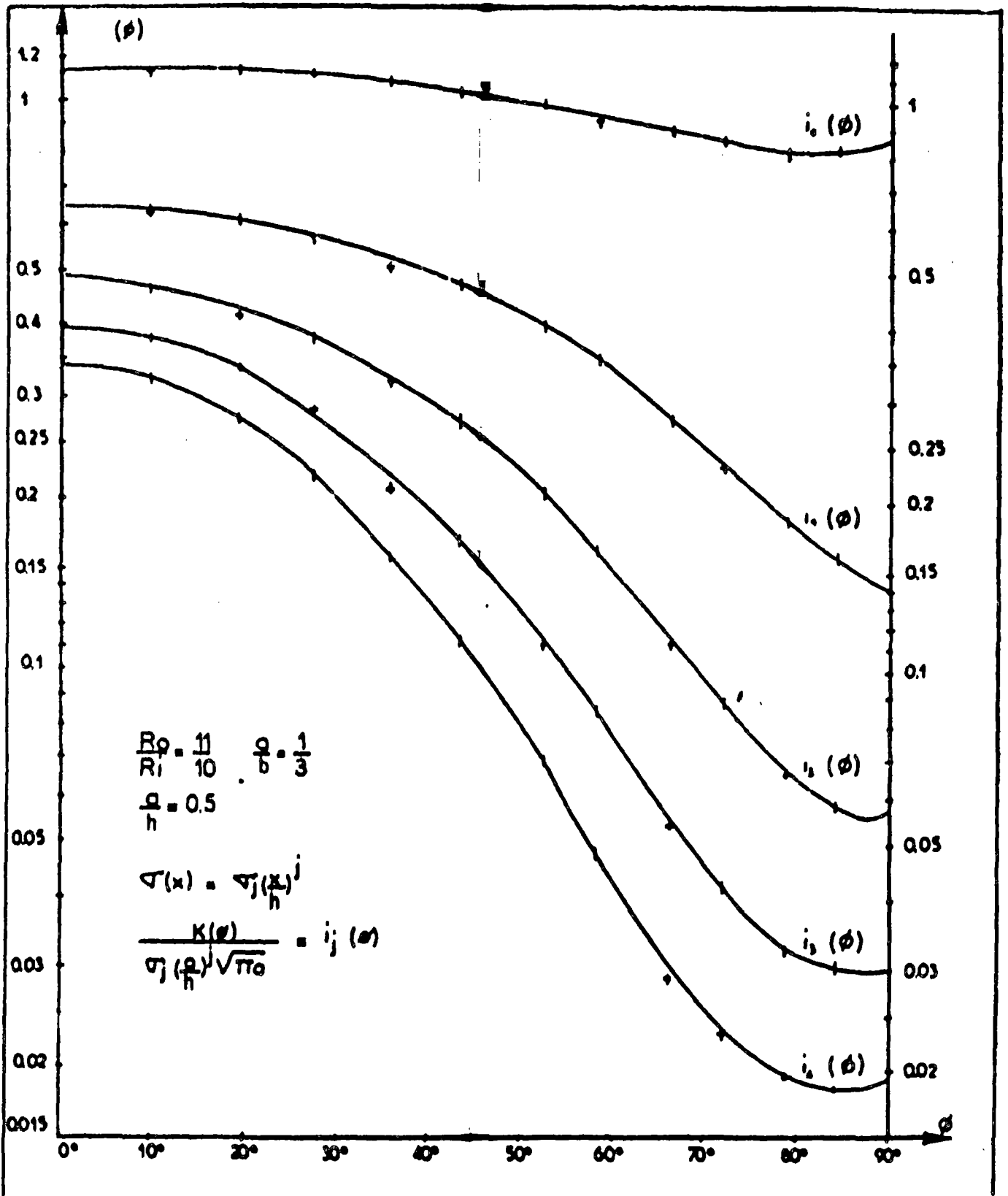


Figure A-6. Functions $i_j(\phi)$ for $\frac{a}{h} = 0.50$ (from Heliot 79).

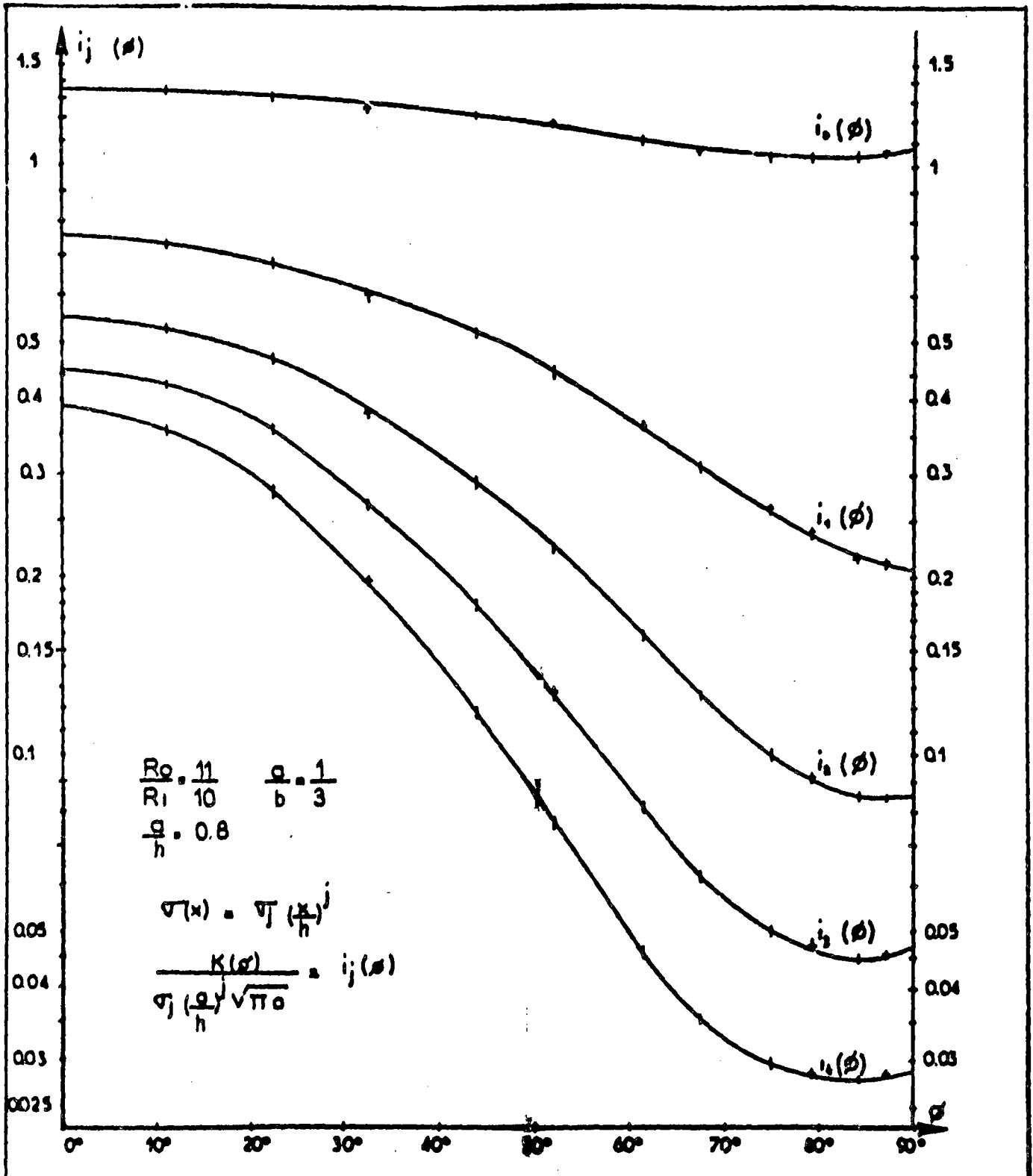


Figure A-7. Functions $i_j(\phi)$ for $\frac{a}{h} = 0.80$ (from Hellot 79).

<u>Reference</u>	γ	β	α
Atluri 77a	2	1	0.5, 0.8
	2	2	0.5
Atluri 77b	2	5	0.8
Kobayashi 77	2-9	5	0.4, 0.6, 0.8
	2-9	1	0.6, 0.8
	2	1.5	0.4
Yagawa 79	∞	1.5	4/30
	∞	2.4	9/30
	∞	5	16/30

All of these solutions are for either a uniform stress on the crack, or a varying hoop stress corresponding to those for an internally pressurized cylinder. A longitudinal crack orientation is considered, and information on the variation of K along the crack front is provided. Note that most of the information is for thick-walled cylinders ($\gamma \sim 2$). Atluri 77b and Kobayashi 77 also contain information on exterior semi-elliptical cracks, which will not be discussed here.

The K solutions included in the above table provide a great deal of information, but are far from providing complete solutions. Trends in the behavior of K with various geometric parameters can be obtained from these existing solutions. Figure A-8 shows the influence of γ ($=R_1/h$) for various β when $\alpha = 0.6$. It is seen that γ is not a strongly influential parameter, and that values for $\gamma = 10$ are not yet approaching flat plate ($\gamma = \infty$) solutions. These are in accordance with earlier observations in regard to Figure A-3. The data plotted in Figure A-8 are from Kobayashi 77; the value for $\gamma = \infty$, $\beta = 1$ is from Newman 79. Variations of K along the crack front for various conditions are presented in Figure A-9. Here it is seen that the value of β is most influential in that large differences are observed between $\beta = 1$ and $\beta = 5$. The values of γ and α have a secondary influence on the normalized variation of K along the crack front.

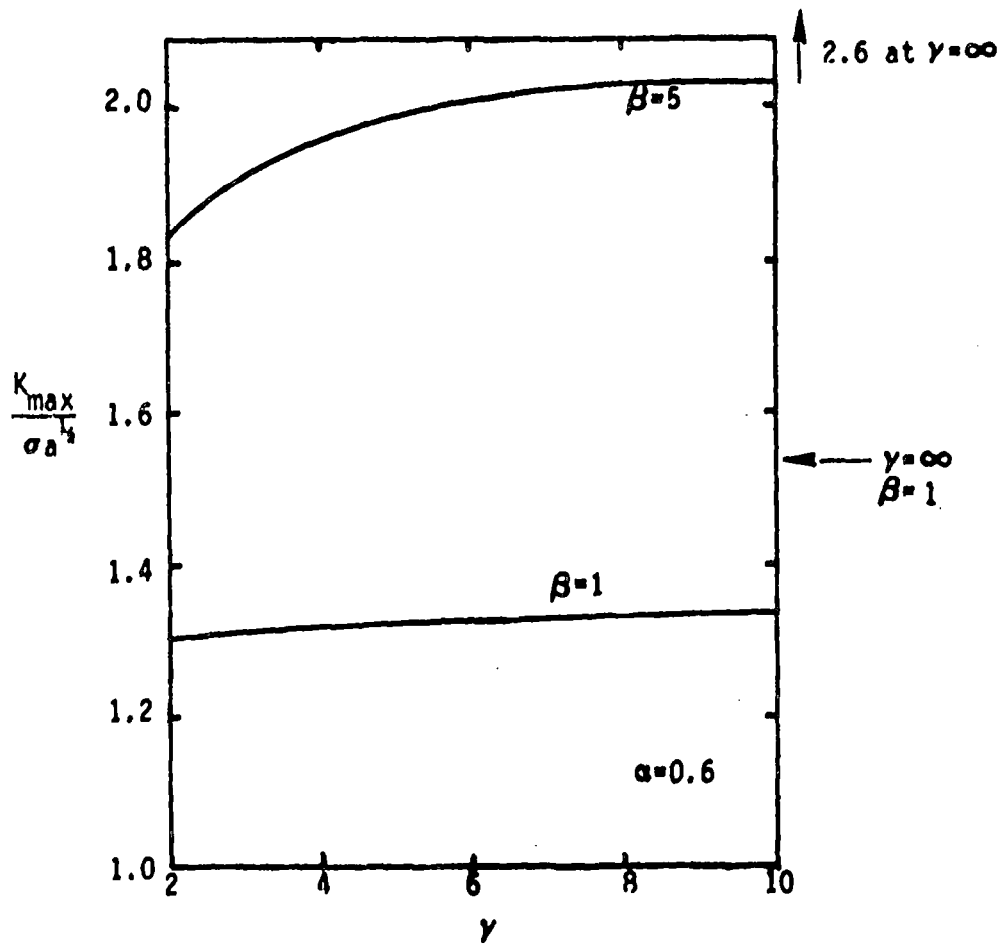


Figure A-8. $K_{max}/\sigma_a h$ as a Function of γ For $\beta=1$ and 5 and $\alpha=0.6$. Results are from Kobayashi 77 and are for uniform or pressure stress.

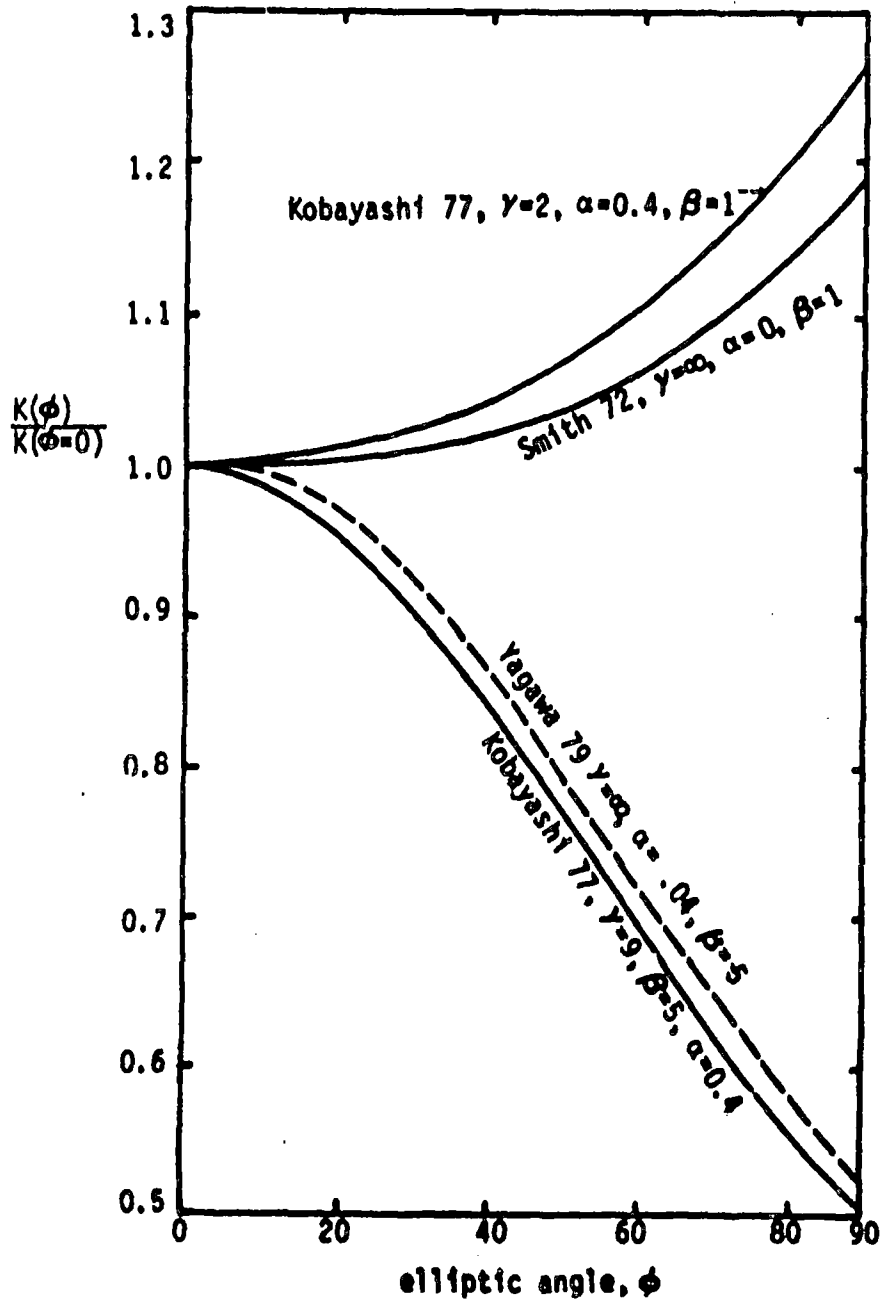


Figure A-9. Normalized Angular Variation of K Along Crack Front for Selected Cases of Uniform or Pressure Stress.

Overall, the above review indicates that existing stress intensity factors for cracks in pipes are available for only a spotty selection of values of the many geometric parameters involved. Such information is especially lacking for cases where thickness gradients of the stress exist, and solutions for part-circumferential cracks are virtually nonexistent. Therefore, in order to be able to adequately treat the bivariate distribution of part-circumferential cracks considered in this investigation, some new stress intensity factor results needed to be generated. The elasticity problem is fully three-dimensional, and numerical techniques must be resorted to. The boundary integral equation (BIE) technique was selected for use. This technique will be briefly reviewed, followed by presentation of results obtained by its use.

A.3 Review of Boundary Integral Equation Techniques

The problem of a part-circumferential crack in a pipe composed of elastic material is a fully three-dimensional problem. Analytic solutions of such problems are usually unobtainable, and numerical techniques must be resorted to. The most commonly known and applied technique for elasticity problems is finite elements. In such cases the complete body, including its interior, must be broken up into small elements. For three-dimensional problems, very large computers and long execution times are generally the rule. Another means of obtaining numerical solutions to three-dimensional elasticity problems is the boundary integral equation technique (BIE). In this technique, only the surface of the body need be broken up into elements, and the numerical solution then directly provides displacements and surface tractions at the surface nodal points. If information in the interior of the body is desired, additional calculations are required. However, crack problems can generally be formulated such that the crack surface and crack plane form a part of the surface of the body to be analyzed. Stress intensity factors are obtainable from crack surface displacements close to the crack tip (see Appendix B). Therefore, numerical information on crack surface displacements is sufficient for the present case, and BIE techniques appear to be especially well suited to provide economical solutions to the three-dimensional crack problem of interest.

The BIE technique is based on some integral results originally obtained by Somigliana which relate displacements to surface integrals of combinations of surface tractions and surface displacements. Such integrals are covered in Section 169 of Love 44. Rizzo, and Cruse and his co-workers pioneered the application of BIE to elasticity problems, and theoretical bases of the procedures employed are covered in Rizzo 67, Cruse 69, 73, 75a. Basically, the surface of the body is broken up into segments, and the variation of stresses and displacements within an area segment are assumed. The surface integrals are then evaluated in terms of the unknown surface displacements and tractions. This results in a set of simultaneous linear equations that can be solved for the unknown nodal displacements or tractions. Since only the surface of the body has to be modelled, the size of the problem is much less than if the entire volume of the body had to be broken up into elements. Hence, BIE techniques can be advantageous over finite element techniques. However, the "matrix of coefficients" of the unknowns is "banded" in finite elements which compensates somewhat for this. Additionally, finite element techniques are more accurate. Nevertheless, BIE techniques were selected for use in this investigation, because high accuracy was not desired, and computer expenses were to be minimized. The computer program described by Cruse 73 was obtained* and applied to the problems of interest. The results obtained are presented in Appendix B.

* The generous assistance of T. Cruse, Pratt and Whitney Aircraft, East Hartford, Connecticut, and P.M. Besuner, Failure Analysis Associates, Palo Alto, California, provided in obtaining and exercising the BIE program is gratefully acknowledged.

APPENDIX B

**STRESS INTENSITY FACTOR RESULTS FROM BOUNDARY
INTEGRAL EQUATION CALCULATIONS**

Appendix B

STRESS INTENSITY FACTOR RESULTS FROM BOUNDARY INTEGRAL EQUATION CALCULATIONS

Existing stress intensity factor solutions are not adequate for treating the bivariate distribution of part-circumferential cracks considered in this investigation--as was extensively discussed in Appendix A. Therefore, boundary integral equation techniques were applied to obtain the desired results. In order to gain familiarity with the code (Cruse 73) and to estimate its accuracy, problems with previously existing solutions were first analyzed. New problems were solved after reproducing previous results with sufficient accuracy. Comparisons with previous solutions and newly generated results will be presented in this Appendix.

The stress intensity factor for a crack problem can be estimated from the results of numerical procedures that do not employ singular elements in a variety of ways - including the following:

- Evaluation of results for two nearly equal crack sizes, then calculating the strain energy release rates and obtaining the stress intensity factor (K) from the energy release rate. This requires roughly twice as many computer runs, and therefore approximately doubles the computer cost (see for instance, Cruse 75a).
- Performing contour integrals around the crack tip and relating values of the integrals to singular conditions at the crack tip. This is analogous to Rice's J - Integral formulation (Rice 68).
- Comparison of stresses near the crack tip with the known singular solution in terms of K .
- Comparison of crack surface opening displacement near the crack front with known solutions in terms of K .

This last procedure will be used here, because only one BIE calculation is required per crack size considered, numerical elasticity solutions generally provide displacements with higher accuracy than stresses, and the crack surface displacements are obtained directly from the BIE calculations. As was mentioned above, extreme accuracy was not required.

The relevant equation relating the stress intensity factor, K , to the crack surface displacement close to the crack tip is derived from classical elasticity (Paris 65, Tada 73). For the standard polar coordinate system with origin at the crack tip, the vertical displacement, v , is given by

$$v(r, \theta) = \frac{K}{G} \left(\frac{r}{2\pi}\right)^{1/2} \sin \frac{\theta}{2} (2 - 2\nu' - \cos^2 \frac{\theta}{2}) \quad (B-1)$$

This equation is for plane strain. On the crack surface, $\theta = 180^\circ$, and the variation of v with distance from the crack tip is

$$v(r, 180^\circ) = \frac{K(1-\nu')}{G} \left(\frac{2r}{\pi}\right)^{1/2} \quad (B-2)$$

In this project, K will be evaluated from the opening displacement at the node closest to the crack front. Denoting this as $v(r_0)$, the equation for K is

$$K = \frac{G}{1-\nu'} v(r_0) \left(\frac{\pi}{2r_0}\right)^{1/2} \quad (B-3)$$

As before r_0 is the distance between the crack front and the closest node. This equation will be used to obtain values of K from the results of BIE calculations.

Comparison with previously existing results will be presented in the following section.

B.1 Complete Circumferential Crack

The axisymmetric geometry of a complete circumferential crack in a pipe was selected as an initial problem to analyze in order to become familiar with running the BIE code. For axisymmetric loading, K results could be compared with corresponding results from Labbens 76. The first loading case considered was axisymmetric, and is shown in Figure B-1, along with the nodalization scheme employed. K due to the ring of pressure loading was evaluated by numerical integration of Labbens 76 weight functions. The loading geometry, and K from the BIE displacements and integration of Labbens results are shown in Figure B-2. This figure also presents results obtained when the pipe length is halved, or when the portion of the crack over which the pressure is applied is altered. K is independent of angular position for this loading and body geometry. This is seen to be borne out by the BIE results, which provides a good check on the program and its inputs. When the pipe length is taken to be half the base case (which was 6 in. from the crack plane to the end of the pipe) K increases, as would be expected. The agreement between the BIE results and Labbens 76 is good, with the BIE results being 9.2% low for $r_0/a = 0.1$ and 6.7% low for $r_0/a = 0.05$. A value of r_0/a of 1/10 thus appears to provide satisfactory results. Additional results were generated in which the row of nodes on the cylindrical surfaces closest to the crack plane were moved only half as far from the crack plane. This was found to have a negligible influence on the stress intensity factor.

These results demonstrated that the code was capable of providing accurate results, that boundary conditions were being properly treated, and that K could be evaluated by use of Equation B-3.

The next problem to be considered retained the axisymmetric geometry of the body, but considered a pressure loading only over a small angular segment. This was intended to check on the accuracy of results where steep gradients of K existed along crack front. Some renodalization was

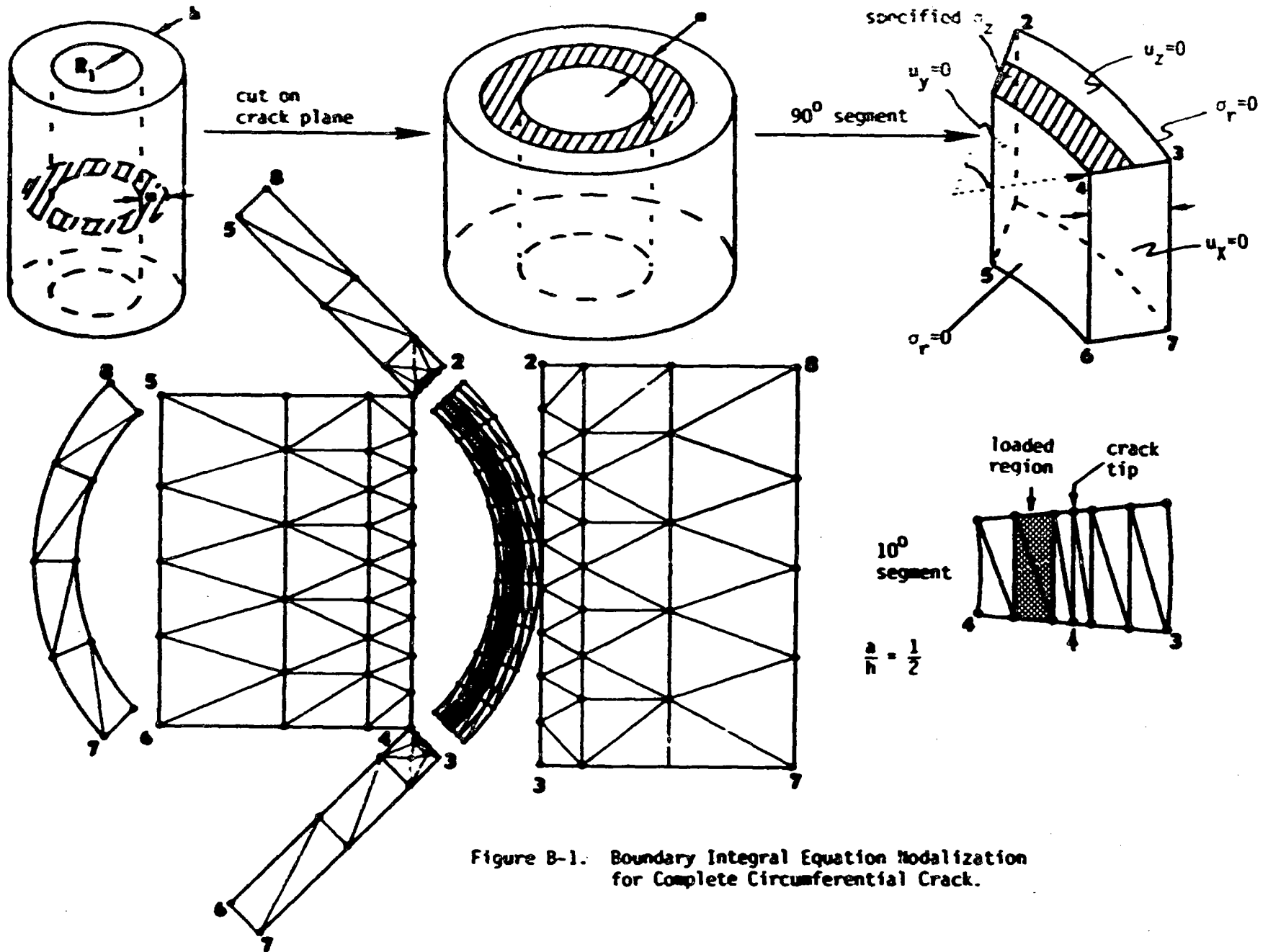


Figure B-1. Boundary Integral Equation Modalization for Complete Circumferential Crack.

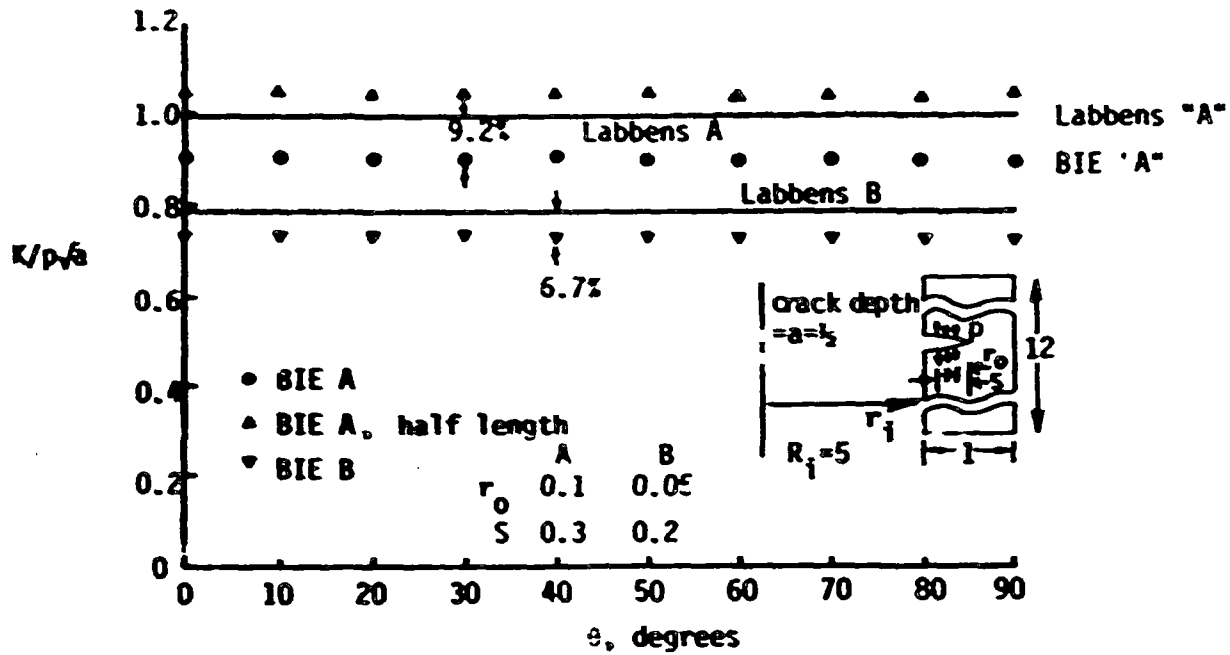


Figure B-2. Various Comparisons of K From BIE Calculations With Corresponding Results Obtainable From Labbens 76.

done, with more nodes being concentrated in regions of steep gradients. The loading geometry considered is shown in Figure B-3, along with various sets of results. The "analytical" solution refers to an estimated K for a point load included in Harris 79 and Harris 80a. The value of θ at which boundary conditions were specified was varied, with a free surface at 30° and a "roller" surface at 90° being considered. Results for these two cases are shown in Figure B-3, from which it is observed that the boundary condition did not have an appreciable influence. This is an expected result, due to St. Venant's principle. Figure B-3 shows good agreement between the BIE results and an approximate analytical solution. This demonstrates the suitability of the BIE code to crack problems when steep K gradients exist along the crack front. Once again, the BIE results appear to be somewhat low.

The next step was to employ the BIE code for a semi-elliptical longitudinal crack. This would exercise the code on a fully three-dimensional problem for which previously existing results are available (Heliot 79, McGowan 79). The results obtained will be presented in the next section.

B.2 Longitudinal Semi-Elliptical Cracks

The BIE code was used to calculate K for semi-elliptical longitudinal cracks in pipes. The results obtained can then be compared to information in the literature in order to assess the accuracy of the BIE results.

The geometry considered is shown in Figure B-4 which also presents the nodalization employed. General expressions for the nodal coordinates were written in terms of the crack depth, crack length, wall thickness and inner pipe radius. This allowed many different crack and pipe sizes to be treated without extensive changes to the BIE input. Results were obtained only for uniform stress; techniques for treating nonuniform stresses will be covered in Appendix C. Results were first generated for $\gamma = R_1/h = 10$, since this value was considered by Heliot 79 and McGowan 79, which are the references with the most complete set of results

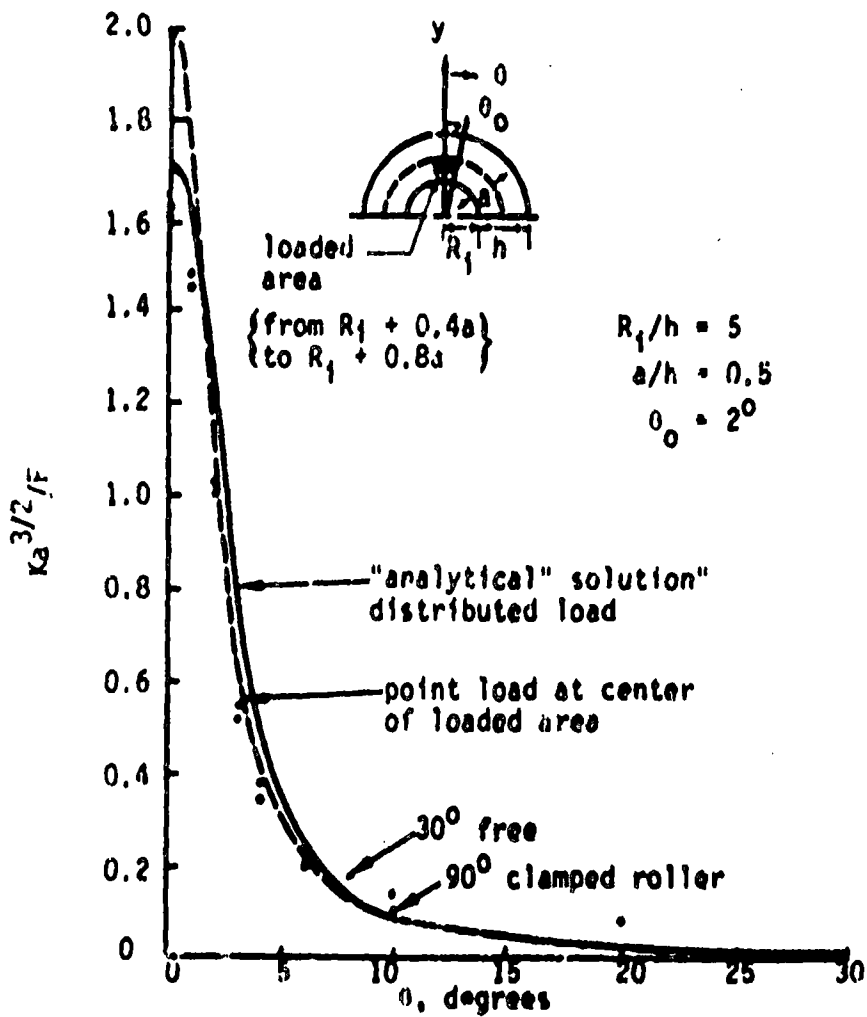


Figure B-3. Stress Intensity Factor as a Function of Position on Crack Front for Pressure Loading on a Small Area of Crack Surface.

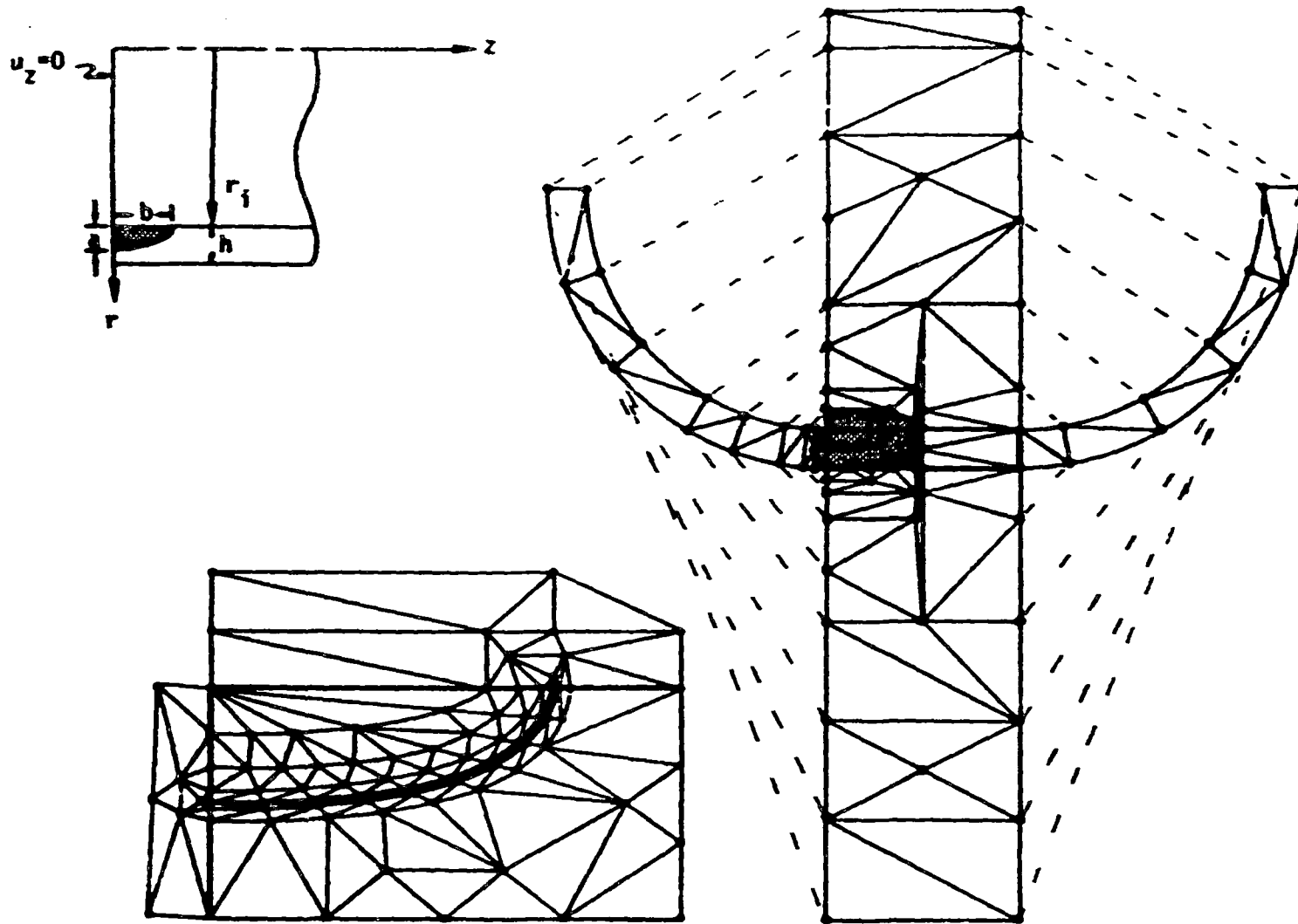


Figure B-4. Nodalization for BIE Analysis of a Longitudinal Semi-Elliptical Crack in a Pipe.

that are directly comparable to the problems of interest here. The results of Heliot 79 were presented in Figure A-5 to A-7. Two aspects of the results for uniform stress are of interest; the maximum value of K , and the variation of K along the crack front. The distance between the crack front and the nearest row of nodes on the crack surface was taken to be $a/10$. Table B-1 summarizes the results of the BIE calculations for K at the central portion of the crack ($\phi = 0$), and compares the results with those of Heliot 79 and McGowan 79. Considering that the execution time of the BIE code was on the order of $\frac{1}{4}$ minute on a CDC7600, and that K was simply evaluated from Equation B-3, the agreement between the various sets of results is quite good. The two sets of results from the literature disagree by some 10%, but the current results are consistently low by some 10 to 20%.

Comparison of the normalized variation of K along the crack front [$K(\phi)/K(0)$] are presented in Figures B-5 to B-7, which provide plots of the current results along with values reviewed earlier and presented in Figures A-5 to A-7. Figure B-5, which is for $\alpha = \frac{1}{4}$, shows McGowan 79 and Heliot 79 agreeing quite well with one another, with the results of the current investigation falling right in with the others. In Figure B-6, which is for $\alpha = \frac{1}{4}$, McGowan 79 and Heliot 79 do not agree so well with one another, and the results of the investigation fall somewhat below McGowan 79. The agreement in Figure B-7 is somewhat poorer; Heliot 79 and McGowan 79 do not agree closely, and the results of this investigation again fall somewhat low. However, the degree of disagreement is distorted by the expanded scales in these figures, and overall the agreement of the results of this investigation with previous results is felt to be really quite good. An interesting point regarding the results of Figures B-5 and B-6 is that the maximum K obtained by Heliot 79 does not occur at the point of maximum crack depth ($\phi = 0$), but at some point away from the crack center. This is not realistic from a symmetry standpoint, and is probably an artifact of the numerical procedures. The results of this investigation exhibit the same feature in Figure B-5. Heliot, et al. also employ boundary integral equation techniques for their calculations, whereas McGowan, et al. employed finite

Table B-1

Comparisons of $K(\phi=0)/\sigma a^{1/2}$ for Uniform Stress on a Longitudinal Interior Surface Semi-Elliptical Crack in a Pipe with $R_1/h=10$, $b/a=3$, Various $\alpha=a/h$

α	Heliot 79	McGowan 79	This Work	$\frac{\text{Heliot}}{\text{This}}$	$\frac{\text{McG \& R}}{\text{This}}$
0.25	1.737	1.654	1.498	1.160	1.104
0.5	1.967	1.949	1.644	1.196	1.186
0.8	2.393	2.226	1.945	1.230	1.144

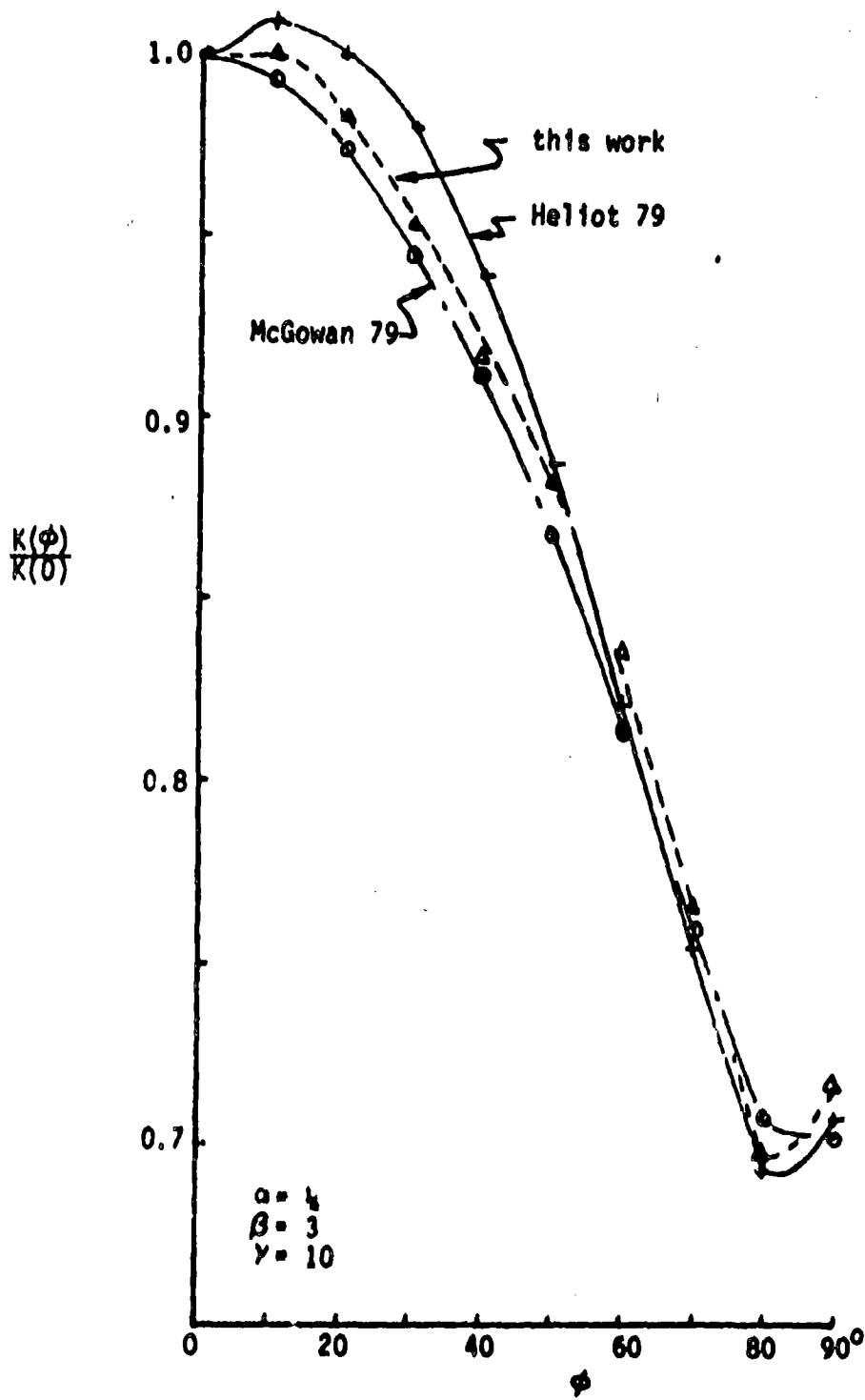


Figure B-5. Comparison of Normalized Variation of K Along Crack Front of Semi-Elliptical Interior Surface Longitudinal Crack in a Pipe.

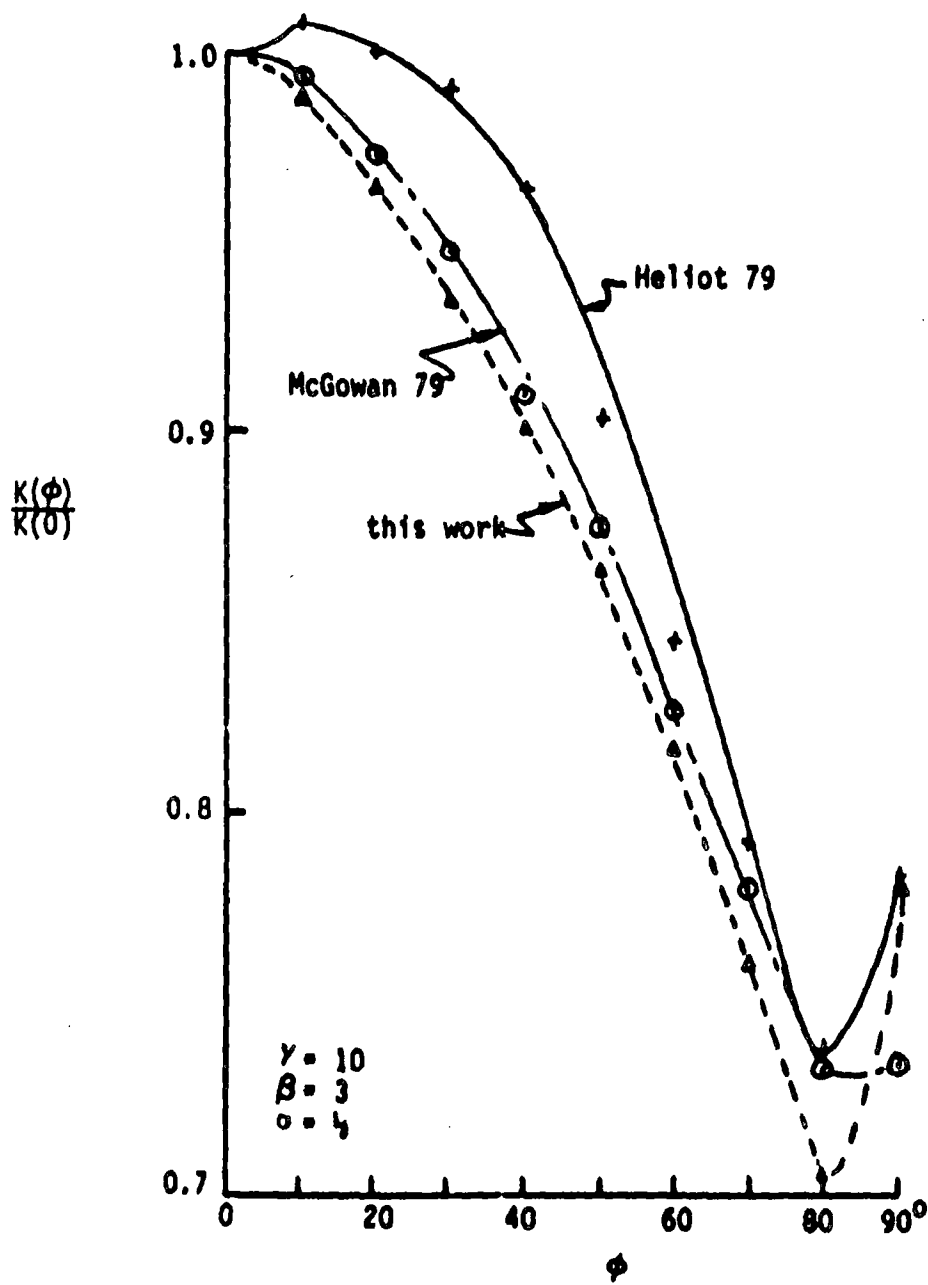


Figure B-6. Comparison of Normalized Variation of K Along Crack Front of Semi-Elliptical Interior Surface Longitudinal Crack in a Pipe.

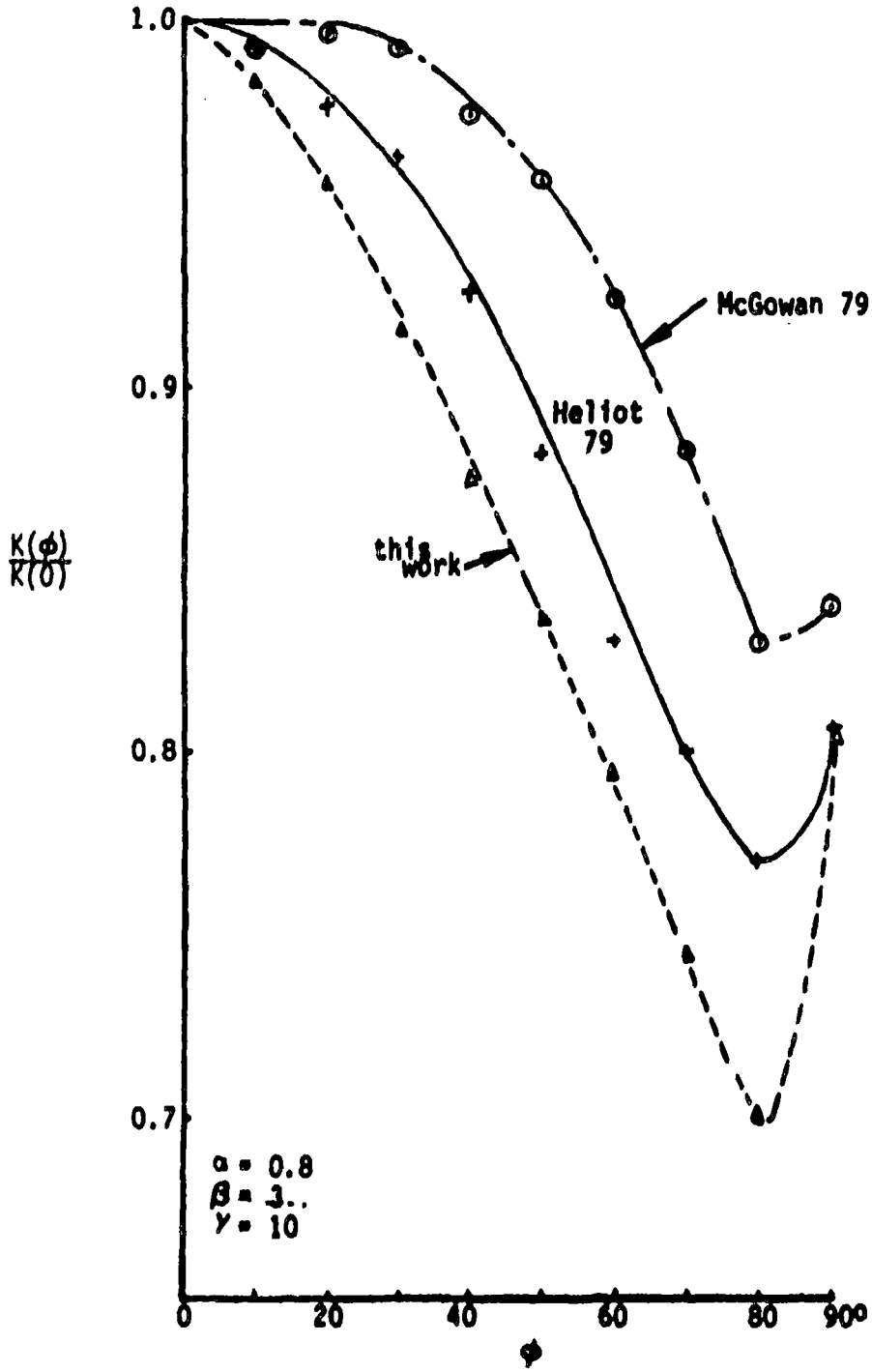


Figure B-7. Comparison of Normalized Variation of K Along Crack Front of Semi-Elliptical Interior Surface Longitudinal Crack in a Pipe.

elements. Another interesting feature is the "hook" observed as ϕ approaches 90° . This is near the free surface, where additional complexities occur (Hartranft 72), and current numerical techniques are incapable of providing reliable details. However, such effects are quite localized, and should not significantly influence the results of interest here.

Additional comparisons of variation of K along the crack front are provided in Figure B-8, which compares results of this investigation with corresponding values that were included in Figure A-9. Results for $\beta = 1$ and $\beta = 5$ are included, which provides a wider range of values than $\beta = 3$ considered in Figure B-5 to B-7. Some flat plate results are included ($\gamma = \infty$). This figure once again shows good agreement with the results of other investigators, and reveals that the influence of γ on the angular variation of K is not large, even for values of γ as small as 2.

Table B-2 summarizes BIE results for longitudinal cracks in pipes with various γ , α , and β . This table shows only small differences between $\gamma = 5$ and $\gamma = 10$ results, which provides additional confirmation on the small influence of γ on stress intensity factors for semi-elliptical longitudinal cracks. The small influence of γ was indicated earlier in Appendix A, with Figure A-8 summarizing such results.

Figure B-9 presents some additional comparisons of absolute values of K at the point of maximum crack penetration. Once again good agreement is observed and it is seen that γ does not have an appreciable influence. However, the current BIE results are again observed to fall below the results of other investigators (except, in this case, for large deep cracks).

The consistent observation that the BIE results obtained as part of this investigation fall below earlier results from the literature suggests that a "correction" applied to the current results would provide more accurate results. Figures B-2 and B-3 showed consistently low results for complete circumferential cracks, and Table B-1 shows that the current results are 10 to 20% lower than the results of other investigators. Multiplying all BIE K results by 1.15 would provide much better agreement.

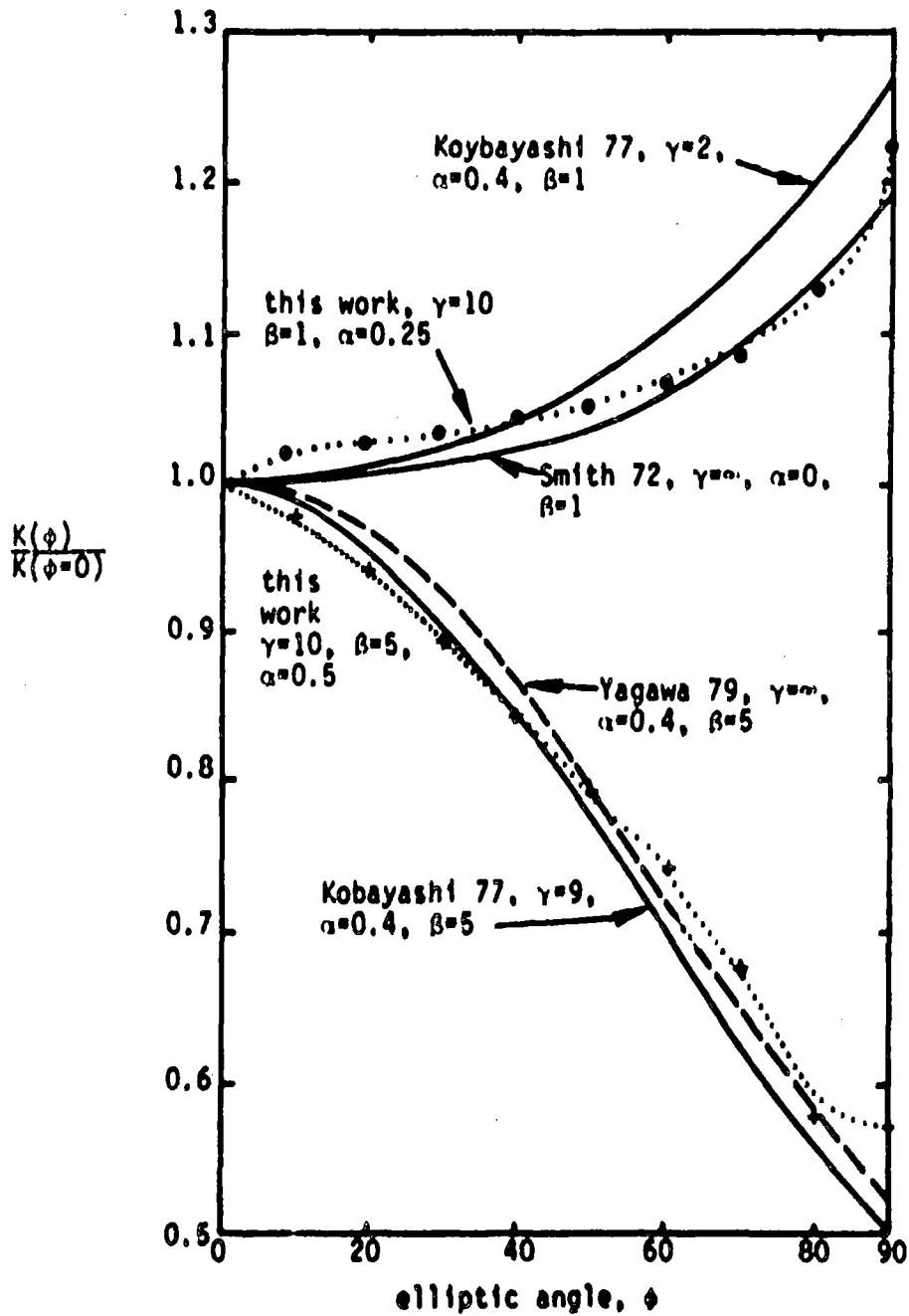


Figure B-8. Various Comparisons of Normalized Variation of K Along Crack Front for Semi-Elliptical Longitudinal Surface Cracks in Pipe, Plates and Half-Spaces.

Table B-2

Comparison of $K(\phi=0)/\sigma a^{3/2}$ for Uniform Stress on a Longitudinal Semi-Elliptical Crack in a Pipe for Various γ , α and β . All Results Generated by BIE, and are not Corrected to Account for Consistently Low BIE Results

β	$\alpha = 0.25$		$\alpha = 0.5$		$\alpha = 0.8$	
	$\gamma=5$	10	$\gamma=5$	10	$\gamma=5$	10
1	0.99	1.01	1.03	1.05	1.15	1.12
3	1.45	1.50	1.61	1.64	1.97	1.95
5	1.59	1.65	1.83	1.86	2.36	2.33
∞*	--	2.48	--	4.08	--	9.84

* from Labbens 1976

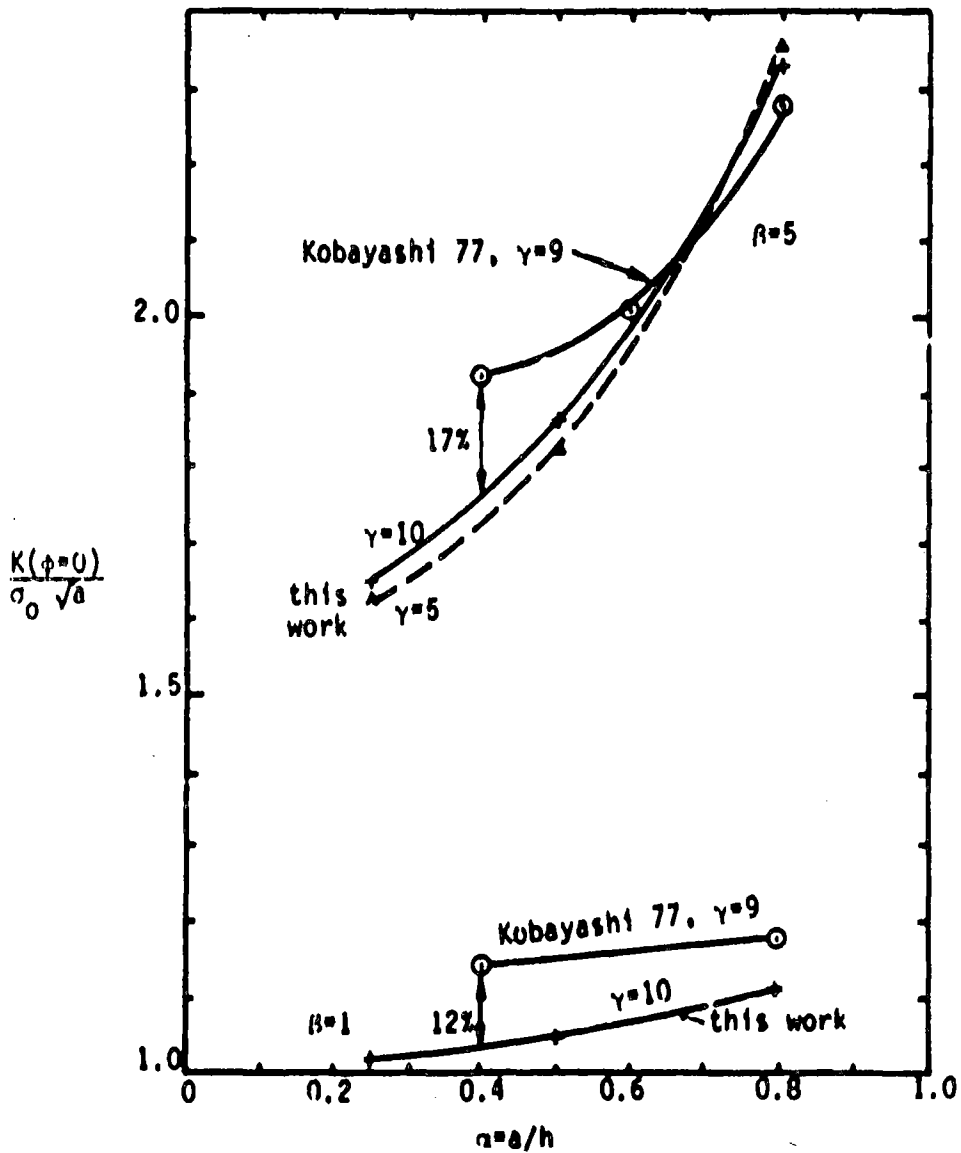


Figure B-9. Various Comparisons of $K(\phi=0)$ for Longitudinal Semi-Elliptical Cracks in Pipes.

and move the current results into the midrange of results of other investigators. This provides a particularly simple correction, and will be applied to all results presented in the remainder of the appendices and in the main body of the text.

Heliot 79 and McGowan 79 include results for stresses that vary as a polynomial with distance from the inner pipe wall. The angular variation of K along the crack front is provided. These polynomial results will be compared with results of the current work in Appendix D, which will serve as a check on the influence functions which were generated to permit the evaluation of stress intensity factors for complex stress conditions. The influence functions themselves are discussed in Appendix C.

The results presented for longitudinal cracks in this section provide a good check on the BIE procedures employed for fully three-dimensional problems. Favorable comparisons with previous results were observed, but a 1.15 multiplicative factor was introduced in order to improve the accuracy. Attention will now be turned to part-circumferential cracks in pipes. This is the crack configuration of primary interest in the current work, and for which no previously existing solutions are available.

B.3 Circumferential Semi-Elliptical Cracks

Stress intensity factors for part-circumferential cracks in pipes with $\gamma = 5$ and 10 were calculated by the boundary integral equation procedures described in Section A.3 and the introductory portion of Appendix B. As mentioned in Section B.2, a multiplicative "correction" term of 1.15 improves the agreement between results obtained by use of the BIE code employed and the results of previous investigators. This correction term will be applied to all BIE results presented in this section.

The body geometry considered, and the nodalization scheme employed are shown in Figure B-10. The distance between the crack front and the row of nodes closest to the crack front and on the crack surface was maintained at $a/10$ in accordance with earlier discussions on longitudinal

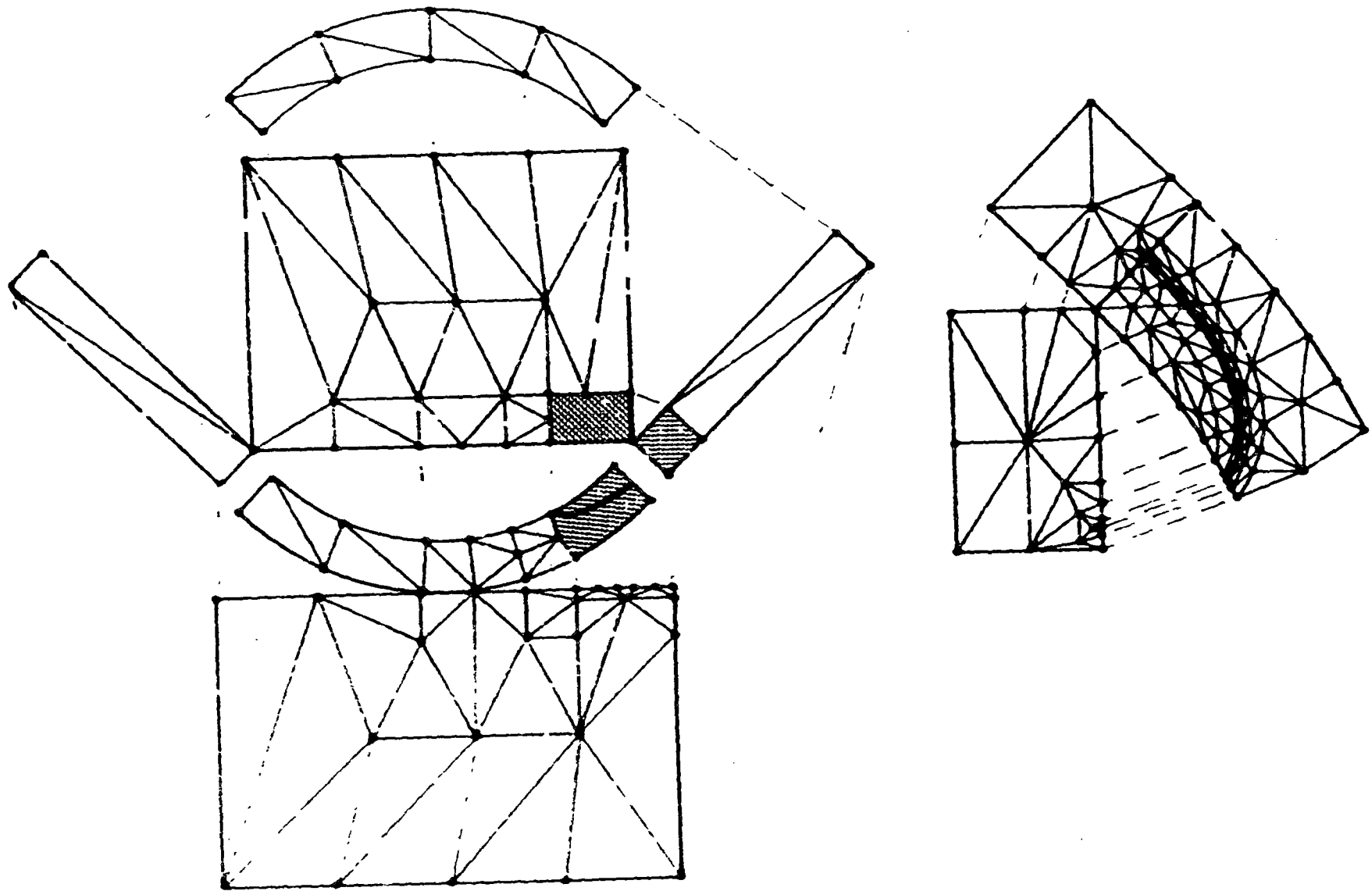


Figure 1. Nodalization of Pipe Circumferential Cracked Pipe of Interest Showing Nodalization

and complete circumferential cracks. General expressions of the nodal coordinates were written in terms of the crack depth, crack length, wall thickness and inside pipe radius. In this manner, the different geometries considered could be remodeled by the computer once the relevant geometric parameters were defined. This greatly facilitates consideration of a wide variety of crack and pipe sizes. Long semi-elliptical circumferential cracks become distorted due to the curvature of the pipe surface. It was therefore required to generalize the equation for an ellipse, which was accomplished by use of the following expression

$$\frac{(r-R_1)^2}{a^2} + \frac{(R_1\theta)^2}{b^2} = 1$$

where r and θ form a polar coordinate system centered at the center of the pipe.

Calculations for uniform applied stress of K as a function of position on the crack front were performed, with the results for K at the point of maximum crack depth ($\phi=0$) summarized in Table B-3. Corresponding results obtained for longitudinal cracks are also included in this table. All values in Table B-3 have been subjected to the 1.15 multiplicative "correction" factor. Hence, the numbers in Table B-3 are 15% higher than the corresponding value in Table B-2. Values of K for a flat plate ($\gamma=\infty$) are from Newman 79, values for finite γ but infinite β are from Labbens 76, and values for $\gamma=\beta=\infty$ are from the single-edge-cracked strip in tension results provided by Tada, Paris and Irwin (Tada 73).

The results presented in Table B-3 reveal only very small differences between longitudinal and circumferential cracks as long as β does not approach ∞ . That is, for semi-elliptical cracks, the K results are virtually independent of whether the crack is longitudinal or circumferential. The only time that the orientation has an effect is when the aspect ratio becomes very large, and the corresponding two-dimensional problem is approached. As shown in Figure A-4, the limiting two-dimensional cases of longitudinal and complete circumferential cracks have quite different

Table B-3

Comparison of $K(\psi=0)/\sigma a^{1/2}$ for Uniform Stress on Semi-Elliptical Cracks in Pipes with Various γ Showing Direct Comparison of Longitudinal and Circumferential Cracks.

		$\alpha = 0.25$			$\alpha = 0.5$			$\alpha = 0.8$		
		$\gamma=5$	$\gamma=10$	$\gamma=\infty$	$\gamma=5$	$\gamma=10$	$\gamma=\infty$	$\gamma=5$	$\gamma=10$	$\gamma=\infty$
$\beta = 1$	circ.	1.06	1.06	1.37	1.21	1.21	1.42	1.33	1.30	1.75
	long.	1.14	1.16		1.18	1.21		1.32	1.29	
$\beta = 3$	circ.	1.58	1.60	--	1.87	1.96	--	2.27	2.32	--
	long.	1.67	1.73		1.85	1.89		2.23	2.24	
$\beta = 5$	circ.	1.70	1.75	2.04	2.06	2.20	2.45	2.75	2.76	3.07
	long.	1.83	1.90		2.10	2.14		2.73	2.68	
$\beta = \infty$	circ.	2.27	2.36	2.67	2.87	3.25	5.02	4.14	4.89	21.2
	long.	--	2.48		--	4.08		--	9.93	

values of K once a/h exceeds about 0.2. Table B-3 reveals that the longitudinal and circumferential cracks have virtually the same K if a three-dimensional configuration with finite β is considered. Thus, the differences expected from consideration of the two-dimensional results (Figure A-4) are not observed in the corresponding three-dimensional values (Table B-3). This is most likely due to the differing effects on global stiffnesses of pipes and plates produced by semi-elliptical versus infinitely long cracks.

The results of Table B-3 again show that γ does not have an appreciable influence on the K values, except in the extreme case of $\beta \rightarrow \infty$. It is also seen that results for $\beta = 5$ are not representative of infinitely long cracks.

The other aspect of the results for part-circumferential cracks that is of interest is the variation of K along the crack front. Figures B-11 and B-12 present selected results normalized to the value at the point of maximum crack penetration. These figures show that there are not significant differences between longitudinal and circumferential cracks as regards variation of K along the crack front. Results presented in Section B.2 showed that K variations along the crack front were nearly the same for longitudinal cracks in pipes and corresponding cracks in flat plates. Thus, it can be concluded that to a satisfactory degree of approximation, stress intensity factors for semi-elliptical cracks are virtually independent of whether they are in a flat plate or oriented circumferentially or longitudinally in a pipe. However, limiting two-dimensional cases, such as plane strain longitudinal cracks or complete circumferential cracks, do exhibit appreciable differences that are not observed for the range of aspect ratio considered here. Such differences were shown in Figure A-4.

Results for uniform applied stresses have been detailed here in Appendix B. As was stated earlier, it is desired to account for stresses which have complex and steep gradients through the thickness of the pipe wall. The use of the BIE code for every thickness distribution of interest would

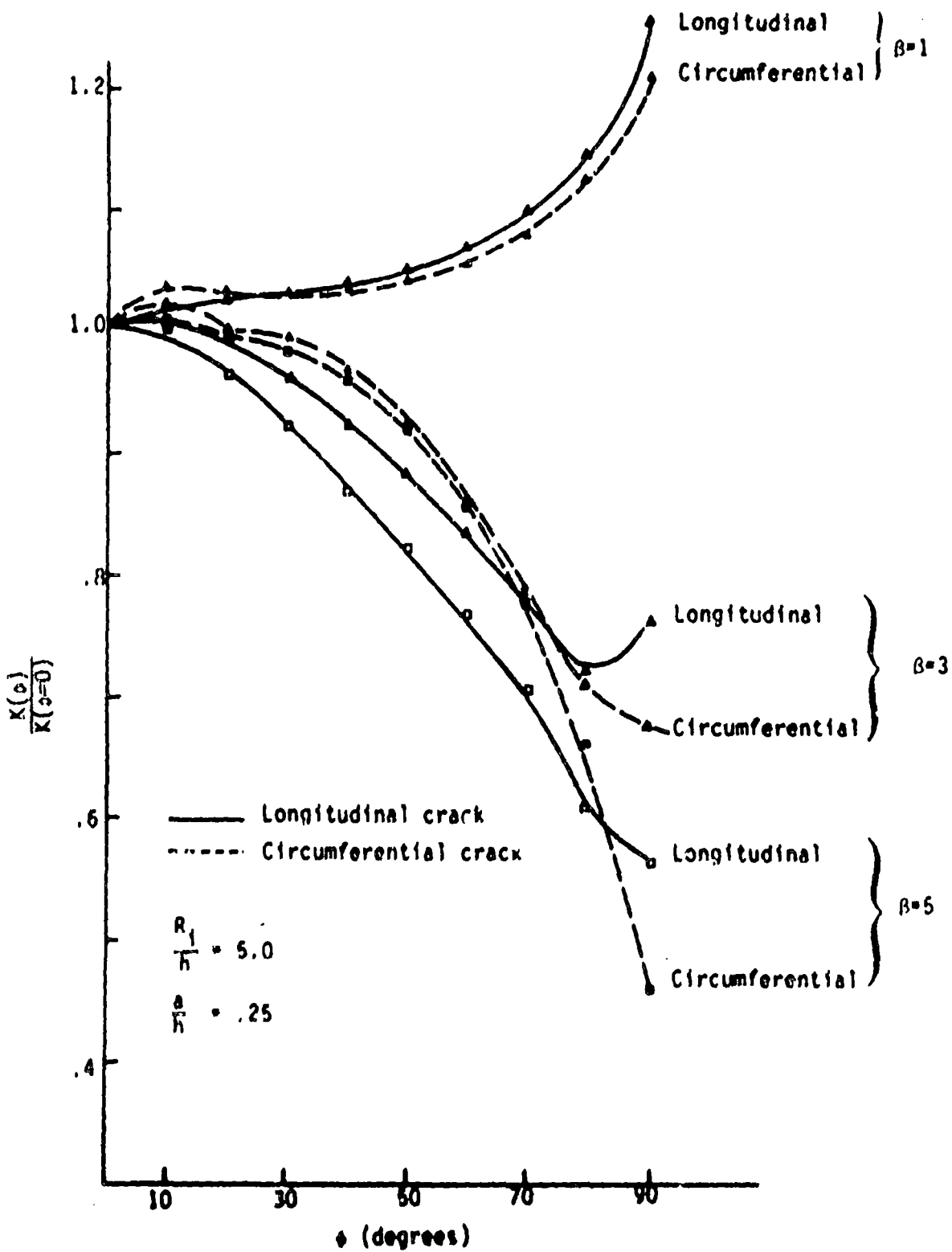


Figure B-11. Normalized Variation of K Along the Crack Front For Various Longitudinal and Circumferential Semi-Elliptical Cracks in Pipes as Obtained by BIE Calculations.

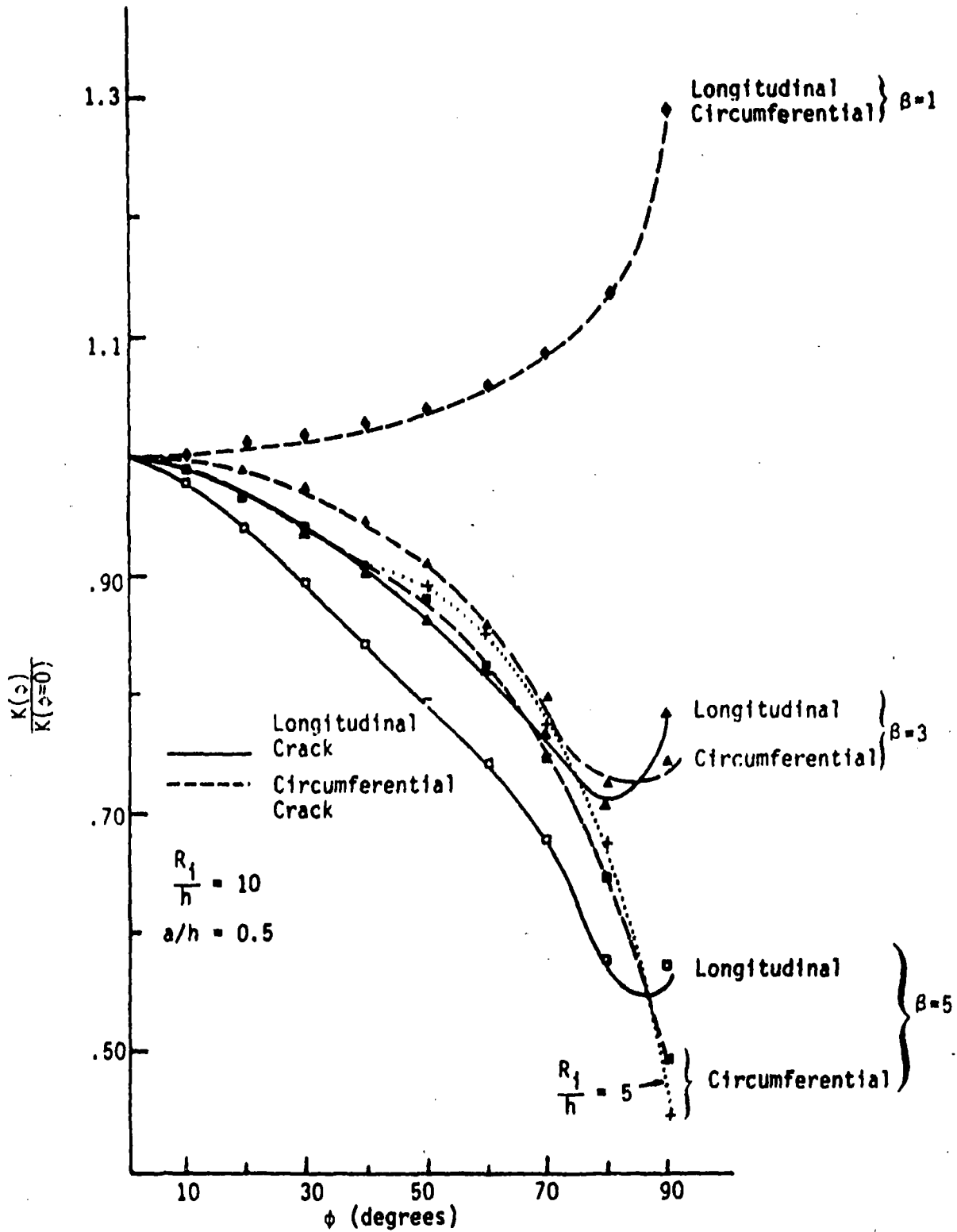


Figure B-12. Normalized Variation of K Along the Crack Front For Various Longitudinal and Circumferential Semi-Elliptical Cracks in Pipes as Obtained by BIE Calculations.

be prohibitively expensive, and would produce more detail than could be effectively used in the fatigue crack growth analysis. Influence function techniques are capable of generating the desired information using only results already obtained as part of the BIE calculations for uniform applied stresses. These techniques will be reviewed in Appendix C, and applied to radial gradient thermal stresses of interest in Appendix D.

APPENDIX C
INFLUENCE FUNCTIONS

APPENDIX C

INFLUENCE FUNCTIONS

The desire to account in the fatigue crack growth analysis for transient stresses which have steep and complex variations through the wall thickness necessitates the generation of stress intensity factor solutions in addition to those provided for uniform stress in Appendix B. The use of boundary integral equation techniques for all stresses considered would be prohibitively expensive, and would produce more information than required for a fatigue crack growth analysis. Influence function techniques based on some results by Rice 72b were therefore resorted to, which was originally suggested by Cruse and Besuner (Cruse 75b, Besuner 76). Some introductory remarks will be provided, followed by a brief review of the underlying theory and a presentation of the results generated for a part-circumferential crack in a pipe.

C.1 Introductory Remarks

A semi-elliptical surface crack such as shown in Figure 2-2 or A-1, is a two-dimensional crack that requires two length dimensions for its specification; a and b . The local value of the stress intensity factor varies along the crack front--even for uniform applied stress. Results presented in Appendices A and B vividly show this. When considering the growth of a semi-elliptical fatigue crack due to cyclic loading, it would be tempting to consider the local value of the crack growth rate to depend on the local value of K . However, this results in considerable complexity in the crack growth analysis, and would quickly lead to cracks that were not semi-elliptical in shape. This, in turn, would lead to the necessity of generating new stress intensity factor results to account for the "non-ellipticity" of the crack. In order to circumvent such problems, it is generally assumed that the crack remains elliptical as it grows so that only a and b need to be considered (Cruse 75b, Besuner 76, 77b, 78, Nair 78). This is discussed more fully in Section 2.6. Basically, two

options are generally considered: (i) the growth rates of a and b are controlled by the local values of K at $\phi=0$ and 90° respectively (see Figure A-1); or (ii) the growth of a and b are controlled by "RMS-averaged" stress intensity factors associated with the growth of cracks in the a and b directions. The second option will be used in this work, for reasons discussed in Section 2.6. One prime advantage to this option is that the "RMS-averaged" stress intensity factors are obtainable from influence functions that can be derived from crack surface displacement results obtained by BIE calculations. Hence, a "two-degree of freedom" model is employed, with "RMS averaged" stress intensity factors controlling the growth rates in each of the directions associated with each degree of freedom. The "RMS-averaged" stress intensities will be denoted by a bar over the symbol, such as \bar{K}_a . This is the RMS-K value for growth in the depth, or a, direction. The other RMS-K is \bar{K}_b , which is associated with growth in the surface length direction.

The values of \bar{K}_a and \bar{K}_b can be determined by the use of influence functions h_a and h_b from the following general expressions (Rice 72b, Cruse 75b, Besuner 76, 77b, 78).

$$\bar{K}_a = \int_A h_a(x,y,a,b) \sigma(x,y) dA$$

$$\bar{K}_b = \int_A h_b(x,y,a,b) \sigma(x,y) dA$$

(C-1)

The integration is carried out over the crack surface A. $\sigma(x,y)$ is the stress on the crack plane that would be present before the crack is introduced, and h_a and h_b are the influence functions associated with growth in the a and b directions (the two degrees of freedom considered). The influence functions will be discussed in the following section.

The relationship between the \bar{K} s and the angular variation of K [$K(\phi)$] is obtainable. The basic relations are the following

$$\bar{k}_a^2 = \frac{1}{\Delta A_a} \int_0^{\frac{\pi}{2}} k^2(\phi) d[\Delta A_a(\phi)] \quad (C-2)$$

$$\bar{k}_b^2 = \frac{1}{\Delta A_b} \int_0^{\frac{\pi}{2}} k^2(\phi) d[\Delta A_b(\phi)]$$

The functions $\Delta A_a(\phi)$ and $\Delta A_b(\phi)$ are related to changes in area as a function of ϕ for a crack growing only in the a or b direction, respectively. Figure C-1 shows a crack extending only in the a direction. The parameter s is the distance along the arc of the ellipse. It can be expressed in terms of ϕ by the following expression (Flügge 62, p. 20-3)

$$s = b E(k, \phi)$$

$$k = \left(1 - \frac{a^2}{b^2}\right)^{1/2}$$

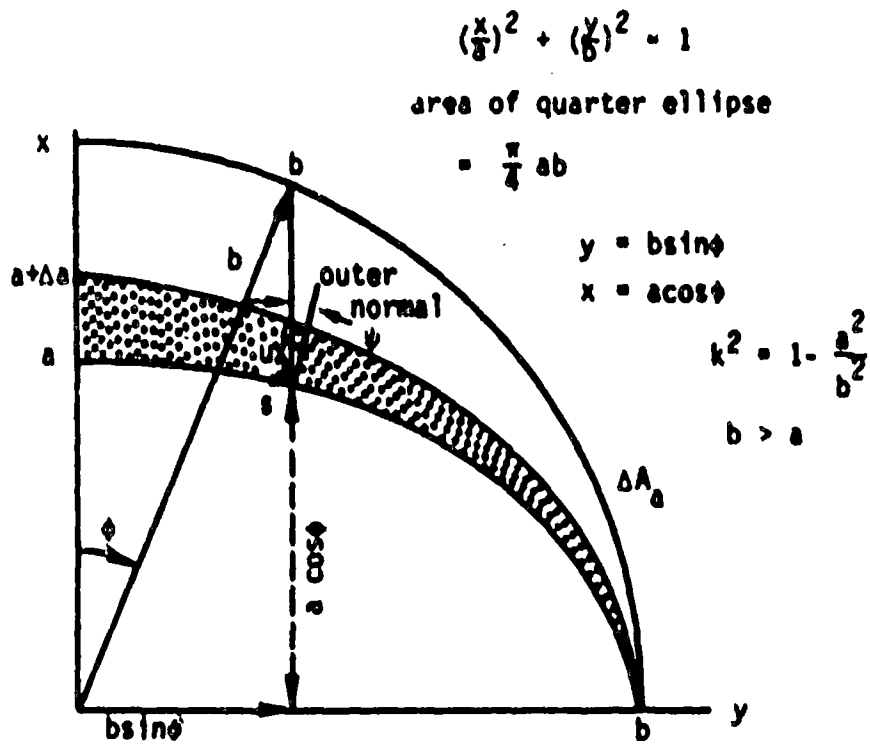
$$E(k, \phi) = \int_0^{\phi} (1 - k^2 \sin^2 \psi)^{1/2} d\psi$$

From this the following expression for ds is obtained

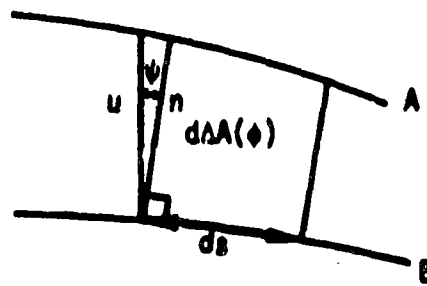
$$ds = b(1 - k^2 \sin^2 \phi)^{1/2} d\phi$$

The area ΔA_a is easily seen to be $\frac{\pi}{4} b \Delta a$. The area $d(\Delta A_a)$, in Figure C-1b is equal to $n ds$. Considering A and B to be nearly parallel (which will be increasingly true as Δa approaches zero), then $n/u = \cos \psi$. Another useful relation which comes directly from geometry is $u = \Delta a \cos \phi$. The angle ψ is a function of ϕ , and the functional relationship obtainable from geometry and differential calculus is

$$\tan \psi = - \frac{dx}{dy} = \frac{a \sin \phi}{b \cos \phi} = \frac{a}{b} \tan \phi$$



(C-1a)



(C-1b)

Figure C-1. Schematic Representation of a Crack Growing Only in the "a" Degree of Freedom.

Combining these results provides the following expressions for $d[\Delta A_a(\phi)]$

$$d[\Delta A_a(\phi)] = n ds = b \Delta a \cos\phi \cos\left[\tan^{-1}\left(\frac{a}{b} \tan\phi\right)\right] \times (1 - k^2 \sin^2\phi)^{1/2} d\phi \quad (C-3)$$

The following corresponding result for ΔA_b is obtainable by similar means

$$d[\Delta A_b(\phi)] = b \Delta b \sin\phi \sin\left[\tan^{-1}\left(\frac{a}{b} \tan\phi\right)\right] (1 - k^2 \sin^2\phi)^{1/2} \quad (C-4)$$

In this case, $\Delta A_b = \frac{\pi}{4} a db$. These expressions for ΔA_a and ΔA_b are to be inserted into Equation C-2 to provide the values of \bar{K}_a and \bar{K}_b if $K(\phi)$ is known.

As a sidelight, if $K(\phi)$ is a constant, then \bar{K}_a and \bar{K}_b are equal to $K(\phi)$. In order for this to be true, the following expressions must be true.

$$\int_0^{\pi/2} \cos\phi \cos\left\{\tan^{-1}\left[(1-k^2)^{1/2} \tan\phi\right]\right\} (1-k^2 \sin^2\phi)^{1/2} d\phi = \frac{\pi}{4}$$

$$\frac{1}{(1-k^2)^{1/2}} \int_0^{\pi/2} \sin\phi \sin\left\{\tan^{-1}\left[(1-k^2)^{1/2} \tan\phi\right]\right\} (1-k^2 \sin^2\phi)^{1/2} d\phi = \frac{\pi}{4}$$

These results must hold independently of k for k between 0 and 1. It is not immediately obvious that this is the case. However, these results can be verified by elementary, but tricky, means. For instance, in the first integral, the change of variable $u = \sin\phi$ is first made. Then $\tan\phi = [u(1-k^2)^{1/2}/(1-u^2)^{1/2}]$ is used as the definition of ϕ , and the corresponding expression for $\cos\phi$ is written. The end result becomes $\int_0^1 (1-u^2)^{1/2} du$, which is easily shown to be equal to $\pi/4$.

Figure C-1 along with Equation C-2 shows that \bar{K}_a is an RMS-averaged value of K along the crack front, but that the averaging process is heavily weighted towards values of K at positions close to where the "a" degree-of-freedom is most prominent. Corresponding remarks can be made regarding \bar{K}_b . The expression C-2 suggests that $(\bar{K}_a)^2$ is closely related to the strain energy release rate associated with crack growth in the "a" degree

of freedom direction. Likewise for \bar{K}_j . This relationship with strain energies becomes more apparent when considering the influence functions, which are derived from information on applied stresses and crack surface displacements--the product of which is related to strain energy. Discussions of the influence functions themselves will now be presented.

C.2 Underlying Theory

The influence function method of calculating the RMS stress intensity factors for semi-elliptical surface defects in material with finite thickness is described here. The underlying theory in this methodology was developed principally by Besuner and Cruse (Besuner 76, 77b, 78, Cruse 75b). Some of the basic relationships developed by them are reproduced here.

Cruse and Besuner (Cruse 75b) show that the RMS K -values for the j -th degree-of-freedom can be obtained from the following expression, which is analogous to Equation C-1

$$R_j = \iint h_{j\sigma}(x,y) dA \quad (C-5)$$

where h_j is the influence function associated with the j -th degree of freedom. Cruse and Besuner (Cruse 75b) also show that

$$h_j = \left[\frac{1}{H} \frac{\partial A}{\partial a_j} \frac{\partial U}{\partial a_j} \right]^{-1/2} \frac{\partial W}{\partial a_j} \quad (C-6)$$

where W = crack opening displacements for the top half of the crack for any arbitrary stresses

U = strain energy for the same arbitrary stresses

$$H = \frac{E}{1-\nu^2}$$

a_j = flaw dimension in the j -th direction

Note that W and U are the EXACT results for the problem under consideration. Unfortunately W and U are available only for very special geometries, such as an embedded elliptical crack in an infinite body. Generally speaking, only approximate solutions denoted by \bar{W} and \bar{U} are available. Hence, evaluation of Equations C-5 and C-6 results in

$$\bar{K}_j = \iint \bar{h}_j \sigma(x,y) dA \quad (C-7)$$

with

$$\bar{h}_j = \left[\frac{1}{H} \frac{\partial A}{\partial a_j} \frac{\partial \bar{U}}{\partial a_j} \right]^{-1} \frac{\partial \bar{W}}{\partial a_j} \quad (C-8)$$

The values of \bar{W} and \bar{U} may be obtained from a numerical solution such as boundary integral equation (BIE) or finite element (FE) techniques.

A more accurate approach uses a slightly modified form of Equation C-6. This modification requires a reference problem for which an exact analytical solution exists. Suppose that this exact solution is denoted by W^* and U^* , or

W^* = exact values for the crack opening displacements for reference problem

U^* = exact value for the strain energy for reference problem

Next assume that the approximate solution to the general problem (\bar{W} , \bar{U}) is related to the exact solution of the general (W , U) problem by

$$\bar{W}(x,y,a,b) = \phi_1(x,y,a,b)W(x,y,a,b) \quad (C-9)$$

$$\bar{U}(a,b) = \psi_1(a,b)U(a,b) \quad (C-10)$$

Furthermore, assume that the approximate solution (\hat{W} and \hat{U}) to the reference problem is related to the exact solution (W^* and U^*) of the reference problem in a manner similar to Equations C-9 and C-10, or

$$\hat{W} = \phi_2 W^* \quad (C-11)$$

$$\hat{U} = \psi_2 U^* \quad (C-12)$$

If $\phi_1 = \phi_2$ and $\psi_1 = \psi_2$ in Equations C-9 to C-12, they can be eliminated by forming the ratios g_1 and g_2 , or

$$g_1(a,b) = \left(\frac{\tilde{U}}{U} \right) = \left(\frac{U}{U^*} \right) \quad (C-13)$$

$$g_2(x,y,a,b) = \left(\frac{\tilde{W}}{W} \right) = \left(\frac{W}{W^*} \right) \quad (C-14)$$

Observe that Equations C-13 and C-11 suggest that

$$U = g_1 U^* \quad (C-15)$$

$$W = g_2 W^* \quad (C-16)$$

Substitution of Equation C-15 and C-16 into Equation C-6 gives

$$\begin{aligned} h_j &= \left[\frac{1}{H} \frac{\partial A}{\partial a_j} \frac{\partial}{\partial a_j} (g_1 U^*) \right]^{-1} \left[\frac{\partial}{\partial a_j} (g_2 W^*) \right] \\ &= \left[\frac{1}{H} \frac{\partial A}{\partial a_j} \left\{ g_1 \frac{\partial U^*}{\partial a_j} + U^* \frac{\partial g_1}{\partial a_j} \right\} \right]^{-1} \left[g_2 \frac{\partial W^*}{\partial a_j} + W^* \frac{\partial g_2}{\partial a_j} \right] \\ &= \left[\frac{1}{H} \frac{\partial A}{\partial a_j} \frac{\partial U^*}{\partial a_j} \left\{ g_1 + U^* \left(\frac{\partial U^*}{\partial a_j} \right)^{-1} \frac{\partial g_1}{\partial a_j} \right\} \right]^{-1} \left(\frac{\partial W^*}{\partial a_j} \right) \left[g_2 + \left(\frac{\partial W^*}{\partial a_j} \right)^{-1} W^* \frac{\partial g_2}{\partial a_j} \right] \\ &= \left[\frac{1}{H} \frac{\partial A}{\partial a_j} \frac{\partial U^*}{\partial a_j} \right]^{-1} \left(\frac{\partial W^*}{\partial a_j} \right) \left[g_1 + U^* \left(\frac{\partial U^*}{\partial a_j} \right)^{-1} \frac{\partial g_1}{\partial a_j} \right]^{-1} \left[g_2 + \left(\frac{\partial W^*}{\partial a_j} \right)^{-1} W^* \frac{\partial g_2}{\partial a_j} \right] \end{aligned}$$

$$h_j = h_j^* r_j \quad (C-17)$$

where

$$h_j^* = \left[\frac{1}{H} \frac{\partial A}{\partial a_j} \frac{\partial U^*}{\partial a_j} \right]^{-1/2} \left[\frac{\partial W^*}{\partial a_j} \right] \quad (C-18)$$

and

$$f_j = \left[g_1 + U^* \left(\frac{\partial U^*}{\partial a_j} \right)^{-1} \frac{\partial g_1}{\partial a_j} \right]^{-1/2} \left[g_2 + \left(\frac{\partial W^*}{\partial a_j} \right)^{-1} W^* \frac{\partial g_2}{\partial a_j} \right] \quad (C-19)$$

Equations C-17, C-18, and C-19 define a general influence function h_j in terms of the influence function h_j^* of the reference problem and a "correction factor" f_j . Substitution of Equation C-17 into Equation C-5 results in

$$\bar{k}_j = \iint_A h_j^*(x,y) \cdot f_j(x,y) \cdot \sigma(x,y) \, dA \quad (C-20)$$

where $\sigma(x,y)$ is the stress distribution for which R_s are desired.

In order to apply Equations C-17 to C-20, one needs the following values

- (a) $g_1 = \tilde{U}/\hat{U}$
- (b) $g_2 = \tilde{W}/\hat{W}$
- (c) U^* , and
- (d) W^*

The ratios g_1 and g_2 are obtained by dividing the numerical solution for the problem of interest by the numerical solution of the reference problem. Since the only relevant 3-D problem with an exact analytical solution is the ellipse buried in an infinite body, it is the natural choice as the reference problem. Solutions for this problem are available in the literature (Green 50, Irwin 62, Besuner 77b). For a uniform stress, on the crack surface

$$W^* = \frac{2\sigma a}{HF} \left[1 - \left(\frac{x}{a}\right)^2 - \left(\frac{y}{b}\right)^2 \right]^{1/2} \quad (C-21)$$

and

$$U^* = \frac{4\pi\sigma a^2 b}{3HF} \quad (C-22)$$

where

σ is a uniform stress applied on the crack surface

a is one-half the minor axis,

b is one-half the major axis,

H is defined following Equation C-8.

F is the complete elliptic integral of the second kind, defined by

$$\int_0^{\pi/2} \left[1 - \left(1 - \frac{a^2}{b^2}\right) \sin^2 \theta \right]^{1/2} d\theta$$

x and y are local coordinates whose origin is located at the intersection of the major and minor axes.

By direct differentiation of Equations C-21 and C-22 one obtains the following relationships

$$\frac{\partial U^*}{\partial a} = U^* \left[\frac{2}{a} - \frac{1}{F} \frac{\partial F}{\partial a} \right] \quad (C-23)$$

$$\frac{\partial U^*}{\partial b} = U^* \left[\frac{1}{b} - \frac{1}{F} \frac{\partial F}{\partial a} \right] \quad (C-24)$$

$$\frac{\partial W^*}{\partial a} = W^* \left[\frac{1}{a} + \frac{x^2}{\xi a^3} - \frac{1}{F} \frac{\partial F}{\partial a} \right] \quad (C-25)$$

$$\frac{\partial W^*}{\partial b} = W^* \left[\frac{y^2}{\xi b^3} - \frac{1}{F} \frac{\partial F}{\partial b} \right] \quad (C-26)$$

where $\xi = 1 - \left(\frac{a}{b}\right)^2 - \left(\frac{y}{b}\right)^2$

Substitution of Equations C-23 through C-26 into Equations C-17 through C-19 yields

$$h_x^* = \frac{\left| \frac{1}{a} - \frac{1}{F} \frac{\partial F}{\partial a} + \frac{x}{a^2} \left(\frac{x}{a} \right) \right| \left| 1 - \left(\frac{x}{a} \right)^2 - \left(\frac{y}{b} \right)^2 \right|^{1/2}}{\pi b \left| \frac{1}{3} F \left(\frac{2}{a} - \frac{1}{F} \frac{\partial F}{\partial a} \right) \right|^{1/2}} \quad (C-27)$$

$$h_y^* = \frac{\left| -\frac{1}{F} \frac{\partial F}{\partial b} + \frac{y}{b^2} \left(\frac{y}{b} \right) \right| \left| 1 - \left(\frac{x}{a} \right)^2 - \left(\frac{y}{b} \right)^2 \right|^{1/2}}{\pi \left| \frac{ab}{3} F \left(\frac{1}{b} - \frac{1}{F} \frac{\partial F}{\partial b} \right) \right|^{1/2}} \quad (C-28)$$

$$r_x = \left\{ g_1 + \frac{\partial g_1}{\partial a} \left| \frac{2}{a} - \frac{1}{F} \frac{\partial F}{\partial a} \right|^{-1} \right\}^{1/2} \left\{ g_2 + \frac{\partial g_2}{\partial a} \left(\frac{1}{a} - \frac{1}{F} \frac{\partial F}{\partial a} + \frac{x^2}{a^3} \right)^{-1} \right\}^{1/2} \quad (C-29)$$

$$r_y = \left\{ g_1 + \frac{\partial g_1}{\partial b} \left| \frac{1}{b} - \frac{1}{F} \frac{\partial F}{\partial b} \right|^{-1} \right\}^{1/2} \left\{ g_2 + \frac{\partial g_2}{\partial b} \left(-\frac{1}{F} \frac{\partial F}{\partial b} + \frac{y^2}{b^3} \right)^{-1} \right\}^{1/2} \quad (C-30)$$

An approximation by Rowe (Newman 79) permits a considerable reduction in the tedium associated with evaluating Equations C-27 to C-30. Specifically, the function F is approximated by

$$F \sim \left| 1 + 1.464(a/b)^{1.65} \right|^{1/2} \quad a < b \quad (C-31)$$

Equation C-31 is accurate to 0.13% for all a/b between 0 and 1. Equation C-31 can also be differentiated to obtain

$$\frac{\partial F}{\partial a} = \frac{G}{F} \quad (C-32)$$

$$\text{and } \frac{\partial F}{\partial b} = \frac{G}{F} \left(\frac{a}{b}\right) = \frac{a}{b} \frac{\partial F}{\partial a} \quad (\text{C-33})$$

$$\text{where } G = \frac{1.464 \times 1.65}{2b} \left(\frac{a}{b}\right)^{0.65} \quad (\text{C-34})$$

Once g_1 and g_2 are defined, such as by the expressions following Equation C-20, then f_j are defined by Equations C-29 and C-30. These can be combined with h_j^* in Equations C-27 and C-28 to obtain h_j (Equation C-17), which is then integrated by use of Equation C-5 to obtain \bar{K}_j for arbitrary stresses on the crack plane, $\sigma(x,y)$. The principal difficulty in the evaluation of \bar{K}_j arises from the necessity to integrate an integral with a $\xi^{-1/2}$ singularity--which comes from the h_j^* . The integration procedure developed to efficiently handle this will be covered in Appendix D. The procedure for obtaining suitable mathematical expressions for g_1 and g_2 will be discussed in the next section.

C.3 Curve Fit to g_1

The function g_1 is required as a part of the desired influence functions, as can be seen in Equation C-19. The following definition of g_1 was provided in Section C.2.

$$g_1 = \frac{\tilde{U}}{\hat{U}} \quad (\text{C-35})$$

\tilde{U} is the strain energy determined from numerical procedures for the crack geometry of interest, and \hat{U} is the strain energy determined numerically for the reference problem (which in this case is the buried elliptical crack subjected to uniform stress). The strain energy in the half of the body on one side of the crack plane is desired, and can be calculated from the work of the surface tractions during the application of loads to the body. Mathematically, this can be expressed as

$$U = \frac{1}{2} \int_A \sigma(x,y) w(x,y) dA$$

The influence functions themselves are independent of the applied stress used to determine g_1 and g_2 . Uniform stress on the crack face was considered, hence the expression for U becomes a simple matter of integrating the nodal values of crack surface displacement, w , over the crack area. In accordance with the assumption in the BIE code that displacements vary linearly within an area segment, the value of U is easily obtained from the nodal coordinates and corresponding displacements. Table C-1 summarizes such results for a surface crack and an embedded crack. These values correspond to a stress on the crack surface of 100 ksi, however, since ratios are taken, the value cancels out and the units of U are irrelevant. Values of \hat{U} for a buried elliptical crack were calculated for $a/h = 0.25$. This is felt to provide results that are representative of an elliptical crack in an infinite body. g_1 for $a/h \neq 0.25$ was scaled according to the following procedure.

The strain energy for an embedded crack in an infinite body is given analytically by the following expression (Irwin 62)

$$U = \frac{4\pi\sigma^2 a^2 b}{3HF} = \frac{4\pi\sigma^2 a^3 (b/a)}{3HF}$$

This shows that for a given $\beta = b/a$, $U = a^3$, therefore

$$\frac{\hat{U}(a/h)}{\hat{U}(a/h=0.25)} = \left(\frac{a/h}{0.25}\right)^3$$

Therefore, for any a/h , the following expression for g_1 holds

$$g_1(a/h) = \frac{\hat{U}(a/h)}{\hat{U}(a/h=0.25)} \left(\frac{0.25}{a/h}\right)^3$$

The values of g_1 obtained by use of this expression and the results included in Table C-1 are presented in Table C-2 as a function of a/h and b/a .

The values of g_1 in Table C-2 were curve fitted by a least squares regression to a polynomial in $\alpha (=a/h)$ and $\beta (=b/a)$. The following result was obtained.

Table C-1
Strain Energies for Surface and Buried Cracks

Strain Energy for Semi-Elliptical Surface Defect, \bar{U}

a/h b/a	.25	.40	.50	.65	.80
1	.03244	.14184	.28813	.66926	1.31974
2	.09012	.40067	.82521	1.96792	4.00456
3	.15036	.67650	1.40172	3.36495	6.92261
4	.21053	.95065	1.96664	4.71548	9.80132
5	.27019	1.21608	2.50587	6.00374	12.69604
6	.32889	1.47130	3.01913	7.27472	15.69383

Strain Energy for Buried Elliptical Defect, (\hat{U})

a/h b/a	.25
1	.03002
2	.07482
3	.11821
4	.16283
5	.20838
6	.25390

$R_1/h = 5$

Table C-2
 g_1 for Various Sizes of Surface
 Cracks

a/h b/a	.25	.40	.50	.65	.80
1	1.08049	1.153364	1.199590	1.268252	1.341442
2	1.20453	1.307434	1.378700	1.496512	1.633422
3	1.27203	1.397231	1.482274	1.619635	1.787220
4	1.29298	1.425405	1.509776	1.647716	1.837011
5	1.29665	1.424790	1.503205	1.639272	1.859377
6	1.29536	1.414749	1.486383	1.630176	1.886328

$$g_1 = (.9701 + .03414\beta) + (-.00176 + .39924\beta - .05512\beta^2)\alpha + (-.16095 + .4112\beta - .15460\beta^2 + .01936\beta^3)\alpha^2 \quad (C-36)$$

Table C-3 presents results for g_1 calculated by use of this expression. Figure C-2 presents a comparison of these results, with the data points representing the original BIE results, and the lines representing the results from the polynomial curve fit. The polynomial g_1 agrees with the original data to better than 5% for any crack geometry, which is felt to provide sufficient accuracy for the present purposes.

C.4 Curve Fit to g_2

The remaining function to be determined in order to define the desired influence function is g_2 . From Section C.2, this function is given by the following ratio

$$g_2 = \frac{\tilde{W}}{W}$$

\tilde{W} is the crack surface opening displacement determined numerically for the crack geometry of interest, and W is the corresponding crack surface opening displacement determined numerically for the reference problem.

The crack opening displacements at various locations on the crack surface for buried elliptical and surface semi-elliptical defects were directly obtained by numerical solution of BIE. The displacements for a buried elliptical defect were obtained only for $a/h = .25$, and therefore, the g_2 values for $a/h \neq .25$ are scaled as follows.

$$\text{Since } W = \frac{2\sigma a}{HF} \left[1 - \left(\frac{x}{a}\right)^2 - \left(\frac{y}{b}\right)^2 \right]^{1/2} = \frac{2\sigma(a/h)h}{HF} \left[1 - \left(\frac{x}{a}\right)^2 - \left(\frac{y}{b}\right)^2 \right]^{1/2}$$

that is, for a given x/a , y/b and aspect ratio, W varies linearly with a/h . Therefore, for any a/h ,

$$g_2 = \frac{\tilde{W}(a/h)}{\tilde{W}\left(\frac{a}{h} = .25\right)} \cdot \frac{1}{\left(\frac{a}{h}\right)_{.25}}$$

Table C-3
 g_1 for Various Crack Geometries-Results From Curve-Fit

b/a a/b	.05	.1	.15	.2	.25	.3	.35	.4	.45	.5	.55	.6	.65	.7	.75	.8
0.5	1.00	1.01	1.01	1.02	1.03	1.04	1.05	1.06	1.07	1.08	1.09	1.10	1.11	1.12	1.13	1.14
1	1.02	1.04	1.06	1.08	1.10	1.12	1.14	1.16	1.18	1.20	1.23	1.25	1.28	1.30	1.33	1.35
1.5	1.05	1.07	1.10	1.12	1.15	1.18	1.21	1.24	1.27	1.30	1.33	1.37	1.40	1.44	1.47	1.51
2	1.07	1.10	1.13	1.16	1.19	1.23	1.26	1.30	1.34	1.38	1.42	1.46	1.50	1.54	1.58	1.63
2.5	1.09	1.12	1.16	1.19	1.23	1.27	1.31	1.35	1.39	1.43	1.48	1.52	1.57	1.61	1.66	1.71
3	1.11	1.14	1.18	1.22	1.26	1.30	1.34	1.39	1.43	1.47	1.52	1.57	1.61	1.66	1.71	1.76
3.5	1.13	1.16	1.20	1.24	1.28	1.32	1.37	1.41	1.46	1.50	1.55	1.60	1.65	1.70	1.75	1.80
4	1.14	1.18	1.22	1.26	1.30	1.34	1.39	1.43	1.48	1.53	1.57	1.62	1.68	1.73	1.78	1.84
4.5	1.14	1.18	1.22	1.26	1.30	1.34	1.39	1.43	1.48	1.53	1.58	1.63	1.68	1.73	1.78	1.84
5	1.14	1.18	1.22	1.26	1.30	1.34	1.39	1.43	1.48	1.53	1.58	1.63	1.68	1.73	1.78	1.84
5.5	1.14	1.18	1.22	1.26	1.30	1.34	1.39	1.43	1.48	1.53	1.58	1.63	1.68	1.73	1.78	1.84
6	1.14	1.18	1.22	1.26	1.30	1.34	1.39	1.43	1.48	1.53	1.58	1.63	1.68	1.73	1.78	1.84

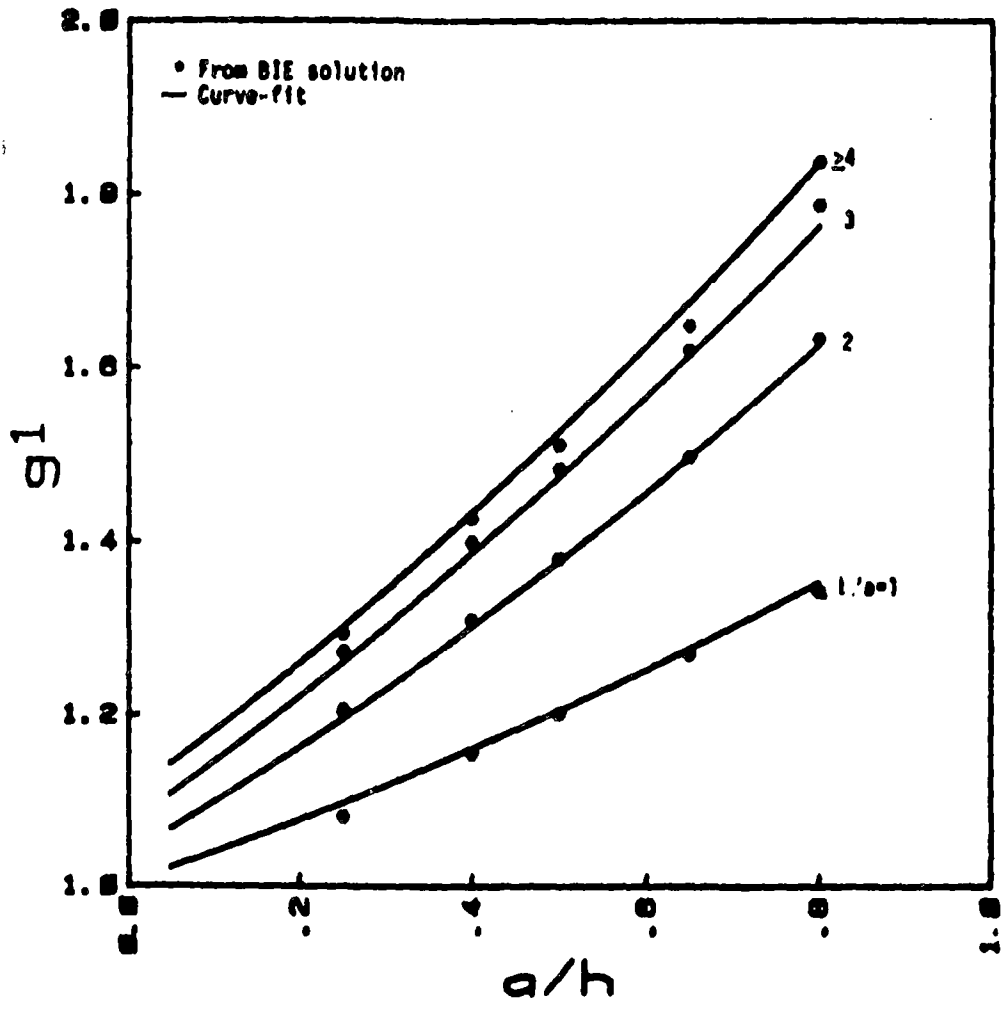


Figure C-2. Comparison of Curve Fit and BIE Data Points for the Function G1.

These are the values of g_2 required for computing influence functions. Unlike in the case of g_1 , a special problem exists for obtaining a mathematical expression for g_2 since g_2 is a function of location (x,y) on the crack surface in addition to it being a function of a/h and b/a . For a given a/h , following the methodology of Besuner 78, $g_2(b/a,x,y)$ for a constant a/h can be curve fitted as follows:

$$g_2|_{a/h} = A_0 + A_1 R^{1.5} \theta^{.15} + A_2 R^{1.5} \theta^{.3} + A_3 R^{2.5} \theta^{.15} + A_4 R^{2.5} \theta^{.3} \\ + A_5 (a/b - 1) + A_6 \left(\frac{a}{b} - 1\right)^2$$

where

$$R = \left[\left(\frac{x}{a}\right)^2 + \left(\frac{y}{b}\right)^2 \right]^{.5}$$

$$\theta = 1 - \frac{2}{\pi} \left\{ \tan^{-1} \left(\frac{y/x}{b/a} \right) \right\}$$

$A_0 - A_6$ = Coefficients obtained by regression analysis.

For each a/h , a set of $A_0 - A_6$ coefficients was obtained. Next, these coefficients were curve fitted as a function of a/h to obtain g_2 as a composite function of a/h , b/a , x and y . Finally a correction factor of the form

$$.15 \left(\frac{a-x}{h}\right) \left(\frac{y}{b}\right)^2 \left(1 + .2 \frac{a}{h}\right) (2b/a - 1.99)$$

was used to improve the curve fit. A function subroutine G2BIE was formulated which returns the value of g_2 for a given x , y , a/h and b/a . A listing of the subroutine is given here. The program is written in terms of l/a which is equal to 2β . x is the distance from the inner pipe wall, and y is the angular distance from the radial line extending through the middle of the ellipse.

FUNCTION G2BIE(X,Y,ELOA,AOH)
 COMMON/G/GG
 COMMON/PIPE/PI,RIN,THICK

C-----
 C G2BIE REVISED ON 29 MAY 1980 C
 C CORRECTION FACTOR ADDED TO G2BIE ON JUNE 6 C
 C CORRECTIN FOR A/H IS INCLUDED IN THIS REVISED VERSION C
 C BR=BESUNER'S R C
 C BT=BESUNER'S THETA C
 C-----

AA=AOH*THICK
 EL=ELOA*AOH*THICK
 DR=SQRT((X/AA)**2+(2.*Y/EL)**2)
 IF(X.EQ.0.) X=0.00001
 UT=1.-(2./PI)*ATAN(2.*Y/(X*ELOA))
 OTT=BT*.15
 URR=BR*SQRT(BR)
 XX1=URR*OTT
 XX2=URR*OTT*BTT
 XX3=URR*BR*OTT
 XX4=URR*BR*BTT*BTT
 XX5=2./ELOA-1.
 XX6=XX5*XX5
 AOH2=AOH*AOH
 AOH3=AOH*AOH2
 AOH4=AOH*AOH3
 AOH5=AOH*AOH4
 A0=0.99568+0.71745*AOH
 A1=3.99268-22.1411*AOH+44.2643*AOH2-32.8078*AOH3
 A2=-3.5431+17.3427*AOH-40.5886*AOH2+31.5185*AOH3
 A3=-2.5524+2.3462*AOH+0.27447*AOH2
 A4=2.5948-0.6154*AOH
 A5=-0.17706-0.5A57*AOH
 A6=-0.1378+0.09001*AOH
 GG=A0+A1*XX1+A2*XX2+A3*XX3+A4*XX4+A5*XX5+A6*XX6
 G2BIE=GG*(1.+(AA-X))*((Y*2./EL)**2)*(1.+AOH/5.)*(ELOA-1.99)*.15/
 SCK)
 10 RETURN
 END

Once g_1 and g_2 are known, the correction factors f_x and f_y can be evaluated using Equations C-29 and C-30. The derivative terms like $\frac{\partial g_2}{\partial a}$ in the expressions for f_x and f_y are evaluated by numerical differentiation as follows:

$$\frac{\partial g_2}{\partial a} = \frac{g_2(a+\Delta a) - g_2(a-\Delta a)}{2\Delta a}$$

All the components for obtaining the RMS stress intensity factors using Equation C-20

$$\bar{K}_j = \iint_A h_j^*(x,y) \cdot f_j(x,y) \cdot \sigma(x,y) dA$$

are now complete. $h_j^*(x,y)$ is the known influence function for a buried elliptical defect and $f_j(x,y)$ is the correction factor for $h_j^*(x,y)$ to obtain the influence functions for semi-elliptical circumferential surface defects in pipes. $\sigma(x,y)$ is the arbitrary stress on the crack surface. The \bar{K}_j for buried elliptical defects for an arbitrary stress $\sigma(x,y)$ is obtained by integrating the above equation with $f_j(x,y) = 1.0$. Similarly, \bar{K}_j for semi-elliptical surface defects with uniform stress on the crack surface are obtained by integration of the above equation with $\sigma(x,y)$ equal to a constant. The \bar{K}_j for buried ellipse with uniform stress are obtained by making $f_j(x,y) = 1$ as well as $\sigma(x,y) = a$ constant. The actual integration procedures and some of the above cases will be discussed in Appendix D. Such special cases provide checks on the accuracy of the approximate influence functions developed in this appendix.

APPENDIX C
APPLICATIONS TO COMPLEX STRESSES

Appendix D

APPLICATIONS TO COMPLEX STRESSES

The influence functions developed in Appendix C will be applied to various stress systems in this Appendix. Integration procedures will be described, followed by the results of verification runs performed to check the accuracy of the integration procedure and influence functions. Finally, results for stress intensity factors for circumferential cracks due to radial gradient thermal stresses will be provided.

D.1 Integration Procedures

The final step in obtaining the RMS stress intensity factors is the integration of Equation C-20 which is reproduced here.

$$\bar{K}_j = \iint_A h_j^*(x,y) \cdot f_j(x,y) \cdot \sigma(x,y) \cdot dA$$

Due to the complexity of the expressions in the above equation, it is imperative that a numerical integration procedure be used. The principal complication in the numerical integration arises due to $r^{-1/2}$ singularity at the crack front in h_x^* and h_y^* functions (Equations C-27 and C-28). The method by which this is overcome is described by considering the integration to obtain \bar{K}_a (the procedure will be exactly similar for \bar{K}_b). For \bar{K}_a , the above equation can be written as

$$\bar{K}_a = \iint_A h_x^*(x,y) \cdot f_x(x,y) \cdot \sigma(x,y) \cdot dA \quad (D-1)$$

where

$$h_x^* = \frac{\left| \frac{1}{a} - \frac{1}{r} \cdot \frac{\partial F}{\partial a} + \frac{K^2}{a^3} \right| c^h}{\pi b \left| \frac{1}{3} F\left(\frac{2}{a} - \frac{1}{r} \frac{\partial F}{\partial a}\right) \right|^h} \quad (D-2)$$

$$\text{and } \xi = 1 - \left(\frac{x}{a}\right)^2 - \left(\frac{y}{b}\right)^2$$

rearranging the equation for h_x^*

$$\begin{aligned} h_x^* &= \frac{\left(\frac{1}{a} - \frac{1}{F} \cdot \frac{\partial F}{\partial a}\right) \xi^{\frac{1}{2}} + \frac{x^2}{a^3 \xi^{\frac{1}{2}}}}{\pi b \left[\frac{1}{3} F \left(\frac{2}{a} - \frac{1}{F} \cdot \frac{\partial F}{\partial a} \right) \right]^{\frac{1}{2}}} \\ &= \frac{\left\{ \left(\frac{1}{a} - \frac{\partial F}{\partial a} \cdot \frac{1}{F} \right) \xi + \frac{x^2}{a^3} \right\} \frac{1}{\xi^{\frac{1}{2}}}}{\pi b \left[\frac{1}{3} F \left(\frac{2}{a} - \frac{1}{F} \cdot \frac{\partial F}{\partial a} \right) \right]^{\frac{1}{2}}} \\ &= h_x^{**} \frac{1}{\xi^{\frac{1}{2}}} \end{aligned} \tag{D-3}$$

These expressions follow directly from results included in Appendix C. The function h_x^{**} has no singularities within the crack area.

Substituting this in the expression for \bar{K}_a ,

$$\bar{K}_a = \iint_A \frac{h_x^{**}(x,y)}{\xi^{\frac{1}{2}}} \cdot r_x(x,y) \sigma(x,y) \cdot dA \tag{D-4}$$

Changing to polar coordinates,

$$x = r \cos \theta, \quad y = r \sin \theta, \quad dA = r \, dr \, d\theta$$

leads to the following expression

$$\xi = 1 - r^2 \left(\frac{\cos^2 \theta}{a^2} + \frac{\sin^2 \theta}{b^2} \right)$$

In turn, this leads to the following expression:

$$\bar{k}_a = \iint_A \frac{h_x^{**}(r,\theta) \cdot f_x(r,\theta)}{\left[1 - r^2 \left(\frac{\cos^2 \theta}{a^2} - \frac{\sin^2 \theta}{b^2}\right)\right]^{1/2}} \sigma(r,\theta) r dr d\theta \quad (D-5)$$

Specifically, for integration over a semi-elliptical area (Figure D-1), the first-integration can be considered as the integration in the r direction of the segment shown by the cross-hatched area, the limits of integration being from $r = 0$ to $r = R(\theta)$, where $R(\theta)$ is the edge of the ellipse, defined by

$$R(\theta) = \left[\frac{\cos^2 \theta}{a^2} + \frac{\sin^2 \theta}{b^2} \right]^{1/2}$$

The second part of the integration would then be to integrate these segments in the θ direction, the limits of integration being $\theta = 0$ to $\theta = \pi/2$, that is, over the semi-elliptical area.

The following expression is obtained from results presented above.

$$1 - r^2 \left(\frac{\cos^2 \theta}{a^2} + \frac{\sin^2 \theta}{b^2} \right) = 1 - r^2 / R(\theta)^2$$

The Equation D-5 can now be rewritten as

$$\bar{k}_a = \int_{\theta=0}^{\pi/2} \int_{r=0}^{R(\theta)} \frac{h_x^{**}(r,\theta)}{\left[1 - r^2 / R(\theta)^2\right]^{1/2}} f_x(r,\theta) \cdot \sigma(r,\theta) r dr d\theta \quad (D-6)$$

The integration along r involves a singularity at $r = R$. A numerical method for integrating this type of singularity is given on p.889, Equation 25.4.36 in Abramowitz 64. This method was used to integrate the right hand side of Equation D-6 over $r = 0$ to $r = R(\theta)$. The integration of the resulting function in the angular direction (from $\theta = 0$ to $\theta = \pi/2$) was then carried out using the standard Gauss Quadrature method, such as given by Equation 25.4.30 of Abramowitz 64. Two computer subroutines

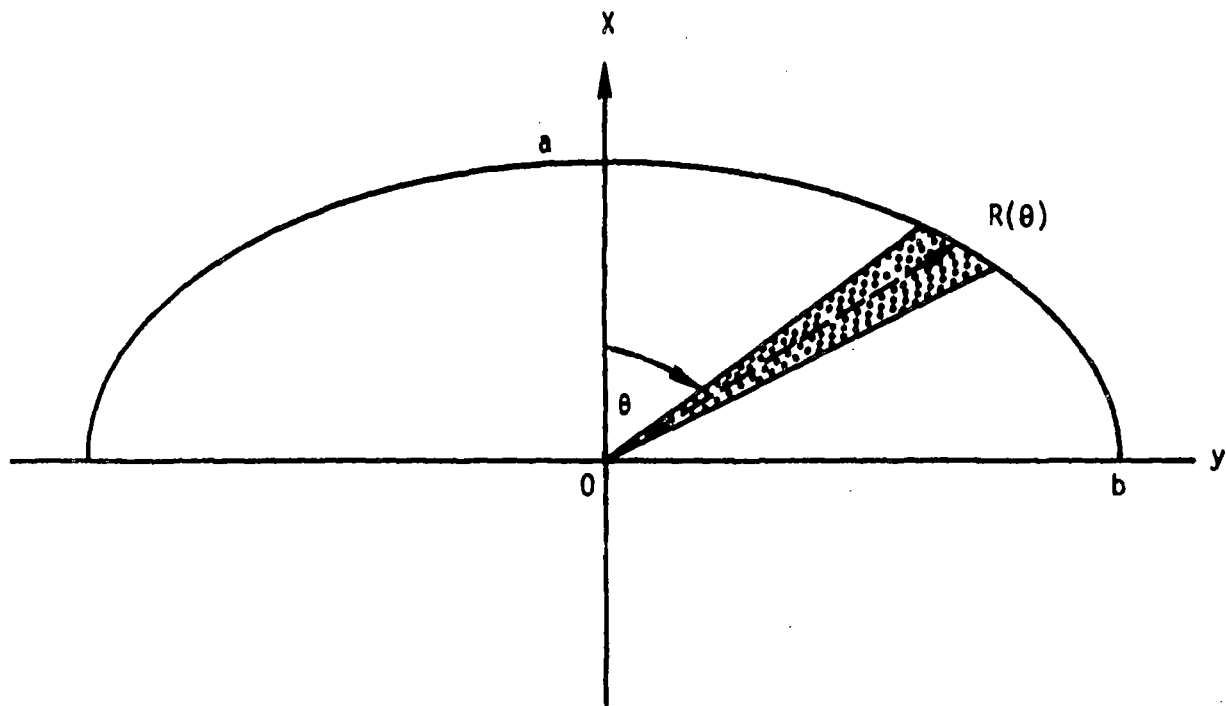


Figure U-1. Coordinate System for Integration Scheme for Integrating Over a Semi-Elliptical Area.

KBARA and KBARB were written to numerically evaluate RMS stress intensity factors for arbitrary stress on the crack surface for semi-elliptical surface cracks in pipes.

D.2 Verification of the Integration Procedures

The accuracy of the numerical integration scheme was verified by obtaining RMS stress intensity factor results using this method for those problems for which the solutions already exist. One such problem is the buried elliptical crack in an infinite body under uniform stress, and another one is a buried circular defect under a non-uniform stress (Tada 73). For both of these cases, stress intensity factors are obtained by the integration schemes and the results are compared with the corresponding analytical solutions.

D.2.1 Uniform Stresses

For a buried elliptical defect in an infinite body under uniform stress, Besuner 77b gives solutions for RMS stress intensity factors as

$$\bar{K}_a = 2\sigma a \left[\frac{1}{3F} \left(\frac{2}{a} - \frac{1}{F} \frac{\partial F}{\partial a} \right) \right]^{1/2}$$

and

$$\bar{K}_b = 2\sigma \left[\frac{ab}{3F} \left(\frac{1}{b} - \frac{1}{F} \frac{\partial F}{\partial b} \right) \right]^{1/2}$$

where $F = \left[1 + 1.464 (a/b)^{1.65} \right]^{1/2}$

The above expressions for \bar{K}_a and \bar{K}_b by simple algebraic manipulation, can be simplified to

$$\bar{K}_a = 2\sigma a^{1/2} \left\{ \frac{1}{3F} \left(2 - \frac{1.208(a/b)^{1.65}}{F^2} \right) \right\}^{1/2}$$

and

$$\bar{K}_b = 2\sigma a^{1/2} \left\{ \frac{1}{3F} \left(1 + \frac{1.208(a/b)^{1.65}}{F^2} \right) \right\}^{1/2}$$

The RMS stress intensity factors for buried elliptical defect in an infinite body under uniform stress using the integration scheme are obtained by integration as described earlier of Equation C-20 with the correction factor $f_j(x,y)$ set equal to unity and $\sigma(x,y) = \text{a constant}$. The results obtained for \bar{K}_a and \bar{K}_b by the integration scheme are compared with that obtained by Besuner 77b in Tables D-1 and D-2. The maximum difference between the two sets of results is less than 0.4%, thus verifying the accuracy of the integration scheme for uniform stress.

D.2.2 Non-Uniform Stresses

To further check the accuracy of the numerical integration scheme, a problem involving non-uniform stresses over the crack surface is considered. Tada et al. (Tada 73) gives a solution for K for a buried circular defect in an infinite body with stresses varying as a power of radial distance (r) from the center of the defect. For a specific case of stresses varying as r^3 , that is, for

$$\sigma = r^3$$

the solution for the stress intensity factor simplifies to

$$K = .6647 a^{3.5}$$

This is an exact solution for K for this particular case. Since for a buried circular defect in an infinite body subjected to an axisymmetric stress system \bar{K}_a , \bar{K}_b and K are all identical, the analytical results obtained from the above expression can be directly compared to \bar{K}_a and \bar{K}_b . The \bar{K}_a and \bar{K}_b from the integration scheme for this case are obtained by integrating Equation C-20 with the correction factor $f_j(x,y) = 1$ and $\sigma = r^3$. The results obtained by both the methods are presented in Table D-3. Again, an excellent agreement with the analytical results was obtained for both \bar{K}_a and \bar{K}_b with the maximum error being less than 0.4 percent.

Table D-1

K_a for Buried Elliptical Defect in an Infinite Body Under Uniform Stress-Comparison of Results Obtained by the Integration Scheme with the Existing Solutions

a (inch)	b/a	K_a from the Integration Scheme	K_a from (Besuner 1977b)
.05	1	.25323	.25322
	3	.33206	.34940
	5	.34940	.34940
.20	1	.50646	.50644
	3	.66411	.66410
	5	.69880	.69879
.35	1	.66998	.66995
	3	.87854	.87852
	5	.92443	.92442
.50	1	.80078	.80075
	3	1.05005	1.05003
	5	1.10490	1.10489
.65	1	.91303	.91299
	3	1.19724	1.19722
	5	1.25978	1.25977
.80	1	1.01291	1.01287
	3	1.32822	1.32820
	5	1.42315	1.39759

K_a in ksi in^{3/2}, $\sigma = \text{constant} = 1 \text{ ksi}$

Table D-2

\bar{K}_b for Buried Elliptical Defect in an Infinite Body Under Uniform Stress-Comparison of Results Obtained by the Integration Scheme with the Existing Solutions

a (inch)	b/a	\bar{K}_b from the Integration Scheme	\bar{K}_b from (Besuner 77b)
.05	1	.251	.252
	3	.264	.263
	5	.262	.261
.20	1	.503	.503
	3	.527	.527
	5	.523	.523
.35	1	.667	.666
	3	.697	.697
	5	.692	.692
.50	1	.796	.796
	3	.833	.833
	5	.827	.827
.65	1	.907	.907
	3	.950	.950
	5	.943	.950
.80	1	1.006	1.006
	3	1.054	1.054
	5	1.046	1.046

\bar{K}_b in ksi-in^{1/2}, $\sigma = \text{constant} = 1 \text{ ksi}$.

Table D-3

K_a and K_b for Buried Circular Defect Under Non-Uniform Stress, in an Infinite Body--Comparison of Analytical Results with that Obtained by the Integration Scheme

a (in)	Numerical		Analytical
	K_a	K_b	$K = .6647a^{3.5}$
.1	.002100	.002100	.002102
.2	.002372	.002372	.002378
.3	.00982	.00982	.00983
.4	.0268	.0268	.0269
.5	.0588	.0588	.0588
.6	.1112	.1112	.1112
.7	.1908	.1908	.1908
.8	.3044	.3044	.3044

K, K_a, K_b in ksi - in⁴

$\sigma = r^3, \sigma$ in ksi

D.3 Comparisons With Existing Solutions

In this section the RMS stress intensity factors for semi-elliptical surface cracks in material with finite thickness obtained by the integration of Equation C-20 will be compared with the existing solutions for the same or similar problems. The \bar{K}_j results obtained from the integration scheme, hereafter referred to as influence function (IF) results, will be first compared with results for uniform stresses. Next the IF results will be obtained for power law stresses for which solutions exist in the open literature (Heliot 79, McGowan 79).

D.3.1 Uniform Stress

The RMS stress intensity factors for semi-elliptical surface cracks in material with finite thickness can be obtained from IF method by integrating Equation C-20 for a given crack geometry defined by a/h and b/a . The \bar{K} for uniform stress are obtained by setting $\sigma(x,y) = 1.0$, that is, a constant. These results (\bar{K}_a and \bar{K}_b) are obtained for a/h varying from .05 to .8 and b/a varying from 1 to 6. The normalized \bar{K}_j ($\bar{K}_j/\sigma a^{3/2}$) are then plotted as a function of a/h (Figures D-2 and D-3) for various b/a . The IF results are shown as dashed lines. The solid lines are the results obtained directly from the BIE calculations, as described in Section 2.7. For a/h larger than .25, the errors in the stress intensity factors obtained by IF method are generally less than 10%. Larger errors, both in \bar{K}_a and \bar{K}_b for a/h less than .25 are not very significant. Plotting the normalized values of \bar{K}_j tends to overemphasize the inaccuracies for small a , because of the $a^{-3/2}$ term. The values of \bar{K}_j for small a are themselves small, so inaccuracies in such values are not of great concern in this investigation.

D.3.2 Non-Uniform Stresses

As was mentioned earlier (Appendix A), the current IF solutions for RMS stress intensity factors were developed for semi-elliptical circumferential cracks in PWR primary pipes ($R_1/h \approx 5$). For non-uniform stresses on the crack surface, the closest available solutions are for

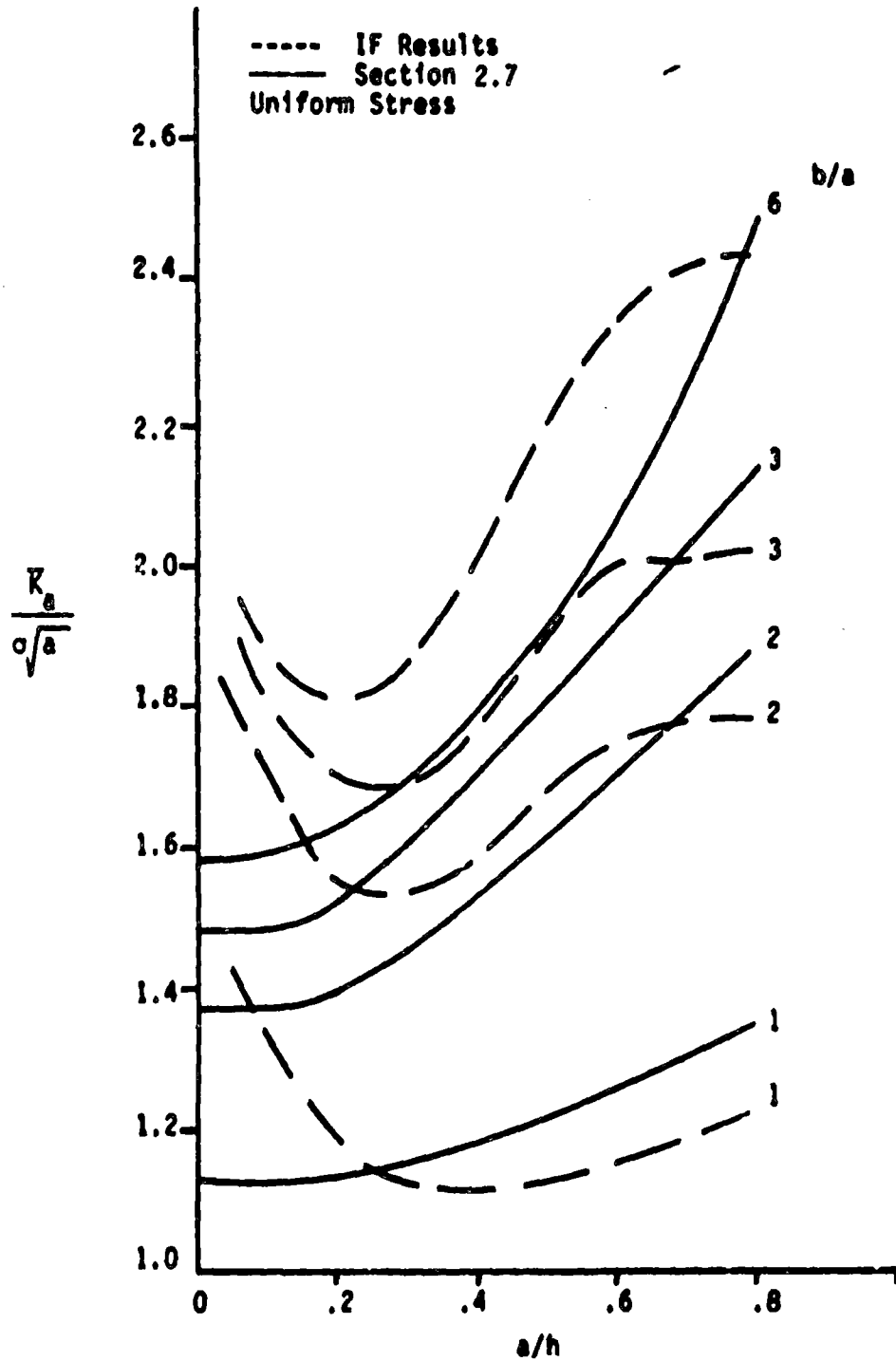


Figure D-2. K_a for Uniform Stress Obtained by IF Method Compared with Direct Results From BIE (Section 2.7).

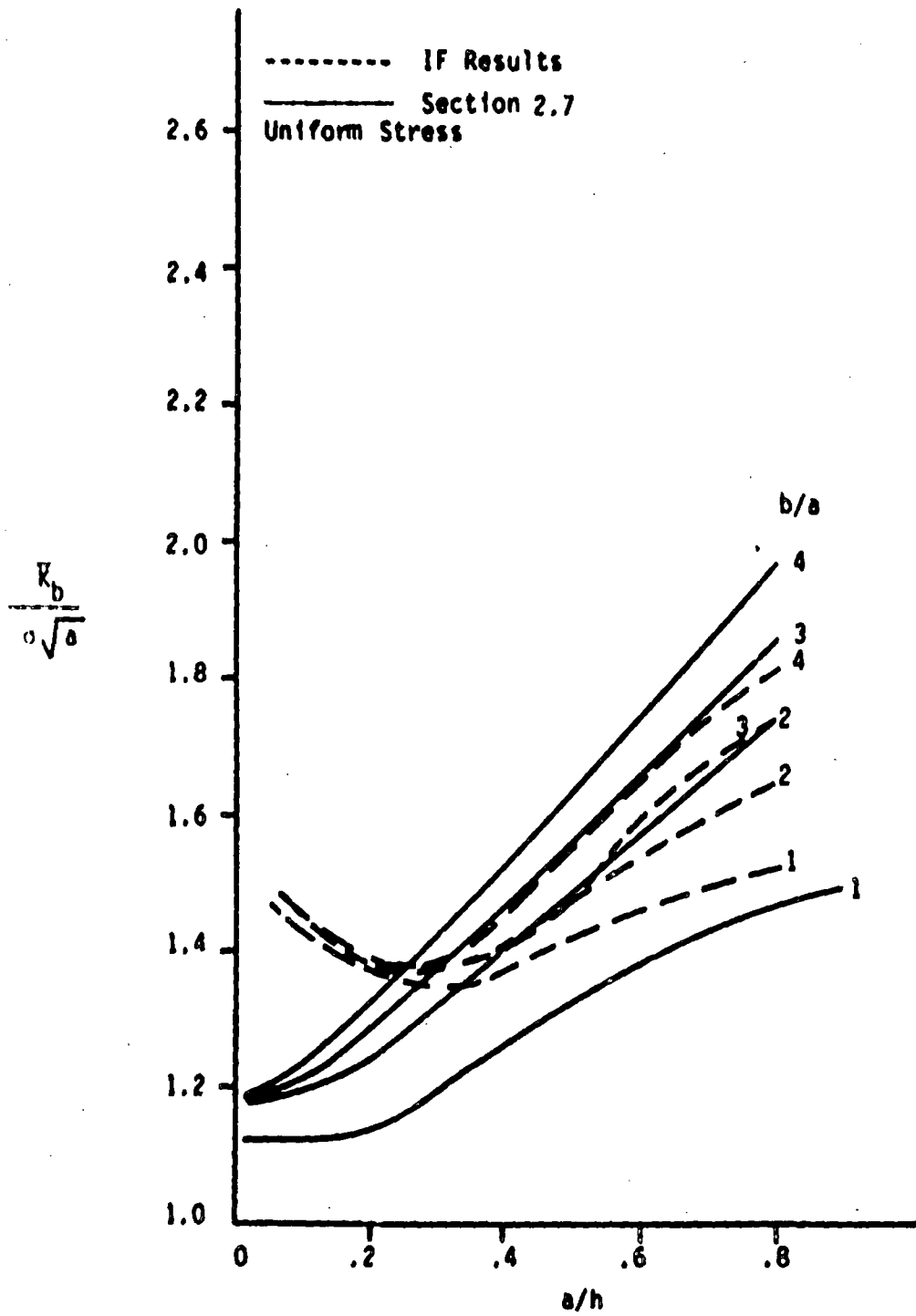


Figure D-3. K_b for Uniform Stress Obtained by IF Method Compared with Direct Results From BIE.

...

longitudinal cracks in cylinders with R_1/h of 10 (Heliot 79, McGowan 79), and only for three crack depths with a fixed aspect ratio ($b/a = 3$). The stress intensity factors for each crack geometry are given by Heliot 79 and McGowan 79 as a function of position on the crack front. Their results are given for non-uniform stresses of the type

$$\sigma(x/h)^p \quad p = 0, 1, 2, 3, 4$$

From the results of McGowan 79, values of \bar{K}_a and \bar{K}_b were computed for each crack geometry and stress state. This was accomplished by numerical integration using Equations C-2 through C-4. The normalized \bar{K}_a and \bar{K}_b are plotted as a function of a/h for various loading conditions (Figures D-4 and D-5).

The IF results were obtained by integrating Equation C-20 for

$$\sigma(x,y) = (x/h)^p \quad p = 0, 1, 2, 3, 4$$

for normalized crack depths varying from .25 to .80 and for an aspect ratio of $b/a = 3$. The IF results are also plotted on the same graph for comparison and are generally within 10% of the results reported by McGowan 79. Some disagreement in the two solutions is expected because of the following two reasons.

- (i) IF solutions are obtained for circumferential cracks whereas McGowan's results are for longitudinal cracks.
- (ii) IF solutions are obtained for pipes with $R_1/h = 5$ whereas McGowan's solutions are for pressure vessels with R_1/h of 10.

However, as was discussed in Appendices A and B, the influence of R_1/h is not strong for semi-elliptical cracks within the range of 5-10, and differences between corresponding circumferential and longitudinal cracks is not large. Overall, the agreement between the IF results and those reported by McGowan 79 shown in Figures D-4 and D-5 is felt to be quite good, and serves as an additional check on the influence functions developed in Appendix C.

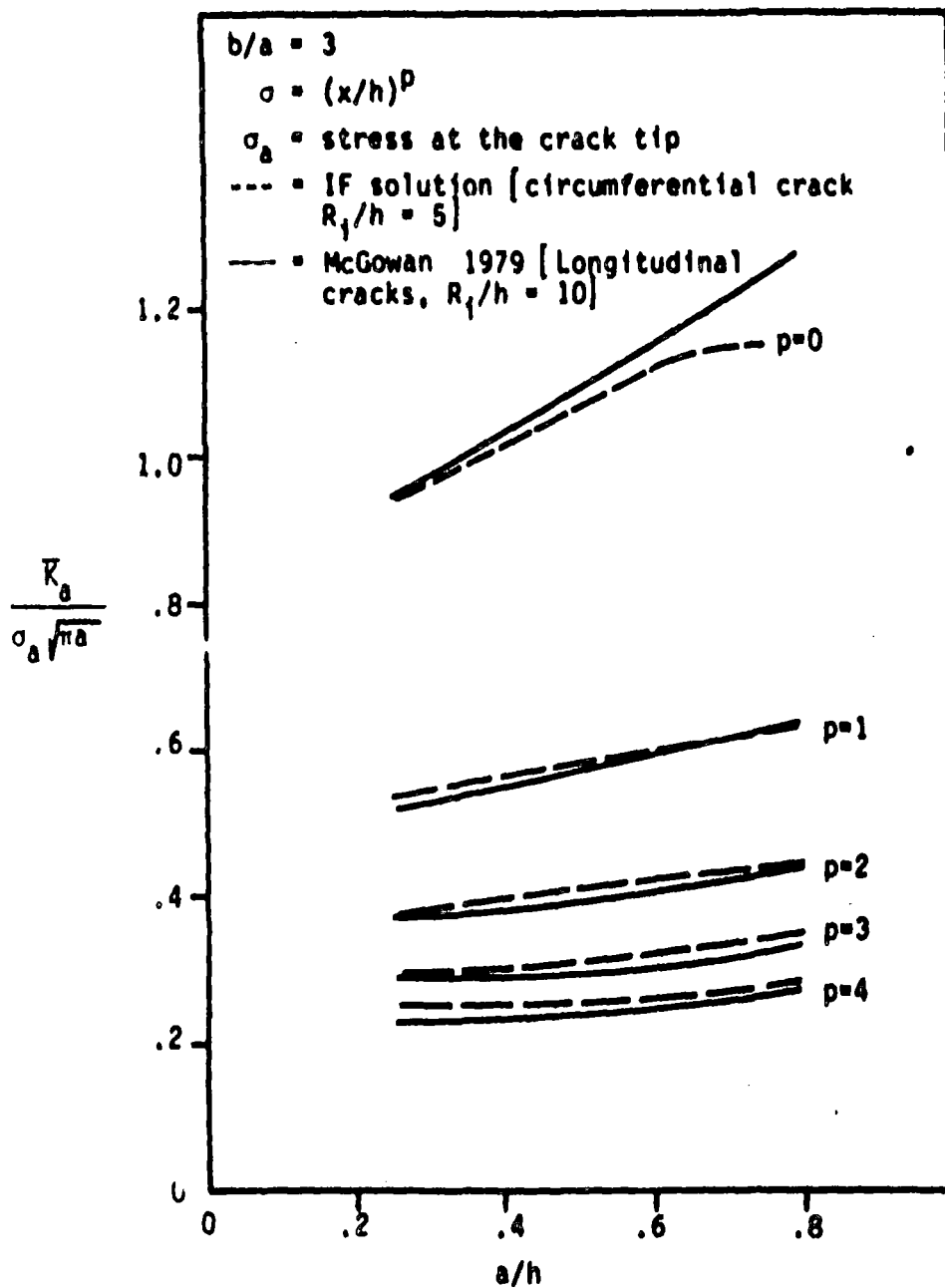


Figure D-4. Comparison of IF Solutions for Non-Uniform Stresses with Existing Solutions.

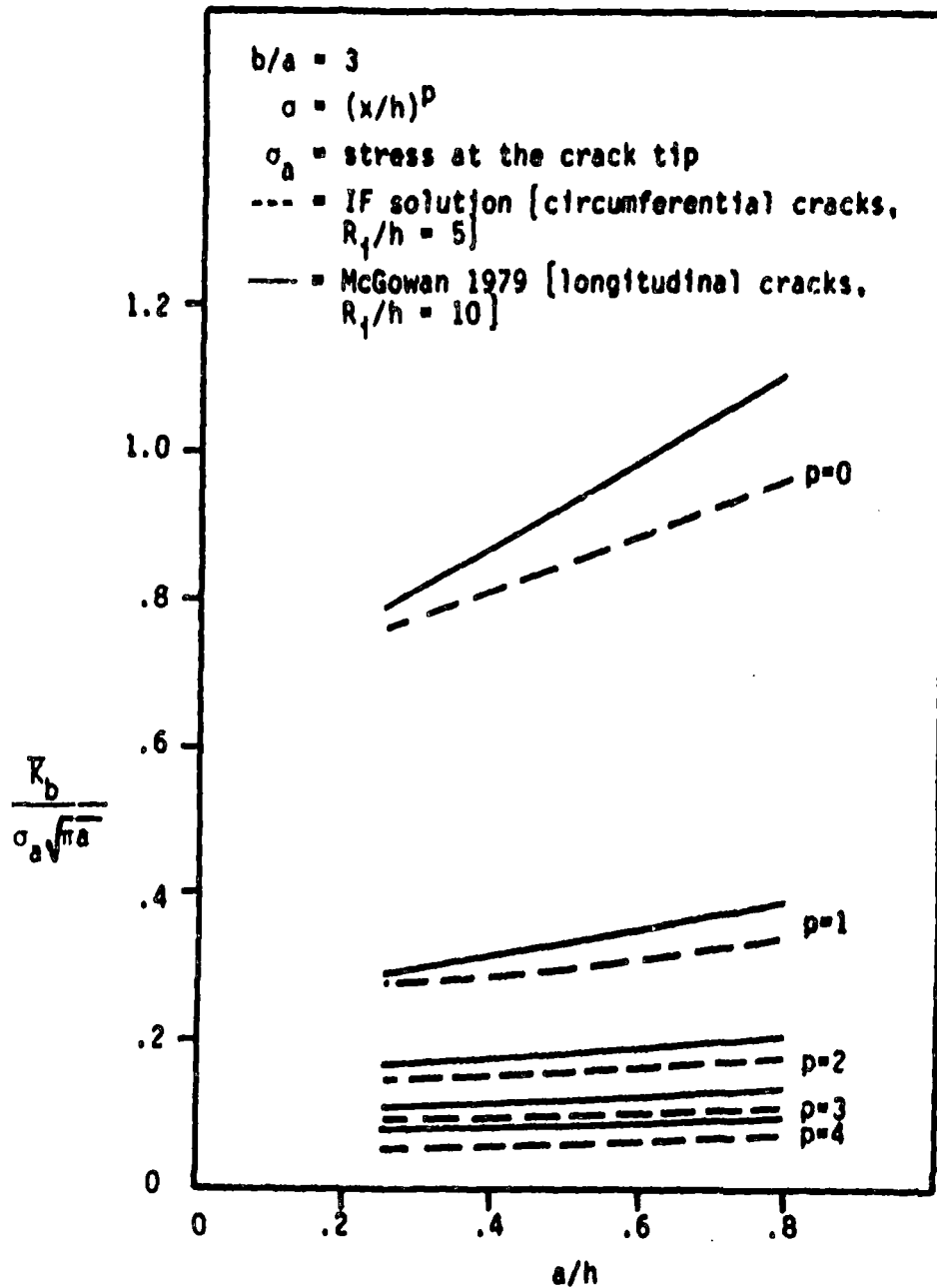


Figure D-5. Comparison of IF Solutions for Non-Uniform Stresses with Existing Solutions.

The influence functions and integration procedures developed and demonstrated above will now be applied to stress systems of actual interest in the fracture mechanics analysis of crack growth in reactor piping.

D.4 Applications to Radial Gradient Thermal Stresses

Transient thermal stresses are produced in the wall of a pipe when the temperature of the coolant in the pipe changes rapidly. Such rapid changes result from various plant operating transients. Pipes being circular objects, these stresses are axisymmetric and change only in the radial direction. Hence, they are called radial gradient thermal stresses. Due to the nonequilibrium nature of the coolant temperature, the radial gradient thermal stresses are transient in nature; that is, they are a function of time.

The component of the radial gradient stress that is of interest here is the axial component, $\sigma_z(r,t)$. The thermal expansion capabilities of the primary pressure boundary can accommodate the average axial thermal stress, which enters into the restraint of thermal expansion contributor to stress. In addition to this, the radial gradient stress is the portion of the stress that cannot be accommodated by overall elongation of the pipe. The average axial component of the radial gradient stress is zero. Such stresses can be calculated from the temperature field in the pipe (Timoshenko 51), but the average value of σ_z is subtracted off. The expression for the radial gradient component of $\sigma_z(r,t)$ is then given by the following

$$\sigma_z(r,t) = \frac{\alpha E}{1-\nu} \{T(r,t) - \bar{T}(t)\} \quad (D-7)$$

$$\bar{T}(t) = \frac{1}{h} \int_0^h T(r,t) dr$$

Thus, it is seen that this component of the stress depends on the elastic properties of the material, the coefficient of thermal expansion, and the parameters that influence the temperature in the wall—such as the thermal diffusivity of the material. Evaluation of the radial gradient stress is seen to be primarily a transient heat conduction problem. These stresses can then be used to calculate the resulting RMS stress

intensity factors by use of the influence functions developed in Appendix C. These cyclic stress intensities in turn are used to calculate fatigue crack growth due to transients.

The computation of the radial gradient thermal stress was performed using a numerical computer code PIPET (Chan 81). The temperature field calculations were performed by treating the pipe of wall thickness h as a flat slab of this same thickness. The slab was considered to be insulated on the outside surface, and subjected to flowing water of varying specified temperature on the inside surface. Convection heat transfer at the inner wall was accounted for.

For a given transient, the primary input to the code was the time-temperature profile of the coolant. Eleven transients (George 80) that produce radial gradient thermal stresses were considered and a short description of these transients is given in Table D-4. The maximum change in the coolant temperature in the hot leg (ΔT) for each transient is also listed in the table. The time-temperature profiles of the coolant in the hot leg (T_H), cold leg (T_C) and steam lines (T_{steam}) for each transient are given in Figures D-6 through D-15. Small differences between the maximum ΔT values in Table D-4 and Figures D-6 through D-15 exist, but are inconsequential.

For each transient, the radial gradient thermal stresses were calculated at various positions through the pipe wall thickness for about every 0.2 seconds, starting from the beginning of the transient and until after the coolant temperature has reached an equilibrium value. Calculations were performed for the various thickness joints in the hot leg, cold leg and cross-over leg. Results to be presented in the remainder of this appendix are limited to the hot leg with a wall thickness of 2.5 in. The hot leg generally sees the largest temperature excursion, and therefore is subjected to the largest radial gradient thermal stresses.

Table D-4
Description of the Transients, Including Maximum
 ΔT in Hot Leg

Transient	Description	Max ΔT ($^{\circ}F$)
1	Plant loading, 5% per minute	39.5
2	Plant unloading, 5% per minute	39.5
3	10% step load decrease	13.4
4	10% step load increase	13.4
5	large step decrease in load	84.0
6	loss of load from full power	89.0
7	loss of power	44.0
8	loss of flow in one loop	120.0
9	loss of flow in other loops	69.0
10	steam line break from no load	339.5
11	reactor trip from full power	73.0

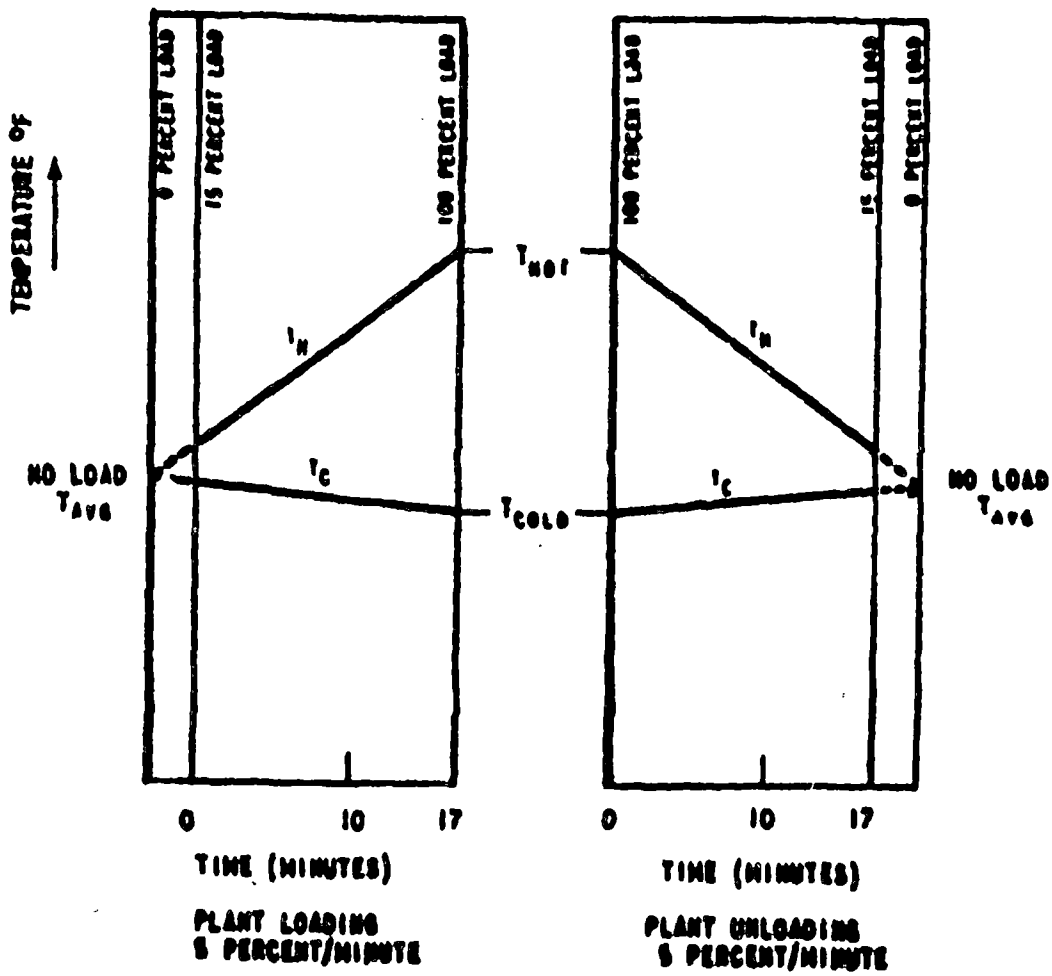


Figure D-6. Plant Loading and Unloading at a Rate of 5% per minute.

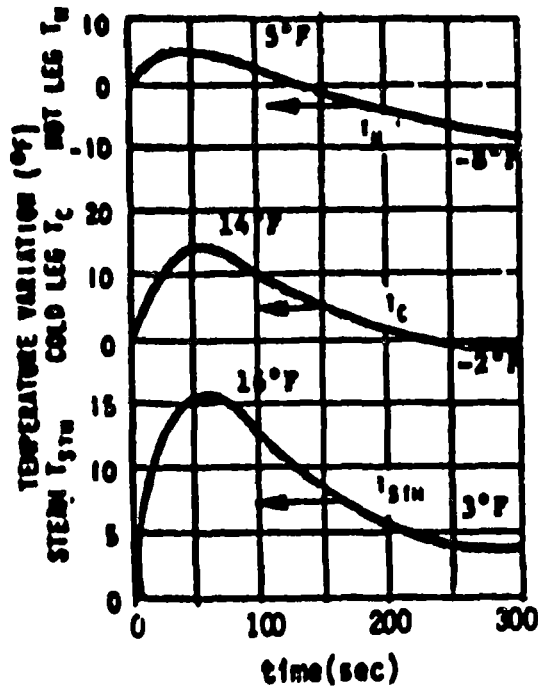


Figure D-7. Ten Percent Step Load Decrease From 100 Percent Power.

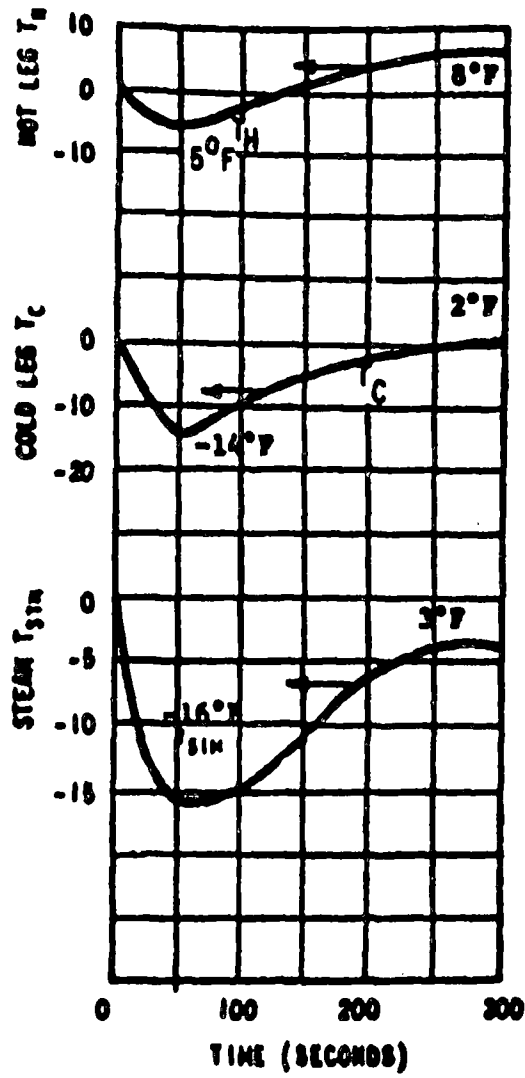


Figure 0-8. Ten Percent Step Load Increase From 90 Percent Power.

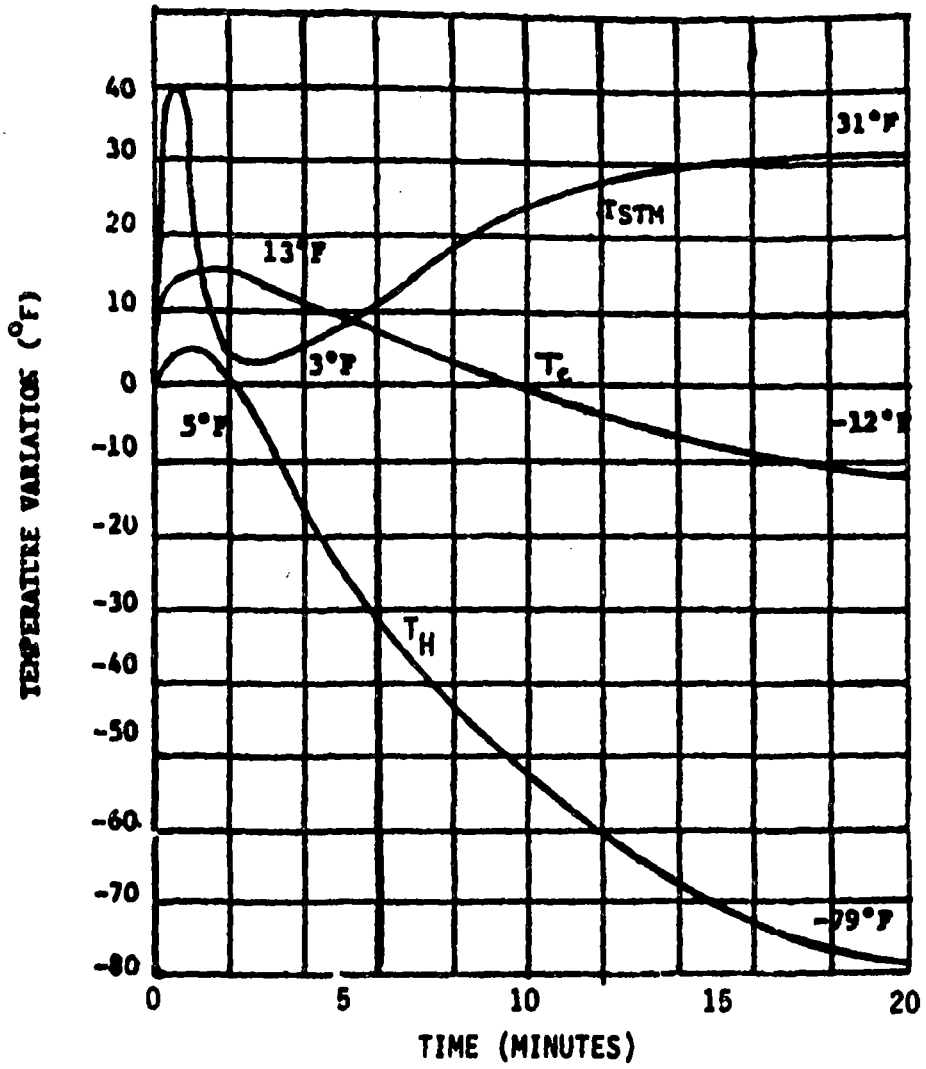


Figure D-9. Large Step Decrease in Load With Steam Dump.

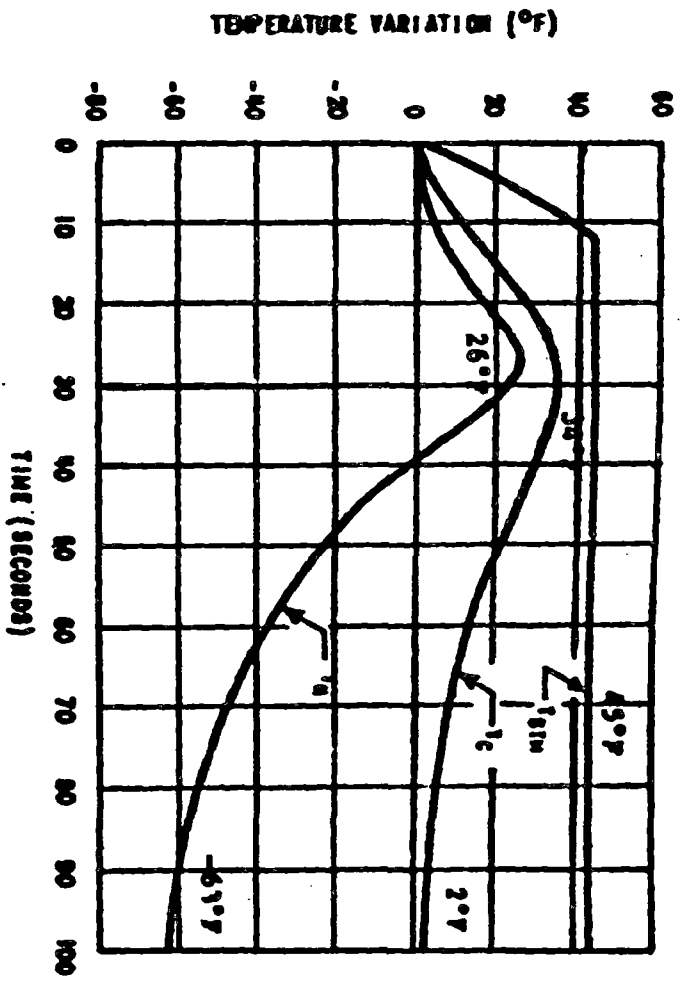


Figure D-10. Loss of Load From Full Power.

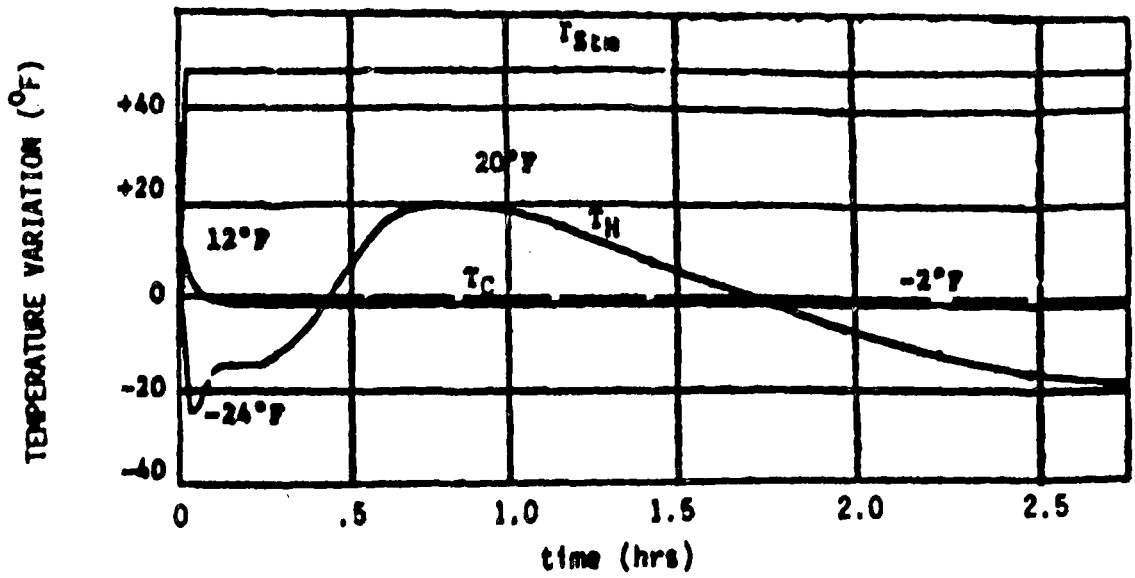


Figure D-11. Loss of Power.

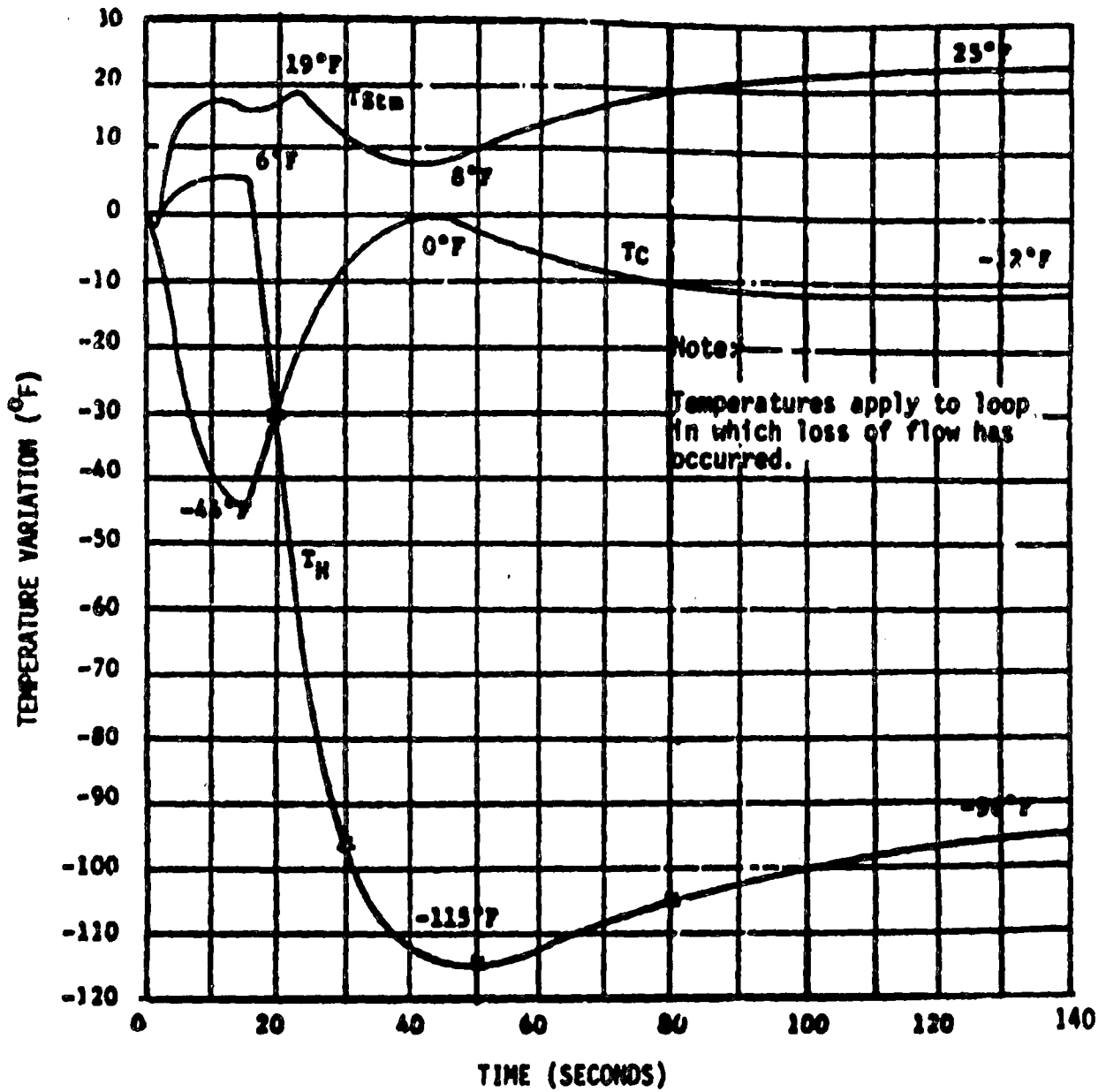


Figure D-12. Loss of Flow in One Loop.

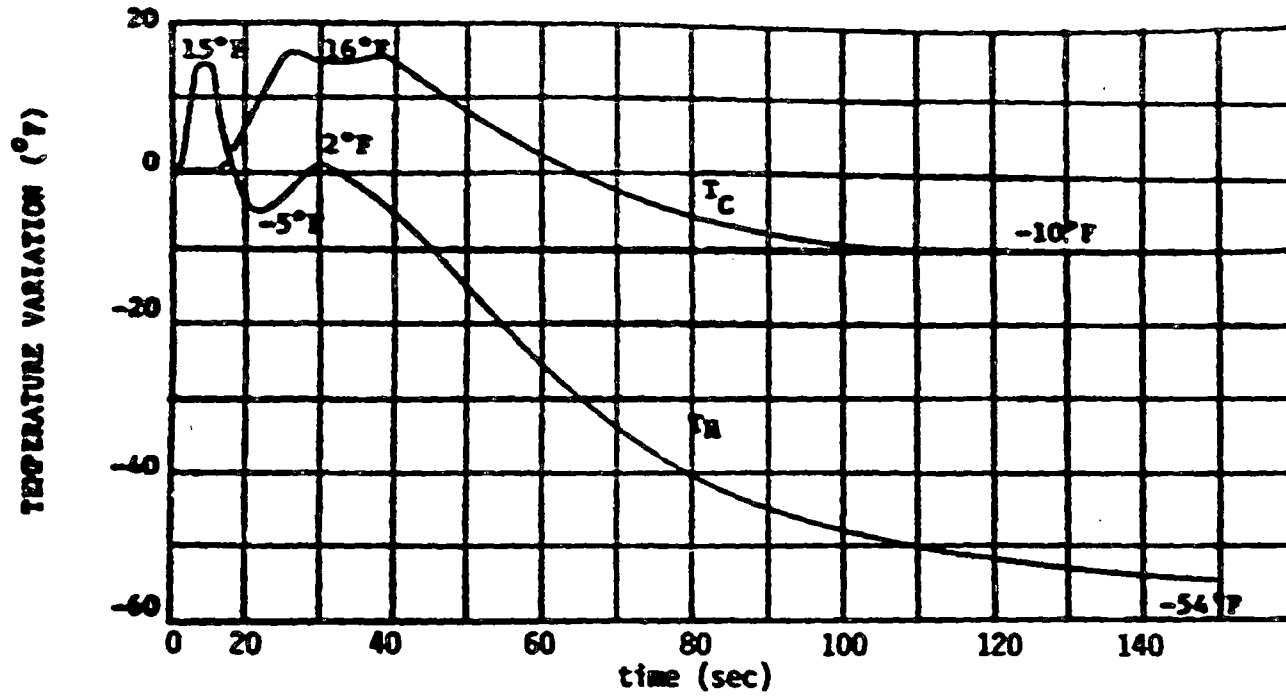


Figure D-13. Loss of Flow in Other Loops.

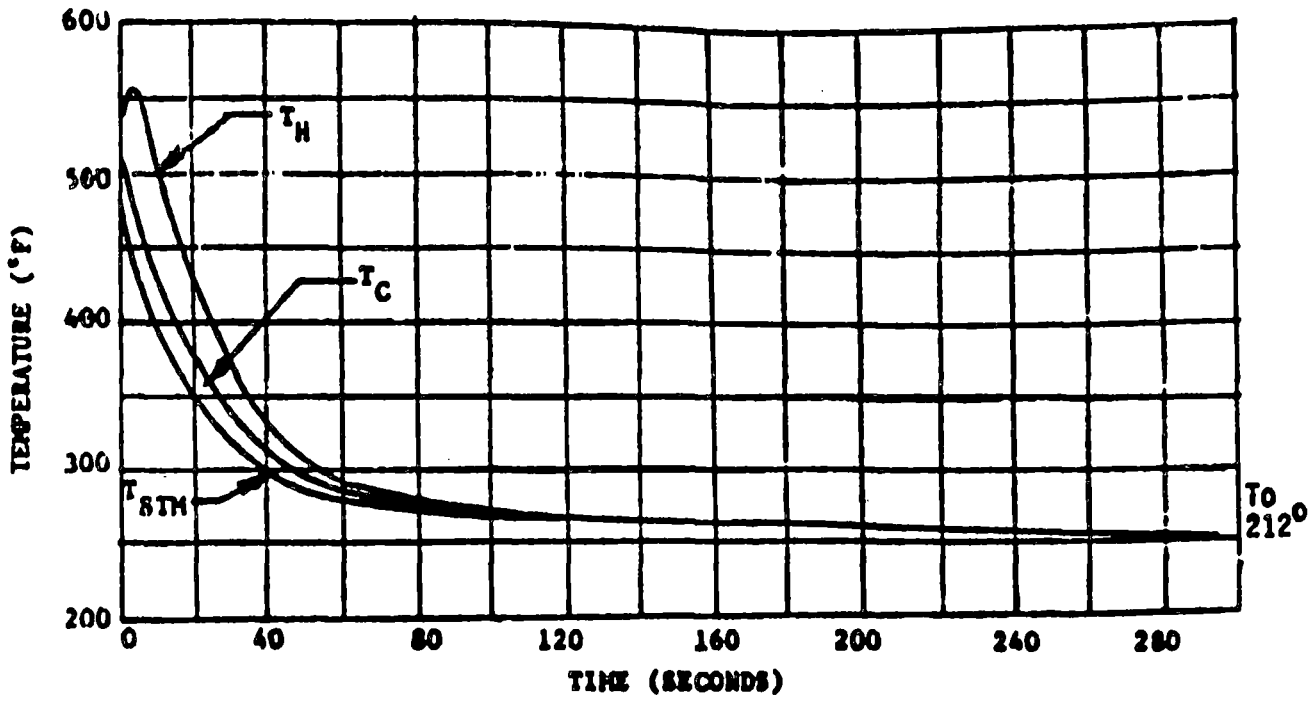


Figure D-14. Steam Line Break From no Load.

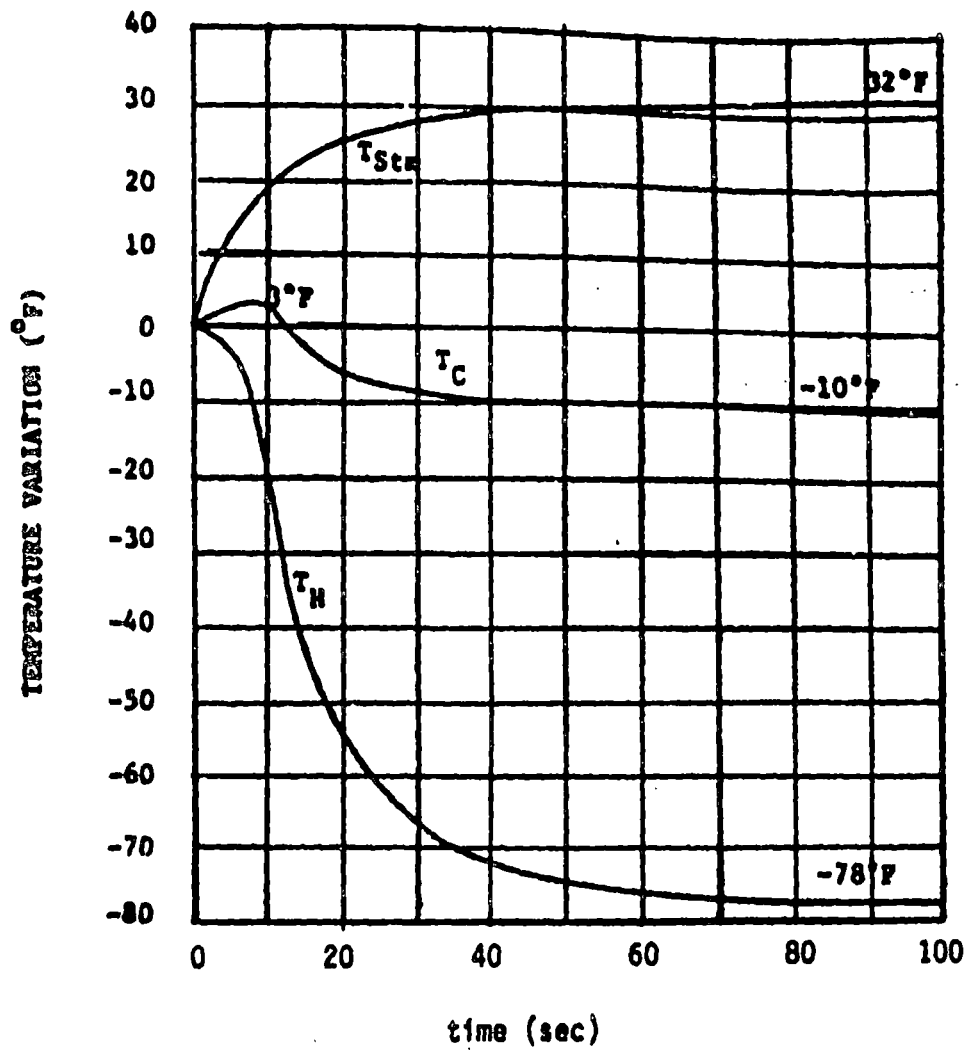


Figure D-15. Reactor Trip From Full Power.

The procedure for computing the fatigue crack growth due to the transient radial gradient thermal stresses will now be illustrated by considering the example of reactor trip from full power (transient 11 in Table D-4). This is one of the most important transients as far as its influence on fatigue crack growth is concerned, because it occurs about 400 times during the lifetime of a plant (see Section 4.1) and the stresses produced during this transient are fairly high.

The time-temperature profiles of the coolant during the reactor trip are given in Figure D-15. For this illustration, the cyclic stress intensity factor occurring at the hot leg-to-pressure vessel joint will be considered. The weld junction is 2.5 inch thick and is a part of the hot leg (joint 1 in Figure 1-2). The time variation of the coolant temperature of the hot leg will be considered for computing the stresses. The radial gradient thermal stresses were computed using the PIPET code (Chun 81) at 51 locations equally spaced from the inner surface of the pipe to the outer surface, for every 0.2 second time interval from the start of the transient. These stresses are shown as a function of time for a few time intervals in Figure D-16. (The stresses shown here are the axial stresses which are relevant for circumferential cracks. Radial and circumferential stresses were also computed in a similar fashion, which could be used if longitudinal cracks are considered.)

For each time interval, the RMS stress intensity factors (K_a and K_b) were calculated by using the influence function (IF) method. For each time interval the radial gradient stresses were read into the computer program as a table and a linear interpolation scheme was used to obtain stresses as a function of position in the pipe wall. Because of the very fine grid (51 points), this linear interpolation scheme was found to be very accurate. Then for each time interval, values of K_a and K_b were computed for a range of crack geometries. For illustration, K_a for selected crack geometries is plotted as a function of time in Figure D-17. These RMS stress intensity factors are referred to as δK_a because these stress intensity factors are those due only to the radial gradient thermal stresses, and

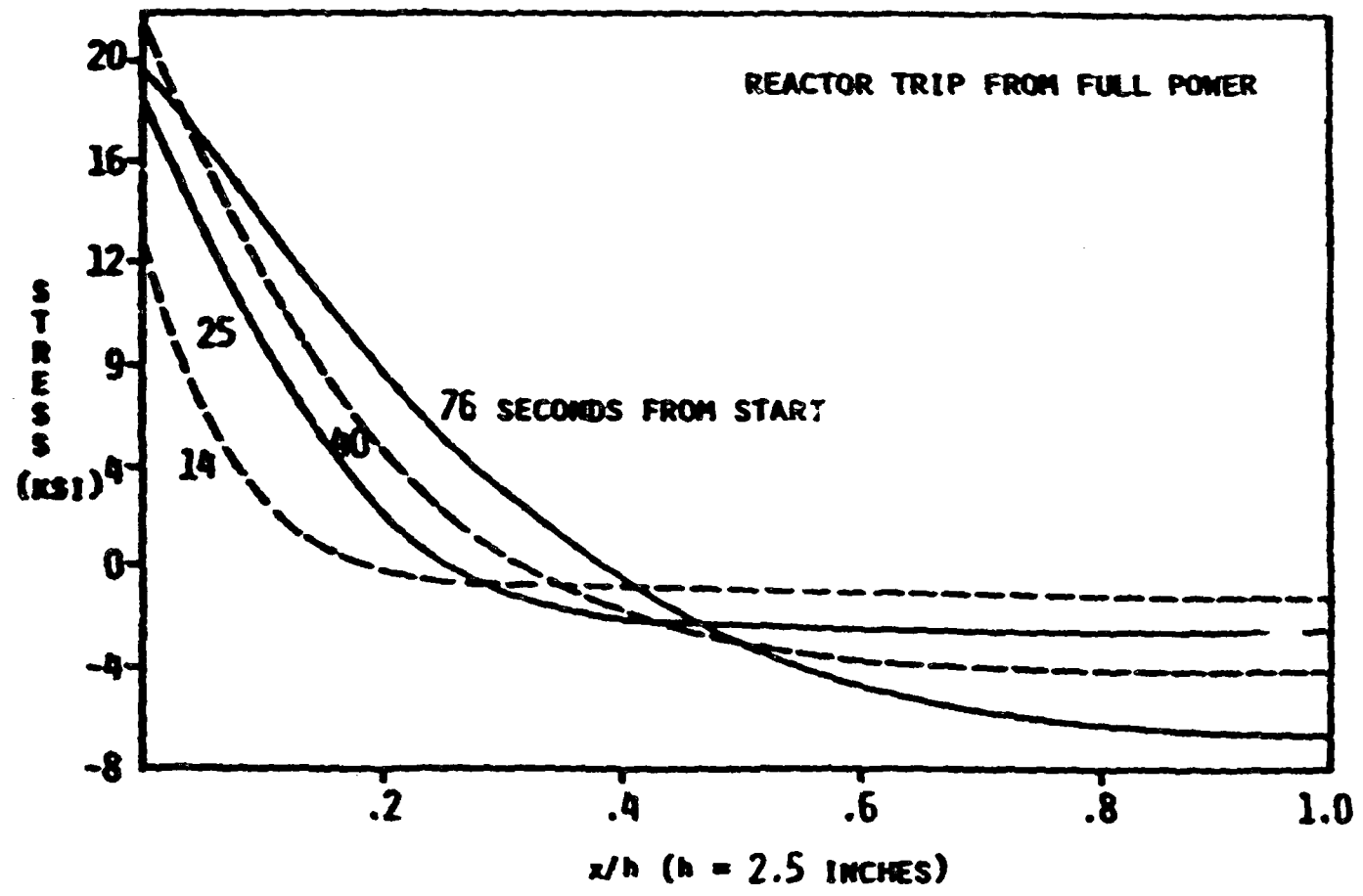


Figure D-16. Radial Gradient Thermal Stresses at Various Times From the Start of the Transient for a 2.5 in. Thick Weld in the Hot Leg.

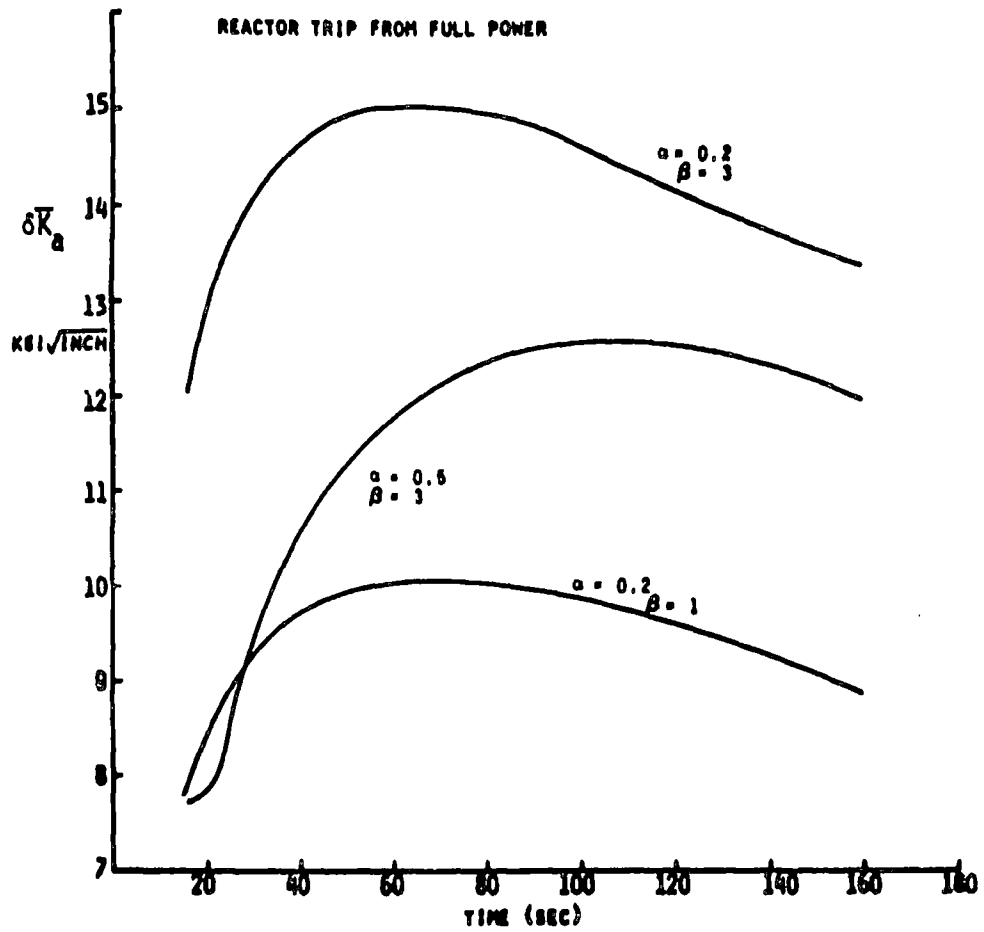


Figure D-17. δK_a as a Function of Time for Three Crack Geometries for a 2.5 Inch Thick Weld in the Hot Leg.

do not include the effect of any other stresses such as dead weight, thermal expansion, residual stresses etc. As shown in Figure D-17, for each crack geometry, $\delta\bar{K}_a$ changes with time and goes through a maximum. This seems very much like a fatigue cycle and during fatigue the crack growth is controlled primarily by the maximum change in the stress intensity. Hence, maximum excursions of \bar{K}_a and \bar{K}_b are of interest, rather than details of the time variations of these stress intensity factors.

The maximum $\delta\bar{K}_a$ reached during the reactor trip for a few crack geometries are

<u>a/h</u>	<u>b/a</u>	<u>maximum $\delta\bar{K}_a$ (ksi - in^{1/2})</u>
.2	1	10.043
.2	3	15.058
.5	3	12.598

The maximum $\delta\bar{K}_a$ and $\delta\bar{K}_b$ for a range of crack geometries can thus be obtained, with the results presented in Figures D-18 and D-19. The maximum $\delta\bar{K}_a$ and $\delta\bar{K}_b$ for any crack size can then be obtained either by curve fitting or by an interpolation scheme from these data.

A couple of interesting observations can be drawn from Figures D-18 and D-19. One is that $\delta\bar{K}_b$ is generally larger than $\delta\bar{K}_a$ for the same crack. This means that this transient will tend to grow cracks in the circumferential direction more than in the depth direction. Therefore, the occurrence of such transients would tend to produce the long cracks that favor LOCA's rather than the deep cracks that favor leaks. This is because the largest stresses occur at the inner pipe wall, with a steep gradient into the wall--as is observed in Figure D-16. Another interesting feature of the \bar{K} 's for a reactor trip is that the stress intensity factors for shallow cracks can actually be larger than for deep cracks. This is in marked contrast to corresponding results for uniform stress, and is again

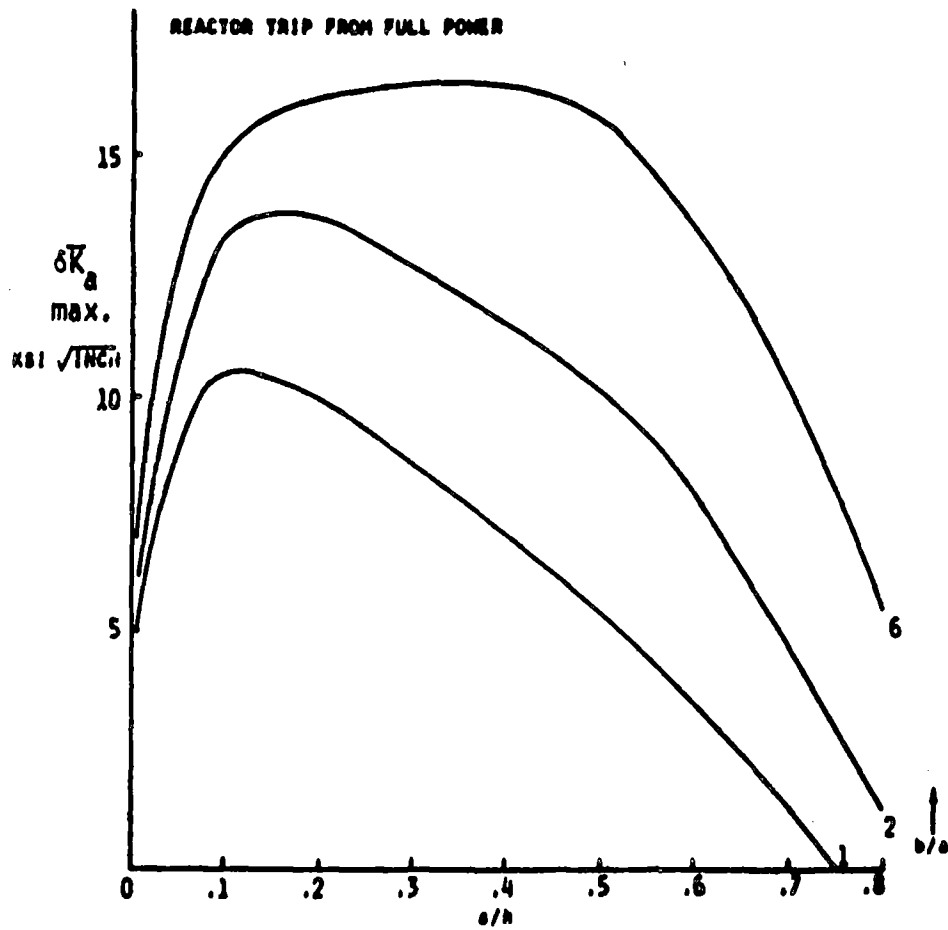


Figure D-18. Maximum δK_a During Reactor Trip as a Function of Crack Geometry for a 2.5 Inch Thick Weld in the Hot Leg.

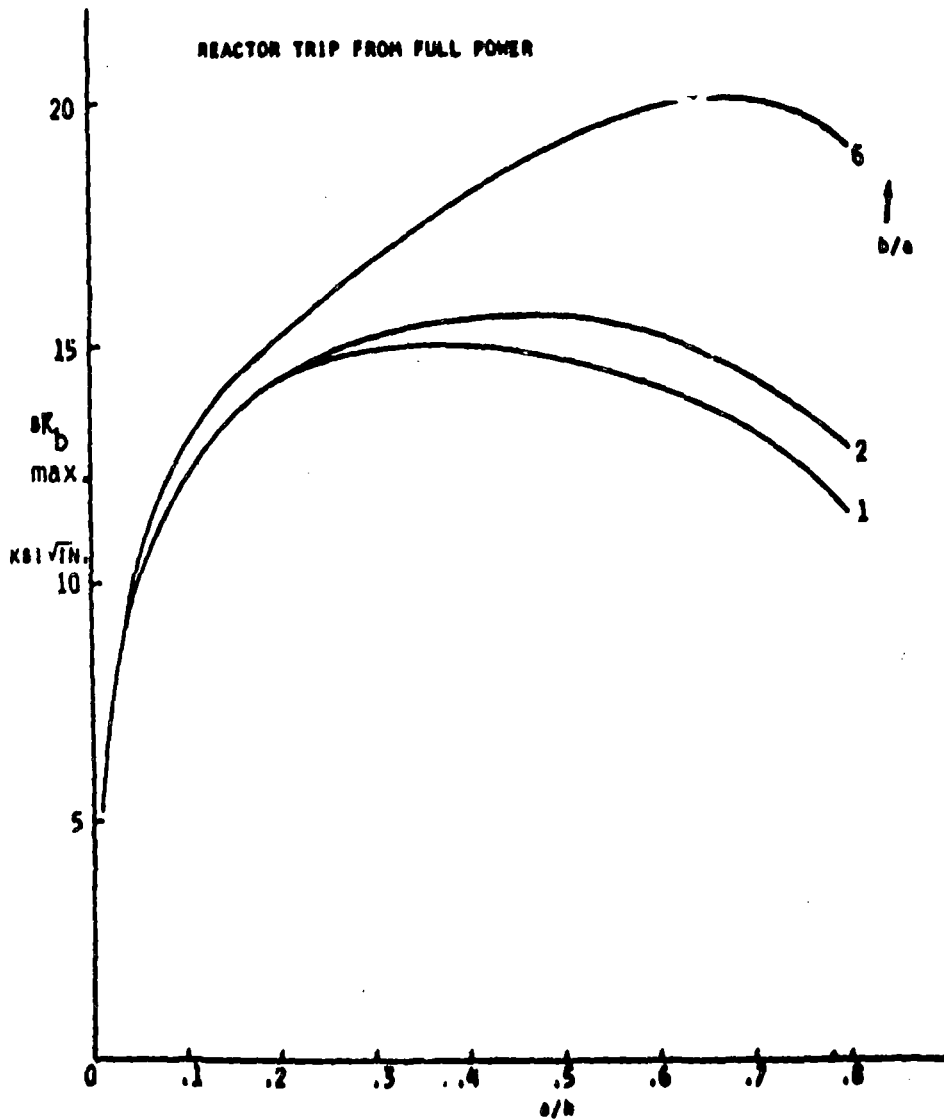


Figure D-19. Maximum δK_D During Reactor Trip as a Function of Crack Geometry for a 2.5 Inch Thick Weld in the Hot Leg.

due to the steep stress gradients through the pipe wall. This means that crack growth in the depth direction due to reactor trips will decelerate with increasing depth, which again points to such transients tending to lead to complete pipe severances more than uniform stress transients. The degree to which this is actually observed in the leak and LOCA probabilities will be addressed in Section 4.3.

The transient considered for the above illustration (reactor trip from full power), has such a time-temperature profile that no negative RMS stress intensity factors are produced. In this case the minimum δK_j are considered all zeroes. On the other hand, during the transient loss of load from full power, the temperature profile goes positive and then negative with respect to the initial coolant temperature. This produces negative radial gradient thermal stresses and therefore the minimum δK_j are negative rather than zero as seen in Figures D-20 and D-21. Even though negative stress intensity factors are physically meaningless, they are still of interest because they represent the influence of radial gradient stresses on cracks in pipes subjected to tensile loads, such as those due to dead weight, pressure, etc. Details on how to combine these radial gradient stress intensity factor results with K_j due to other stresses, and then to calculate fatigue crack growth are discussed in Section 2.6.

The RMS stress intensity factors described here were calculated for radial gradient thermal stresses in 2.5 inch thick pipes with Youngs modulus $E = 2.87 \times 10^7$ psi and coefficient of thermal expansion $\alpha' = 9.1 \times 10^{-6} \text{ } ^\circ\text{F}^{-1}$ for a given time-temperature profile of the coolant. The maximum and minimum δK_j data thus obtained are normalized to make them dimensionless as

$$\frac{\delta K_j}{\Delta T \alpha' E a^{3/2}}$$

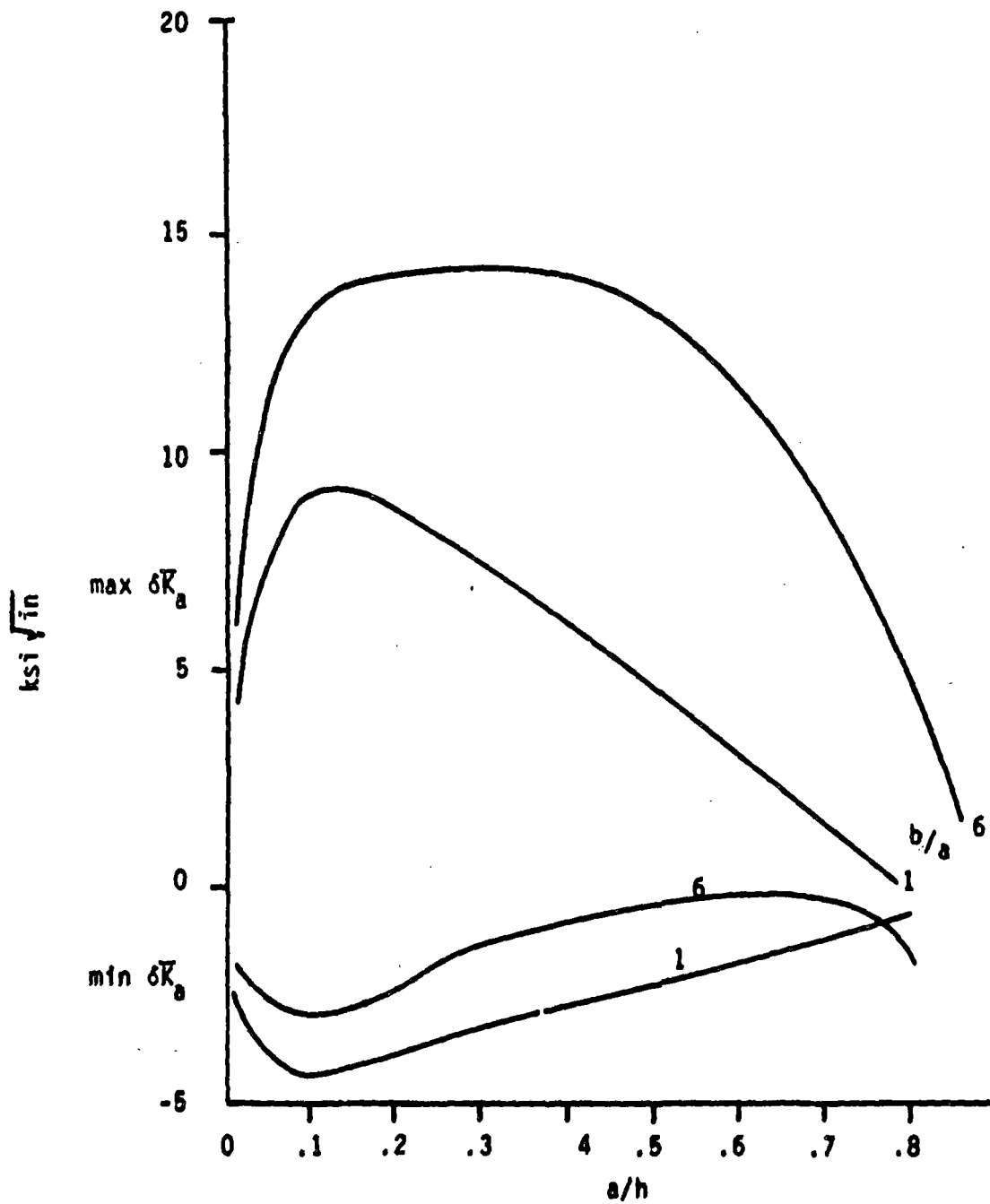


Figure D-20. Maximum and Minimum δK_a During the Transient-Loss of Load From Full Power for a 2.5 Inch Thick Weld in the Hot Leg.

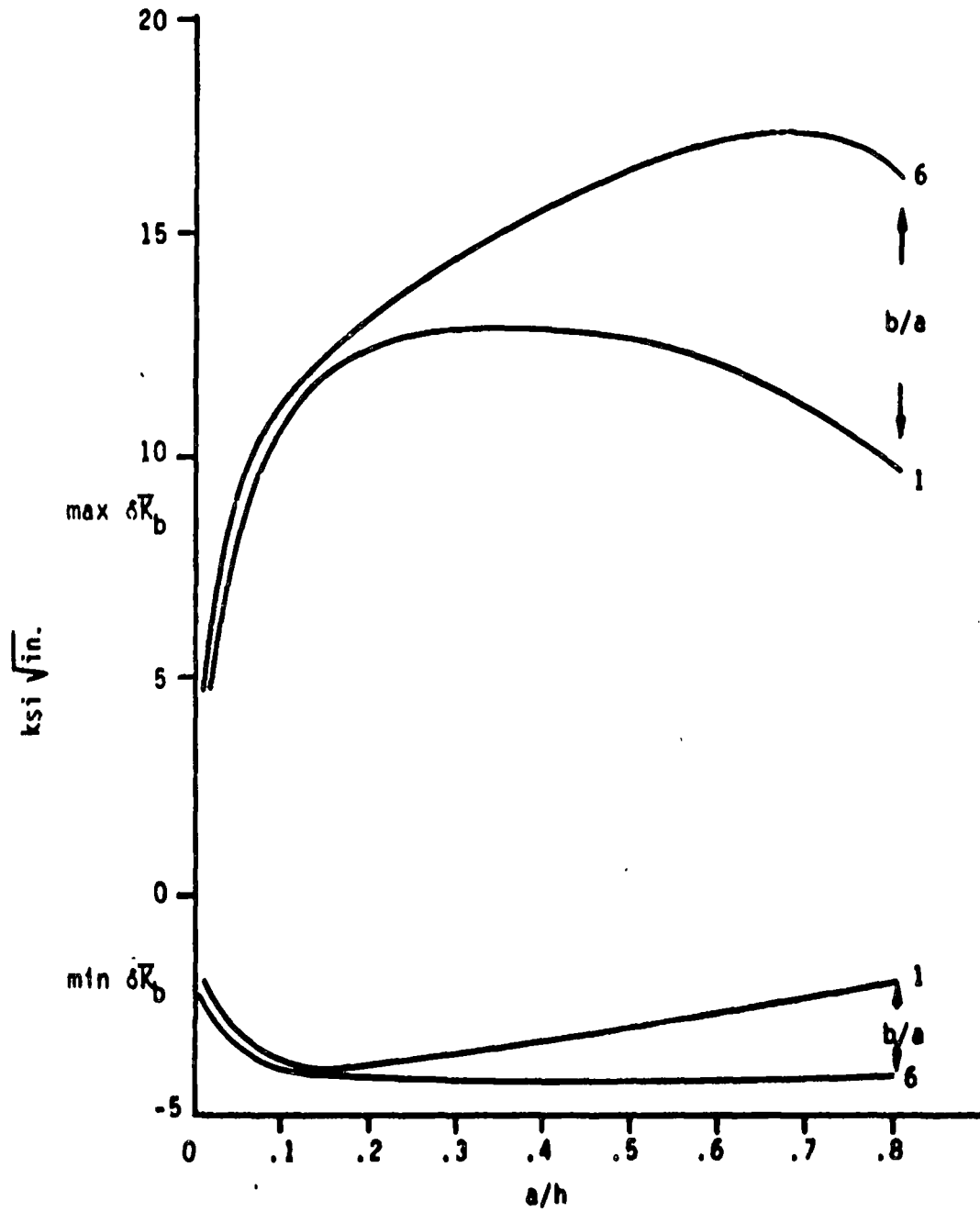


Figure D-21. Maximum and Minimum δK_b During the Transient Loss of Load From Full Power for a 2.5 Inch Thick Weld in the Hot Leg.

where ΔT = maximum change in the coolant temperature during a transient
E = Youngs modulus
 α' = coefficient of thermal expansion
a = crack depth

The normalized maximum and minimum $\delta \bar{I}_a$ and $\delta \bar{K}_b$ data for each transient are listed in Table D-5. This normalization makes it possible to use these tabulated data for the transient when it has the same temperature time variation but with a different ΔT_{max} . It is also possible to use the same table for materials with different thermal coefficient of expansion (but the same thermal diffusivity).

This concludes the characterization of the radial gradient thermal stresses, which will be used in the fatigue crack growth analysis.

Table D-5

Normalized RMS Stress Intensity Factors $\left(\frac{\delta K_I}{\alpha \sqrt{EAT} \sqrt{a}}\right)$ for Transients in the Hot Leg of ZION 1.

Thickness = 2.5 inch
 $\alpha' = 9.1 \times 10^{-6}$ / OF
 $E = 2.87 \times 10^7$ psi
 δK_I in ksi in^{3/2}
 $L/A = 2b/a = 28$

Reproduced from
 best available copy.

TRANSIENT No. 1

DELTA T (Sec) 39.8

DEL 00000 000000

Delta T (Sec)	0.000	0.1000	0.2000	0.3000	0.4000	0.5000	0.6000	0.7000	0.8000
L/A									
2	0.0000000	0.0000000	0.0000000	0.0000000	0.0000000	0.0000000	0.0000000	0.0000000	0.0000000
4	0.0000000	0.0000000	0.0000000	0.0000000	0.0000000	0.0000000	0.0000000	0.0000000	0.0000000
6	0.0000000	0.0000000	0.0000000	0.0000000	0.0000000	0.0000000	0.0000000	0.0000000	0.0000000
8	0.0000000	0.0000000	0.0000000	0.0000000	0.0000000	0.0000000	0.0000000	0.0000000	0.0000000
10	0.0000000	0.0000000	0.0000000	0.0000000	0.0000000	0.0000000	0.0000000	0.0000000	0.0000000
12	0.0000000	0.0000000	0.0000000	0.0000000	0.0000000	0.0000000	0.0000000	0.0000000	0.0000000

DEL 00000 000000

Delta T (Sec)	0.100	0.200	0.300	0.400	0.500	0.600	0.700	0.800
L/A								
2	0.0000000	0.0000000	0.0000000	0.0000000	0.0000000	0.0000000	0.0000000	0.0000000
4	0.0000000	0.0000000	0.0000000	0.0000000	0.0000000	0.0000000	0.0000000	0.0000000
6	0.0000000	0.0000000	0.0000000	0.0000000	0.0000000	0.0000000	0.0000000	0.0000000
8	0.0000000	0.0000000	0.0000000	0.0000000	0.0000000	0.0000000	0.0000000	0.0000000
10	0.0000000	0.0000000	0.0000000	0.0000000	0.0000000	0.0000000	0.0000000	0.0000000
12	0.0000000	0.0000000	0.0000000	0.0000000	0.0000000	0.0000000	0.0000000	0.0000000

DEL 00000 000000

Delta T (Sec)	0.100	0.200	0.300	0.400	0.500	0.600	0.700	0.800
L/A								
2	0.0000000	0.0000000	0.0000000	0.0000000	0.0000000	0.0000000	0.0000000	0.0000000
4	0.0000000	0.0000000	0.0000000	0.0000000	0.0000000	0.0000000	0.0000000	0.0000000
6	0.0000000	0.0000000	0.0000000	0.0000000	0.0000000	0.0000000	0.0000000	0.0000000
8	0.0000000	0.0000000	0.0000000	0.0000000	0.0000000	0.0000000	0.0000000	0.0000000
10	0.0000000	0.0000000	0.0000000	0.0000000	0.0000000	0.0000000	0.0000000	0.0000000
12	0.0000000	0.0000000	0.0000000	0.0000000	0.0000000	0.0000000	0.0000000	0.0000000

DEL 00000 000000

Delta T (Sec)	0.100	0.200	0.300	0.400	0.500	0.600	0.700	0.800
L/A								
2	0.0000000	0.0000000	0.0000000	0.0000000	0.0000000	0.0000000	0.0000000	0.0000000
4	0.0000000	0.0000000	0.0000000	0.0000000	0.0000000	0.0000000	0.0000000	0.0000000
6	0.0000000	0.0000000	0.0000000	0.0000000	0.0000000	0.0000000	0.0000000	0.0000000
8	0.0000000	0.0000000	0.0000000	0.0000000	0.0000000	0.0000000	0.0000000	0.0000000
10	0.0000000	0.0000000	0.0000000	0.0000000	0.0000000	0.0000000	0.0000000	0.0000000
12	0.0000000	0.0000000	0.0000000	0.0000000	0.0000000	0.0000000	0.0000000	0.0000000

338

Table D-5 (cont.d)

TRANSIENT NO. 2

DELTA T (SEC) 36.5

CEL 0400 P171000

Area	0333	0400	0433	0500	0533	0600	0633	0700	0800
L/A									
2	0.	0.	0.	0.	0.	0.	0.	0.	-0.226319
0	0.	0.	0.	0.	0.	0.	0.	0.	0.
0	0.	0.	0.	0.	0.	0.	0.	0.	0.
0	0.	0.	0.	0.	0.	0.	0.	0.	0.
10	0.	0.	0.	0.	0.	0.	0.	0.	0.
20	0.	0.	0.	0.	0.	0.	0.	0.	0.

CEL 0400 P211000

Area	0333	0400	0433	0500	0533	0600	0633	0700	0800
L/A									
2	0.334952	0.098712	0.207574	0.2363975	-0.1714704	-0.1179135	0.0692935	-0.2230774	0.3008605
0	0.0277005	0.0597305	0.0110372	0.0337392	0.270202	-0.2210011	0.1959194	0.0403307	0.0237160
0	0.0200171	0.0291330	0.020011	0.0303700	0.3235602	-0.2692069	0.2310332	0.1229560	0.0909779
0	0.0349020	0.034917	0.0310736	0.040121	0.2904374	-0.066912	0.2206554	0.1075002	0.0670263
10	0.0210000	0.020020	0.0200423	0.0261199	0.370723	-0.3107250	0.2072950	0.1607200	0.0620979
20	0.0000000	0.000000	0.0000000	0.0000000	0.3090774	-0.3300396	0.2672000	0.1926700	0.0961360

CEL 0400 P171000

Area	0333	0400	0433	0500	0533	0600	0633	0700	0800
L/A									
2	0.	0.	0.	0.	0.	0.	0.	0.	0.
0	0.	0.	0.	0.	0.	0.	0.	0.	0.
0	0.	0.	0.	0.	0.	0.	0.	0.	0.
0	0.	0.	0.	0.	0.	0.	0.	0.	0.
10	0.	0.	0.	0.	0.	0.	0.	0.	0.
20	0.	0.	0.	0.	0.	0.	0.	0.	0.

CEL 0400 P211000

Area	0333	0400	0433	0500	0533	0600	0633	0700	0800
L/A									
2	0.0210797	0.0200000	0.0210704	0.0200000	0.0200000	0.0200000	0.0200000	0.0200000	0.0200000
0	0.0000000	0.0000000	0.0000000	0.0000000	0.0000000	0.0000000	0.0000000	0.0000000	0.0000000
0	0.0000000	0.0000000	0.0000000	0.0000000	0.0000000	0.0000000	0.0000000	0.0000000	0.0000000
0	0.0000000	0.0000000	0.0000000	0.0000000	0.0000000	0.0000000	0.0000000	0.0000000	0.0000000
10	0.0000000	0.0000000	0.0000000	0.0000000	0.0000000	0.0000000	0.0000000	0.0000000	0.0000000
20	0.0000000	0.0000000	0.0000000	0.0000000	0.0000000	0.0000000	0.0000000	0.0000000	0.0000000

339

Table D-5 (cont'd)

Temperature (°C)		DELTA T (°F) = 13.0								
ΔT (°C)	0.100	0.200	0.300	0.400	0.500	0.600	0.700	0.800	0.900	
2	-0.017050	-0.0017733	-0.0007012	-0.3235760	-0.2260700	-0.1559002	-0.0921559	-0.6313199	-0.6256602	
4	-0.0110057	-0.0027067	-0.0010124	-0.0004516	-0.3726057	-0.2930050	-0.2050762	-0.1142630	-0.8313176	
6	-0.0061097	-0.0037102	-0.0012010	-0.5322310	-0.0017009	-0.3505259	-0.2636360	-0.1617037	-0.8660701	
8	-0.0017000	-0.0011120	-0.0000017	-0.5070250	-0.0703207	-0.3903509	-0.2993319	-0.1937516	-0.8895070	
10	-0.0010027	-0.0000017	-0.0000017	-0.5000223	-0.5000223	-0.0191016	-0.3205209	-0.2162156	-0.1305000	
12	-0.0000000	-0.0000000	-0.0000000	-0.0000000	-0.5269056	-0.0000000	-0.3513591	-0.2305035	-0.1256600	
DELTA T (°C) = 0.100										
ΔT (°C)	0.100	0.200	0.300	0.400	0.500	0.600	0.700	0.800	0.900	
2	0.0000000	0.0000000	0.0000000	0.0000000	0.0000000	0.0000000	0.0000000	0.0000000	0.0000000	
4	0.0000000	0.0000000	0.0000000	0.0000000	0.0000000	0.0000000	0.0000000	0.0000000	0.0000000	
6	0.0000000	0.0000000	0.0000000	0.0000000	0.0000000	0.0000000	0.0000000	0.0000000	0.0000000	
8	0.0000000	0.0000000	0.0000000	0.0000000	0.0000000	0.0000000	0.0000000	0.0000000	0.0000000	
10	0.0000000	0.0000000	0.0000000	0.0000000	0.0000000	0.0000000	0.0000000	0.0000000	0.0000000	
12	0.0000000	0.0000000	0.0000000	0.0000000	0.0000000	0.0000000	0.0000000	0.0000000	0.0000000	
DELTA T (°C) = 0.200										
ΔT (°C)	0.100	0.200	0.300	0.400	0.500	0.600	0.700	0.800	0.900	
2	0.0000000	0.0000000	0.0000000	0.0000000	0.0000000	0.0000000	0.0000000	0.0000000	0.0000000	
4	0.0000000	0.0000000	0.0000000	0.0000000	0.0000000	0.0000000	0.0000000	0.0000000	0.0000000	
6	0.0000000	0.0000000	0.0000000	0.0000000	0.0000000	0.0000000	0.0000000	0.0000000	0.0000000	
8	0.0000000	0.0000000	0.0000000	0.0000000	0.0000000	0.0000000	0.0000000	0.0000000	0.0000000	
10	0.0000000	0.0000000	0.0000000	0.0000000	0.0000000	0.0000000	0.0000000	0.0000000	0.0000000	
12	0.0000000	0.0000000	0.0000000	0.0000000	0.0000000	0.0000000	0.0000000	0.0000000	0.0000000	
DELTA T (°C) = 0.300										
ΔT (°C)	0.100	0.200	0.300	0.400	0.500	0.600	0.700	0.800	0.900	
2	0.0000000	0.0000000	0.0000000	0.0000000	0.0000000	0.0000000	0.0000000	0.0000000	0.0000000	
4	0.0000000	0.0000000	0.0000000	0.0000000	0.0000000	0.0000000	0.0000000	0.0000000	0.0000000	
6	0.0000000	0.0000000	0.0000000	0.0000000	0.0000000	0.0000000	0.0000000	0.0000000	0.0000000	
8	0.0000000	0.0000000	0.0000000	0.0000000	0.0000000	0.0000000	0.0000000	0.0000000	0.0000000	
10	0.0000000	0.0000000	0.0000000	0.0000000	0.0000000	0.0000000	0.0000000	0.0000000	0.0000000	
12	0.0000000	0.0000000	0.0000000	0.0000000	0.0000000	0.0000000	0.0000000	0.0000000	0.0000000	

Reproduced from
best available copy.

Table D-5 (cont'd)

TEMPERATURE		DELTA T (F) x 10 ⁻³								
		0.100	0.200	0.300	0.400	0.500	0.600	0.700	0.800	
DEL 04041 04100										
TEMP	0.100	0.200	0.300	0.400	0.500	0.600	0.700	0.800		
L/A										
2	-0.09-2560	-0.02-0051	-0.12-0067	-0.22-0086	-0.31-0098	-0.41-0107	-0.50-0115	-0.60-0122	-0.70-0129	-0.80-0135
4	-0.12-2300	-0.07-0051	-0.14-0067	-0.23-0086	-0.32-0098	-0.42-0107	-0.51-0115	-0.61-0122	-0.71-0129	-0.81-0135
6	-0.12-1533	-0.07-0051	-0.14-0067	-0.23-0086	-0.32-0098	-0.42-0107	-0.51-0115	-0.61-0122	-0.71-0129	-0.81-0135
8	-0.13-1713	-0.07-0051	-0.14-0067	-0.23-0086	-0.32-0098	-0.42-0107	-0.51-0115	-0.61-0122	-0.71-0129	-0.81-0135
10	-0.13-1983	-0.07-0051	-0.14-0067	-0.23-0086	-0.32-0098	-0.42-0107	-0.51-0115	-0.61-0122	-0.71-0129	-0.81-0135
12	-0.13-2029	-0.07-0051	-0.14-0067	-0.23-0086	-0.32-0098	-0.42-0107	-0.51-0115	-0.61-0122	-0.71-0129	-0.81-0135
DEL 04041 04110										
TEMP	0.100	0.200	0.300	0.400	0.500	0.600	0.700	0.800		
L/A										
2	-0.06-2529	-0.02-0021	-0.11-0056	-0.20-0066	-0.29-0075	-0.38-0084	-0.47-0092	-0.56-0100	-0.65-0108	-0.74-0115
4	-0.07-2220	-0.02-0021	-0.11-0056	-0.20-0066	-0.29-0075	-0.38-0084	-0.47-0092	-0.56-0100	-0.65-0108	-0.74-0115
6	-0.07-2124	-0.02-0021	-0.11-0056	-0.20-0066	-0.29-0075	-0.38-0084	-0.47-0092	-0.56-0100	-0.65-0108	-0.74-0115
8	-0.07-2001	-0.02-0021	-0.11-0056	-0.20-0066	-0.29-0075	-0.38-0084	-0.47-0092	-0.56-0100	-0.65-0108	-0.74-0115
10	-0.07-1960	-0.02-0021	-0.11-0056	-0.20-0066	-0.29-0075	-0.38-0084	-0.47-0092	-0.56-0100	-0.65-0108	-0.74-0115
12	-0.07-1917	-0.02-0021	-0.11-0056	-0.20-0066	-0.29-0075	-0.38-0084	-0.47-0092	-0.56-0100	-0.65-0108	-0.74-0115
DEL 04041 04120										
TEMP	0.100	0.200	0.300	0.400	0.500	0.600	0.700	0.800		
L/A										
2	-0.10-2020	-0.07-0075	-0.14-0091	-0.21-0103	-0.28-0115	-0.35-0126	-0.42-0137	-0.49-0147	-0.56-0157	-0.63-0167
4	-0.10-2000	-0.07-0075	-0.14-0091	-0.21-0103	-0.28-0115	-0.35-0126	-0.42-0137	-0.49-0147	-0.56-0157	-0.63-0167
6	-0.10-1980	-0.07-0075	-0.14-0091	-0.21-0103	-0.28-0115	-0.35-0126	-0.42-0137	-0.49-0147	-0.56-0157	-0.63-0167
8	-0.10-1960	-0.07-0075	-0.14-0091	-0.21-0103	-0.28-0115	-0.35-0126	-0.42-0137	-0.49-0147	-0.56-0157	-0.63-0167
10	-0.10-1940	-0.07-0075	-0.14-0091	-0.21-0103	-0.28-0115	-0.35-0126	-0.42-0137	-0.49-0147	-0.56-0157	-0.63-0167
12	-0.10-1920	-0.07-0075	-0.14-0091	-0.21-0103	-0.28-0115	-0.35-0126	-0.42-0137	-0.49-0147	-0.56-0157	-0.63-0167
DEL 04041 04130										
TEMP	0.100	0.200	0.300	0.400	0.500	0.600	0.700	0.800		
L/A										
2	-0.07-2070	-0.03-0037	-0.07-0052	-0.11-0066	-0.15-0077	-0.19-0088	-0.23-0098	-0.27-0108	-0.31-0118	-0.35-0128
4	-0.08-2000	-0.03-0037	-0.07-0052	-0.11-0066	-0.15-0077	-0.19-0088	-0.23-0098	-0.27-0108	-0.31-0118	-0.35-0128
6	-0.07-1970	-0.03-0037	-0.07-0052	-0.11-0066	-0.15-0077	-0.19-0088	-0.23-0098	-0.27-0108	-0.31-0118	-0.35-0128
8	-0.07-1940	-0.03-0037	-0.07-0052	-0.11-0066	-0.15-0077	-0.19-0088	-0.23-0098	-0.27-0108	-0.31-0118	-0.35-0128
10	-0.07-1910	-0.03-0037	-0.07-0052	-0.11-0066	-0.15-0077	-0.19-0088	-0.23-0098	-0.27-0108	-0.31-0118	-0.35-0128
12	-0.07-1880	-0.03-0037	-0.07-0052	-0.11-0066	-0.15-0077	-0.19-0088	-0.23-0098	-0.27-0108	-0.31-0118	-0.35-0128

Table D-5 (cont'd)

TABLE D-5		DELTA T (F) vs. DELTA T (C)								
DELTA T (C) = 100		.100	.200	.300	.400	.500	.600	.700	.800	
DELTA T (C)	DELTA T (F)									
2	35.8	36.8	37.8	38.8	39.8	40.8	41.8	42.8	43.8	
4	37.8	38.8	39.8	40.8	41.8	42.8	43.8	44.8	45.8	
6	39.8	40.8	41.8	42.8	43.8	44.8	45.8	46.8	47.8	
8	41.8	42.8	43.8	44.8	45.8	46.8	47.8	48.8	49.8	
10	43.8	44.8	45.8	46.8	47.8	48.8	49.8	50.8	51.8	
12	45.8	46.8	47.8	48.8	49.8	50.8	51.8	52.8	53.8	
14	47.8	48.8	49.8	50.8	51.8	52.8	53.8	54.8	55.8	
16	49.8	50.8	51.8	52.8	53.8	54.8	55.8	56.8	57.8	
18	51.8	52.8	53.8	54.8	55.8	56.8	57.8	58.8	59.8	
20	53.8	54.8	55.8	56.8	57.8	58.8	59.8	60.8	61.8	
22	55.8	56.8	57.8	58.8	59.8	60.8	61.8	62.8	63.8	
24	57.8	58.8	59.8	60.8	61.8	62.8	63.8	64.8	65.8	
26	59.8	60.8	61.8	62.8	63.8	64.8	65.8	66.8	67.8	
28	61.8	62.8	63.8	64.8	65.8	66.8	67.8	68.8	69.8	
30	63.8	64.8	65.8	66.8	67.8	68.8	69.8	70.8	71.8	
32	65.8	66.8	67.8	68.8	69.8	70.8	71.8	72.8	73.8	
34	67.8	68.8	69.8	70.8	71.8	72.8	73.8	74.8	75.8	
36	69.8	70.8	71.8	72.8	73.8	74.8	75.8	76.8	77.8	
38	71.8	72.8	73.8	74.8	75.8	76.8	77.8	78.8	79.8	
40	73.8	74.8	75.8	76.8	77.8	78.8	79.8	80.8	81.8	
42	75.8	76.8	77.8	78.8	79.8	80.8	81.8	82.8	83.8	
44	77.8	78.8	79.8	80.8	81.8	82.8	83.8	84.8	85.8	
46	79.8	80.8	81.8	82.8	83.8	84.8	85.8	86.8	87.8	
48	81.8	82.8	83.8	84.8	85.8	86.8	87.8	88.8	89.8	
50	83.8	84.8	85.8	86.8	87.8	88.8	89.8	90.8	91.8	
52	85.8	86.8	87.8	88.8	89.8	90.8	91.8	92.8	93.8	
54	87.8	88.8	89.8	90.8	91.8	92.8	93.8	94.8	95.8	
56	89.8	90.8	91.8	92.8	93.8	94.8	95.8	96.8	97.8	
58	91.8	92.8	93.8	94.8	95.8	96.8	97.8	98.8	99.8	
60	93.8	94.8	95.8	96.8	97.8	98.8	99.8	100.8	101.8	
62	95.8	96.8	97.8	98.8	99.8	100.8	101.8	102.8	103.8	
64	97.8	98.8	99.8	100.8	101.8	102.8	103.8	104.8	105.8	
66	99.8	100.8	101.8	102.8	103.8	104.8	105.8	106.8	107.8	
68	101.8	102.8	103.8	104.8	105.8	106.8	107.8	108.8	109.8	
70	103.8	104.8	105.8	106.8	107.8	108.8	109.8	110.8	111.8	
72	105.8	106.8	107.8	108.8	109.8	110.8	111.8	112.8	113.8	
74	107.8	108.8	109.8	110.8	111.8	112.8	113.8	114.8	115.8	
76	109.8	110.8	111.8	112.8	113.8	114.8	115.8	116.8	117.8	
78	111.8	112.8	113.8	114.8	115.8	116.8	117.8	118.8	119.8	
80	113.8	114.8	115.8	116.8	117.8	118.8	119.8	120.8	121.8	
82	115.8	116.8	117.8	118.8	119.8	120.8	121.8	122.8	123.8	
84	117.8	118.8	119.8	120.8	121.8	122.8	123.8	124.8	125.8	
86	119.8	120.8	121.8	122.8	123.8	124.8	125.8	126.8	127.8	
88	121.8	122.8	123.8	124.8	125.8	126.8	127.8	128.8	129.8	
90	123.8	124.8	125.8	126.8	127.8	128.8	129.8	130.8	131.8	
92	125.8	126.8	127.8	128.8	129.8	130.8	131.8	132.8	133.8	
94	127.8	128.8	129.8	130.8	131.8	132.8	133.8	134.8	135.8	
96	129.8	130.8	131.8	132.8	133.8	134.8	135.8	136.8	137.8	
98	131.8	132.8	133.8	134.8	135.8	136.8	137.8	138.8	139.8	
100	133.8	134.8	135.8	136.8	137.8	138.8	139.8	140.8	141.8	

Table D-5 (cont'd)

74-5107-2		5076 7 0908 129-8								
2000		2100	2200	2300	2400	2500	2600	2700	2800	
0	00000000	00000000	00000000	00000000	00000000	00000000	00000000	00000000	00000000	
1	00000000	00000000	00000000	00000000	00000000	00000000	00000000	00000000	00000000	
2	00000000	00000000	00000000	00000000	00000000	00000000	00000000	00000000	00000000	
3	00000000	00000000	00000000	00000000	00000000	00000000	00000000	00000000	00000000	
4	00000000	00000000	00000000	00000000	00000000	00000000	00000000	00000000	00000000	
5	00000000	00000000	00000000	00000000	00000000	00000000	00000000	00000000	00000000	
6	00000000	00000000	00000000	00000000	00000000	00000000	00000000	00000000	00000000	
7	00000000	00000000	00000000	00000000	00000000	00000000	00000000	00000000	00000000	
8	00000000	00000000	00000000	00000000	00000000	00000000	00000000	00000000	00000000	
9	00000000	00000000	00000000	00000000	00000000	00000000	00000000	00000000	00000000	
10	00000000	00000000	00000000	00000000	00000000	00000000	00000000	00000000	00000000	
11	00000000	00000000	00000000	00000000	00000000	00000000	00000000	00000000	00000000	
12	00000000	00000000	00000000	00000000	00000000	00000000	00000000	00000000	00000000	

Table D-5 (cont'd)

TABLE OF ...

DELTA T (P) = 339.5

DEL ...

Delta	-100	-150	-200	-250	-300	-350	-400	-450	-500	-550	-600	-650	-700	-750	-800
2	-0.0107514	-0.0602207	-0.0010021	-0.0004874	-0.0033947	-0.0001715	-0.0000184	-0.0119953	-0.0093002						
4	-0.0175473	-0.0672427	-0.0020537	-0.0015754	-0.0042376	-0.0007861	-0.0003866	-0.0031279	-0.0082408						
6	-0.0210036	-0.0707142	-0.0030292	-0.00219665	-0.0049907	-0.0013672	-0.0006354	-0.0020979	-0.0060958						
8	-0.0219422	-0.0707429	-0.0034925	-0.0021744	-0.0051709	-0.0011701	-0.0008134	-0.0020177	-0.0061599						
10	-0.0210175	-0.0690791	-0.00337641	-0.00223850	-0.0047336	-0.0013215	-0.0009577	-0.0020542	-0.0062472						
12	-0.0210015	-0.0690736	-0.0034917	-0.0022353	-0.0045496	-0.0014829	-0.0011234	-0.0020906	-0.0063118						

DEL ...

Delta	-100	-150	-200	-250	-300	-350	-400	-450	-500	-550	-600	-650	-700	-750	-800
2	1.0020022	0.0020083	0.5701246	0.0000959	0.2433692	0.2002462	0.1171851	0.0399162	0.0000000						
4	1.0050007	0.0070003	0.7010071	0.0000356	0.4757903	0.3760137	0.2640276	0.1450614	0.0000054						
6	1.0070054	0.0100031	0.8573305	0.0000211	0.617973	0.5002303	0.3419755	0.2072966	0.0000460						
8	1.0070100	0.0090110	0.9003704	0.0000224	0.6362108	0.5099568	0.3002070	0.2491907	0.0000764						
10	1.00900542	0.0100013	0.915377	0.0000669	0.6379111	0.5368447	0.281217	0.2705103	0.0000469						
12	1.0110020	0.0090000	0.9200052	0.0000954	0.6699990	0.5710015	0.2501197	0.3090650	0.0000953						

DEL ...

Delta	-100	-150	-200	-250	-300	-350	-400	-450	-500	-550	-600	-650	-700	-750	-800
2	0	0	0	0	0	0	0	0	0	0	0	0	0	0	0
4	0	0	0	0	0	0	0	0	0	0	0	0	0	0	0
6	0	0	0	0	0	0	0	0	0	0	0	0	0	0	0
8	0	0	0	0	0	0	0	0	0	0	0	0	0	0	0
10	0	0	0	0	0	0	0	0	0	0	0	0	0	0	0
12	0	0	0	0	0	0	0	0	0	0	0	0	0	0	0

DEL ...

Delta	-100	-150	-200	-250	-300	-350	-400	-450	-500	-550	-600	-650	-700	-750	-800
2	1.0000000	0.0000000	0.0000000	0.0000000	0.0000000	0.0000000	0.0000000	0.0000000	0.0000000	0.0000000	0.0000000	0.0000000	0.0000000	0.0000000	0.0000000
4	1.0000000	0.0000000	0.0000000	0.0000000	0.0000000	0.0000000	0.0000000	0.0000000	0.0000000	0.0000000	0.0000000	0.0000000	0.0000000	0.0000000	0.0000000
6	1.0000000	0.0000000	0.0000000	0.0000000	0.0000000	0.0000000	0.0000000	0.0000000	0.0000000	0.0000000	0.0000000	0.0000000	0.0000000	0.0000000	0.0000000
8	1.0000000	0.0000000	0.0000000	0.0000000	0.0000000	0.0000000	0.0000000	0.0000000	0.0000000	0.0000000	0.0000000	0.0000000	0.0000000	0.0000000	0.0000000
10	1.0000000	0.0000000	0.0000000	0.0000000	0.0000000	0.0000000	0.0000000	0.0000000	0.0000000	0.0000000	0.0000000	0.0000000	0.0000000	0.0000000	0.0000000
12	1.0000000	0.0000000	0.0000000	0.0000000	0.0000000	0.0000000	0.0000000	0.0000000	0.0000000	0.0000000	0.0000000	0.0000000	0.0000000	0.0000000	0.0000000

347

Table D-5 (cont'd)

DELTA T (°C) = 73.3		DELTA T (°C) = 73.3								
DELTA T (°C)	DELTA T (°C)	DELTA T (°C)	DELTA T (°C)	DELTA T (°C)	DELTA T (°C)	DELTA T (°C)	DELTA T (°C)	DELTA T (°C)	DELTA T (°C)	DELTA T (°C)
2	0	2	3	3	0	0	3	-0.8174853	-0.8657949	
4	0	4	0	0	0	0	0	0	-0.8872523	
6	0	6	0	3	0	0	0	0	0	
8	0	8	0	3	0	0	0	0	0	
10	0	10	0	3	0	0	0	0	0	
12	0	12	0	3	0	0	0	0	0	
14	0	14	0	3	0	0	0	0	0	
DELTA T (°C) = 73.3										
DELTA T (°C)	DELTA T (°C)	DELTA T (°C)	DELTA T (°C)	DELTA T (°C)	DELTA T (°C)	DELTA T (°C)	DELTA T (°C)	DELTA T (°C)	DELTA T (°C)	DELTA T (°C)
2	1.0007302	1.0090000	1.0172700	1.0255400	1.0338100	1.0420800	1.0503500	1.0586200	1.0668900	1.0751600
4	1.0007302	1.0090000	1.0172700	1.0255400	1.0338100	1.0420800	1.0503500	1.0586200	1.0668900	1.0751600
6	1.0007302	1.0090000	1.0172700	1.0255400	1.0338100	1.0420800	1.0503500	1.0586200	1.0668900	1.0751600
8	1.0007302	1.0090000	1.0172700	1.0255400	1.0338100	1.0420800	1.0503500	1.0586200	1.0668900	1.0751600
10	1.0007302	1.0090000	1.0172700	1.0255400	1.0338100	1.0420800	1.0503500	1.0586200	1.0668900	1.0751600
12	1.0007302	1.0090000	1.0172700	1.0255400	1.0338100	1.0420800	1.0503500	1.0586200	1.0668900	1.0751600
14	1.0007302	1.0090000	1.0172700	1.0255400	1.0338100	1.0420800	1.0503500	1.0586200	1.0668900	1.0751600
DELTA T (°C) = 73.3										
DELTA T (°C)	DELTA T (°C)	DELTA T (°C)	DELTA T (°C)	DELTA T (°C)	DELTA T (°C)	DELTA T (°C)	DELTA T (°C)	DELTA T (°C)	DELTA T (°C)	DELTA T (°C)
2	1.0720000	1.0317702	1.0205000	1.0092300	0.9979600	0.9866900	0.9754200	0.9641500	0.9528800	0.9416100
4	1.0720000	1.0317702	1.0205000	1.0092300	0.9979600	0.9866900	0.9754200	0.9641500	0.9528800	0.9416100
6	1.0720000	1.0317702	1.0205000	1.0092300	0.9979600	0.9866900	0.9754200	0.9641500	0.9528800	0.9416100
8	1.0720000	1.0317702	1.0205000	1.0092300	0.9979600	0.9866900	0.9754200	0.9641500	0.9528800	0.9416100
10	1.0720000	1.0317702	1.0205000	1.0092300	0.9979600	0.9866900	0.9754200	0.9641500	0.9528800	0.9416100
12	1.0720000	1.0317702	1.0205000	1.0092300	0.9979600	0.9866900	0.9754200	0.9641500	0.9528800	0.9416100
14	1.0720000	1.0317702	1.0205000	1.0092300	0.9979600	0.9866900	0.9754200	0.9641500	0.9528800	0.9416100

GLOSSARY

Artificial accelogram

A numerically simulated acceleration time-history plot of an earthquake's ground motion.

Aspect ratio

Half-length-to-depth ratio of a semi-elliptical surface crack, b/a .
The half length is measured along the surface of the pipe.

Availability

The percent of time that the reactor plant is actually in operation during its 40-yr life. For Zion, the estimated availability is 70%.

Boundary integral equation (BIE) technique

A mathematical solution of three-dimensional elasticity problems which divides a body's surface into elements and provides displacements and tractions at surface nodal points. Results are a set of simultaneous linear equations that are solved for the unknown nodal displacements or tractions.

BWR

Boiling water reactor.

Cold leg

Portion of the primary coolant loop piping which connects reactor coolant pump to reactor pressure vessel.

Conditional probability

If A and B are any two events, the conditional probability of A relative to B is the probability that A will occur given that B has occurred or will occur.

Confidence interval (estimator)

An interval estimator with a given probability (the confidence coefficient) that it will contain the parameter it is intended to estimate.

Containment

A concrete shell designed to house the NSSS, the polar crane, and other internal systems and components of a nuclear power plant.

Correlation

The relation between two or more variables.

Couple

To combine, to connect for consideration together.

Covariance

The expected value of the product of the deviations of two random variables from their respective means. The covariance of two independent random variables is zero, but a zero covariance does not imply independence.

Crossover leg

Portion of the primary coolant loop piping which connects the steam generator to the reactor coolant pump.

Cumulative distribution function (cdf)

A function that gives the probability that a random variable, X , is less than or equal to a real value, x .

Decouple

The opposite of couple; disconnecting two events.

Estimate

A number or an interval, based on a sample, that is intended to approximate a parameter of a mathematical model.

Estimator

A real-valued function of a sample used to estimate a parameter.

Fatigue crack growth

Growth of cracks due to cyclic stresses.

Flow stress

The average of the yield strength and ultimate tensile strength of a material. Approximate stress at which gross plastic flow occurs.

Fracture

See pipe fracture.

Girth butt weld

Circumferential weld connecting adjacent pipe ends. The girth butt welds referred to in this report are in the primary coolant loop piping.

Hazard curve (seismic)

The probability that one earthquake will generate a specified value of the peak ground acceleration in a time interval of specified length, usually one year.

Hot leg

Portion of the primary coolant loop piping which connects the reactor pressure vessel to steam generator.

Independent events

Two events are independent if, and only if, the probability that they will both occur equals the product of the probabilities that each one, individually, will occur. If two events are not independent, they are dependent.

Independent random variables

Two or more random variables are independent if, and only if, the values of their joint distribution function are given by the products of the corresponding values of their individual (marginal) distribution functions. If random variables are not independent, they are dependent.

Large LOCA

Large loss-of-coolant accident. For the purpose of this report the large LOCA is equivalent to a pipe fracture in the primary coolant loop pipe. (See pipe fracture).

Leak-before-break situation

A pipe defect that grows to become a through-wall crack but is of insufficient length to result immediately in a complete pipe severance.

Load-controlled stress

Stress upon a pipe that cannot be relaxed by displacement. As such, the load is not relieved by crack extension. In this analysis pressure, dead weight, and seismic stresses are assumed to be load controlled.

Mean

(1). A measure of the center of a set of data. The sample mean of n numbers is their sum divided by n . (2). A population mean is a measure of the center of the probability density function. This is also called the mathematical expectation.

NSSS

Nuclear steam supply system.

OBE

Operating basis earthquake.

Operating stress

Stress in the piping due to normal operating loads, e. g., dead weight, pressure, start ups, etc.

Pipe fracture

A double-ended guillotine pipe break; also referred to in this report as a LOCA and a large LOCA. Refers to a circumferential pipe fracture in which pipe sections on either side of the fracture are completely severed from each other.

Pipe severance

See pipe fracture.

Poisson process

A random process, continuous in time, for which the probability of the occurrence of a certain kind of event during a small time interval t is approximately λt , the probability of occurrence of more than one such event during the same time interval is negligible, and the probability of what happened during such a small time interval does not depend on what happened before.

PRAISE

A computer code, Piping Reliability Analysis Including Seismic Events, developed to estimate the time to first failure for individual joints in a piping system. It is used to analyze the Zion 1 primary coolant loop. PRAISE is written in FORTRAN.

Primary cooling loop

Cold leg, hot leg, and crossover leg.

Probability density function (pdf)

A non-negative, real-valued function whose integral from a to b (a less than or equal to b) gives the probability that a corresponding random variable assumes a value on the interval from a to b .

PWR

Pressurized water reactor.

Radial gradient thermal stress

Axially symmetric stress in the pipe arising from temperature variations through the pipe wall thickness. In this report, the radial gradient thermal stress is a result of temperature transients in the reactor coolant.

Random variable

A real-valued function defined over a sample space.

Response spectrum analysis

A response analysis that estimates the maximum response from response spectra.

RCL

Reactor coolant loop.

RCP

Reactor coolant pump.

Risk

Expected loss.

RPV

Reactor pressure vessel.

Sample space

A set of points that represent all possible outcomes of an experiment.

S factor

Stress factor used for fatigue analysis to account for multiple stress cycles.

Seismic hazard curve

See hazard curve.

SG

Steam generator.

Simulation

Numerical technique employed to simulate a random event, artificial generation of a random process. The PRAISE computer code uses Monte Carlo Simulation to estimate the probability of failure in nuclear reactor piping.

Soil impedance functions

Forces required to oscillate the foundation through unit displacements different directions.

SSE

Safe shutdown earthquake.

Standard deviation

(1). A measure of the variation of a set of data. The sample standard deviation of a sample of size n is given by the square root of the sum of the deviations from the mean divided by $(n-1)$. (2). A measure of the variability of a random variable. The population standard deviation is the square root of the variance; the mean of the square of the random variable minus its mean.

Response spectrum analysis

A response analysis that estimates the maximum response from response spectra.

RCL

Reactor coolant loop.

RCP

Reactor coolant pump.

Risk

Expected loss.

RPV

Reactor pressure vessel.

Sample space

A set of points that represent all possible outcomes of an experiment.

S factor

Stress factor used for fatigue analysis to account for multiple stress cycles.

Seismic hazard curve

See hazard curve.

SG

Steam generator.

Simulation

Numerical technique employed to simulate a random event, artificial generation of a random process. The PRAISE computer code uses Monte Carlo Simulation to estimate the probability of failure in nuclear reactor piping.

Soil impedance functions

Forces required to oscillate the foundation through unit displacements different directions.

SSE

Safe shutdown earthquake.

Standard deviation

(1). A measure of the variation of a set of data. The sample standard deviation of a sample of size n is given by the square root of the sum of the deviations from the mean divided by $(n-1)$. (2). A measure of the variability of a random variable. The population standard deviation is the square root of the variance; the mean of the square of the random variable minus its mean.

Statistically dependent

Two events are statistically dependent if they do not fit the criterion for statistical independence.

Statistically independent

See independent events.

Stratified random sampling

A method of sampling in which portions of the total sample are allocated to individual subpopulations and randomly selected from those strata. The principal purpose of this kind of sampling is to guarantee that population subdivisions of interest are represented in the sample, and to improve the precision of whatever estimates are to be made from the sample data.

Stress corrosion cracking

Cracking due to the combined effects of stress and corrosion.

Stress intensity factor

A fracture mechanics parameter that describes the state of stress at the tip of a crack.

Surge line

Piping that connects pressurizers to the reactor coolant loop. In the Zion I PWR the surge line is a branch from the hot leg in Loop 4.

Time-history response analysis

A response analysis that estimates the maximum response from response spectra.

Transient

An event in the operation of the PWR that gives rise to a load in the piping over a specified length of time.

Uncertainty

Absence of certainty due to randomness of a random variable or lack of knowledge of the edf of a random variable.

Uniform hazard method (uhm)

A procedure for estimating frequency of occurrence distributions for various ground motion parameters.

UT

Ultrasonic testing.

Variance

The mean of the squares of the deviations from the mean of a random variable.

ZPGA

Zero period ground acceleration; defines the size of M₀ earthquake.

NRC FORM 335 (7-77)		U.S. NUCLEAR REGULATORY COMMISSION BIBLIOGRAPHIC DATA SHEET		1. REPORT NUMBER (Assigned by DDCI) NUREG/CR-2189, Vol. 5 UCID-18967, Vol. 5	
4. TITLE AND SUBTITLE (Add Volume No., if appropriate) Probability of Pipe Fracture in the Primary Coolant Loop of a PWR Plant Volume 5: Probabilistic Fracture Mechanics Analysis				2. (Leave blank)	
7. AUTHOR(S) D. O. Harris, E. Y. Lim, D. D. Dedhia				3. RECIPIENT'S ACCESSION NO.	
9. PERFORMING ORGANIZATION NAME AND MAILING ADDRESS (Include Zip Code) Lawrence Livermore National Laboratory P.O. Box 808 Livermore, California				5. DATE REPORT COMPLETED MONTH YEAR June 1981	
12. SPONSORING ORGANIZATION NAME AND MAILING ADDRESS (Include Zip Code) Division of Engineering Technology Office of Nuclear Regulatory Research U.S. Nuclear Regulatory Commission Washington, DC 20555				DATE REPORT ISSUED MONTH YEAR August 1981	
13. TYPE OF REPORT Technical				6. (Leave blank) UB00450	
15. SUPPLEMENTARY NOTES				8. (Leave blank)	
16. ABSTRACT (200 words or less) The purpose of the portion of the Load Combination Program covered in this volume was to estimate the probability of a seismic induced loss-of-coolant accident (LOCA) in the primary piping of a commercial pressurized water reactor (PWR). Such results are useful in rationally assessing the need to design reactor primary piping systems for the simultaneous occurrence of these two potentially high stress events. The primary piping system at Zion I was selected for analysis. Attention was focussed on the girth butt welds in the hot leg, cold leg and cross-over leg, which are centrifugally cast austenitic stainless steel lines with nominal outside diameters of 32 - 37 inches.				10. PROJECT/TASK/WORK UNIT NO.	
17. KEY WORDS AND DOCUMENT ANALYSIS				11. CONTRACT NO. FIN A0133	
17b. IDENTIFIERS/OPEN-ENDED TERMS				13. PERIOD COVERED (Inclusive dates)	
18. AVAILABILITY STATEMENT UNLIMITED				14. (Leave blank)	
19. SECURITY CLASS (This report) UNCLASSIFIED				21. NO. OF PAGE	
20. SECURITY CLASS (This page) UNCLASSIFIED				22. PRICE \$	